

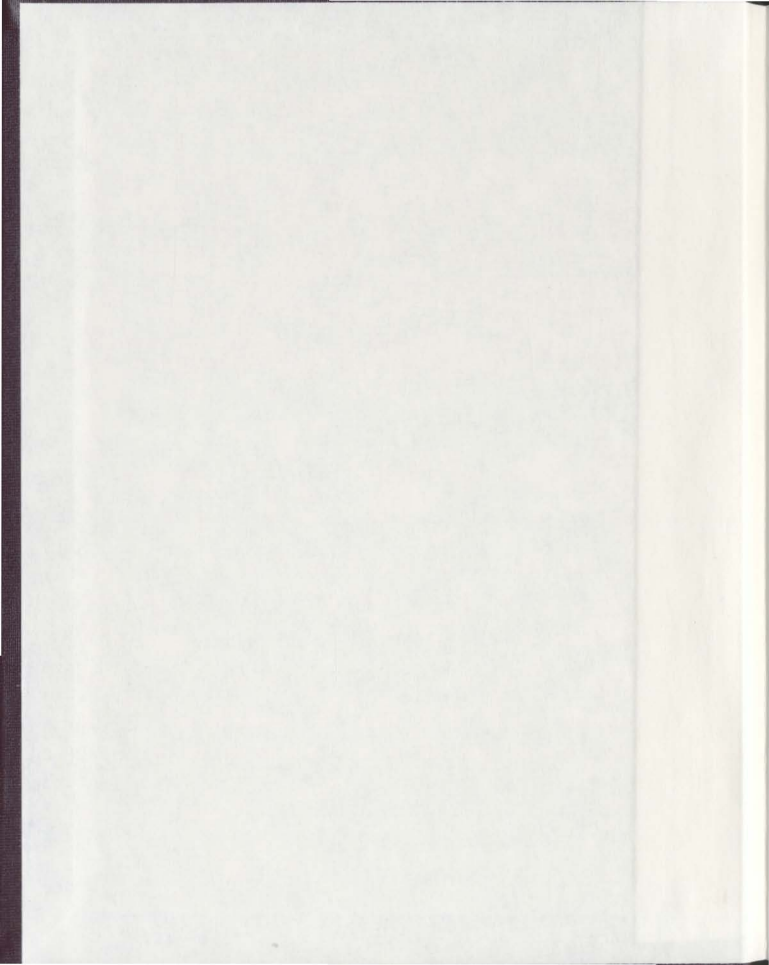
GEOLOGY, STRUCTURE AND GEOCHEMISTRY  
OF GOLD MINERALIZATION IN THE  
GERALDTON AREA, NORTHWESTERN ONTARIO

CENTRE FOR NEWFOUNDLAND STUDIES

**TOTAL OF 10 PAGES ONLY  
MAY BE XEROXED**

(Without Author's Permission)

CAROLYN DIANE ANGLIN





ABSTRACT

GEOLOGY, STRUCTURE AND GEOCHEMISTRY OF GOLD MINERALIZATION IN THE GERALDTON AREA, NORTHWESTERN ONTARIO. The area is bounded by the Huronian province to the north and the Quebec subprovince to the south.

Regionally, the deposits are linearly distributed (east-west) parallel to the southern margin of the Wabigoon belt. Virtually all rock types host gold mineralization, except for the youngest intrusions, diabase and langrophyre dykes.

A thesis submitted in partial fulfillment of the requirements for the degree of Master of Science: 1) in quartz and quartz-carbonate veins in fractured graywacke, felsic and mafic intrusions and mafic volcanic rocks, 2) in disseminated sulphide-bearing, highly fractured, Department of Earth Sciences Memorial University of Newfoundland in oxide iron formation. 1987

St. John's is no primary sulphide or carbon Newfoundland iron formation in the belt. All sulphide and carbonate minerals in iron formation are secondary alteration features associated with gold mineralization. The

## ABSTRACT

Gold mineralization in the Beardmore-Geraldton area occurs in a major, long-lived deformation zone, spatially coincident with the boundary between the Wabigoon subprovince to the north and the Quetico subprovince to the south.

Regionally, the deposits are linearly distributed (east-west) parallel to the strata of the southern margin of the Wabigoon belt. Virtually all rock types host gold mineralization, except for the youngest intrusions, diabase and lamprophyre dykes.

Gold mineralization in the Geraldton area occurs; 1) in quartz and quartz-carbonate veins in; fractured greywacke, felsic and mafic intrusions and mafic volcanic rocks, 2) in disseminated sulphide-bearing, highly fractured, zones in greywacke and quartz-feldspar porphyry, and 3) in massive quartz-sulphide lenses in oxide iron formation.

There is no primary sulphide or carbonate facies iron formation in the belt. All sulphide and carbonate minerals in iron formation are secondary alteration features associated with gold mineralization. The

alteration is characterized by addition of  $\text{CO}_2$ , S, As, K, Ba and  $\text{H}_2\text{O}$ , and loss of Sr. There is no primary enrichment of gold in any of the rocks, background gold content of all rock types is less than 10 ppb.

Gold-bearing veins occur in relatively young structures that crosscut all local Archean rock, and overprint several earlier phases of deformation. The major control on emplacement of veins is cleavage- and foliation-parallel fractures and dilations, and zones of intense deformation localized at the contacts of rocks of differing ductility.

The U/Pb zircon age of felsic porphyry intrusions in the Geraldton area is  $2691 \pm 3/-2$  Ma, significantly younger than volcanic rocks in the Onaman Lake area to the north, which are  $2769 \pm 6/-5$  Ma.

The age of gold mineralization is  $2556 \pm 72/-76$  Ma as determined by a lead isochron on pyrite from mineralized felsic porphyries. This age is approximately 130 Ma younger than the age of the felsic porphyritic rocks and therefore there does not appear to be a direct magmatic-hydrothermal link between these intrusive rocks and the gold mineralization.

## ACKNOWLEDGEMENTS

The writer gratefully acknowledges the Geological Survey of Canada for funding of field work and subsequent research time, and also for providing analytical and photographic services; and the Natural Sciences and Engineering Research Council for granting me a postgraduate scholarship, and Memorial University for the use of their analytical facilities, and for granting me a teaching assistantship.

The writer would also like to thank, in particular, her advisors, Dr. J.M. Franklin of the Geological Survey of Canada, and Dr. B.J. Fryer of Memorial University, for their guidance and support.

Thanks are also expressed to the numerous geologists at both the Geological Survey of Canada in Ottawa and the Ontario Geological Survey in Toronto and Thunder Bay, with whom I have had many interesting and informative discussions of Geraldton geology.

My most heartfelt appreciation goes to all my friends who have helped in this effort, directly or indirectly, particularly through their unfailing patience; and most especially to Jill for all her help in the field and otherwise.

1.5 Chlorite schists	64
2.5 Intermediate Intrusive rocks	70

TABLE OF CONTENTS		Page
LIST OF TABLES	.....	ix
LIST OF FIGURES	.....	xi
CHAPTER 1. INTRODUCTION AND REGIONAL GEOLOGY		
1.0 Introduction	.....	1
1.0.1 Purpose of study	.....	1
1.0.2 Location and access	.....	5
1.0.3 History and geological setting of the deposits	.....	6
1.1 Regional Geology	.....	8
1.1.1 Regional setting	.....	8
1.1.1.1 Interpretations of stratigraphy	.....	9
1.1.1.2 Structure	.....	10
1.1.1.3 Metamorphism	.....	11
1.1.2 The Beardmore-Geraldton Belt	.....	11
CHAPTER 2. GENERAL GEOLOGY - DESCRIPTION OF ROCK TYPES		
2.0 Introduction	.....	15
2.1 Sequence of lithologies	.....	15
2.2 Mafic volcanic rocks	.....	19
2.3 Sedimentary rocks	.....	19
2.3.1 Group B greywacke-siltstone	.....	20
2.3.2 Group A sedimentary rocks	.....	23
2.3.2.1 Greywacke and siltstone	.....	24
2.3.2.2 Conglomerate	.....	29
2.3.2.3 Alteration of clastic sedimentary rocks	.....	33
2.3.2.4 Iron formation	.....	34
2.3.2.5 Alteration of iron formation	.....	42
2.3.3 Sedimentological summary of the sedimentary rocks in the Geraldton area	.....	53
2.4 Mafic intrusive rocks	.....	55
2.5 Chlorite schists	.....	64
2.6 Intermediate intrusive rocks	.....	70

2.7 Felsic intrusive rocks .....	71
2.7.1 Western porphyries (WP) .....	75
2.7.2 Eastern Porphyries (EP) .....	80
2.7.3 Interpretation of the origin of the two porphyry groups .....	81
 CHAPTER 3. STRUCTURAL GEOLOGY	
3.0 Introduction .....	87
3.1 Structural observations in the Geraldton area .....	88
3.1.1 Bedding and younging direction .....	88
3.1.2 Cleavage .....	89
3.1.3 Structural facing .....	93
3.1.4 Folds .....	95
3.1.4.1 Description of minor folds .....	96
3.1.5 Shear zones and faults .....	104
3.1.5.1 Fabrics within shear zones .....	104
3.1.5.2 Faults .....	107
3.1.5.3 Displacement along the Bankfield- Tombill Fault .....	110
3.1.5.4 Timing of faulting .....	114
3.1.6 Timing of quartz veining .....	114
3.2 Interpretation of structural observations .....	120
3.2.1 Interpretation of structural facing reversals .....	120
3.2.2 Interpretation of minor folds .....	121
3.2.3 Interpretation of shear zones and faults .....	122
3.3 Summary .....	124
3.4 Structural model .....	125
 CHAPTER 4. GEOCHEMISTRY	
4.0 Introduction .....	128
4.1 Sedimentary rocks .....	129
4.1.1 Clastic sedimentary rocks .....	129
4.1.1.1 Comparison of Geraldton sedimentary rocks with average Archean sedimentary rocks .....	135
4.1.1.2 Comparison of group A and group B sedimentary rocks .....	135
4.1.1.3 Background gold contents of Geraldton clastic sedimentary rocks .....	137
4.1.2 Iron formation .....	140
4.1.2.1 Gold and base metals in iron formation .....	145

4.2	Intrusive rocks .....	150
4.2.1	Mafic intrusive rocks and chlorite schists ..	150
4.2.1.1	Mass balance studies of gabbro and chlorite schist .....	156
4.2.2	Felsic intrusive rocks .....	164
4.2.2.1	Comparison of eastern and western felsic porphyritic rocks .....	167
4.2.2.2	Alteration of the felsic porphyritic rocks .....	174
4.2.2.3	Gold - porphyritic intrusion association .....	183
4.3	Isotopic studies .....	184
4.3.1	Uranium-lead zircon dating of a felsic porphyritic intrusion .....	184
4.3.2	Lead isotopes .....	188
4.3.2.1	Lead isotope methods .....	190
4.3.2.2	Theory of lead isotopes .....	192
4.3.2.3	Discussion of the lead isotope data ..	195
4.3.3	Implications of U/Pb zircon and Pb isotope results for genetic models of gold deposits .....	204
4.4	Summary .....	206
CHAPTER 5. GOLD MINERALIZATION IN THE GERADLTON AREA: SELECTED EXAMPLES		
5.0	Introduction .....	210
5.1	Relationship of gold mineralization to iron formation; North Ore Zone, Hard Rock Mine ...	210
5.2	Porphyry-associated mineralization; MacLeod- Cockshutt, Hard Rock and Bankfield Mines .....	224
5.3	Other types of mineralization .....	231
5.4	Summary and interpretation of gold mineralization in the Geraldton area .....	233

CHAPTER 6. SUMMARY AND DISCUSSION .....	237
6.1 Summary of observations .....	237
6.1.1 Sedimentary environment .....	237
6.1.2 Intrusive rocks .....	239
6.1.3 Structural setting .....	240
6.1.4 Structural controls on and relative timing of quartz vein emplacement .....	242
6.1.5 The absolute timing of emplacement of gold mineralization .....	243
6.1.6 Alteration .....	245
6.1.7 Source of the mineralization fluids .....	246
6.2 Discussion .....	247
CHAPTER 7. CONCLUSIONS .....	252
REFERENCES .....	254
APPENDICES .....	262
A. Listing of all results of whole rock and trace element analyses .....	262
B. Analytical methods .....	276
C. Lead isotope error determinations .....	281
D. Listing of rare earth element analyses and chondrite normalization factors .....	282
Table 3. Representative analyses of sedimentary rocks from group A and group B .....	131
Table 4. Average whole rock analyses of Geraldton rocks .....	132
Table 5. Results of statistical analysis of t-tests on whole rock analyses .....	133
Table 6. Average gold content of Geraldton clastic sedimentary rocks .....	139
Table 7. Average major element and trace element analyses of iron formation subdivided by sulphur content .....	141
Table 8. Means ranges and standard deviation of major and trace element analyses of mafic intrusions and chlorite schists .....	151
Table 9. Comparison of Geraldton mafic rocks with average Archean Superior Province basalts, and average Archean mafic flows, and diorites and gabbros from Western Australia .....	152
Table 10. Mass balance chemical and specific gravity data and calculations of volume changes .....	162

## LIST OF TABLES

	Page
Table 1. Production statistics for the Beardmore-Geraldton area .....	7
Table 2. Table of formations .....	16
Table 3. Results of electron microprobe analyses of Western quartz feldspar porphyries .....	79
Table 4. Results of electron microprobe analyses of Eastern feldspar porphyries .....	84
Table 5. Representative analyses of sedimentary rocks from group A and group B .....	131
Table 6. Average whole rock analyses of Geraldton greywacke and siltstone from group A and group B .....	134
Table 7. Average compositions of Archean greywackes and argillites .....	136
Table 8. Results of F-tests and pooled variance t-tests on whole rock analyses of group A versus group B sedimentary rocks .....	138
Table 9. Average gold content of Geraldton clastic sedimentary rocks .....	139
Table 10. Average major element and trace element analyses of iron formation subdivided by sulphur content .....	141
Table 11. Means ranges and standard deviation of major and trace element analyses of mafic intrusions and chlorite schists .....	151
Table 12. Comparison of Geraldton mafic rocks with average Archean Superior Province basalts, and average Archean mafic flows, and diabases and gabbros from Western Australia .....	152
Table 13. Mass balance chemical and specific gravity data and calculations of volume changes.....	162

Table 14. Major and trace element compositions of selected Geraldton quartz-feldspar and feldspar porphyritic intrusions .....	165
Table 15. Normative mineralogy of Geraldton felsic porphyritic intrusive rocks .....	171
Table 16. Results of U-Pb zircon analyses .....	186
Table 17. Lead isotope analytical results .....	191
Table 18. Model lead ages of Geraldton galenas and pyrites .....	197
Table 19. Results of linear regression calculations on colinear $^{207}\text{Pb}/^{204}\text{Pb}$ versus $^{206}\text{Pb}/^{204}\text{Pb}$ compositions .....	202a
Figure 1. Photographs of group A graywacke and siltstone .....	22
Figure 2. Map of Mosher East (hydroline exposure east of Mosher Lake) .....	27
Figure 3. Photographs of conglomerate in the group A sequence .....	31
Figure 4. Photographs of iron formation in the group A sequence .....	36
Figure 5. Map of island in Barton Bay and detailed map of Algona trenches .....	38
Figure 6. Photomicrograph of iron formation .....	40
Figure 7. Composite photomicrograph of graded magnetite-siltstone beds .....	44
Figure 8. Photomicrographs of sedimentary structures in iron formation .....	46
Figure 9. Photographs of sulphide replacement of oxide iron formation .....	48
Figure 10. Photomicrographs of sulphides replacing oxide iron formation .....	50

	Page
Figure 15. Photomicrograph of quartz-carbonate vein crosscutting iron formation	32
LIST OF FIGURES	
Figure 16. Detailed geology map of the Bankfield property	33
Figure 1. Maps of the Wabigoon Subprovince of the Superior Province of the Canadian Precambrian Shield.	2
Figure 2. Map of the eastern end of the Beardmore-Geraldton belt (After Pye et al, 1965)	4
Figure 3. Map of the southern half of Errington and part of Ashmore Townships (after Pye, 1952, and Horwood and Pye, 1955)	18
Figure 4. Photographs of group B greywacke and siltstone	22
Figure 5. Photographs of group A greywacke and siltstone	26
Figure 6. Map of Mosher East (hydroline exposure east of Mosher Lake)	27
Figure 7. Photographs of conglomerate in the group A sequence	31
Figure 8. Photographs of iron formation in the group A sequence	36
Figure 9. Map of island in Barton Bay and detailed map of Algoma trenches	38
Figure 10. Photomicrograph of iron formation	40
Figure 11. Composite photomicrograph of graded magnetite-siltstone beds	44
Figure 12. Photomicrographs of sedimentary structures in iron formation	46
Figure 13. Photographs of sulphide replacement of oxide iron formation	48
Figure 14. Photomicrographs of sulphides replacing oxide iron formation	50

Figure 15. Photomicrograph of quartz <sup>z</sup> -carbonate vein crosscutting thin-banded iron formation .....	52
Figure 16. Detailed geology map of the Bankfield property .....	58
Figure 17. Photographs of mafic intrusions .....	60
Figure 18. Photomicrographs of mafic intrusions .....	63
Figure 19. Photographs of hornblende gabbro and chlorite schist from the Fault Rock Outcrop .....	66
Figure 20. Photographs of intrusive nature of the Geraldton quartz feldspar porphyry .....	74
Figure 21. Photomicrographs of western felsic porphyritic intrusive rocks .....	78
Figure 22. Photomicrographs of eastern felsic porphyritic intrusive rocks .....	83
Figure 23. Ternary Ab-An-Or plot of electron microprobe analyses of plagioclase phenocrysts in felsic intrusions .....	86
Figure 24. Photographs of cleavage in sedimentary rocks .....	91
Figure 25. Sketch illustration of bedding-cleavage- structural facing relationships .....	94
Figure 26. Photographs of folds .....	98
Figure 27. Tracings of folds from hand samples of banded oxide iron formation .....	99
Figure 28. Photographs of shear discontinuities in folds .....	103
Figure 29. Fabrics in chlorite schist shear zones .....	106
Figure 30. Geologic map of the Roxmark (McLellan) Property .....	109
Figure 31. Photographs of structural dislocation features .....	113

Figure 32.	Photographs of quartz veining .....	117
Figure 33.	Detailed sketch maps of selected outcrops at the Open Stope exposure of the Hard Rock North Ore Zone .....	118
Figure 34.	Frequency distributions of $\text{SiO}_2$ , $\text{Al}_2\text{O}_3$ , $\text{Fe}_2\text{O}_3\text{T}$ , and $\text{MgO}$ in clastic sedimentary rocks .....	132
Figure 35.	Probability curves for $\text{SiO}_2$ and $\text{Al}_2\text{O}_3$ in clastic sedimentary rocks .....	133
Figure 36.	X-Y plots of iron formation geochemical analyses; $\text{SiO}_2$ vs $\text{Fe}_2\text{O}_3\text{T}$ ; $\text{Al}_2\text{O}_3$ vs $\text{Fe}_2\text{O}_3\text{T}$ ; $\text{Cr}$ vs $\text{Fe}_2\text{O}_3\text{T}$ ; $\text{TiO}_2$ vs $\text{Fe}_2\text{O}_3\text{T}$ ; $\text{Ni}$ vs $\text{Al}_2\text{O}_3$ ; $\text{Co}$ vs $\text{Al}_2\text{O}_3$ ; $\text{Cr}$ vs $\text{Al}_2\text{O}_3$ ; $\text{TiO}_2$ vs $\text{Al}_2\text{O}_3$ ; $\text{Ni}$ vs $\text{Fe}_2\text{O}_3\text{T}$ ; $\text{Co}$ vs $\text{Fe}_2\text{O}_3\text{T}$ ; and $\text{TiO}_2$ vs $\text{SiO}_2$ .....	142
Figure 37.	X-Y plots of sulphur, gold and arsenic in iron formation .....	146
Figure 38.	Histograms of gold and arsenic content of iron formation .....	147
Figure 39.	X-Y plots of selected base metals versus sulphur and gold in iron formation .....	149
Figure 40.	Chondrite-normalized rare earth element plots of mafic intrusive rocks .....	154
Figure 41.	Chondrite-normalized rare earth element plots of Archean basaltic komatiites and tholeiites .....	155
Figure 42.	Zr versus $\text{TiO}_2$ and Cr versus $\text{MgO}$ in hornblende gabbro and chlorite schist .....	157
Figure 43.	Mass balance plots of chlorite schist versus hornblende gabbro .....	159
Figure 44.	Sketch map and photograph of Highway 11 Fault Rock Outcrop .....	161
Figure 45.	Chondrite-normalized rare earth element plots of felsic porphyritic intrusive rocks .....	166

Figure 46.	X-Y plots of selected elements for comparison of Eastern versus Western porphyries .....	169
Figure 47.	Normative quartz-plagioclase-K-feldspar content of felsic intrusive rocks plotted on the IUGS ternary classification plot for plutonic rocks .....	173
Figure 48.	Plots of a) Zr versus $TiO_2$ , b) $FeOT + MgO$ versus $SiO_2$ , and c) Ni versus $MgO$ for comparison of felsic and mafic intrusive rocks .....	175
Figure 49.	Mass balance plot comparing two Eastern porphyritic intrusive rocks .....	177
Figure 50.	Mass balance plots of the Western porphyries .....	179
Figure 51.	Plots of $K_2O$ and Sr versus $Al_2O_3$ for Eastern versus Western felsic porphyritic intrusive rocks .....	181
Figure 52.	Concordia diagram for U/Pb zircon analyses of the Wods-Mac porphyry and the Onaman Lake rhyolitic volcanic .....	187
Figure 53.	Geraldton lead isotope data superimposed on a Stacey-Kramers (1975) growth curve and selected isochrons .....	199
Figure 54.	$^{207}Pb/^{204}Pb$ versus $^{206}Pb/^{204}Pb$ plot of lead isotope analyses .....	200
Figure 55.	$^{208}Pb/^{204}Pb$ versus $^{206}Pb/^{204}Pb$ plot of lead isotope analyses .....	201
Figure 56.	Aerial photograph of the Open Stope exposure of the North Ore Zone on the Hard Rock property .....	212
Figure 57.	Detailed map of the Open Stope exposure of the North Ore Zone, Hard Rock property .....	215
Figure 58.	Photographs and sketches of sulphide replacement lenses at the Open Stope exposure .....	217

Figure 59. Cross-section of the North Ore Zone, MacLeod-Cockshutt Mine .....	219
Figure 60. Plan of the North Ore Zone, Hard Rock Mine ..	220
Figure 61. Photograph of quartz veins and sulphide replacement lenses, Open Stope exposure ....	223
Figure 62. Photomicrographs of gold in pyrite- arsenopyrite sulphide replacement lenses ...	226
Figure 63. Plan of the South Ore Zone, 349-foot level, of the MacLeod-Cockshutt Mine .....	229
Figure 64. Block diagram of the porphyry nose and the F-zone on the MacLeod-Cockshutt property .....	230
Figure 65. Plans of the Little Long Lac Mine .....	232

oxide iron formation.

### 1.3.1 Purpose of study

The purpose of this study is: 1) to characterize the geological environment in which the gold occurs, 2) to determine the timing of emplacement of and the controls on the site of the gold mineralization, 3) to determine the nature and importance of the relationship between gold mineralization and iron formation and 4) to assess the relationship of the felsic intrusive rocks to the gold mineralization.

This study was conducted primarily south of Geraldton in an area approximately 15 kilometres long by 3 kilometres wide comprising the southern half of Errington Township and the southwestern quarter of Ashcroft Township in the District of Thunder Bay (Figures 1 and 2). Within

## CHAPTER 1

## INTRODUCTION AND REGIONAL GEOLOGY

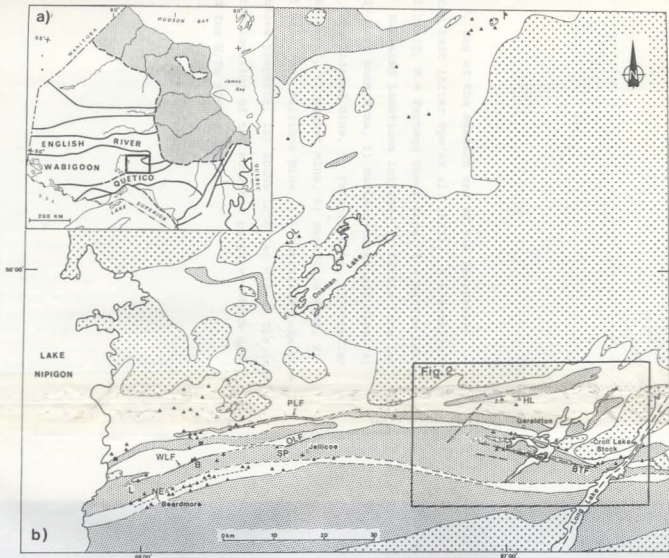
## 1.0 Introduction

Gold mineralization in the Geraldton area occurs; 1) in quartz and quartz-carbonate veins in fractured greywacke, quartz-feldspar porphyry, gabbro and volcanic rocks, 2) in disseminated sulphide-bearing, highly fractured, zones in greywacke and quartz-feldspar porphyry, and 3) in massive quartz-sulphide lenses in oxide iron formation.

## 1.0.1 Purpose of study

The purpose of this study is; 1) to characterize the geological environment in which the gold occurs, 2) to determine the timing of emplacement of and the controls on the site of the gold mineralization, 3) to determine the nature and importance of the relationship between gold mineralization and iron formation and 4) to asses the relationship of the felsic intrusive rocks to the gold mineralization.

This study was conducted primarily south of Geraldton in an area approximately 15 kilometres long by 5 kilometres wide comprising the southern half of Errington Township and the southwestern quarter of Ashmore Township in the District of Thunder Bay (Figures 1 and 2). Within



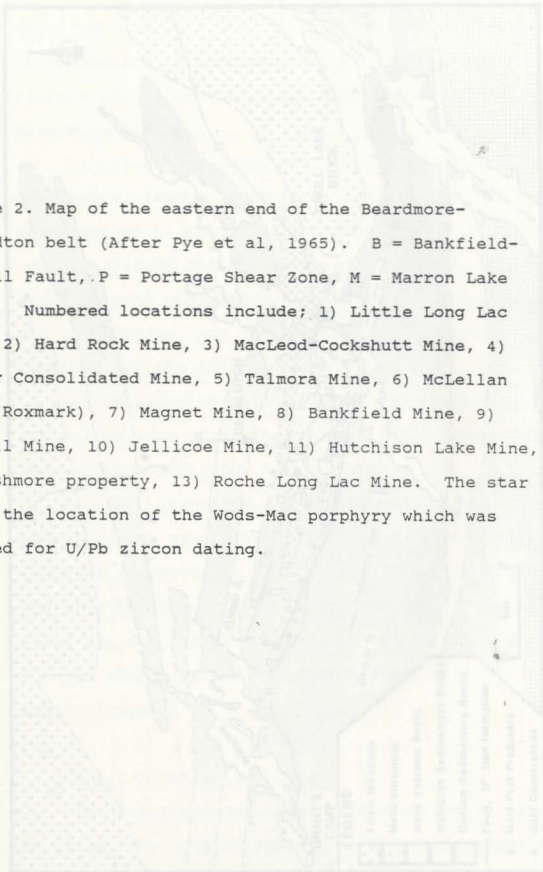
#### LEGEND

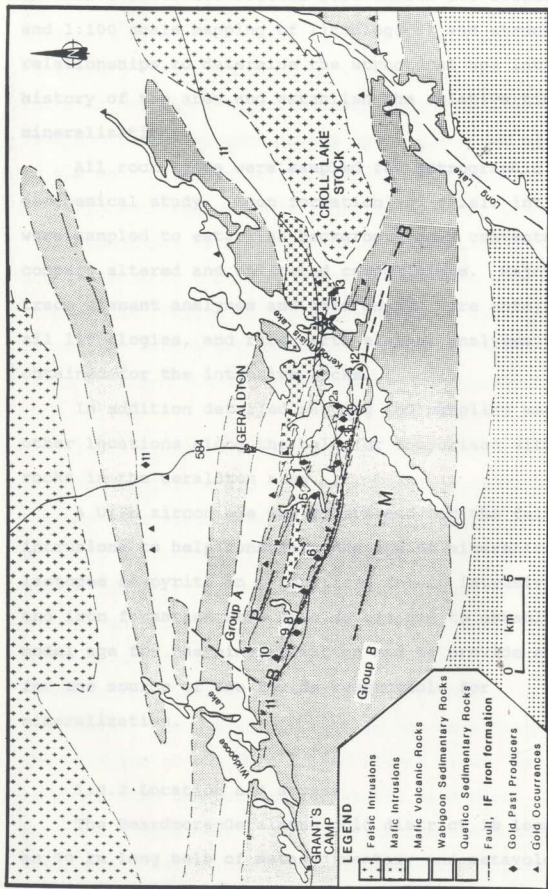
	Felsic Intrusives	B	Bema Property (Watson Lake)
	Mafic Intrusives	HL	Hutchison Lake Mine
	Metasedimentary Rocks	L	Leitch Mine
	Metavolcanic Rocks	NE	Northern Empire Mine
	Geological Boundary	SP	Solomon's Pillars (Oremond Property)
	Faults	WLF	Watson Lake Fault
	Lineament (Probable Fault)	PLF	Paint Lake Fault
	Gold Occurrences	OLF	Oxaline Lake Fault
	Past Producing Mines	BTF	Bankfield-Tombill Fault

Figure 1. a) Map of Northern Ontario showing the English River, Wabigoon and Quetico belts in central Superior Province of the Canadian Shield. The stipple pattern indicates Phanerozoic rocks. The Beardmore-Geraldton area is outlined in the black rectangle. b) Map of the eastern Wabigoon belt. The subprovince boundary between the Wabigoon metavolcanic-plutonic subprovince and the Quetico metasedimentary subprovince is presently defined as the southern boundary of the southernmost linear metavolcanic belt (Williams, 1986). Gold past-producers and occurrences are marked by open and closed triangles, respectively. The Onaman Lake massive sulphide property is marked OL.

page 3  
inserted  
incorrectly

Figure 2. Map of the eastern end of the Beardmore-Geraldton belt (After Pye et al, 1965). B = Bankfield-Tombill Fault, P = Portage Shear Zone, M = Marron Lake Fault. Numbered locations include; 1) Little Long Lac Mine, 2) Hard Rock Mine, 3) MacLeod-Cockshutt Mine, 4) Mosher Consolidated Mine, 5) Talmora Mine, 6) McLellan Mine (Roxmark), 7) Magnet Mine, 8) Bankfield Mine, 9) Tombill Mine, 10) Jellicoe Mine, 11) Hutchison Lake Mine, 12) Ashmore property, 13) Roche Long Lac Mine. The star marks the location of the Wods-Mac porphyry which was sampled for U/Pb zircon dating.





this area several locations were chosen for detailed 1:500 and 1:100 scale mapping of lithological and structural relationships to determine the structural and intrusive history of the area and establish the relative timing of mineralization.

All rock types were sampled for petrographic and geochemical study. Iron formation and felsic intrusions were sampled to establish background gold contents, and to compare altered and unaltered compositions. Major and trace element analyses and gold assays were obtained for all lithologies, and rare earth element analyses were obtained for the intrusive rocks.

In addition detailed mapping and sampling was done at other locations along the belt for comparison with the rocks in the Geraldton area.

A U/Pb zircon age was determined for the felsic intrusions to help constrain the age of mineralization. Pb isotopes of pyrite in mineralized felsic intrusive rocks and iron formation were also determined to establish a model age for the mineralization and to provide evidence for the source of the fluids responsible for mineralization.

#### 1.0.2 Location and access

The Beardmore-Geraldton gold district is located in an 90 km long belt of metasedimentary and metavolcanic rocks (the prefix meta will subsequently be omitted), east

of Lake Nipigon, approximately 160 to 250 kilometres northeast of Thunder Bay (Figure 1a). The belt is relatively easily accessed by Highway 11, the northern route of the Trans-Canada Highway, which follows the belt from south of Beardmore in the west to east of Geraldton in the east (Figure 1b). Several north-south secondary highways and logging roads allow additional access.

Topography is moderately flat with numerous swampy areas. Much of the belt is drift-covered. Good outcrop exposure is limited to highway rock cuts, old mine properties (where not obscured by waste or tailings) and areas stripped and trenched recently by prospectors.

### 1.0.3 History and geological setting of the deposits

In the 1920's and 30's gold-bearing quartz vein systems were discovered in the area, and gold has been produced intermittently for the past 50 years, from 18 mines (Table 1). Numerous gold occurrences are located in the volcanic terrain to the north of the area, but the major producers were all located in a narrow east-west trending zone between Geraldton and Beardmore.

Sedimentary and intrusive rocks in the Geraldton area at the east end of the belt hosted eleven mines, the largest of which were the MacLeod-Cockshutt, Hard Rock, Little Long Lac, Magnet Consolidated, Consolidated Mosher and Bankfield mines. This area produced, over a period of 34 years, approx 2,900,000 ounces of gold with an average

Table 1. Production statistics for the Beardmore-Geraldton area (modified after Mason et al., 1983)

Mine	Years in Production	Ounces Gold	Ounces Silver	Tons of Ore Milled	Average Au Grade	oz/ton Average Ag Grade	Host Lithology	References
GERALDTON AREA:								
MacLeod-Cockshutt	1938-48	1,475,728	101,388	10,337,229	0.14	0.09	greysacke porphyry iron formation	Horwood and Pye (1955)
Little Long Lac	1938-39 1956	603,949	32,750	1,780,516	0.34	0.03	greysacke quartzawacke (iron formation)	Buce (1936, 1937) Pye (1952)
Mosher Longlac	1962-66	330,265	34,604	2,710,657	0.12	0.01	diorite iron formation porphyry greysacke	Pye (1952)
Hard Rock	1938-51	269,081	9,009	1,458,375	0.18	0.01	greysacke iron formation porphyry	Matheson and Douglas (1948) Horwood and Pye (1955)
Magnet Consolidated	1938-43 1948-52	152,089	16,879	339,912	0.42	0.05	greysacke iron formation porphyry	Pye (1952)
Tombill	1938-42 1955	69,120	8,595	190,622	0.36	0.05	greysacke porphyry	Matheson (1948) Pye (1952)
Bankfield	1937-42 1944-47	66,917	7,590	231,009	0.29	0.03	greysacke porphyry iron formation gabbro	Matheson (1948) Pye (1952)
Theresa	1935-38 1941-43, 45 1950-53, 55	4,785	202	26,120	0.18	0.01	quartz diorite mafic to intermediate volcanic	Johnson (1981)
Jellicoe Talmora Longlac	1939-41 1947, 48	5620 1417	145 36	14,000 6,634	0.40 0.21	0.01 0.01	greysacke iron formation gabbro	Matheson (1948) Pye (1952)
BEARDMORE AREA:								
Leitch	1936-48	847,090	31,802	920,745	0.92	0.03	greysacke iron formation	McKay et al. (1948)
Northern Empire	1934-41 1949	149,093	19,803	475,866	0.35	0.05	mafic to intermediate volcanics	Benedict and Titcomb (1948)

grade of 0.1 oz/ton. In the Beardmore area at the west end of the belt (Figure 1b), gold production was largely from an area of sedimentary rocks (the largest being the Leitch and Sand River mines) and one mine hosted in volcanic rocks (the Northern Empire Mine). This area produced over 1,135,000 ounces with an average grade of 0.66 oz/ton (Mason and McConnell, 1982).

On a regional scale the deposits are linearly distributed in an east-west direction broadly parallel to the strike of the sedimentary and volcanic stratigraphy (Figure 1b), and concentrated along the southern margin of the Wabigoon greenstone belt. Virtually all rock types in the belt contain mineralization, except for the youngest intrusive units, diabase and lamprophyre dykes.

The gold occurs predominantly in quartz and quartz-carbonate vein systems in greywacke, felsic porphyritic rocks, and conglomerate, as well as in silicified sulphidic fracture zones in the above rock types and hornblende gabbros, and sulphidic zones in iron formation.

## 1.1 Regional Geology

### 1.1.1 Regional setting

The Beardmore-Geraldton area is in the eastern end of the Wabigoon Subprovince, a major subdivision of the Superior province of the Canadian Shield (Figure 1a). Wabigoon Subprovince extends in an east-west direction for

approximately 900 km and attains widths up to 150 km. It emerges from under Phanerozoic cover just west of the Manitoba-Ontario border and extends eastward under Lake Nipigon (aeromagnetic data ODM-GSC 1970a) past Longlac, where it again passes under Phanerozoic cover (Blackburn et al., 1985) (Figure 1a).

The Wabigoon Subprovince is a typical granite-greenstone terrain of Archean age, consisting of a supracrustal assemblage of predominantly volcanic rocks and lesser amounts of sedimentary rocks, into which were emplaced plutons varying in composition from granite, to syenite and gabbro (Card, 1983; Blackburn et al, 1985). To the north, the Wabigoon Subprovince is bounded by the English River Subprovince, and to the south by the Quetico Subprovince, both of which consist predominantly of "Couchiching type" turbiditic sedimentary rocks, and migmatites, as well as granitoid rocks of both anatexitic and magmatic derivation (McGlynn, 1970; Blackburn et al, 1985).

#### 1.1.1.1 Interpretations of stratigraphy

Ayres (1978) interpreted the Wabigoon Subprovince to be the dismembered and deformed remnant of a linear chain of volcanic islands whose lower and middle parts coalesced to form a continuous unit. The chain was bounded on the south by a penecontemporaneous turbidite sedimentary basin now represented by the Quetico Subprovince. Within the

western Wabigoon Subprovince, Blackburn et al (1985) suggested that "...there was a consistent development through time from initial, thick mafic, tholeiitic, quiescent submarine flows, with little or no associated clastic sediments, to more silicic, calc-alkaline, pyroclastic, violent, in part subaerial, volcanism. Clastic sedimentation associated with the latter was widespread, and consisted of proximal alluvial fan, braided river, and lacustrine facies, and distal submarine facies." Ayres (1978) stated that the original volcanic chain is now highly deformed and dismembered.

#### 1.1.1.2 Structure

The Wabigoon granite-greenstone terrain is dominated by elliptical to amoeboid domal structures, which are related to batholith emplacement. The supracrustal rocks are distributed in arcuate patterns that wrap around the domes (Figure 1). The ends of these arcuate zones are strongly attenuated, but in the interiors of the supracrustal areas there are zones of relatively coherent volcano-sedimentary assemblages (Blackburn, et al, 1985). The Beardmore-Geraldton belt corresponds to the latter. There the rocks strike dominantly east to east-northeast, whereas in the north part of the Wabigoon, the strike directions are much more variable and tend to warp around the granitoid plutonic bodies (Figure 1b). In the south

part of the eastern Wabigoon, east-west trending lineaments and faults are prominent structures.

#### 1.1.1.3 Metamorphism

The Wabigoon subprovince is characterized by low greenschist facies assemblages, with metamorphic grade increasing rather abruptly to amphibolite facies at the margins of plutonic and batholithic bodies. Ayres (1978) noted that the increase in grade toward the granitic batholiths is probably a contact metamorphic effect. The relatively low metamorphic grades in the interior of the belts indicate a relatively shallow burial, probably less than 10 km (Ayres, 1978).

#### 1.1.2 The Beardmore-Geraldton Belt

The Beardmore-Geraldton belt is at the southern margin of the Wabigoon Subprovince (Figure 1b). In this study the Beardmore-Geraldton belt is defined as the southern part of the Wabigoon greenstone belt, where the strike of the supracrustal units is predominantly east-west, and the volcanic rocks are predominantly mafic in composition. Felsic intrusive and extrusive units are volumetrically minimal. In contrast, the volcanic rocks to the north range from mafic through intermediate to felsic in composition. Granitic intrusions are also a major component of this part of the Wabigoon greenstone belt.

In the Beardmore-Geraldton belt the rocks are distributed in lens-shaped elongate panels which alternate between domains dominated by mafic volcanic rocks and those dominated by sedimentary rocks (Figure 1b).

Within Errington and Ashmore townships, Pye (1952) and Horwood and Pye (1955) divided the greywacke unit south of Geraldton into two distinct sedimentary assemblages. The northern assemblage consists of greywacke, quartz-rich greywacke, siltstone, polymict conglomerate and iron formation, with a minor amount of mafic volcanic strata in the southeast part of Ashmore Township. They named this assemblage 'group A'. To the south of group A, the sedimentary assemblage consists of a very homogeneous, laterally extensive sequence of interbedded, medium to fine grained greywacke and siltstone. This southern package, 'group B', is notably lacking in iron formation and contains only very minor conglomerate.

The group A sedimentary sequence is intruded by hornblende gabbro, felsic porphyritic rocks and Proterozoic diabase dykes. Intrusive rocks, other than Proterozoic dykes, are absent in group B.

These two distinctive sedimentary groups (A and B) are continuous along the strike length of the belt. The iron formation-bearing strata are continuous along the entire belt from east of Geraldton, west to Beardmore and southwest under Lake Nipigon to north of Thunder Bay. The

Geraldton area has an anomalous proportion of iron formation relative to the rest of the belt. This may result from tectonic thickening of the iron formation in this highly deformed area (see Chapter 3). Tectonic thickening and thinning of units most certainly takes place at the outcrop scale. However, this greater development of iron formation in the Geraldton area may also be due to a change in depositional environment along the belt.

Conglomerate beds throughout the Beardmore-Geraldton belt also occur typically as narrow, laterally extensive units, confined to the northern heterogeneous sedimentary sequence. These conglomeratic horizons are commonly located near and parallel to sedimentary-volcanic rock contacts and/or fault contacts (Bruce, 1937a; Bruce, 1937b).

Numerous east-west striking faults are identified throughout the area. Many of the contacts between sedimentary rock- and volcanic rock-dominant terrains are occupied by faults, for example the Paint Lake Fault and the Watson Lake Fault (Figure 1b). Bruce (1937a) described schistose contacts between sedimentary and volcanic rocks at several locations in the belt. He suggested that movement had occurred along these zones obliterating all primary contact relationships.

In addition to east-west faults, the Beardmore-Geraldton belt is characterized by isoclinal folding.

Kehlenbeck (1986) identified the entire Beardmore-Geraldton belt as a complex folded terrain. He observed that the rocks of the southern part of the belt form a series of isoclinal antiforms and synforms. Fold axes are generally parallel to the strike of the units. Minor fold hinge lines and bedding ( $S_0$ )/ cleavage ( $S_1$ ) intersection lineations vary both in trend and plunge along the strike of the belt. Beds dip steeply to vertically and strike dominantly east-west.

Déformation in the belt is most intense in the east around Geraldton, where Pye (1952) and Horwood and Pye (1955) identified in the south part of Errington and Ashmore townships, an elliptical zone of intense deformation, to the north of a major strike-slip fault (Figure 1b, and Figure 2). The deformation zone extends along strike for over 15 km and may attain widths up to 5 km (Buck and Williams, 1984).

Author's Note: The work for this thesis was done at the same time that the Ontario Geological Survey had several geologists working in the Beardmore - Geraldton area (Macdonald 1983, 1984; Lavigne, 1983; Kehlenbeck, 1984, 1986; Barrett and Fralick, 1985; and, Buck and Williams, 1984). Other than the occasional mutual exchange of ideas, all of the observations and conclusions in this thesis (except where referenced) were based on my own, independent, field and laboratory work.

## CHAPTER 2

## GENERAL GEOLOGY - DESCRIPTION OF ROCKTYPES

## 2.0 Introduction

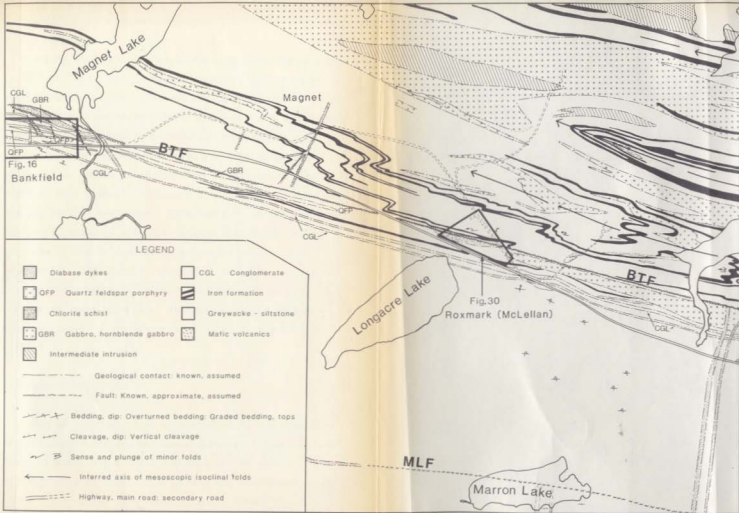
The thesis area, which measures approximately 15 kilometres east-west by 5 kilometres north-south, is located in the southern half of Errington and southwestern quarter of Ashmore Townships, centred on Horwood and Pye's (1955) southern sedimentary belt, groups A and B (Figures 2 and 3).

## 2.1 Sequence of lithologies

A generalized sequence of the lithologies is presented in Table 2. Although the absolute timing of events is poorly constrained, the relative timing of intrusive, and deformational events has been well established through field observations. Intrusive relationships will be discussed with respect to each intrusive lithology. The relationship between the sedimentary and the volcanic rocks is unknown. No primary contacts were observed. (See chapter 3 for more discussion of this relationship.)

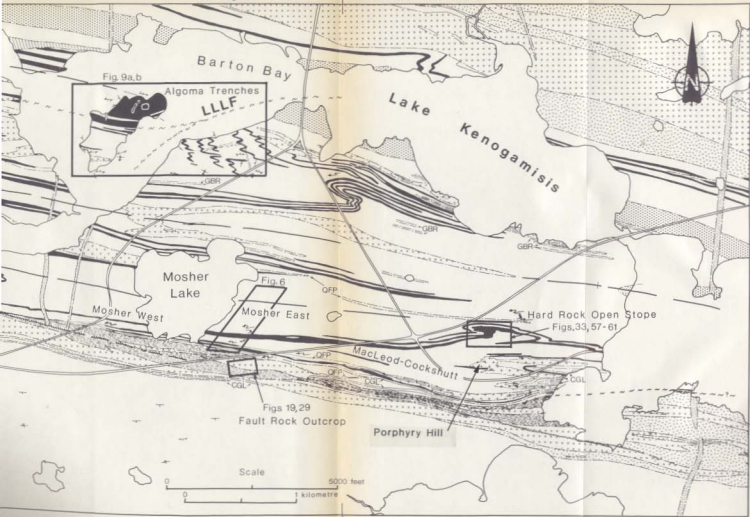


Figure 3. Map of the southern half of Errington and part of Ashmore Townships (after Pye, 1952, and Horwood and Pye, 1955). Locations of detailed maps are outlined in black and labelled with their respective figure numbers.



Errington Township

Ashmore Township



## 2.2 Mafic volcanic rocks

Within the Geraldton area, mafic volcanic rocks occur in the southeast part of Ashmore township (in the group A belt), and in the two linear east-west panels to the north of the central sedimentary belt (Figures 2 and 3). Though the volcanic rocks were not studied in detail, a few representative samples were taken for petrographic examination. These rocks are fine to medium grained, light to dark green, with some outcrops pillowed and some showing remnant amygdules. Interbedded with the flows are beds of agglomerate and well-layered tuff which, along with the pillows, indicate a submarine depositional environment. The mineral assemblage is typical of lower greenschist grade mafic rocks, consisting of varying amounts of Na-plagioclase, fibrous amphibole, chlorite, epidote, sericite, and carbonate, with minor quartz and biotite.

## 2.3 Sedimentary rocks

The sedimentary rocks were studied in the Geraldton area where deformation was least intense, (Figure 3); and, along highway 11, at Grant's Cabins and at several outcrops east of Jellicoe (Figure 2 and 1b), where group B rocks are exposed. The classification scheme used for naming these rocks follows that of Pettijohn, (1957).

### 2.3.1 Group B greywacke-siltstone

The sedimentary rocks of group B are composed primarily of a homogeneous sequence of fine to medium grained feldspathic greywacke interbedded with fine-grained chloritic siltstone. Minor thin lenses of intraformational conglomerate have been reported (Pye, 1952). The coarser beds, which weather a light grey to white, typically vary in thickness from 10 to 30 cm, and are locally up to approximately one metre thick. The fine-grained beds, which weather a darker grey-green, due to their higher chlorite content, locally attain thicknesses of up to a metre, but on average they are 1 to 3 cm thick (Figure 4a,b,c).

The thicker beds are commonly massive (Figure 4d), but in many places they have regular variations in grain size from a coarse gritty to pebbly base, through to a finer-grained, slaty, top (Figure 4a, b). Rip-up clasts, flame structures, and poorly-developed cross-laminations are present. The coarser, sandy beds commonly have very sharp bases (Figure 4a,b,d). Rootless folds, in two outcrops along Highway 11 are in strata that are not correspondingly deformed. These are probably soft sedimentary folds, indicative of tectonic instability during sedimentation.

Petrographically, the coarser grained layers consist mainly of angular quartz and feldspar grains with minor

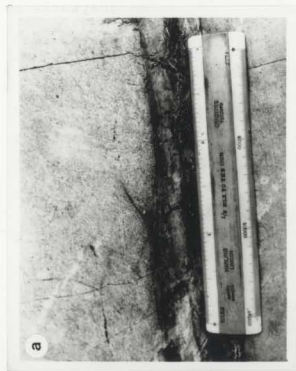
Figure 4. Photographs of group B greywacke and siltstone. Photographs were taken at Grant's Camp on Highway 11 and in each case the top of the photograph is to the northeast.

4a. Flame structure and small rip-up clasts of shale in overlying coarse-based graded greywacke bed.

4b. Rhythmic graded bed sequence with thin sandy bases that grade stratigraphically upward into shale. The sequence in the photo is capped by a massive greywacke bed.

4c. Scours of coarser greywacke into laminated shale layer.

4d. Load casts of coarse greywacke into finer greywacke. Note the shear zone with sigmoidal fractures cross-cutting layering.



chert fragments. No lithic fragments were observed. The quartz and feldspar grains range from 0.3 to 0.8 mm. The feldspar grains are fresh, and like the quartz, are angular to subangular. Some of the quartz grains are composite and some are strained, even though the rock has only a faint foliation. The matrix, which comprises 30 to 50% of the rock, is a fine-grained groundmass of quartz and altered feldspar, plus chlorite, sericite and carbonate. Minor magnetite is present.

The finer grained layers have essentially the same constituents as the coarser layers, but in different proportions. The chlorite content is up to 35% in the fine-grained layers. The foliation in these layers is much more pronounced, with the chlorite and sericite in preferred dimensional alignment, wrapping around the larger quartz and feldspar grains.

#### 2.3.2 Group A sedimentary rocks

This group consists of interlayered greywacke and slate, polymict, sandy conglomerate lenses and oxide iron formation. These rocks were intruded by hornblende gabbro, diorite and quartz and feldspar porphyritic felsic intrusions. In addition, local zones of chlorite schist are developed along faults and contacts of different rock types.

In other locations, such as the hydro line exposure west of Koshar Lake (Figures 3 and 6) individual beds are

### 2.3.2.1 Greywacke and siltstone

Greywacke and siltstone are the most abundant lithologies of the group A panel. They vary from relatively coarse, massive sandy feldspathic greywacke to finely-laminated chloritic siltstone. The coarse layers weather light grey to white, commonly with a pebbly surface due to differential weathering of the more resistant quartz and feldspar fragments. The finer-grained layers weather a darker grey due to their higher chlorite content. In some outcrops, the chloritic layers contain abundant magnetite which imparts a darker colour.

On the island in Barton Bay (Figure 3) well-graded, 10-15 cm thick, greywacke siltstone beds were observed, tops to the south (Figure 5a). In one outcrop area on the south shore of Barton Bay, just west of the Little Long Lac mine property (Figure 3), the greywacke beds are up to approximately a metre thick, with coarse pebbly bases (clasts up to 2cm long). These beds have rip-up features at their bases, and they grade up through a massive sandy interval into very fine, magnetite-rich chloritic tops, the magnetite laminae being no thicker than one cm, and usually less (Figure 5b). In the same area, features similar to load casts are seen in sandy greywacke where it overlies 3 to 4 cm thick magnetite layers (Figure 5c). These features have been accentuated by deformation.

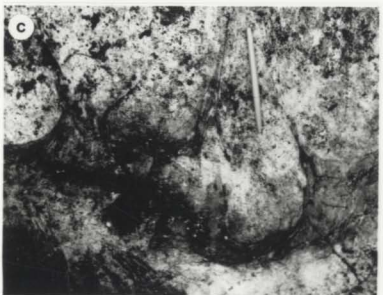
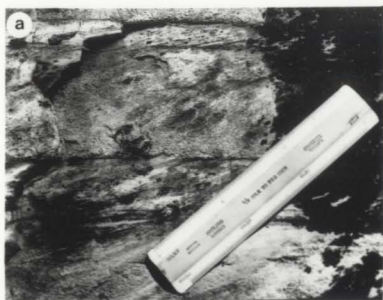
In other locations, such as the hydro line exposure west of Mosher Lake (Figures 3 and 6) individual beds are

Figure 5. Photographs of group A greywacke and siltstone.

5a. Graded sandy greywacke beds. Photograph of outcrop on the island in Barton Bay. Top of photograph is to the south.

5b. Greywacke bed, 80cm thick, grading from massive sandy base into finer siltstone, with a very fine, magnetite-rich top. Overlying bed repeats sequence of siltstone to magnetite over a 10cm interval. Note the magnificent refracted cleavage.

5c. Load casts of sandy greywacke into finer-grained, magnetite-rich, siltstone.





thinner, ranging from several cm to several tens of cm thick and finer-grained than those described above. They are composed dominantly of sandy and silty greywacke with a significant portion of oxide iron formation. Where it is most abundant, over an interval of several metres, the magnetite layers are up to 30 cm thick. These layers are actually compound units of narrow magnetite laminae with very minor chert and very narrow siltstone laminae. Individual laminae are usually less than a few mm thick. In addition, narrow interbeds of green, fine-grained chloritic layers, contain abundant disseminated magnetite grains. These may be mafic tuffaceous interlayers.

Petrographically, the greywacke and siltstone of group A are very similar to those of group B. The principal difference is the generally coarser-grained nature of the greywacke, and the high proportion of magnetite in some of the chloritic slaty layers, of group A. These sedimentary rocks are composed of angular to subangular quartz and feldspar grains, 0.15 to 0.5 mm in size, in a variable fine grained matrix of quartz, highly altered feldspar (to sericite), chlorite, sericite and carbonate. Horwood and Pye (1955) and Pye (1952) distinguished a separate lithology in the group A panel that they called arkose. In thin section this unit is coarser-grained, with more quartz grains and less matrix than the greywackes. Quartz greywacke is probably a more appropriate term for

this rock than arkose because in the sections examined the rock contained at least 15% matrix.

#### 2.3.2.2 Conglomerate

Elongate, narrow, locally lensoid, conglomerate horizons extend across Errington and Ashmore townships within the group A panel (Figure 3). Good exposures are present on the Bankfield property, on Highway 11 south of the McLellan property (now Roxmark mines), on the east-west hydroline right-of-way, west of Mosher lake (Mosher West), and on Highway 11 at the entrance to the old Mosher-Consolidated property (Mosher East) (Figure 3).

The conglomerate units are polymict, clast-supported and matrix-supported pebble-cobble beds, and alternate with sandy to silty greywacke beds. At the Roxmark property the individual sandy beds are from 5 to 20 cm wide and the conglomeratic layers average 50 cm in thickness but may attain thicknesses of up to 1 metre. The matrix here is very sandy (Figures 3 and 7a).

On the Bankfield property, conglomerate is exposed at both the northern and southern edges of the outcrop area. The conglomerate here is more massive and occurs in thicker beds, up to 2 metres wide, which are bounded on either side by massive greywacke beds.

Individual conglomeratic beds are moderately sorted with respect to size of clasts, but there is a wide variation in clast size between beds. In some outcrops

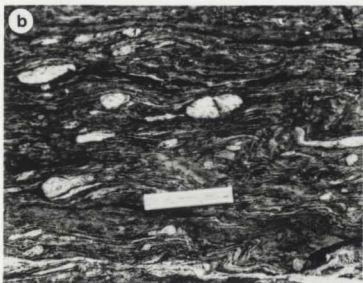
98

Figure 7. Photographs of conglomerate in the group A sequence.

7a. Conglomerate with sandy interbeds, on Highway 11 south of Roxmark trenches. Note the lens cap for scale.

7b. Deformed conglomerate layers with finer-grained matrix and stretched-out volcanic clasts, Mosher West.

7c. Deformed conglomerate, southeast of Mosher Lake, east of "Gabbro Fault Rock" outcrop. Note the consistent asymmetry to the minor folds.



maximum clast size is 2-3 cm in diameter, for example south of Highway 11 between Little Long Lac and Eldee Lake, whereas, at the Bankfield and Roxmark properties the clasts attain sizes of 10 to 15 cm in the long dimension (even longer in the case of deformed mafic volcanic clasts). There appears to also be some variation in clast sizes along the strike of the beds.

Clast lithologies are very variable: granitic, granodioritic and quartz feldspar porphyritic clasts appear to be the most abundant, followed by mafic volcanic (and some felsic volcanic), quartz and a few chert and jasper pebbles. It may be that the intrusive lithologies appear to be more abundant than the extrusive ones because the latter are obscured somewhat by deformation (Figure 7b,c) and, especially in the case of the mafic clasts which are difficult to distinguish from the matrix of the conglomerate. The petrography and provenance of these clasts were not studied in detail.

The shape of the clasts depends on the composition and amount of deformation. Felsic plutonic and quartzitic clasts are typically more spherical than other clast types, and may have length to width ratios from 1:1 to 5:1. Felsic volcanic clasts tend to be more elongate, parallel to foliation, whereas the mafic volcanic clasts are stretched by as much as 15:1. Clasts are typically oblate spheroids ("pancakes") flattened in the N-S dimension and elongate E-W and vertically.

Petrographically, the matrix of these conglomerates is the same as the enclosing greywacke, varying from fine to medium grained, from slaty (schistose) to massive, and from chloritic to sandy (quartzitic and feldspathic). The matrix is composed dominantly of subrounded to angular quartz grains (some composite) and variable amounts of plagioclase, chlorite, carbonate, sericite and minor magnetite.

#### 2.3.2.3 Alteration of clastic sedimentary rocks

Where these rocks are crosscut by quartz or quartz-carbonate veins the sedimentary rocks in some cases develop a chloritic-pyritic-sericitic selvage on the veins, and in others a sericite-carbonate selvage. This seems to depend on the original composition of the rock with the finer-grained sediments tending to develop chloritic selvages, which commonly contain fine-grained pyrite. In all instances the alteration selvages on the veins are very narrow and are seldom greater than the width of the veins themselves.

Extreme carbonate alteration of sedimentary rocks is developed at the open stope exposure on the Hard Rock property. Here, the rocks are so extensively altered that it is difficult in hand specimen and in thin section to determine their primary composition. These rocks are identified as sedimentary however because of their stratiform association with iron formation, and the

presence of what appears to be bedding in one short drill core. These rocks have also been extensively deformed and transposition of bedding has been extreme along the south side of the open stope (see Chapter 3).

#### 2.3.2.4 Iron formation

The most distinctive member of the sedimentary sequence is iron formation which occurs at a number of stratigraphic levels within the sedimentary rocks of group A, interbedded with sandy and silty greywacke (Figure 3, 8a,b,c and d). Sedimentary sequences containing magnetite occur at several discrete, fairly laterally continuous horizons, however, it is evident from Figure 3 that many of the stratigraphic occurrences of iron formation are due to fold repetition. Structural thickening and thinning of the sedimentary package and frequent repetition of the sequence occurs at centimetre and metre scale (Figure 8c,d).

At the outcrop scale, these bands, which are composite units composed of alternating magnetite and clastic sedimentary laminae 10's of centimetres to metres wide, are traceable for 100's of metres. Similar to the distribution of the conglomerate, however, the iron formation actually appears to have a lensoid local distribution, with individual laminae thinning out rapidly along strike.

Figure 8. Photographs of iron formation in group A sequence.

8a. Magnetite and hematite-rich iron formation interlaminated with fine-grained sil<sup>l</sup>stone in trench on island in Barton Bay.

8b. Deformed magnetite-rich layers 5 to 10 cm wide in greywacke, Roxmark property.

8c. Highly deformed magnetite-rich layers in greywacke and silstone, Mosher East (hydroline exposure east of Mosher Lake.

8d. Very narrow magnetite-rich laminae in greywacke-silstone beds, Mosher East. Note isoclinal folding of sedimentary layers.



The iron formation varies from an almost purely chemical (Figure 8a), to an almost entirely clastic end-member (Figure 8d). The chemical end-member consists of magnetite(-hematite)-rich intervals intercalated with minor siltstone beds. The best exposure of this type is on an island in Barton Bay (Figure 3), where the iron formation has been exposed in a pit and trench (Figure 9a,b, Algoma trenches). Finely laminated bands of magnetite and hematite, with minor reddish jasper bands, are intercalated with narrow siltstone laminae (Figure 8a). These laminae form compound iron-oxide dominated packages which are interlayered with more coarse-grained clastic laminae.

In thin section, the Barton Bay iron formation consists of fine-grained magnetite-dominated and hematite-dominated layers, interlaminated with very fine-grained quartz-rich siliciclastic layers or narrow chert and jasper bands. The hematite grains have a tabular habit and are oriented with their long dimensions parallel to cleavage. Magnetite grains are generally equant and coarser-grained than the hematite grains (Figure 10). The iron oxide-rich bands are made up of many individual laminae with varying proportions of iron oxide and siliceous material. Individual beds tend to be discontinuous.

A complete spectrum of compositions exists between the two end-members. At the Roxmark property, Mosher

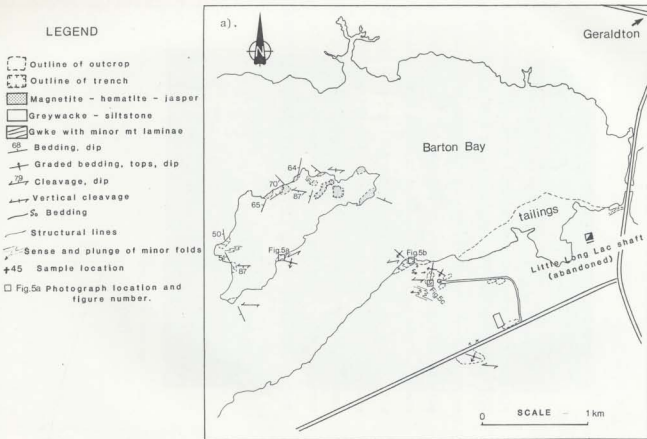


Figure 9. a) Map of the island in and shoreline of Barton Bay; and, b) Detailed structural map of the Algoma trenches. Sample locations are marked with crosses. Photograph locations are outlined by small squares and labelled with their respective figure numbers.

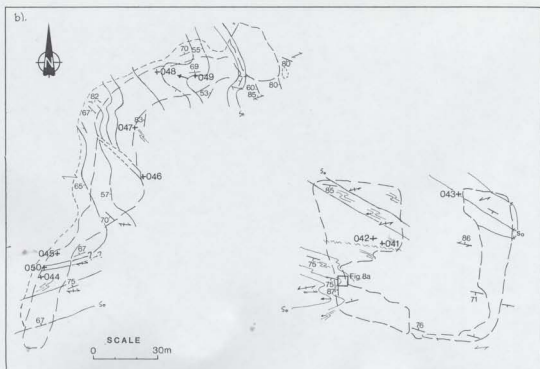


Figure 10. Photomicrograph of iron formation sample 045. This sample is from the western Algoma trench on the island in Barton Bay. The photograph was taken under transmitted, polarized light at 2 X 2.5 magnification. Magnetite-dominated and hematite-dominated layers are interlaminated with very fine-grained quartz-rich siliciclastic or chert and jasper bands. The magnetite grains are generally equant and coarser than the hematite grains which have a tabular habit. Note the cleavage perpendicular to layering and the very slight offset of layering along this cleavage.



1 mm

East, and the Bankfield property, the magnetite-rich laminae are intercalated with more clastic-rich beds resulting in the intermediate member (Figures 3, 8b).

In the south part of the Mosher East section (Figure 6), magnetite laminae (<1 centimetre wide) are intercalated with sandy-silty greywacke beds (these are actually representative of the clastic-dominated end-member). The next 65 metres of section to the north (some structural repetition is present) consists only of siliciclastic material. The next 60 metres of section contains more magnetite-rich beds. These beds are up to 20 centimetres wide composed of finely laminated magnetite (described above). The section alternates from being entirely clastic-dominated to being dominated by magnetite layers.

The clastic-dominated iron formation (LIF for lean iron formation) is characterized by laminae of almost pure magnetite which occur at the uppermost, finest-grained parts of thick, graded, greywacke-siltstone units, as seen in outcrops on the shore of Barton Bay just west of the site of the old Little Long Lac mine shaft, and east of the island. These were described above under group A greywacke and siltstone.

In the clastic-dominated sections, chert and jasper bands are absent. This is different from the more characteristic magnetite-hematite-chert interbanding of Algoma-type iron formation as described by Gross (1965).

In the Geraldton area, magnetite laminae often form the tops of graded greywacke beds. Graded bedding is seen in thin section (Figure 11), with the amount of magnetite increasing as grain-size of the clastic material decreases. Laminae of almost pure magnetite may occur at the tops of these units (Shegelski, 1978). What appear to be scour marks or load casts of siliciclastic material into magnetite layers are preserved in some samples (Figure 12a,b).

#### 2.3.2.5 Alteration of iron formation

In no place were primary carbonate, silicate or sulphide facies of iron formation observed in the Geraldton area. However, carbonate and sulphide alteration is common on the selvages of quartz-carbonate veins that crosscut the iron formation. Hand specimen photographs and photomicrographs clearly illustrate the replacement and overgrowth textures of carbonate and sulphide minerals in the oxide iron formation (Figures 13a,b 14 and 15). The carbonate minerals weather an orange-brown, and have variable relief in thin section, suggesting that they are iron carbonates, but the exact composition is unknown.

Sulphide and carbonate alteration of iron formation is very pronounced at the Open Stope exposure. Where veins are parallel to the bedding in iron formation the secondary nature of the sulphides is difficult to see;

Figure 11. Composite photomicrograph of iron formation siltstone sample 004. Note graded nature of sample from darker coarse-grained fragmental material to finer-grained magnetite and quartz-rich material at the tops of beds. The photographs were taken under transmitted, plane light. The scale bar is 1.0mm.

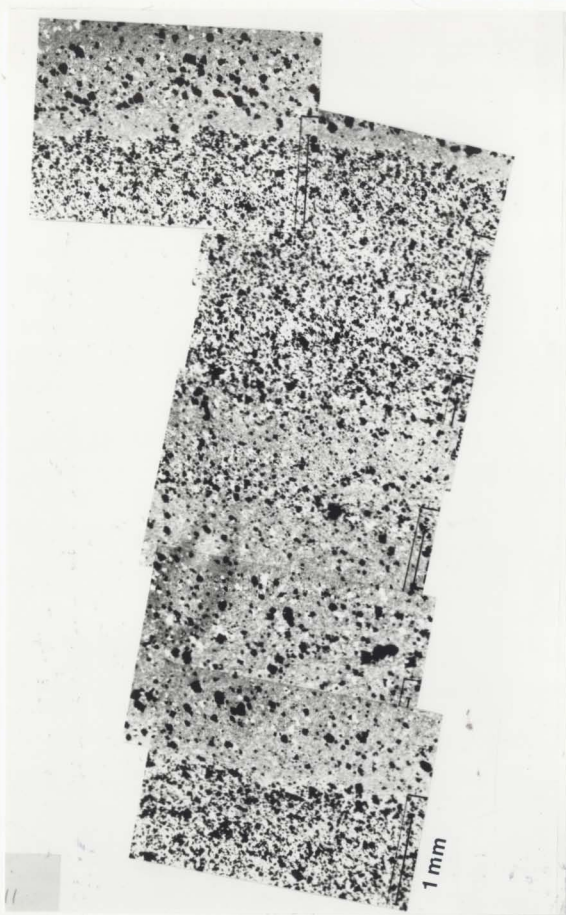
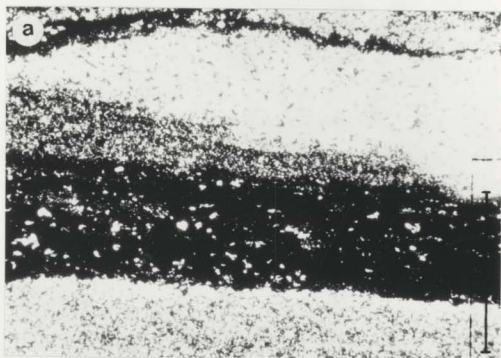


Figure 12. Photomicrographs of sedimentary structures in iron formation sample 153; a) scour marks, and b) load casts, of siliceous clastic material into magnetite-rich laminae. The photographs were taken in transmitted light. The scale bar is 1.0mm.



1 mm

Handwritten notes or signatures in the bottom right corner of the page.

Figure 13. Photographs of sulphide replacement of iron formation in hand samples; a) A sample of thin-banded magnetite-hematite-jasper-siltstone iron formation from the Solomon's Pillars property northwest of Jellico (see Figure 1b). Sulphides (pyrite with minor arsenopyrite) replace the iron oxide minerals outwards from a small crosscutting quartz-carbonate vein. (Photograph courtesy of A.J. Macdonald, Ontario Geological Survey, Toronto, Ontario.), b) A sample of banded magnetite-hematite-siltstone iron formation from the Hard Rock dump. Sulphides (pyrite and arsenopyrite) replace oxide minerals along and across folded bedding. Small quartz veinlets are hosted in fractures parallel to the axial plane of the minor folds.

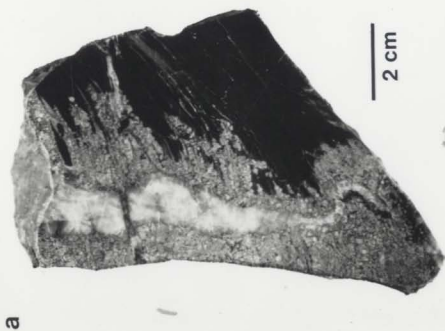
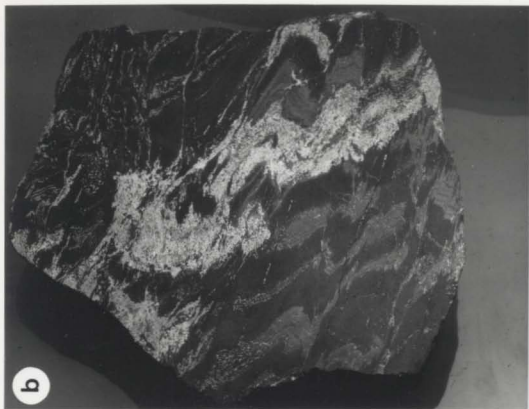
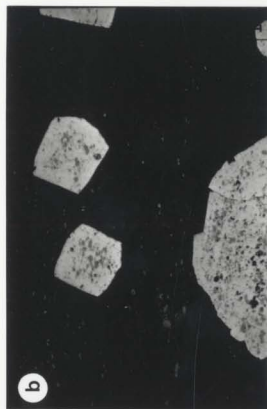
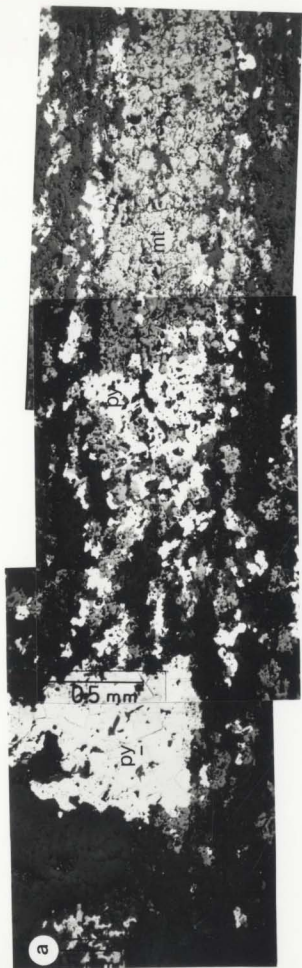
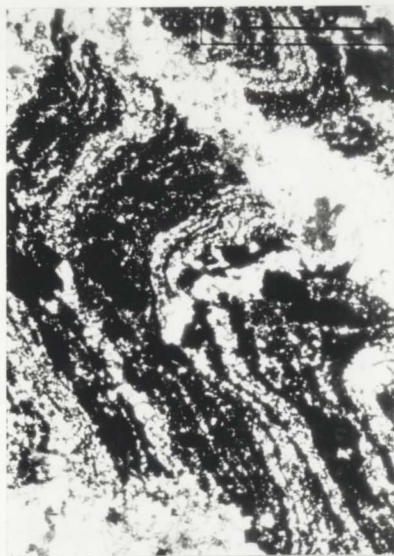


Figure 14. Photomicrographs of sulphides replacing oxide iron formation; a) from the Open Stope exposure on the Hard Rock property. Sulphides (pyrite with very minor arsenopyrite and pyrrhotite) replace magnetite along bedding, outwards from a cross-cutting quartz vein (dark area to left of the large pyrite grain). Note how the replacement front appears to be localized along the contact between the magnetite and the darker clastic laminae (right hand part of the photograph). This sample assayed at greater than 10,000 ppb.; b) from the Roxmark property. Pyrite porphyroblasts overgrow fine-grained magnetite in an iron-rich chloritic slate. This sample assayed at 4400 ppb Au.

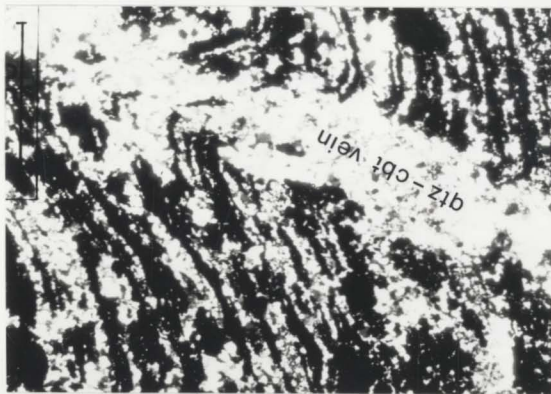


0.5 mm

Figure 15. Photomicrograph of quartz-carbonate vein crosscutting thin-banded iron formation. This sample is from the Open Stope exposure on the Hard Rock property. The photograph was taken in transmitted light. The scale bar is 0.5 mm.



0.5 mm



however, where veins cut the layering at a high angle the replacement nature of the sulphides is clear (Figures 13a,b ,15). In photomicrographs of sulphides from the open stope, pyrite and arsenopyrite progressively replace magnetite-hematite layers away from quartz veins (Figure 14a). The magnetite layers were first replaced along their contacts with siliceous layers, clastic or chert. The sulphides selectively replaced the magnetite layers. Pyrite grains overgrow smaller magnetite grains in slaty iron formation from the Roxmark property (Figure 14b).

### 2.3.3 Sedimentological summary of the sedimentary rocks in the Geraldton area

Due to limited outcrop and extensive deformation in the Geraldton area, sedimentary structures and stratigraphic relationships tend to be obscured. However, the associations of certain lithologies may be used to fit the area into a generalized sedimentological model.

The greywacke described from both group A and B sequences fits Walker's (1979) model of turbidite sediments. Turbidite beds are laterally extensive, tend to be parallel-sided and vary little in thickness laterally (Walker, 1979). The group B and group A sedimentary rocks appear to be comprised of A and E beds of the Bouma model. Several other facies which Walker (1979) stated are commonly associated with classical turbidites are observed in the group A sequence. These

include, pebbly sandstones, and clast-and matrix-supported conglomerates. This association of rock types fits the Resedimented (Turbidite) Facies Association described by Ojakangas (1985) for Archean sedimentary rocks. In this model, the turbidite sequences are developed on a submarine fan. These turbidites are commonly interbedded with conglomerate that is graded and lacks cross-bedding, and represents resedimented conglomerates deposited from mass flows.

The occurrence of iron formation in turbidites was noted as early as 1936 by Rittenhouse (Shegelski, 1978) who observed magnetite bands occurring in the top layer of a graded sequence, which passed from greywacke through argillite to iron formation. Shegelski (1978) noted that the turbidite-hosted iron formation commonly occurs between turbidite beds and is finely laminated. He called this type "laminated iron formation" and interpreted these layers to be equivalent to the ambient pelagic sedimentation in the deeper water turbidite environments. Only oxide facies iron formation was observed in the Geraldton area. *delta and no outcrops have been found in*

There are two distinct sedimentary environments in the Geraldton area. The group A sediments consist of graded greywacke-siltstone (mudstone) turbidites with minor coarse greywacke, polymict matrix-supported conglomerate and iron formation, consistent with a proximal, turbidite fan environment. To the south, the

group B sequence consists entirely of graded greywacke-siltstone mudstone with no conglomerate or iron formation, indicating a more distal turbidite environment. The lack of iron formation in the group B assemblage indicates that there was either no source of iron chemical precipitate in this area, or the deposition rates were higher and/or more consistent so that no distinctive iron-sediments were produced. However, crosscutting relationships

were observed on the Bankfield Mines property, where mafic intrusions intrude primary strata at low angles (Figure 16, 17a).

Large mafic bodies, several kilometres in length, intrude the volcanic rocks to the north of Geraldton. Similar, but smaller bodies intrude the sedimentary and volcanic rocks of the group A panel. There is an anomalous concentration of mafic intrusions in the Geraldton area relative to the rest of the Beardmore-Geraldton belt (Figure 1a). Horwood and Pye (1955, p16) noted that exposures of the mafic intrusions are more numerous and more extensive in the volcanic belts than in the sedimentary belts and no outcrops have been found in either the sedimentary belt underlying the town of Geraldton or in the southern group B part of the southern sedimentary belt. However, numerous intrusions are found in the group A sedimentary belt.

Outcrops of the mafic intrusions were examined on the Bankfield property, outcrops west and south of Mosher

Lake, on the Ashmore and Roche Long Lac properties at the east end of the study area, and several other outcrops to the north of the highway.

The mafic intrusions are dyke-like and sill-like masses that vary from a few centimetres to approximately 1500 metres in width (Horwood and Pye 1955). Their contacts are generally parallel to the sedimentary units which they intrude. However, crosscutting relationships were observed on the Bankfield Mines property, where mafic sills crosscut the sedimentary strata at low angles (Figure 16, 17a).

On the Bankfield property the mafic bodies range from a knobby-weathering, dark green variety (the "knobs" being blocky hornblende crystals) (Figure 17b); to a finer-grained dark greenish-grey rock which forms narrow sill-like bodies. In some outcrops the matrix surrounding the hornblende crystals weathers almost white rather than the normal greyish-green due to epidotization of the plagioclase in the matrix. The mafic intrusions are cut by narrow albitized zones which in turn are cross-cut by thin hematite-bearing fractures. The hematite-filled fractures are cut by small felsic dykes (Figure 17c). Within the central part of the mafic bodies, these dykes have variable strikes, that locally occur at high angles to the regional foliation.

The interiors of the mafic intrusions are relatively massive with foliation increasing toward the margin

Figure 16. Detailed geology map of the Bankfield property. Sample locations are marked with crosses. Note the crosscutting relationships of the mafic intrusions into the sedimentary rocks, and the felsic intrusions into both the sedimentary rocks and the mafic intrusions.

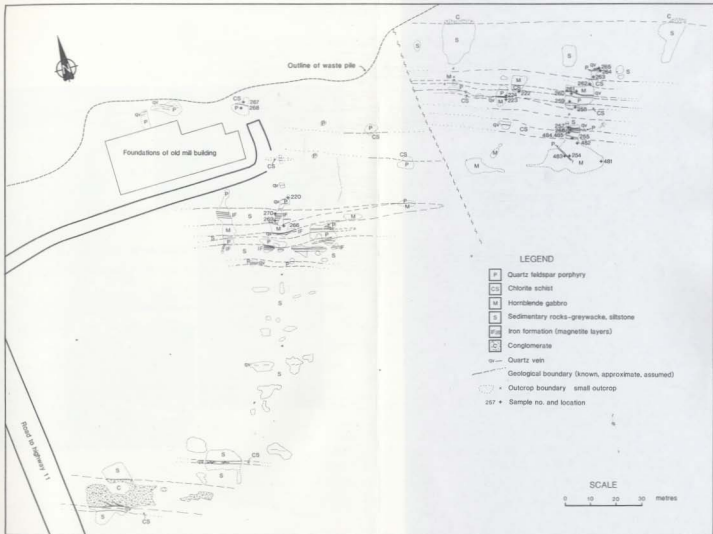


Figure 17. Photographs of mafic intrusions on the Bankfield property.

17a. Mafic sill crosscutting greywacke. The intrusive contact is located just above the lens cap and is marked with two small black arrows. A fragment of banded oxide iron formation (marked IF) is included within the mafic intrusion.

17b. Coarse-grained hornblende crystals in the centre of a mafic sill, away from its deformed margins (see 17d).

17c. Felsic intrusive material crosscutting coarse-grained relatively undeformed gabbro.

17d. Chlorite schist developed at the margins of a mafic intrusion. Note the lighter material in the vicinity of the lens cap at the bottom of the photograph. This is felsic material that has been deformed subsequent to crosscutting the mafic sill.



(Figure 17d). Where the intrusions have been subjected to intense deformation, they are transformed into a strongly foliated, rubbly-weathering chlorite schist (Figure 17d). Similarly, at the margins of the mafic intrusions the cross-cutting felsic dykes are rotated to be sub-parallel with the foliation, and where felsic dykes are caught up in the schist zones, they form boudinaged lenses surrounded by chloritic, mafic material (Figure 17d).

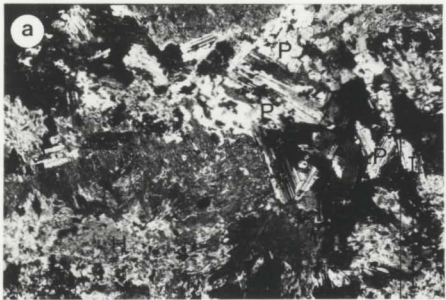
Petrographically, the mafic intrusive rocks consist of stubby to elongate crystals of hornblende, which impart a porphyritic texture, and twinned plagioclase laths, in a fine grained matrix of altered plagioclase, epidote, sericite, carbonate, and locally fine-grained biotite and quartz (Figure 18a,b). In samples where the hornblende crystals are elongate, they have an ophitic texture with plagioclase laths of approximately the same size (Figure 18a). The hornblende in these rocks is commonly partially altered to chlorite and minor carbonate. In one sample (228) remnants of clinopyroxene were observed in the interiors of several of the stubby hornblende crystals. In some samples, the plagioclase is almost entirely altered to epidote, carbonate and sericite. Opaques consist of less than 5% magnetite and less than 2% sulphide in most sections. The magnetite contains abundant ilmenite intergrowths.

Figure 18. Photomicrographs of mafic intrusions.

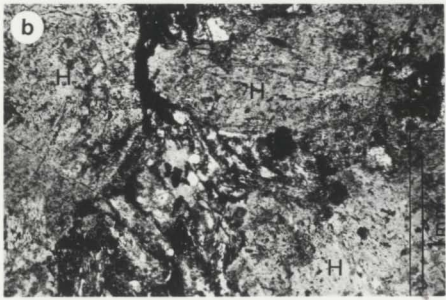
18a. Coarse-grained equigranular plagioclase and hornblende crystals with ophitic texture.

18b. Very coarse hornblende crystals in fine grained plagioclase-quartz matrix.

Some remnant pyroxene within hornblende was observed in one thin section. Most of the hornblende is now altering to chlorite.



1 mm



material (Figure 19c). At this location, however, the

## 2.5 Chlorite schists

Chlorite schist units occur as: 1) narrow layers at the contacts of mafic intrusions with other rock types, as on the Bankfield property (above); 2) as narrow bands entirely enclosed within massive hornblende gabbro; and, 3) at the contacts of felsic intrusions and sedimentary rocks. Outcrops of this schist were examined immediately south of the Bankfield-Tombill Fault, on the Roxmark property; associated with gabbroic intrusions in outcrops on the hydroline exposure west of Mosher Lake and south of the lake to outcrops on Highway 11; and, further southeastward along strike to an area south of the MacLeod-Cockshutt and Hard Rock properties (Figure 3).

In the series of outcrops from west of Mosher Lake southwest to south of the Hard Rock property, lenses and layers of chlorite schist are intercalated with coarse-grained hornblende gabbro (Figure 19a,b,c,d). These rocks outcrop along a narrow zone that is parallel to the strike of the enclosing sedimentary rocks and the Bankfield-Tombill Fault (BTF), and in several places appears to enclose the fault. Similar to the chlorite schist units at the margins of the gabbroic intrusives on the Bankfield property, these are dark green, highly foliated, schistose, rubbly-weathering outcrops (Figure 19d), interbanded with very finely laminated, highly chloritic, material (Figure 19c). At this location, however, the

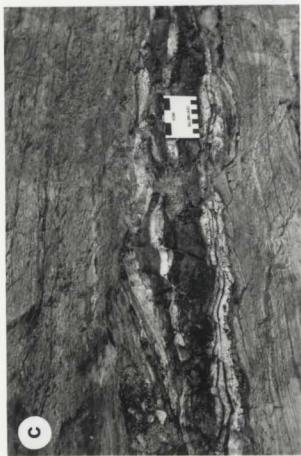
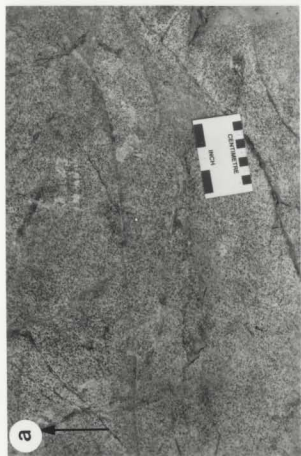
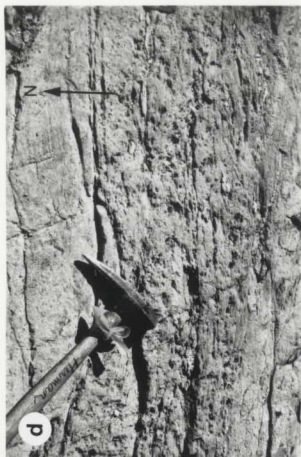
Figure 19. Photographs of hornblende gabbro and chlorite schist from the Fault Rock Outcrop.

19a. Fairly massive, coarse-grained hornblende gabbro.

19b. Slightly foliated hornblende gabbro. Narrow chloritic seams are developed parallel to foliation direction.

19c. Strongly foliated gabbro with prominent chloritic laminae and boudinaged and rotated quartz veins parallel to foliation direction.

19d. Extremely foliated, rubbly-weathering, chlorite schist zone with narrow, discontinuous, quartz lenses.



chlorite schist units are more extensive, up to several metres wide. They are not exclusively localized at contacts of different rock types but are enclosed entirely by gabbro, and locally are at gabbro-sediment contacts.

These outcrops were originally mapped by Horwood and Pye (1955) and Pye (1952) as tuff and volcanic breccia, intruded by gabbro. Pye (1952, p13-14) interpreted the rubbly-weathered outcrops to be volcanic breccia, composed of highly altered, schistose elliptical fragments. The finely banded schist that is interbanded with the "fragmentals" he interpreted to be waterlain tuffs, the banding being due to more abundant chlorite in some layers than in others. In thin sections Pye observed that the two rocks had a similar mineral assemblage; chlorite, altered plagioclase, quartz, and small amounts of sericite, carbonate and epidote; however, the "tuff" bands had constituent minerals arranged in parallel laminae, with chlorite-dominated laminae alternating with those containing dominantly quartz and feldspar.

Detailed examination of this series of outcrops indicates that these "fragmental" and "tuffaceous" units are actually gradational into the surrounding gabbro bodies which were thought, by the above authors, to be intrusive into them. It is postulated that these chlorite schist zones are not a primary rock type as suggested by Horwood and Pye (1955), but were derived from the deformation and alteration of massive hornblende gabbro.

Massive gabbro (Figure 19a) may be followed across strike into moderately foliated gabbro where the hornblende phenocrysts start to become elongated and parallel (Figure 19b). This transition continues into more foliated rock in which narrow (less than 1 cm) anastomosing chloritic "sheared" zones have developed (Figure 19c), and finally into the intensely foliated, rubbly weathering schist and the very finely laminated bands (Figure 19d). This entire transition may take place within 2 or 3 metres.

The gradational nature of these chlorite schists with massive gabbro is also documented in thin sections. The sequence from massive hornblende gabbro to chlorite schist is represented by progressive destruction of the hornblende crystals by alteration to chlorite and minor epidote, and by progressive decrease in grain size. Plagioclase is altered to epidote, carbonate and chlorite. As the rock becomes finer-grained, chlorite, carbonate and quartz become dominant, with the chlorite forming almost monomineralic dark bands. In the most schistose sections irregular streaks of dusty-brown semi-opaque material form parallel to the chlorite. In reflected light these masses are a semi-opaque bluish-grey and are probably hematite + titanium oxides, probably leucoxene, formed as an alteration of ilmenite-magnetite intergrowths. Sulphides are minor in abundance, less than 2%, and consist of pyrite and chalcopyrite.

Geochemical analysis and mass balance calculations were done to further test the hypothesis that the chlorite schist was derived directly from the hornblende gabbro (see Chapter 4). The presence of texturally and mineralogically similar-looking chlorite schists at the contacts of hornblende gabbro on the Bankfield property described above supports this hypothesis. The presence of leucoxene also indicates that they probably underwent a major hydrothermal alteration as leucoxene is not typically a primary igneous phase.

Although some of the chlorite schist, that Horwood and Pye (1955) and Pye (1952) mapped as tuff and agglomerate, was originally gabbro, on the Ashmore property there are true tuff and agglomerate units interbedded with mafic flows. Thus some of the chlorite schist along the fault zone may be volcanic material that has been deformed in a major fault, but not all the chlorite schist units along the fault in the study area can be explained as primary, intercalated, volcanic strata. This interpretation would relieve the difficulty Horwood and Pye (1955) had in explaining the relationship of these "tuff and breccia" zones to the surrounding sedimentary rocks. Many of the chlorite schist zones in the area may be fault zones. The mechanism by which these units were formed is discussed in Chapter 3 (shear zones and faults).

## 2.6 Intermediate intrusive rocks

A suite of intrusions that are petrographically and geochemically "intermediate" between the mafic and felsic intrusive rocks occur in a few outcrops within the Geraldton area. The relative age of these rocks with respect to the felsic intrusions is unknown from this study as cross-cutting relationships were not observed, but they are grouped with the mafic intrusions because of their close spatial association with these rocks.

Contacts of this rock type with the surrounding rocks are exposed only on the Ashmore property. Here the intrusion cuts across mafic volcanic rocks and a mafic gabbroic intrusion. According to Pye (1952), they are generally small bodies, either narrow sills or dykes intrusive into sedimentary rock, or larger masses spatially associated with gabbroic intrusions.

In outcrop these bodies are massive, fine to medium grained, greyish-white on the weathered surface, and darker grey with white plagioclase crystals visible on the fresh surface. In some outcrops they are porphyritic in others they are essentially equigranular. In two locations (the Roxmark and Ashmore properties) these bodies contain up to 7% arsenopyrite and a few samples contain anomalous gold values.

intrusive nature of this rock. For example, Reid (1949) suggested that the porphyry was of sedimentary origin because of: 1) its

## 2.7 Felsic intrusive rocks

Felsic porphyritic rocks outcrop along a narrow zone restricted to the group A sedimentary belt in the west, and the southern part of the volcanic belt in the east (Figures 3). This roughly linear distribution is spatially coincident with the distribution of the mines in the area, with the BTF, and to some degree also with the mafic intrusions.

The porphyry bodies in all areas crosscut all other rock types except the diabase and lamprophyre dykes. (Their relationship to the intermediate intrusions is unknown.) Underground at the MacLeod-Cockshutt Mine the porphyry truncates folded sedimentary rocks, implying some deformation prior to intrusion (Pye, 1952). Similarly, included fragments of highly foliated gabbro suggests that the latter rock type had undergone some deformation prior to and/or during intrusion of the porphyries. The porphyries themselves are intensely deformed in some places and therefore must have been emplaced prior to the end of deformation.

In most outcrops the porphyry contacts are conformable with the enclosing stratigraphy. Very few cross-cutting relationships are exposed. This led to confusion in the past as to the intrusive nature of this rock. For example, Reid (1945) suggested that the porphyry was of sedimentary origin because of; 1) its

generally conformable nature, "interbedded" with greywacke and iron formation; and, 2) its similarity in appearance to an arkosic sedimentary rock.

However, cross-cutting relationships are exposed on the Bankfield property (Figures 3, 16, 20a) and on the hydroline exposure west of Mosher Lake (Figures 3, 4 and 20 a,b). At the latter location a 30 centimetre long fragment of greywacke, with interbedded folded iron formation, is enclosed entirely within porphyry (Figure 20b). The fragment may have originated from a few 10's of centimetres away, where the porphyry is in contact with the sediments. Throughout the remainder of this outcrop area the porphyry contacts are conformable with the enclosing sedimentary rocks.

On the Bankfield property the porphyry crosscuts greywacke and lean iron formation at a high angle, with very irregular margins (Figure 20 a). Narrow felsic dykes cut the hornblende gabbro at a relatively high angle to the foliation, and a small fragment of highly foliated gabbro is included within a porphyry dyke. Commonly these contacts are the site of development of chlorite schist and also of quartz veins and some associated pyrite deposition.

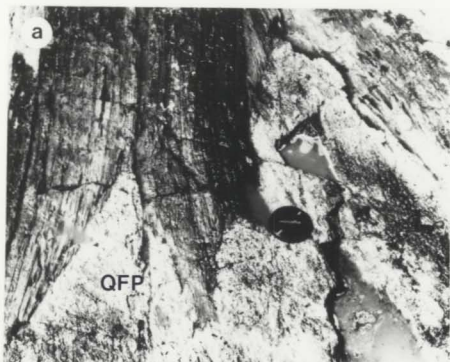
Based on field evidence and spatial distribution the felsic porphyritic rocks are divided into two distinct groups; the western porphyries and the eastern porphyries.

Figure 20. Photographs of intrusive nature of the Geraldton quartz feldspar porphyry.

20a. Quartz feldspar porphyry nose crosscuts banded oxide iron formation and greywacke at the Bankfield property. No evidence of a chilled margin was observed on the border of the porphyry.

20b. Quartz feldspar porphyry crosscuts iron formation and greywacke on the Mosher West hydroline exposure (west of Mosher Lake). Note the fragment of iron formation included within porphyry in the left centre part of the photograph.

IF



### 2.7.1 Western porphyries (WP)

The porphyries in the western area, west of Lake Kenogamis, form sheet-like intrusions which are oriented parallel to the regional foliation and orientation of the stratigraphy. The western porphyries weather a light grey to white and are commonly fine-grained. Phenocrysts of both quartz and feldspar are visible, but they are usually small and rounded, and are not conspicuous on the weathered surface. This rock is easily mistaken for a sedimentary rock, especially where a strong foliation has developed, giving it a "bedded" appearance.

The intensity of foliation varies considerably between outcrops. The grain size of these rocks is also variable. On the Bankfield property, in an outcrop just north of Highway 11, is a fairly coarse grained exposure with abundant, relatively large, quartz phenocrysts (up to 8-10 mm). In contrast, the small felsic dykes that crosscut the hornblende gabbro in outcrops to the north on the Bankfield Property are equigranular.

Weathering colour and texture are variable depending on the intensity of deformation and alteration. Where deformation has been intense a distinct foliation is developed. Most of the porphyries in the western group are moderately to extremely foliated. The more highly foliated rocks tend to assume a greenish colour, due to an increase in white mica.

They commonly show undulose extinction and development of pressure shadows, evidence of their having been strained.

The western porphyries contain variable proportions of quartz and albite phenocrysts (Figure 21a,b,c,d). Phenocryst size may vary from 2 to 8 mm in diameter, with an average of 3.5mm, and they may comprise anywhere from 15 to 50 % of the rock. The albite phenocrysts are nearly pure albite ( $Ab_{96-100}$ ) (Table 3), and are very homogeneous in composition. Many of the plagioclase phenocrysts are twinned, but none show any evidence of zonation. The quartz phenocrysts often have corroded margins.

The matrix is fine crystalline material composed of quartz and plagioclase and is homogeneous. Two small K-feldspar grains were analysed during probe analysis of the phenocrysts, but they were very small and very rare. Samples of all the porphyries were stained for K-feldspar and only the granitic stock to the east, the Croll Lake Stock, gave a positive indication of K-feldspar.

All of the WP show evidence of alteration. A variable amount of sericite and carbonate alteration of both phenocrysts and groundmass is present. In some samples up to 85% of the rock consists of carbonate and sericite. Bands of sericite impart a foliation to many of these rocks. In many samples the fabric penetrates the albite phenocrysts. There is no foliation developed in the quartz phenocrysts but they commonly show undulose extinction and development of pressure shadows, evidence of their having been strained.

Figure 21. Photomicrographs of western felsic porphyritic intrusive rocks. All photographs were taken in transmitted light under crossed nicols. Black lines on photos b, and d are ink outline guides for microprobe analysis. The scale bar is 1 mm. The photographs were all taken at the same scale.

21a. Twinned albite phenocrysts in fine-grained quartz-plagioclase-sericite-carbonate matrix. Sample from the Bankfield property.

21b. Twinned and untwinned albite phenocrysts in fine-grained, moderately foliated matrix. Sample from the Mosher East area.

21c. Quartz and albite phenocrysts in altered, moderately foliated, fine-grained matrix of quartz, plagioclase, carbonate and sericite, and minor pyrite. The section is cut by a small quartz veinlet which has been slightly deformed. The sample is from the Porphyry Hill outcrop.

21d. Highly altered and foliated porphyry. Pyrite and arsenopyrite are abundant in this rock. This sample is also from the Porphyry Hill outcrop.

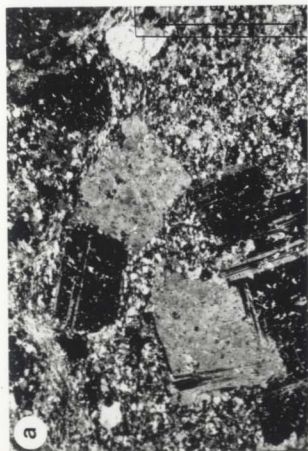


Table 3. Electron microprobe analyses of western quartz-feldspar porphyries.

Sample N +	PLAGIOCLASE						
	011 8 phenos	011 3 (a)	214 8 phenos	214 4 matrix	220 5 phenos	220 1 (a)	220 3 matrix
wt %							
SiO <sub>2</sub>	67.40	64.96	67.52	67.34	68.34	63.37	68.37
Al <sub>2</sub> O <sub>3</sub>	20.30	18.96	20.12	20.07	20.06	18.89	19.69
FeO	0.11	0.09	0.05	0.11	0.05	0.00	0.03
CaO	0.15	0.07	0.33	0.24	0.31	0.20	0.16
Na <sub>2</sub> O	11.60	0.34	11.54	11.32	11.42	0.00	11.31
K <sub>2</sub> O	0.49	15.97	0.14	0.30	0.12	15.80	0.51
TOTAL	100.05	100.39	99.69	99.37	100.3	98.26	100.7
WT % PROPORTIONS							
AN	0.7	0.4	1.6	1.2	1.5	1.0	0.8
AB	98.1	2.9	97.7	95.7	96.7	0.0	95.7
OR	2.9	94.4	0.8	1.8	0.7	93.4	3.0
TOTAL	101.8	97.7	100.1	98.7	98.9	94.4	99.5

a = one small grain analysed.

Sample N +	SERICITE			CHLORITE	CARBONATE	
	011 3	214 6	220 4	011 5	214 6	220 2
wt %						
SiO <sub>2</sub>	46.02	47.63	49.52	25.97	0.01	0.01
TiO <sub>2</sub>	0.36	0.45	0.41	0.13	0.00	0.00
Al <sub>2</sub> O <sub>3</sub>	34.50	35.46	28.82	19.09	0.00	0.00
Cr <sub>2</sub> O <sub>3</sub>	0.01	0.03	0.01	0.06	0.00	0.00
FeO	4.06	1.77	5.42	31.42	14.95	0.22
MnO	0.01	0.02	0.02	0.02	0.23	0.11
MgO	2.04	1.39	3.02	11.63	13.88	0.61
CaO	0.02	0.22	0.01	0.06	27.03	54.90
Na <sub>2</sub> O	0.75	1.00	0.15	0.00	0.00	0.00
K <sub>2</sub> O	7.35	7.49	8.05	0.06	0.00	0.00
TOTAL	95.13	95.45	95.43	88.44	56.11	55.84
PROPORTIONS						
Fe	52.63	60.16	50.15	60.16	20.12	0.31
Mg	47.10	39.69	49.70	39.69	33.28	1.51
Ca	0.28	0.16	0.15	0.16	46.60	98.19
FM Ratio	0.53	0.60	0.50	0.60	0.37	0.16

(Values reported are averages of N number of analyses.)

Electron microprobe analyses of carbonate composition in two samples are given in Table 3. In one sample the carbonate was almost pure calcite, while in the other it was ankerite. The variation in carbonate species with rock type or degree of alteration was not studied in detail but is an important area for further study of these rocks. The ferromagnesian mineral in these rocks consists of a minor amount of chlorite (and epidote). Electron microprobe data on chlorite in one sample indicates that it is iron-rich (Table 3). No biotite or hornblende was observed in these rocks.

2.7.2 Eastern porphyries (EP)

The porphyries to the east of Lake Kenogamisis intrude sedimentary and volcanic rocks and massive gabbro (Figure 2). The contacts of the porphyry here are more irregular than where they intrude sedimentary rocks in the west. On the Roche Long Lac property to the east their strike varies from N70W to N80E (Horwood and Pye, 1955 p97).

The eastern porphyries are darker grey in colour on the fresh and weathered surface than the western porphyries. Phenocrysts are an off-white colour and consist entirely of plagioclase. The groundmass of these rocks contains more ferromagnesian minerals than the western porphyries. At Wods-Mac the ferromagnesian

mineral is dominantly chlorite, while at Roche Long Lac it is biotite.

The EP consist of large (5-8 mm) plagioclase phenocrysts that make up 20-40% of the rock (Figure 22a,b,c,d,) set in a fine-grained groundmass. The phenocrysts are both twinned and untwinned, and zoned and unzoned. The zoning is oscillatory, and compositions vary from approx  $Ab_{66}$  to  $Ab_{75}$ . Electron microprobe results on phenocryst and matrix compositions are given in Table 4. The phenocrysts are generally very angular, retaining their primary igneous texture, but they are variably altered to sericite and minor carbonate. The carbonate composition of one sample is Ca-Mg rich ankerite. The groundmass, which makes up approximately 50-60% of the rock, is composed of fine grained quartz and plagioclase, with minor sericite and carbonate. Chlorite and biotite make up approximately 10% of the groundmass and are coarser grained than the other groundmass constituents.

Alteration of these samples appears to be weak to moderate. They are only weakly foliated, and thus do not seem to have undergone nearly as much deformation or alteration as those porphyries to the west.

### 2.7.3 Interpretation of the origin of the two porphyry groups

These two groups may represent a fractionation trend from more ferromagnesian in the east to more siliceous in

Figure 22. Photomicrographs of eastern felsic porphyritic intrusive rocks. Black lines are ink guides for microprobe analyses. The scale bar is 1 mm. All photographs were taken at the same scale.

22a. Twinned and zoned An<sub>30</sub> plagioclase phenocrysts in fine-grained plagioclase-quartz-chlorite matrix. The zoning is oscillatory. The plagioclase is altering slightly to sericite and minor carbonate. This sample is from the Wods-Mac Porphyry. The photograph was taken under transmitted, plane light.

22b. Photograph of the same section as 22a, taken under polarized light.

22c. Twinned and zoned phenocrysts of An<sub>30</sub> composition in a fine-grained matrix of quartz-plagioclase-biotite. This sample is only weakly altered, with some sericite forming at the expense of the plagioclase. This sample is from the Roche Long Lac property. The photograph was taken under transmitted, plane light.

22d. Photograph of the same section as 22c, taken under polarized light.

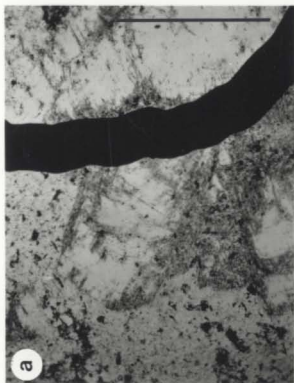


Table 4. Electron microprobe analyses of eastern quartz-feldspar porphyries.

Sample No. N #	PLAGIOCLASE							
	207 5	207 5	207 8	209 9	209 7	209 8	209 4	209 4
	1 pheno osc. zon.	same grain	1 pheno osc. zon.	2 phenos osc. zon.	2 phenos osc. zon.	1 pheno osc. zon.	1 pheno osc. zon.	matrix
wt %								
SiO <sub>2</sub>	60.61	60.02	58.03	61.09	60.83	59.89	59.47	64.93
Al <sub>2</sub> O <sub>3</sub>	25.08	25.38	26.42	24.67	24.67	25.49	25.44	21.97
FeO	0.16	0.10	0.10	0.18	0.16	0.14	0.10	0.18
CaO	5.84	6.15	7.37	5.56	5.57	6.38	6.29	2.78
Na <sub>2</sub> O	8.55	8.35	7.43	8.46	8.50	8.02	7.92	9.66
K <sub>2</sub> O	0.14	0.11	0.12	0.19	0.15	0.12	0.11	0.60
TOTAL	100.37	100.11	99.47	100.16	99.88	100.04	99.32	100.12
WT % PROPORTIONS								
AN	29.0	30.5	36.5	27.6	27.6	31.6	31.2	13.8
AB	72.3	70.6	62.9	71.6	71.9	67.9	67.0	81.7
OR	0.8	0.7	0.7	1.1	0.9	0.7	0.6	3.5
TOTAL	102.1	101.8	100.1	100.3	100.4	100.2	98.8	99.0
Sample N #	BIOTITE				CHLORITE			
	207 5			209 5				
wt %								
SiO <sub>2</sub>	37.84			26.72				
TiO <sub>2</sub>	1.95			0.11				
Al <sub>2</sub> O <sub>3</sub>	16.78			20.73				
Cr <sub>2</sub> O <sub>3</sub>	0.02			0.07				
FeO	18.81			23.94				
MnO	0.16			0.21				
MgO	12.33			17.51				
CaO	0.00			0.10				
Na <sub>2</sub> O	0.00			0.00				
K <sub>2</sub> O	9.15			0.03				
TOTAL	97.04			89.46				
PROPORTIONS								
Fe	46.12			43.30				
Mg	53.88			56.46				
Ca	0.00			0.24				
FM Ratio	0.46			0.43				

(Values reported are averages of N number of analyses.)

the west, or the western porphyry may represent an alteration of the eastern porphyry, or both of the above; or they may be two entirely unrelated rocks.

The outcrop appearance and relative timing of the two porphyry groups are similar. Both porphyries are cut by quartz veins which carry gold. However, the western porphyries have a lower ferromagnesian component than the eastern porphyries, and contain phenocrysts of both quartz and albite, whereas the eastern porphyries have only feldspar phenocrysts of oligoclase composition. This suggests that either a fractionation trend exists between the two rock types, or they have been derived from two different sources.

On the other hand, the western porphyry have variable amounts of sericite-carbonate alteration. In addition the feldspar phenocrysts in the WP are homogeneous in composition (which can not be a primary igneous composition), while those in the EP have oscillatory zoning from An 25 to An 33, suggesting that the western porphyries are more altered rocks than the eastern porphyries (Figure 23). The relationships will be explored further through examination of the chemical composition of these rocks (Chapter 4).

Probe results on feldspar phenocryst composition of sample 209 (Eastern Porphyry)  
and sample 214 (Western Porphyry)

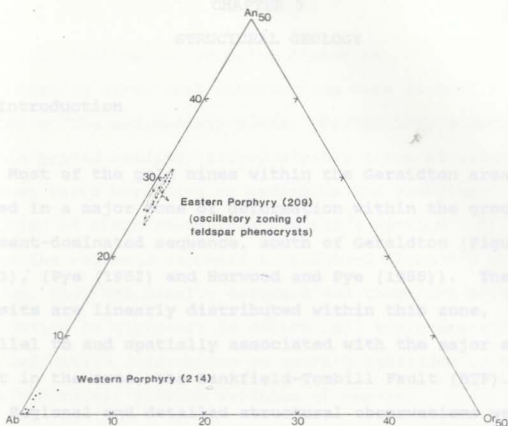


Figure 23. Ternary Ab-An-Or plot of electron microprobe analyses of plagioclase phenocrysts in Eastern and Western felsic porphyritic intrusions.

## CHAPTER 3

## STRUCTURAL GEOLOGY

## 3.0 Introduction

Most of the gold mines within the Geraldton area were hosted in a major zone of deformation within the group A, sediment-dominated sequence, south of Geraldton (Figures 2 and 3), (Pye (1952) and Horwood and Pye (1955)). The deposits are linearly distributed within this zone, parallel to and spatially associated with the major strike fault in the area, the Bankfield-Tombill Fault (BTF).

Regional and detailed structural observations were made to 1) describe the structural style in the Geraldton area, 2) to determine the relative timing of structural events and emplacement of quartz veins (gold) and, 3) the degree to which structural conditions controlled the emplacement of the gold. These observations were made in part through detailed mapping of selected areas, usually near gold mineralization, and also by detailed examination of selected outcrops along Highway 11 and other properties west of the main study area.

### 3.1 Structural observations in the Geraldton area

#### Structural Setting

#### 3.1.1 Bedding and younging direction

Detailed structural observations were generally limited to the sedimentary rocks. Sedimentary structures such as graded bedding, rip-up clasts, flame structures and load casts were used to determine the younging direction of these rocks (see Chapter 2 section 2.2). Within the volcanic succession, pillowed flows are common, however, they are usually deformed and therefore primary orientation is difficult to determine. Agglomerate beds give definitive information on bedding attitudes in these rocks but rarely provide evidence of way-up.

Bedding,  $S_0$ , is well preserved in the sedimentary succession, particularly in the southern and western parts of the Beardmore -Geraldton belt where deformation is not extreme. Toward the Quetico belt to the south, primary bedding surfaces become progressively subordinate to a schistosity, into which bedding appears to be transposed (Kehlenbeck, 1984).

Where observed, bedding in the Geraldton area consistently dips steeply to vertically and strikes approximately east to east-southeast. Within much of the thesis area, particularly in the group A sedimentary rocks, deformation has largely obliterated any sedimentary structures, so younging directions were only determined in secondary examination appears to be bedding, but upon closer

a few localities (Figure 3). (See section 3.2.3 Structural facing).

### 3.1.2 Cleavage

Two cleavages are developed in the rocks in the Geraldton area. An earlier, penetrative cleavage,  $S_1$ , is ubiquitous throughout all the Archean age rocks in the Beardmore-Geraldton belt. The orientation of the dominant cleavage is  $260-270^\circ$ , and is commonly co-planar with the axial surfaces of folds (Figure 24a,b), but is also observed to transect folds (Figure 24c).

The cleavage is defined by the parallel alignment of mica and chlorite, and the flattening of grains, fragments and crystals within the various rock types. Refraction of cleavage is commonly observed in graded beds where ductility differs from the coarse to the fine grained portions of the beds (Figure 24d). The coarser-grained sedimentary layers tend to develop a spaced cleavage, but finer, more chloritic layers tend to develop a penetrative cleavage.

In most outcrops the cleavage is close to, or, bedding-parallel. which, as deformation increases, makes it difficult to determine original bedding. A characteristic feature of the deformation in the Geraldton area is the transposition and disruption of sedimentary layering, giving rise to a "stripey" cleavage which upon cursory examination appears to be bedding, but upon closer

Figure 24. Photographs of cleavage in sedimentary rocks.

24a. Cleavage oriented  $260-270^{\circ}$ , axial planar to the mesoscopic fold. Grant's Camp outcrops.

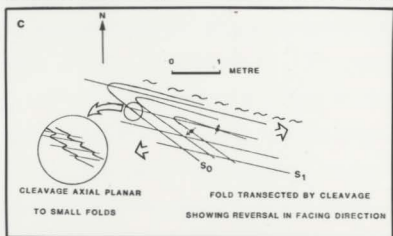
24b. Photomicrograph of sample FRA063 (scale bar is 1 mm). Isoclinal fold in greywacke-siltstone unit with thin magnetite bands.

24c. Sketch map of greywacke outcrop on the north side of Highway 11, approximately 1 km east of Jellicoe, illustrating cleavage crosscutting earlier isoclinal fold.

24d. Cleavage refraction in thin, graded, greywacke-siltstone beds with small pressure solution, or displacements along, cleavage, at Grant's Camp outcrops.

24e. Two cleavages in greywacke from the Mosher West hydroline exposure. The earlier cleavage, which is approximately horizontal in the photo, is kinked by a later cleavage which makes an angle of approximately  $75^{\circ}$  with the earlier one.

24e,f. Highly deformed sedimentary rocks at the Roxmark property. What appears to be bedding is actually transposed lenses of coarser-grained (lighter-coloured) material in highly deformed (darker) silty matrix, which is equivalent to the  $S_1$  cleavage. The  $S_2$  cleavage is axial planar to the minor kink/chevron folds. Note the Z-asymmetry of these later folds.



examination reveals elongate, narrow lenses of coarser-grained sedimentary material within a matrix of intensely deformed finer-grained sedimentary material (Figures 24 f,g). Note the slight transposition of layering along cleavage in Figure 24 d. This process taken to an extreme could produce the features observed in Figures 24 f and g.

Another common feature of the deformation in the Geraldton area is its inhomogeneity with well-preserved sedimentary packages juxtaposed against strongly disrupted packages. This inhomogeneity of deformation is also observed within originally homogeneous rocks such as gabbroic intrusions (see section 3.2.5 Shear zones).

In zones of intense deformation, particularly along the Bankfield-Tombill Fault Zone, a second cleavage,  $S_2$ , is developed which overprints the earlier cleavage and is consistent with the axial planar orientation of minor asymmetric folds (see Section 3.2.4.1) and small kink folds (Figure 24 e,f,g). In one outcrop, a small dyke (less than a few cm wide) of porphyry intrusion was observed which contained an earlier cleavage and was folded by an asymmetric fold consistent with the second cleavage. This places intrusion of the porphyry as prior to much of the tectonic deformation.

No evidence of stretching lineations was observed in outcrops in the Geraldton area. In the conglomerates the pebbles are flattened in the plane of the cleavage, and do

not show evidence of greater stretching in one direction than another within this plane.

### 3.1.3 Structural facing

Bedding, cleavage and younging relationships were used to determine the structural facing of the stratigraphic sequence. Structural facing is defined as the younging direction of strata at the hinge of a fold (Cummins and Shackleton, 1955;). Borradaile (1976) showed that the structural facing of a fold can be determined at any point on a folded surface by projecting the younging direction at that point onto the axial planar cleavage. This observation can be very useful in polydeformed terrains (Poulsen, et al, 1980) as the structural facing of later folds may be obtained by projecting local younging directions onto their accompanying axial planar cleavage. Reversals in the structural facing may indicate areas where the strata was affected by an earlier deformational event (Kehlenbeck, 1985).

Structural facing measurements were made locally along the Beardmore-Geraldton belt. Opposing facing directions are developed at several locations within the sedimentary sequences of the belt (Figure 25). Within the group A sedimentary rocks in the Geraldton area a consistent westward structural facing was observed in outcrops north of the Bankfield-Tombill Fault (BTF)

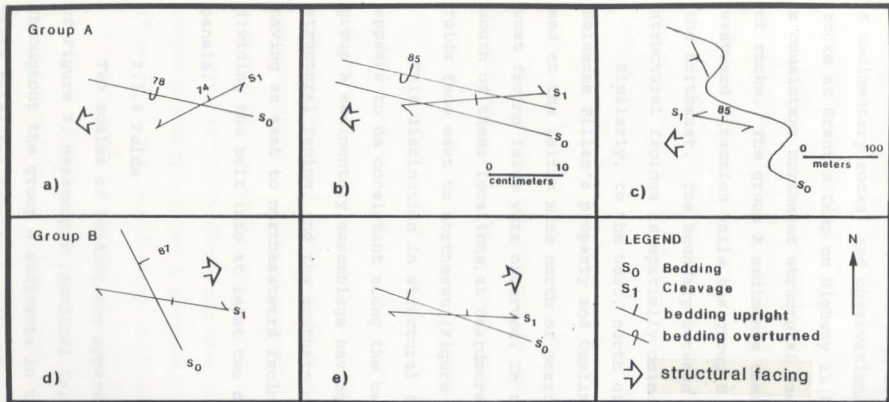


Figure 25. Sketch illustration of bedding-cleavage-structural facing relationships from selected localities along the Beardmore-Geraldton Belt; a) Leitch Mine, b) Oxaline Lake, c) Little Long Lac Mine, d) Highway 11 outcrops at Jellicoe, and e) Grant's Camp outcrops.

(Figure 25c). Horwood and Pye's observations on the group B sedimentary rocks, and observations on the sedimentary rocks at Grant's Camp on Highway 11 (Figure 25e), document a consistent northeast structural facing for this package of rocks. The group A sediments therefore young in a westward direction while the group B sediments young to the northeast. The boundary between these two differing structural facings is spatially coincident with the BTF.

Similarly, to the west, north of Jellicoe at the Solomons Pillar's property and Oxaline Lake (Figure 25b), and at the Leitch mine north of Beardmore (Figure 25a), west facing folds were observed. In the greywacke to the south of these locations at Beardmore and Jellicoe, the folds face east to northeast (Figure 25d).

This distinction in structural facing direction appears to be consistent along the belt, with the northern group A sedimentary assemblage having a westward structural facing, and the southern group B assemblage having an east to northeastward facing direction, thus dividing the belt into at least two discrete structural panels.

#### 3.1.4 Folds

Two scales of folding are apparent from examination of Figure 3. Mesoscopic isoclinal folds are developed throughout the group A sediments in the Geraldton area. These folds are isoclinal, with hinge axes parallel to the

regional strike of the stratigraphy. At Geraldton the hinge spacing of these folds is on the order of hundreds of metres (Figure 3).

Within the group A package north of the BTF and in lithologies immediately south of the fault, minor folds are extensively developed. Some of these folds are consistent with the mesoscopic isoclinal folds, but they are dominated by z-asymmetry which is in places inconsistent with the larger-scale fold structures.

#### 3.1.4.1 Description of minor folds

Minor folds are extensively developed within the sedimentary and volcanic rocks immediately adjacent to the Bankfield-Tombill Fault in the Geraldton area. They are well-developed in the heterogeneous assemblage of rock types to the north of the BTF, especially in finely laminated layered rocks such as oxide iron formation, and finely interbedded sandy and silty greywacke. These folds are dominantly of Z-shaped asymmetry, with a gentle westward plunge, which varies from 30-60°.

Many of the folds in the Geraldton area strongly resemble Ramsay's Class 2 geometry of similar folds (Figures 26 and 27a) in that they tend to be thickened in the hinge zone and thinned on the limbs, and the shape of the folds is repeated from one layer to the next. Similar folds are defined by Ramsay (1967) as having parallel dip isogons, i.e. "the changes of curvature of the surfaces of

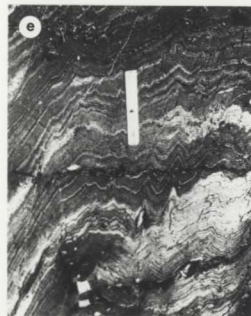
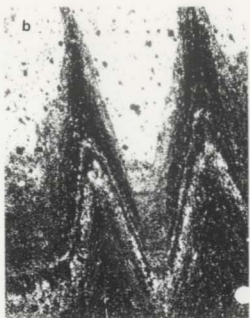
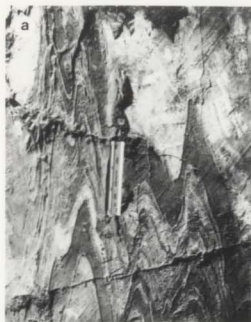
Figure 26. Photographs of folds.

26a. Similar-looking folds in thinly laminated greywacke-siltstone-magnetite iron formation at the Roxmark property. Note the thinning of the limbs and the thickening of the hinge zones of the folds.

26b. Photomicrograph of sample FRA045 from the west trench on the island in Barton Bay. The photo is approximately 2 mm wide.

26c, e, f. Iron formation exposed northwest of the Roxmark trenches. Similar-looking folds with neutral to Z-asymmetry.

26d. Closeup of area in 24c. These folds show evidence of two cleavages. An earlier "stripey" cleavage (especially noticeable in the darker silty layers) is folded by the asymmetric minor folds. The very dark layer at the top of the photo is magnetite.



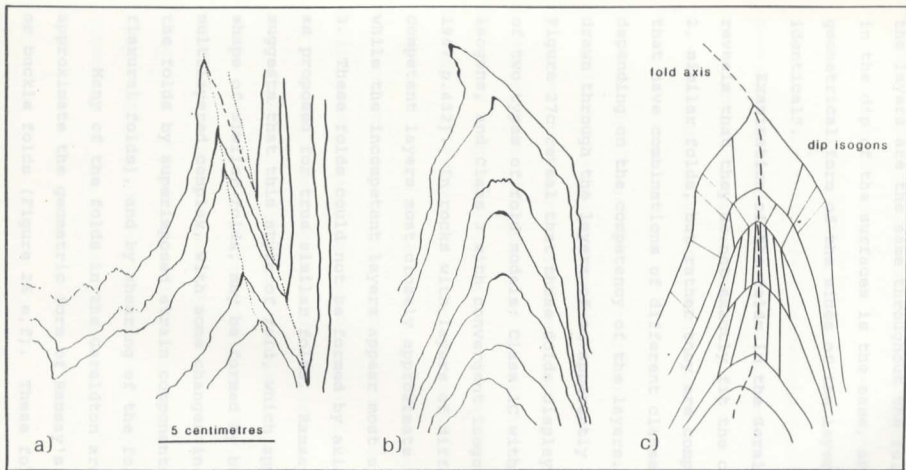


Figure 27. Tracings of folds from hand samples of banded oxide iron formation. a) Hard Rock property. Note the slight offset of some layers along narrow zones parallel to the axial plane of the folds. The plane of this section is at  $30^{\circ}$  to the plunge of the folds. b) MacLeod-Cockshutt property. The plane of this section is perpendicular to the plunge of the fold. c) Idealized fold tracing based on (b). Dip isogons (Ramsay, 1967) are sketched for compound packages of magnetite-hematite-siltstone-chert layers. The scatter of the isogons broadly represents the behaviour of the layers on a millimetre scale.

the layers are the same throughout the fold, the variation in the dip of the surfaces is the same, and the geometrical form of the sides of the layers are identical".

Examination of the folds in the Geraldton area reveals that they do not exactly fit the criteria of Class 2, similar folds, but rather they are composed of folds that have combinations of different classes of folds, depending on the competency of the layers. Dip isogons drawn through the layers of an apparently similar fold in Figure 27c reveal that these folds display a combination of two types of fold models; Class 1C with divergent dip isogons, and Class 3 with convergent isogons (see Ramsay, 1967 p.432). In rocks with layers of differing ductility, competent layers most closely approximate the Class 1C while the incompetent layers appear most similar to Class 3. These folds could not be formed by axial-surface flow as proposed for true similar folds. Ramsay (1967) suggests that this style of fold, which approximates the shape of similar folds, may be formed by buckling a multilayered complex, with some changes in the shapes of the folds by superimposed strain components (flattened flexural folds), and by shearing of the fold limbs.

Many of the folds in the Geraldton area more closely approximate the geometric form of Ramsay's Class 1B folds or buckle folds (Figure 26 e,f). These folds are formed by a compressive stress acting along the length of the

layers. In rocks with strong competency contrasts, the more competent layers tend to buckle, while the less competent layers take a different form. Many fold shapes were observed that were intermediate between buckle and similar-looking folds, suggesting that the similar-looking folds in the Geraldton area may have been formed by a progressive flattening of what were initially buckle folds.

A significant feature of the folds in the Geraldton area is the development of distinct shear discontinuities parallel to the axial surfaces of the folds. Slip along these surfaces is common and may displace fold hinges very slightly (Figure 27a, 28a,b) or in extreme cases, bedding is entirely transposed along cleavage, juxtaposing unrelated layers (Figure 24 f,g). These shear discontinuities occur at both thin section and outcrop scale, and probably on a much larger scale. Thus bedding on a local scale cannot be used to determine stratigraphy.

In addition to the asymmetric z-folds there are folds which appear to be refolded (Figure 28 c,d). These folds approximate the shape of Type 3 interference patterns as described by Ramsay (1967), where the axis of the later folds coincide, or nearly coincide, with the axial direction of the earlier folds.

Figure 28. Photographs of shear discontinuities in folds.

28a,b. Highly contorted sedimentary material at the north end of the Roxmark trenches. Folds have been disrupted and dislocated along narrow zones approximately parallel to cleavage.

28c,d. Highly folded magnetite laminae in greywacke at the Mosher East hydroline exposure. These folds resemble Ramsay's (1967) Class 3 refolded folds, in which both fold axes are parallel, suggesting at least two periods of deformation in a similar stress field.



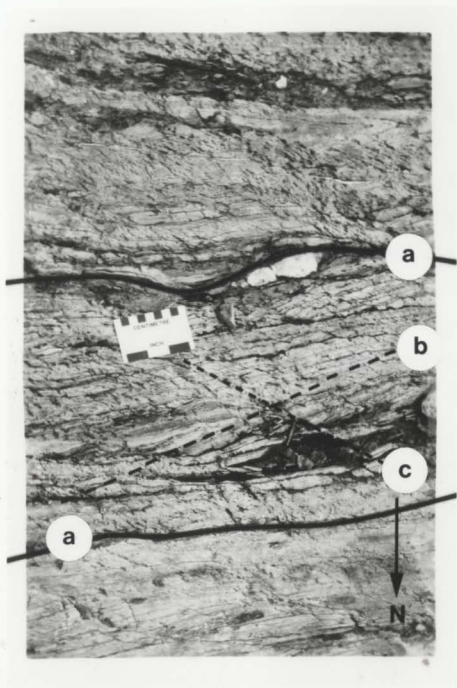
### 3.1.5 Shear zones and faults

A common feature of the deformation in the Geraldton area is its inhomogeneity. Well-preserved packages of rock are often juxtaposed against strongly disrupted and transposed lithologies. Discrete shear zones are present in many outcrops within the Geraldton area. They are most easily recognized at the contacts of differing rock types where the less competent lithology has been extensively deformed, and as chlorite schist within relatively massive hornblende gabbro intrusive rocks. The change from relatively massive, undeformed gabbro, through to shear zones of chlorite and quartz schist is accomplished by the progressive development of a penetrative foliation and reduction in grain size and alignment of minerals, (especially obvious in the flattening and destruction of hornblende crystals). (Figure 19 a,b,c,and d, Chapter 2).

#### 3.1.5.1 Fabrics within the shear zones

Within the chlorite schist zones, three distinct foliations are recognized; 1) The first are represented by through-going chloritic seams, labelled (a) in Figure 29. This fabric is subvertical and is consistent in orientation throughout the outcrop, striking  $270^{\circ}$  to  $280^{\circ}$ ; 2) Oblique to the (a) surfaces is another subvertical foliation, labelled (b). These surfaces define the plane of preferred mineral orientation and correspond to a schistosity, and strike approximately  $260^{\circ}$ ; and 3) A

Figure 29. Fabrics in chlorite schist shear zones. Three main fabrics are observed within the chlorite schist shear zones. Those labelled "a" are subvertical, through-going chloritic seams, consistent in orientation throughout the outcrop, striking  $270$  to  $280^{\circ}$ . The fabrics labelled "b" are also subvertical and are oriented obliquely to the "a" surfaces. These surfaces are defined by the preferred mineral orientation, and therefore correspond to a schistosity, and strike approximately  $260^{\circ}$ . The "c" surfaces make an angle of approximately  $30$  to  $40^{\circ}$  to the "b" planes. The photograph was taken at the Fault Rock Outcrop on Highway 11 (see Figure 3).



third foliation is sometimes present which makes an angle of approximately  $30^{\circ}$  to the (b) planes, striking  $130^{\circ}$  to  $140^{\circ}$ , labelled (c).

In other places, as on the property of Boxer Mines Ltd. (see 3.1.5.2 Faults on property), the fault zone

The Bankfield-Tombill Fault is the largest and best-defined strike fault in the area. It has been traced by diamond drill holes and outcrops from the property of Tombill Gold Mines in Lindsley Tp (just west of the Bankfield Property) eastward through outcrops of chlorite schist material south of Mosher Lake, to a strongly sheared and brecciated zone in mafic rocks south of the Hard Rock Mine, a distance of over 10 km (Pye, 1952; Horwood and Pye, 1955) (Figure 3). In addition, outcrops of extremely sheared volcanic material were observed by this author on the Ashmore Property further to the east along strike from the Hard rock property and it is postulated here that this zone represents the further continuation of the fault zone.

The zone strikes  $100-110^{\circ}$  and dips steeply south at  $60-70^{\circ}$  for its entire length. The width and nature of the fault zone is very variable and seems at least partly to be determined by the type of rock the fault is transgressing. In some places, where the fault zone intersects massive hornblende gabbro, it consists of discrete zones of ductile shear up to 3 metres in width within relatively undeformed gabbro (described above).

These zones contain quartz veins, which are boudinaged and rotated. Carbonatization of the matrix is another feature of these zones.

In other places, as on the property of Roxmark Mines Ltd (formerly the McLellan property), the fault zone intersects a dominantly sedimentary succession (Figure 30). Here the fault itself is represented by a "fault gouge" of brecciated fragments in a clay-rich mud, which is surrounded by a zone up to 60 metres wide of highly silicified and carbonatized material with small amounts of chalcopyrite and pyrite. As the actual fault plane is approached the rock becomes increasingly fragmented and shows evidence of multiple brecciation. The "gouge" material may be up to ten centimetres in width. On either side of the fault the rocks are intensely deformed. To the south of the fault outcrops of chlorite schist are intensely stockworked with narrow quartz veinlets. To the north of the fault, outcrops of medium to fine grained greywacke and siltstone are intensely cleaved and fractured. Further to the north in the sedimentary rocks the penetrative cleavage and fracturing gives way to intense asymmetric folding (Figures 26a,c,d,e,f and 28a,b).

Numerous small east-west faults and shear zones occur within the area. Outcrops of highly schistose material are commonly observed at the contacts between rocks of differing ductilities. This indicates that within the

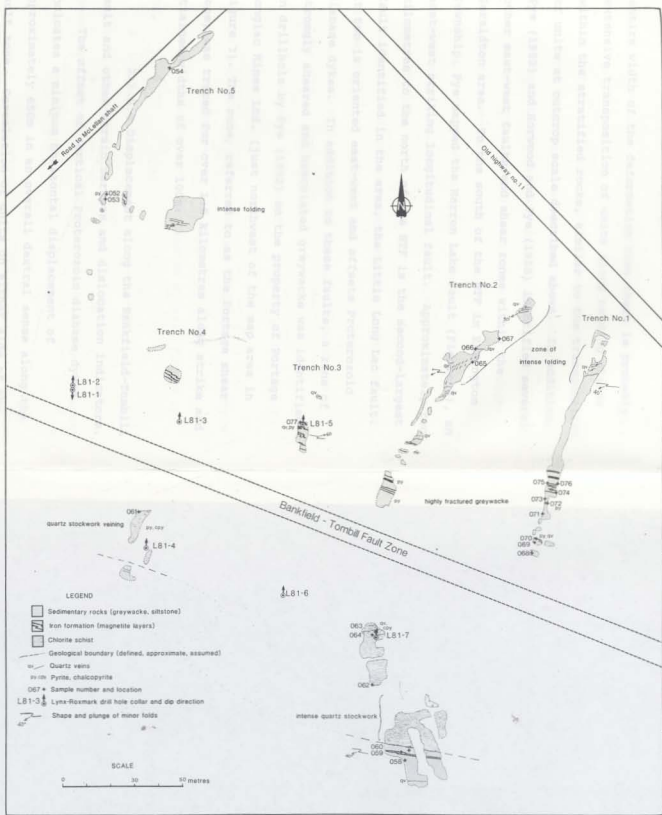


Figure 30. Geologic map of the Roxmark (McLellan) Property. The location of the Bankfield-Tombill Fault Zone is inferred from diamond drill hole information and outlined by dashed lines.

entire width of the deformation zone there is probably extensive transposition of units along bedding planes within the stratified rocks, similar to the transposition of units at outcrop scale described above. In addition, Pye (1952) and Horwood and Pye (1955) identified several other east-west faults and shear zones within the Geraldton area. To the south of the BTF in Errington Township Pye mapped the Marron Lake Fault (Figure 3), an east-west striking longitudinal fault. Approximately two kilometres to the north of the BTF is the second-largest fault identified in the area, the Little Long Lac fault. It too is oriented east-west and offsets Proterozoic diabase dykes. In addition to these faults, a zone of strongly sheared and brecciated greywacke was identified in drillhole by Pye (1952) on the property of Portage Longlac Mines Ltd. (just northwest of the map area in Figure 3). The zone, referred to as the Portage shear zone, was traced for over 1.5 kilometres along strike and attained widths of over 100m.

#### 3.1.5.3 Displacement along the Bankfield-Tombill Fault and other strain markers and dislocation indicators.

The offset of vertical Proterozoic diabase dykes indicates a minimum horizontal displacement of approximately 650m in an overall dextral sense along the fault zone. Correlation of units on either side of the fault other than these dykes is very difficult due to the

subparallel orientation of the fault and lithological boundaries. Because of this, it is very difficult to determine the sense and amount of displacement along the fault. For this reason, a combination of strain markers and dislocative features were documented to determine sense of movement along the fault zone. Most of these features if taken alone would be suspect as indicators, but the fact that they all give a consistent sense of movement suggests that they are reliable. The features observed include:

1. fractured and transposed pebbles in conglomerate, (Figure 31a);

2. offset of layers along brittle fractures, and cleavage (Figure 28a,b);

3. shear bands and foliation fish in gabbro (Figure 31b);

4. sense of asymmetric folds - predominantly Z-style asymmetry (Figures 26, 28 and 31c);

5. offset of Proterozoic diabase dykes, (Figure 3);

and,

6. boudinage and rotation of quartz veins and other competent layers, (Figure 31d);

These strain markers all indicate a dextral sense of shear movement.

Figure 31. Photographs of structural dislocation features.

31a. A fractured and offset pebble in conglomerate south of the Roxmark Property. The offset of the pebble fragment is in a dextral sense. Photograph was taken looking south.

31b. "Foliation" fish" in sheared gabbro at the Fault Rock Outcrop on Highway 11. These features are described by Hanmer (1984) as asymmetric pull-apart features. They occur as elliptical packets whose internal foliation is oblique to the general foliation of the enveloping rocks. The internal foliation of these features commonly undergo back rotation during shearing thus indicating a dextral sense of shear in this case. (See Hanmer, 1984, Figures 15.8 E and F, p.140).

31c. Z-asymmetry of minor folds indicates a dextral sense of displacement of the limbs of the folds.

31d. Z-asymmetry of folding, boudinage and offset of quartz veinlet crosscutting finely laminated (stripey cleavage) sedimentary material.



#### 3.1.5.4 Timing of faulting

Faulting must at least in part follow folding because the fault zone itself is not folded. Proterozoic diabase dykes have been offset along the fault, and all of the lithologies have been cut by the fault, therefore it is at least partly syn- to post-Proterozoic in age (Figure 3). However, the strong spatial coincidence between the fault zone and rocks of intrusive origin (Figure 3) suggests that the fault, or some related structural break, may have served as a locus for emplacement of late Archean magmas. The fault may be a long-lived feature. Note on Figure 3 the very close spatial association between the fault zone and the long narrow conglomerate horizons. Throughout the Beardmore-Geraldton belt these conglomerate horizons are commonly found in association with faulted contacts (Chapter 1). This may indicate a long-lived instability along this zone that was active at the time of sedimentation (Figure 3).

#### 3.1.6 Timing of quartz veining

Veins may be hosted in a variety of settings. No underground exposures were available in this study, but surface exposures clearly reveal the timing and setting of quartz veins.

At the Bankfield property veins are hosted in sheared rock at the contact of quartz feldspar porphyry dykes with hornblende gabbro and with sediments; and quartz

stringers, with associated disseminated pyrite, cut massive sheared quartz feldspar porphyry, (see Figure 16, map of Bankfield property, and Figure 32a,b).

At the Roxmark property (see Figure 30, map of the Roxmark property) different styles of veining include; (a) contorted veins in highly folded and sheared sedimentary rocks north of the BTF (Figure 32c); (b) stockwork veining in the fault zone with later, open space filling quartz, associated with chalcopyrite; (c) veins in fractures cross-cutting small folds, parallel to the axial planar cleavage of the small folds; and, (d) veins occupying cleavage in sedimentary rocks.

On Mosher property, west of Mosher Lake, veins are hosted in very sheared sedimentary rock; (a) parallel to the latest cleavage; (b) at a high angle to this later cleavage, occupying an earlier, folded, cleavage (Figure 32d); and deformed veinlets with tourmaline are hosted in very sheared quartz feldspar porphyry.

On the Hard Rock property, at the open stope exposure, veins occur; (a) as parallel sets of veins occupying fractures parallel to both earlier and later cleavage (Figure 33a); (b) along very sheared and brecciated contacts of iron formation and intrusive rock or sedimentary rock (Figure 33b); (c) crosscutting small asymmetric folds in orientations roughly parallel to axial planar cleavage (Figure 33b, and Figure 15, Chapter 2);

Figure 32. Photographs of quartz veining.

32a,b. Quartz veining in sheared quartz feldspar porphyry on the Bankfield Property. The veins are hosted in fractures that parallel the schistosity in the rock. The wallrock is mineralized with abundant pyrite and arsenopyrite.

32c. Contorted veins in highly folded and sheared sedimentary rocks at the north end of the Roxmark trenches.

32d. Quartz veinlets occupying two cleavages in highly deformed greywacke at the Mosher West hydroline exposure.

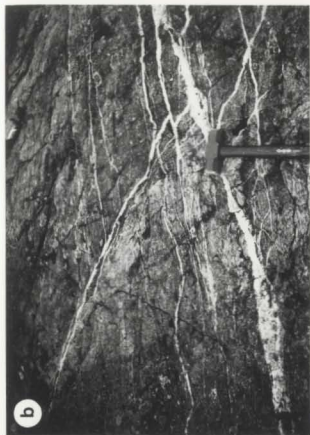
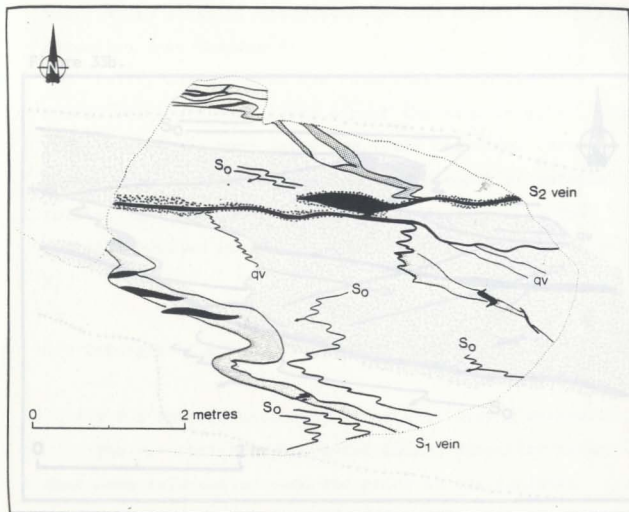


Figure 33a.



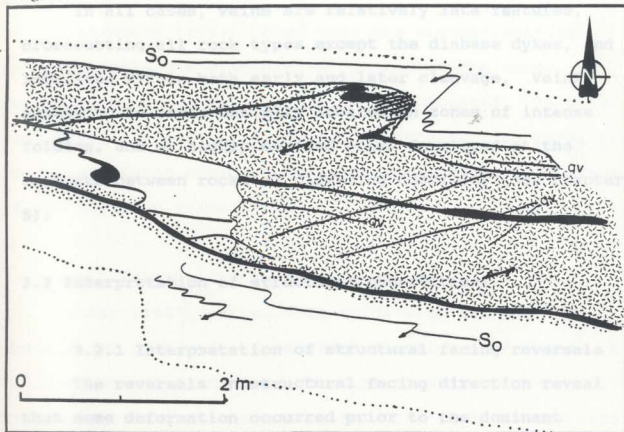
## LEGEND

Figure 33. Detailed sketch maps of selected outcrops at the Open Stope exposure of the Hard Rock North Ore Zone.

33a. Outcrop map from the east end of the Open Stope (see Fig. 57, Chapter 5). Early  $S_1$  carbonate veins, which in this location crosscut bedding at a low angle, are folded into Z-asymmetric minor folds and are cut by later,  $S_2$ , quartz and quartz-carbonate veins. The  $S_2$  veins are hosted in fractures parallel to the axial planes of the minor folds. Auriferous pyrite-arsenopyrite replacement haloes are developed along the borders of these veins where they crosscut iron formation. The host rock lithology is finely laminated magnetite-hematite-siltstone. (See next page for legend).

33b. Outcrop map from the north edge of the Open Stope. Auriferous pyrite-arsenopyrite replacement lenses are developed at the margins of the late quartz and quartz-carbonate veins, which are localized at the contact between finely laminated oxide iron formation and highly carbonatized intrusive rock. These veins crosscut asymmetric Z-folds in the iron formation.

Figure 33b.



## LEGEND

-  Quartz-sulphide (-carbonate) veins which occupy  $S_2$  cleavage, parallel to axial planes of asymmetric z-folds.
-  Pyrite-arsenopyrite replacement halo.
-  Carbonate-quartz veins which occupy  $S_1$  cleavage, which crosscuts bedding at a low angle.
-  Magnetite-hematite iron formation with siltstone interlaminae.
-  Carbonatized, sericitized, and pyritized intrusive.
- $S_0$   Trace of bedding, and sense and plunge of minor folds.
- qv  Quartz veinlet.
-  Schistosity.

and, (d) in zones of brecciation within highly folded iron formation (see Chapter 5).

In all cases, veins are relatively late features, crosscutting all rock types except the diabase dykes, and localized within both early and later cleavage. Veins appear to be preferentially located in zones of intense folding, and or highly sheared zones developed at the contacts between rocks of differing ductility (see Chapter 5).

### 3.2 Interpretation of structural observations

#### 3.2.1 Interpretation of structural facing reversals

The reversals in structural facing direction reveal that some deformation occurred prior to the dominant period of folding. This prior deformation may represent an early folding episode, i.e. recumbent or nappe-style, and/or an early faulting of the stratigraphy, that juxtaposed back-to-back and front-to-front facing lithostratigraphic packages. This interpretation, combined with the observation of the prevalence of transposition and shearing of lithologies at the outcrop scale, implies that the belt may be composed of numerous narrow "slices" or panels of strata in which the structural facing, and therefore the overall younging direction, of each sequence is different from that in the adjacent panel. The Beardmore-Geraldton belt therefore

appears to be composed of a disrupted and discontinuous stratigraphy. During deformation.

Kehlenbeck (1984) noted that the discontinuities which separate the distinctive "packages" are zones in which evidence for shearing is very pronounced. He also stated that in most outcrops the shear direction parallels the axial planar cleavage and therefore the axial surface of the dominant folds. foliations are thought by the

some authors to be characteristic of zones of simple

### 3.2.2 Interpretation of minor folds

Ramsay (1967<sup>p. 471</sup>) stated that folds with similar fold geometrical form, or a form which closely approximates it "...are generally found in the central parts of belts of regional folding and metamorphism. The zones in the crust where these folds are most common were probably in a very ductile state during fold formation.", i.e. they were probably high temperature and/or high pressure. He suggested that all folds, whatever their initial class, may come to resemble shear folds with increased compression and deformation. These folds probably formed from an initial compressive stress acting along the layers, with subsequent flattening of the folds by continued compression, acting across the layers.

Formation of minor folds in the Geraldton area is consistent with an approximately north-south maximum compression and a later component of shear acting northwest-southeast. From the fold features observed it

is reasonable to postulate that the rocks were in a fairly ductile state during deformation.

### 3.2.3 Interpretation of shear zones and faults

Studies of shear zones by Berthe et al (1979), Platt (1984), and Ponce de Leon and Choukroune (1980) have described foliations that are very similar to those described above. These foliations are thought by the above authors to be characteristic of zones of simple shear.

The through-going chlorite seams, (a) surfaces (Figure 29) correspond to Berthe et al's (1979) C surfaces. They found that these were surfaces along which essentially horizontal displacement had occurred and that they maintained a constant orientation within each defined shear band. They also found that these fabrics parallel the "cartographic trace of the major shears, and are specific to zones of simple shear".

The (b) fabric (Figure 29) is similar to the S surfaces of Berthe et al (1979). They stated that these surfaces define the plane of preferred mineral orientation and contain the maximum extension direction of the deformed minerals.

According to Platt (1984), S and C surfaces develop together at the start of deformation and do not overprint each other. The angle between these two sets of surfaces is originally  $45^\circ$ , but diminishes progressively with

continued deformation by rotation of the S surfaces toward the C surfaces while the latter maintain a relatively constant orientation (Berthe et al, 1979). Associated with the rotation of the S surfaces, Ponce de Leon and Choukroune (1980) identified a concomitant decrease in grain sizes and an increase in the frequency of C planes. Both of these features are recognized in the sheared gabbro outcrops. At a given stage in the evolution of zones of simple shear, the C' planes appear, making an angle of  $30^{\circ}$  to the C planes (Ponce de Leon and Choukroune, 1980).

Weijermars and Rondeel (1984) showed that shear band foliation may be used as an indicator of the sense of shear. Shear bands show a consistent angular relationship to the shear zone boundaries and the rotated early foliation, such that the acute angle between the shear zone boundary and the shear band cleavage point in the opposite direction to the relative movement of the country rock outside of the shear zone. Using this criteria, the sense of shear indicated by the shear zones within the hornblende gabbros is dextral. (Figure 29). This observation is consistent with other dislocation features observed within the belt.

The faulting in the Geraldton area appears to be a later, more brittle expression of the same dextral stress that was responsible for the minor folds and the shear zones. Note that the extension of the BTF eastward from

the Roxmark property passes through the gabbro outcrops where the shear zones are developed. Buck and Williams (1984) suggest that the late brittle stage of deformation may be the result of strain hardening or an increased strain rate producing a lower apparent rock ductility.

3.3 Summary above, the structures which are crosscut by quartz-bearing veins include relatively late features, and

1. An early deformation is postulated which produced opposing facing directions within the sequence but was not accompanied by the development of a cleavage.

2. A later deformation event took place with the development of a pervasive regional cleavage, possibly in conjunction with the development of mesoscopic isoclinal folds;

3. Asymmetric folding and dextral shearing, with the development of a later cleavage in the most intensely deformed areas, overprinted the isoclinal folds and the earlier cleavage;

4. Several generations of quartz veins were introduced during deformation, both prior to and subsequent to the later episode of cleavage formation.

5. Deformation was probably progressive over a long period of time, evidenced by cleavage overprints and sets of deformed and undeformed quartz veins.

6. Dextral strike slip faulting continued at least into the Proterozoic. The fault may be a very long-lived

feature, as is suggested by its spatial coincidence with both the mafic and felsic intrusions, and also with long linear conglomerate horizons.

7. Veins are hosted within highly fractured and/or sheared zones which are later than intrusions, cleavage, and asymmetric folds which overprint both of the former. As outlined above, the structures which are crosscut by gold-bearing veins include relatively late features, and therefore the veins are themselves a later feature.

#### 3.4 Structural model

The discontinuity in facing direction coincides with a major zone of intensely deformed rocks within the Geraldton area and this zone shows pronounced evidence of shearing. The discontinuity also parallels the major strike fault in the area, the Bankfield - Tombill Fault (BTF), and several lesser faulted and sheared zones. As noted in the introduction to this chapter, most of the mines in the area are also found in spatial association with this zone.

The structural facing reversal may be related to some early, large-scale deformation. This deformation may have resulted in the juxtaposition of at least two unrelated terrains (group A and group B) along a major break or suture by faulting or some other large-scale tectonic mechanism. This feature has very little expression other

than the structural facing reversal and the apparent facies change that coincides with this reversal. The BTF may merely be a later structure that is superimposed on this long-lived zone of weakness. It is interesting to note the proximity of the Beardmore-Geraldton belt and this structural discontinuity to the subprovince boundary between the Wabigoon and Quetico Belts, presently located at the southern boundary of the southernmost volcanic belt. This long-lived zone of structural weakness may represent a major tectonic suture, similar to that envisioned for accreted "suspect terranes" in the Cordillera and Appalachians (Williams and Hatcher, 1983).

North-south compressive stress caused the sequence to be isoclinally folded along east-west hinges, and this was followed by compression with a component of dextral shear. Continued deformation resulted in more brittle failure, with the development of the BTF and other east-west faults in the area.

The transposition of bedding which is observed in outcrop throughout much of the Geraldton area may be envisioned to be occurring on a much larger scale. This may involve transposition of major lithological units along cleavage parallel fault and shear zones, and may in fact be the process responsible for juxtaposing the different facies of sedimentary rock observed in group A and group B, as well as the alternating panels of mafic volcanic and sedimentary rocks.

Gold-bearing quartz and quartz-carbonate veins occupy a later cleavage and crosscut folds. They therefore are relatively late in the tectonic development of the belt. Many quartz veins are folded, indicating that deformation may have continued over a significant period of time.

The major and trace element composition of the igneous rock units in the study area, the rare earth element (REE) composition of the intrusive rocks, a U/Pb zircon age of the felsic intrusions and the Pb isotope composition of pyrite in felsic intrusions and iron formation are discussed in this chapter. Gold analyses were obtained for the sedimentary rocks in the Geraldton area, and also for iron formation from both within the Geraldton area and from several locations along the Western-Geraldton belt, to determine the distribution of gold in these rocks.

The objectives of this geochemical study are:

(i) sedimentary rocks

(i) clastic sedimentary rocks:

- i) to determine if the Geraldton sedimentary rocks are distinctive in any way compared to other Archean sedimentary rocks
- ii) to determine if there is any geochemical difference between the two groups of sedimentary rocks - group A which hosts gold deposits versus group B which does not.
- iii) to determine if there is any primary enrichment of gold in these rocks.

(ii) iron formation:

- i) to establish the background gold content of the rocks throughout the area and assess the hypothesis that these rocks served as a source for the gold in the

## CHAPTER 4

## GEOCHEMISTRY

## 4.0 Introduction

The major and trace element composition of the various rock units in the study area, the rare earth element (REE) composition of the intrusive rocks, a U/Pb zircon age of the felsic intrusions and the Pb isotope composition of pyrite in felsic intrusions and iron formation are discussed in this chapter. Gold analyses were obtained for the sedimentary rocks in the Geraldton area, and also for iron formation from both within the Geraldton area and from several locations along the Beardmore-Geraldton belt, to determine the distribution of gold in these rocks.

The objectives of this geochemical study are;

## A. Sedimentary rocks

## I) clastic sedimentary rocks:

- i) to determine if the Geraldton sedimentary rocks are distinctive in any way compared to other Archean sedimentary rocks
- ii) to determine if there is any geochemical difference between the two groups of sedimentary rocks - group A which hosts gold deposits versus group B which does not
- iii) to determine if there is any primary enrichment of gold in these rocks.

## II) iron formation;

- i) to establish the background gold content of these rocks throughout the area and assess the hypothesis that these rocks served as a source for the gold in the area

ii) to ascertain which elements are introduced along with gold into these rocks, and that therefore may be used as a geochemical indicator of gold

#### B. Intrusive rocks:

##### I) mafic intrusions and chlorite schists;

i) to establish the composition of these rocks and compare them with other Archean mafic rocks

ii) to geochemically test the hypothesis that the chlorite schist in the fault zone south to southeast of Mosher Lake is derived from the deformation of the hornblende gabbro

##### II) felsic intrusions

i) to compare the eastern and western porphyries

ii) to outline the changes in these rocks due to alteration associated with gold mineralization, and

iii) to comment on a possible association of these rocks with gold mineralization.

#### C. Isotope studies:

##### I) U/Pb zircon

i) to constrain the age of gold mineralization

##### II) Pb isotopes

i) to constrain age of gold mineralization and to investigate the possible source of fluids responsible for the mineralization.

### 4.1 Sedimentary rocks

#### 4.1.1 Clastic sedimentary rocks

50 samples of greywacke and siltstone, 41 from group A and 9 from group B, were analyzed for major and trace elements, and 39 samples from both groups were analyzed for Au. All data are listed in Appendix A. Analytical methods are discussed in Appendix B. Samples were analysed for gold by delayed neutron activation analysis at X-Ray Assay Laboratories, Ltd. (Toronto) and Chemex Laboratories Ltd. (Vancouver). A suite of representative analyses of sedimentary rocks from each group is presented

in Table 5. When sampled, these rocks were not separated into greywacke and siltstone as commonly a sample consists of both rock types finely interbedded. To better compare these samples with reported averages for Archean clastic sedimentary rocks, the samples were classified according to a geochemical criteria. Samples with greater than 61.0%  $\text{SiO}_2$  were arbitrarily classified as greywacke, and those with less than 61.0%  $\text{SiO}_2$  as siltstone. In addition, altered samples and those with quartz vein material were deleted. Using these criteria, 26 samples were classified as greywacke, 19 as siltstone and 5 cases were deleted (all from group A). To test the validity of this assumption, frequency distributions (histograms) were plotted for the entire sample population of sedimentary rocks for  $\text{SiO}_2$ ,  $\text{Al}_2\text{O}_3$ ,  $\text{MgO}$  and  $\text{Fe}_2\text{O}_3\text{T}$ , and probability curves were plotted for  $\text{SiO}_2$  and  $\text{Al}_2\text{O}_3$  (Sinclair, 1976), (Figures 34 and 35). The  $\text{SiO}_2$  and  $\text{Al}_2\text{O}_3$  probability plots clearly show the existence of two distinct sample populations with the change in slope occurring at 62-63%  $\text{SiO}_2$ . Therefore the original estimate of 61%  $\text{SiO}_2$  is considered valid. In addition the  $\text{Al}_2\text{O}_3$  probability plot breaks in slope at 15%  $\text{Al}_2\text{O}_3$ . The average of the Geraldton greywacke samples is <15% (Table 6), and that of the siltstone samples is >15% based on the original 61%  $\text{SiO}_2$  distinction.

**Table 5:** Selected major and trace element analyses of clastic sedimentary rocks representative of group A and group B

	Roxmark Property Trenches					Grants Camp outcrops			
	058 "sand"	067 "mud"	068 "sand"	071 "mud"	076 "mud"	001 "mud"	002 "sand"	037 "mix"	038 "mud"
SiO <sub>2</sub>	64.9	59.1	62.0	60.9	55.6	58.6	62.7	54.7	55.1
TiO <sub>2</sub>	.60	.76	.64	.69	.62	.66	.54	.79	.66
Al <sub>2</sub> O <sub>3</sub>	15.0	17.1	16.2	17.2	15.9	18.0	14.7	19.0	19.3
Fe <sub>2</sub> O <sub>3</sub>	1.5	2.2	2.4	1.8	3.0	1.4	2.3	1.4	.9
FeO	4.5	5.6	6.2	5.6	8.9	5.3	4.2	6.7	5.3
MnO	.06	.08	.05	.11	.09	.08	.06	.09	.12
MgO	2.63	3.15	3.05	3.52	3.45	4.04	2.97	4.17	3.41
CaO	1.23	.44	.28	.83	1.98	1.25	1.81	.64	.99
Na <sub>2</sub> O	2.8	1.8	2.8	.8	1.1	1.9	3.9	5.2	6.5
K <sub>2</sub> O	2.30	3.18	2.52	3.42	2.54	4.41	1.93	3.48	3.09
P <sub>2</sub> O <sub>5</sub>	.13	.14	.14	.13	.13	.17	.17	.16	.19
H <sub>2</sub> O <sub>T</sub>	2.8	4.8	3.7	4.2	4.4	3.7	2.8	3.3	2.8
CO <sub>2</sub> T	1.5	1.3	.1	1.0	2.6	1.1	1.9	.9	1.9
S	.07	.13	.95	0.00	0.00	.03	.20	0.00	0.00
Total	100.2	100.0	100.3	100.4	100.5	100.9	100.4	100.8	100.5
Au	1	10	10	< 1	16	< 1	-	2	2
As	20	267	6	25	0	54	25	20	15
Rb	82	113	102	130	86	133	56	101	93
Sr	151	75	73	62	73	256	242	173	336
Zr	130	136	139	125	101	146	159	146	165

Note: major elements are reported in wt %, Au in ppb, and As, Rb, Sr and Zr in ppm.

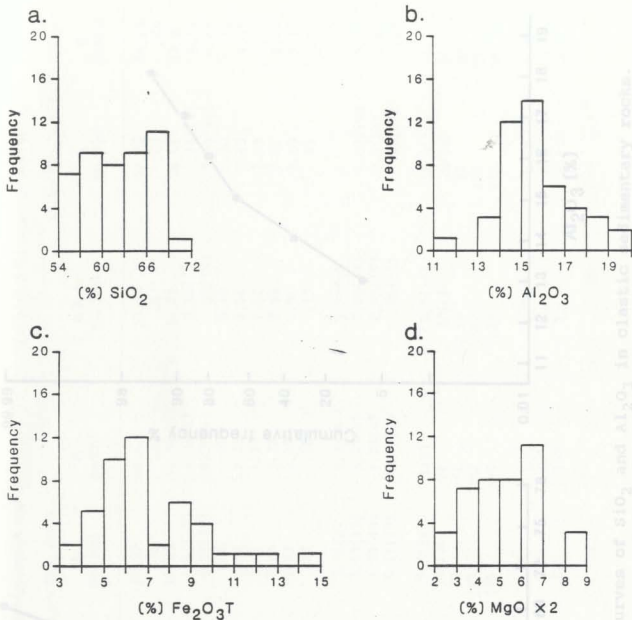


Figure 34. Frequency distributions of; a) SiO<sub>2</sub>, b) Al<sub>2</sub>O<sub>3</sub>, c) Fe<sub>2</sub>O<sub>3</sub>T, and d) MgO (in weight per cent); in clastic sedimentary rocks.

TABLE 6: Average of shale rock analyses for Cevalfion greywacke and siltstone from group A and group B. (Yoshida, 1970)

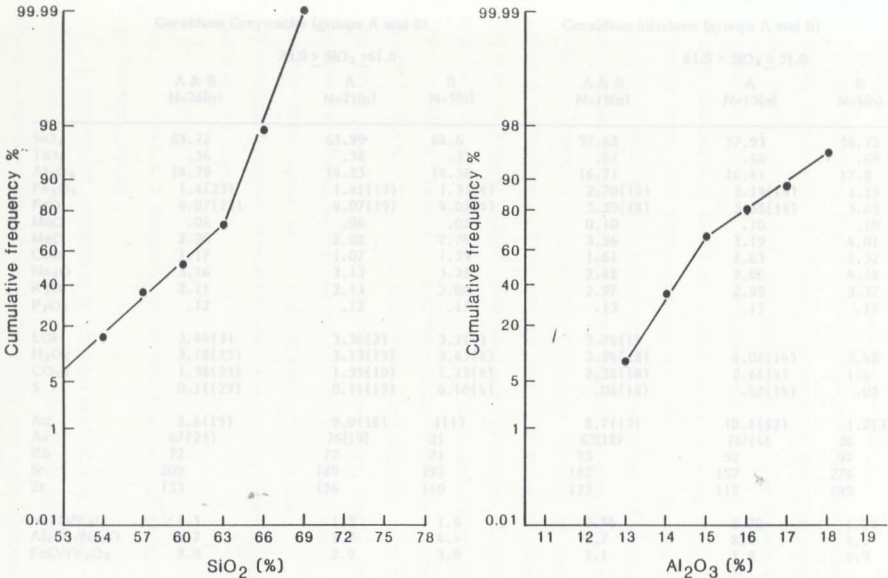


Figure 35. Probability curves of SiO<sub>2</sub> and Al<sub>2</sub>O<sub>3</sub> in clastic sedimentary rocks.

TABLE 6: Average of whole rock analyses for Geraldton greywacke and siltstone from group A and group B. (Weight percent)

	Geraldton Greywacke (groups A and B)			Geraldton Siltstone (groups A and B)		
		73.0 > SiO <sub>2</sub> > 61.0			61.0 > SiO <sub>2</sub> > 51.0	
	A & B N=26(n)	A N=21(n)	B N=5(n)	A & B N=19(n)	A N=15(n)	B N=4(n)
SiO <sub>2</sub>	65.72	65.99	64.6	57.68	57.93	56.73
TiO <sub>2</sub>	.56	.56	.53	.67	.66	.69
Al <sub>2</sub> O <sub>3</sub>	14.79	14.85	14.56	16.71	16.41	17.8
Fe <sub>2</sub> O <sub>3</sub>	1.4(23)	1.41(19)	1.35(4)	2.70(18)	3.14(14)	1.15
FeO	4.07(23)	4.07(19)	4.08(4)	5.59(18)	5.58(14)	5.63
MnO	.06	.06	.07	0.10	.10	.10
MgO	2.20	2.08	2.74	3.36	3.19	4.01
CaO	1.17	1.07	1.59	1.61	1.63	1.52
Na <sub>2</sub> O	3.16	3.13	3.28	2.48	2.02	4.18
K <sub>2</sub> O	2.11	2.13	2.04	2.97	2.89	3.37
P <sub>2</sub> O <sub>5</sub>	.12	.12	.15	.15	.15	.17
LOI	3.44(3)	3.56(2)	3.2(1)	3.74(1)		
H <sub>2</sub> O <sub>T</sub>	3.18(23)	3.13(19)	3.45(4)	3.94(18)	4.07(14)	3.48
CO <sub>2</sub> T	1.58(23)	1.55(19)	1.73(4)	2.38(18)	2.6(14)	1.6
S	0.11(23)	0.11(19)	0.10(4)	.06(18)	.07(14)	.02
Au	8.6(19)	9.0(18)	1(1)	8.7(15)	10.4(12)	1.7(3)
As	67(23)	76(19)	21	65(18)	76(14)	26
Rb	72	72	71	93	92	97
Sr	209	189	292	182	157	276
Zr	153	156	140	125	118	149
Na <sub>2</sub> O/K <sub>2</sub> O	1.5	1.5	1.6	0.84	0.70	1.24
Al <sub>2</sub> O <sub>3</sub> /Na <sub>2</sub> O	4.7	4.7	4.4	6.7	8.1	4.3
FeO/Fe <sub>2</sub> O <sub>3</sub>	2.9	2.9	3.0	2.1	1.8	4.9

#### 4.1.1.1 Comparison of Geraldton sedimentary rocks with average Archean sedimentary rocks

The averages for all greywacke and all siltstone samples are listed in Table 6 along with the averages for these rocks subdivided into group A and group B samples. Comparison of these samples with Condie's data (1981, p.140, Tables 4.4 and 4.5) (reproduced here as Table 7) reveals that, for most elements and ratios reported, the Geraldton sedimentary rocks are very similar to average Archean sedimentary rocks. The Geraldton greywacke has a slightly lower  $\text{FeO}/\text{Fe}_2\text{O}_3$  than Condie's average as does the group A siltstone. This may be due to a greater magnetite content in these rocks. The average Geraldton siltstone has only slightly lower  $\text{SiO}_2$ ,  $\text{Al}_2\text{O}_3/\text{Na}_2\text{O}$  and  $\text{FeO}/\text{Fe}_2\text{O}_3$  than Condie's averages; however, group B samples have a slightly higher  $\text{Na}_2\text{O}$  and therefore also higher  $\text{Na}_2\text{O}/\text{K}_2\text{O}$  and lower  $\text{Al}_2\text{O}_3/\text{Na}_2\text{O}$  than Condie's averages, while group A samples have similar values to Condie's. Therefore, it appears that there is no significant geochemical difference between Geraldton and average Archean clastic sedimentary rocks.

#### 4.1.1.2 Comparison of group A versus group B sedimentary rocks

A series of student's t statistical tests were conducted on the geochemical analyses of the group A and group B sedimentary rocks to test for any significant

TABLE 7: Average compositions of Archean greywackes and argillites

	1	2	3	4	5	6	7	8	9	10	11	12
SiO <sub>2</sub>	63.7	66.2	63.3	64.4	69.2	66.9	70.5	65.2	57.8	59.2	60.6	63.0
Al <sub>2</sub> O <sub>3</sub>	0.57	0.52	0.56	0.62	0.53	0.57	0.3	0.57	0.70	0.69	0.67	0.8
Fe <sub>2</sub> O <sub>3</sub>	14.9	10.2	13.3	15.5	13.7	15.7	14.6	15.8	18.4	20.2	12.6	18.2
CaO	1.01	1.63	1.0	1.05	1.14	1.33	0.77	1.2	1.67	1.15	2.35	1.3
MgO	4.67	5.38	4.9	4.94	3.05	2.59	1.50	3.4	6.21	4.85	8.24	4.5
Na <sub>2</sub> O	2.99	4.50	3.7	3.12	1.6	1.57	1.44	2.2	3.93	3.34	4.71	2.5
K <sub>2</sub> O	2.63	1.97	3.4	2.22	1.8	3.56	3.55	3.3	1.89	1.38	0.68	1.0
SiO <sub>2</sub> /Al <sub>2</sub> O <sub>3</sub>	3.14	1.80	2.9	3.74	3.1	3.84	4.45	3.7	2.19	2.67	0.84	1.3
SiO <sub>2</sub> /Fe <sub>2</sub> O <sub>3</sub>	2.30	1.58	2.1	2.44	2.0	3.07	1.32	3.23	3.26	2.49	2.28	3.5
Al <sub>2</sub> O <sub>3</sub> /Fe <sub>2</sub> O <sub>3</sub>	2.17	2.76	2.0	2.4	2.4	0.65	0.75	0.8	3.11	3.60	4.0	4.0
CaO/SiO <sub>2</sub>	1.49	2.59	1.0	0.3	0.3	0.21	0.12	0.2	0.17	0.05	2.6	0.2
Na <sub>2</sub> O/SiO <sub>2</sub>	0.14	0.08	0.15	0.12	0.12	0.21	0.12	0.17	0.19	0.15	0.10	0.2
Al <sub>2</sub> O <sub>3</sub> /SiO <sub>2</sub>	0.11	0.10	0.1	0.10	0.10	0.07	0.05	0.08	0.09	0.06	0.08	0.1
Na <sub>2</sub> O/K <sub>2</sub> O	1.4	1.1	1.4	1.5	1.6	1.3	3.4	1.1	0.67	1.1	0.37	0.37
Al <sub>2</sub> O <sub>3</sub> /Na <sub>2</sub> O	4.8	5.7	4.6	4.2	4.4	4.1	3.3	4.3	8.4	7.6	15	14
SiO <sub>2</sub> /Fe <sub>2</sub> O <sub>3</sub>	4.6	3.3	4.9	4.7	2.7	2.0	2.0	2.8	3.7	4.2	3.5	3.5

Note: Analyses are reported in weight percent.

(from Condie, 1981 p. 140-141)\*

- 1 = average of 20 Archean graywackes
- 2 = average of 17 Archean greywackes from the Sheba Formation, South Africa
- 3 = composite Archean greywacke
- 4 = average of 23 Archean greywackes, South Pass greenstone belt, Wyoming
- 5 = average Phanerozoic greywacke
- 6 = average granodiorite
- 7 = average Archean tonalite
- 8 = average Precambrian continental crust
- 9 = average of 20 Archean slates
- 10 = average Archean slate from greywacke - argillite couplet
- 11 = average pelite from the Sheba Formation, South Africa
- 12 = average Phanerozoic argillite from greywacke - argillite couplet

\* see Condie (1981) for references for each average analysis reported

difference in the major and trace element content between these two groups. The results of F-tests and pooled variance estimate t-test are presented in Tables 8 a and b. The tests were done to evaluate the hypothesis that the means of the two sample populations are the same, assuming a 5% (0.05) level of significance. F-tests to determine the equality of variances of the samples are evaluated to determine the validity of the t-test statistic. The results indicate that for all those comparisons for which the test is statistically valid, only MgO and  $P_2O_5$  show any significant difference in the greywacke groups and  $Na_2O$  in the siltstone groups. Thus the two groups are essentially identical in major element composition.

#### 4.1.1.3 Background gold content of Geraldton clastic sedimentary rocks

Most of the sampling of these rocks was done away from mineralization. For example, a detailed sampling cross-section was completed over a 330m across-strike section of greywacke-siltstone and iron formation east of Mosher Lake (Figures 3 and 6). The average gold contents for all 39 sedimentary rocks analyzed, subdivided by rock type and area, are presented in Table 9. The average gold contents of these rocks are all very low, ranging from 10.4 ppb for the group A siltstone to 1 ppb for the group B greywacke (only one analysis). The averages of all

Table 8. Results of F-tests and pooled variance estimate t-tests on whole rock geochemical analyses of group A versus group B sedimentary rocks: a) "sands"  $\text{SiO}_2 > 61.0\%$  b) "muds"  $\text{SiO}_2 \leq 61.0\%$

a) "sands" A vs B.		b) "muds" A vs B.					
SiO <sub>2</sub>	N of A	N of B	F-value	NIM n/ENOM	T-value	Pooled Variance Estimate deg of freedom	2-tail probability
SiO <sub>2</sub>	21	5	1.31	A/B	1.22	24	.235
TiO <sub>2</sub>	21	5	2.53	A/B	.48	24	.639
Al <sub>2</sub> O <sub>3</sub>	21	5	3.78	B/A	.52	24	.606
FeO	19	4	22.35	A/B	-.01	21	.992
Fe <sub>2</sub> O <sub>3</sub>	19	4	2.04	A/B	.12	21	.909
MnO	21	5	1.44	B/A	-1.47	24	.155
MgO	21	5	1.65	A/B	-1.89	24	.070
CaO	21	5	2.29	B/A	-1.40	24	.176
Na <sub>2</sub> O	21	5	1.44	A/B	-.45	24	.657
K <sub>2</sub> O	21	5	1.12	A/B	.33	24	.748
P <sub>2</sub> O <sub>5</sub>	21	5	2.86	B/A	-3.08	24	.005
Fe <sub>2</sub> O <sub>3</sub> T	21	4	12.07	A/B	.37	23	.718
H <sub>2</sub> O	19	4	1.74	B/A	-1.35	21	.190
CO <sub>2</sub>	19	4	1.59	A/B	-.35	21	.729
S	19	4	1.58	A/B	-.23	21	.824
SiO <sub>2</sub>	15	4	1.01	B/A	1.02	17	.323
TiO <sub>2</sub>	15	4	5.31	B/A	-.29	17	.774
Al <sub>2</sub> O <sub>3</sub>	15	4	2.67	B/A	-1.76	17	.097
FeO	14	4	5.43	A/B	-.05	16	.958
Fe <sub>2</sub> O <sub>3</sub>	14	4	30.14	A/B	1.90	16	.075
MnO	15	4	10.75	B/A	-.15	17	.882
MgO	15	4	6.85	B/A	-1.41	17	.177
CaO	15	4	1.05	A/B	.18	17	.857
Na <sub>2</sub> O	15	4	1.89	B/A	-2.36	17	.030
K <sub>2</sub> O	15	4	1.30	B/A	-1.26	17	.225
P <sub>2</sub> O <sub>5</sub>	15	4	5.82	A/B	-1.47	17	.160
H <sub>2</sub> O	14	4	2.11	A/B	1.37	16	.189
CO <sub>2</sub>	14	4	9.55	A/B	-.85	16	.410
S	14	4	11.47	A/B	.92	16	.372

**TABLE 9: Average gold content of Geraldton clastic sedimentary rocks**

	Mean Au(ppb)	Standard Deviation	No. of Samples
<u>Group A</u>			
greywacke	9.0	21.4	18
siltstone	10.4	15.7	12
<u>Group B</u>			
greywacke	1.0	-	1
siltstone	1.7	0.6	3
<u>Groups A &amp; B</u>			
greywacke	8.6		19
siltstone	8.7		15

greywacke and all siltstone are both less than 9 ppb gold (greywacke, 8.6 ppb; siltstone, 8.7 ppb).

#### 4.1.2 Iron formation

92 samples of iron formation were collected and analyzed for major and trace elements and gold. The complete results are listed in Appendix A. For purposes of sampling, iron formation refers to a sedimentary rock with visible magnetite laminae. In some cases the laminae are very narrow, in others they are up to a centimetre in width but make up less than 10% of the sample, and in others a sample of iron formation may be greater than 80% magnetite-hematite, therefore there is a great variation in the composition of these rocks.

The average major and trace element composition of all 92 samples, and the average compositions of these rocks subdivided by sulphur content are presented in Table 10. Plots of  $\text{Fe}_2\text{O}_3/\text{T}$  against  $\text{SiO}_2$ ,  $\text{Al}_2\text{O}_3$ ,  $\text{TiO}_2$ , Ni, Cr, and Co, and  $\text{SiO}_2$  against  $\text{TiO}_2$  are presented in Figure 36. All of these plots show negative correlations except the  $\text{SiO}_2$ - $\text{TiO}_2$  plot which shows a weak positive correlation. Plots of  $\text{Al}_2\text{O}_3$  against  $\text{TiO}_2$ , Cr, Ni, and Co are presented in Figure 36. These plots show good positive correlation. The consistency of these plots suggest that although there is a great variation in the composition of these rocks as outlined above, the variation is due to a binary mixing of a clastic sedimentary and a chemical sedimentary

TABLE 10: Average major and selected trace element analyses of Geraldton iron formation; total sample population and population subdivided by sulphur content

	Total Iron Formation N=92				Iron Formation; S <0.5% N=80				Iron Formation S >0.5% N=12			
	mean	min.	max.	S.Dev.	mean	min.	max.	S.Dev.	mean	min.	max.	S.Dev.
SiO <sub>2</sub>	41.79	20.7	60.6	8.13	42.98	27.9	60.6	7.22	33.86	20.7	56.3	9.67
TiO <sub>2</sub>	0.23	0.03	0.60	0.13	0.23	0.03	0.60	0.13	0.22	0.09	0.38	0.10
Al <sub>2</sub> O <sub>3</sub>	6.08	0.90	16.6	3.36	6.12	0.90	16.6	3.42	5.83	2.60	13.5	3.09
Fe <sub>2</sub> O <sub>3</sub>	33.25(82)	2.7	59.2	12.16	33.75	2.70	59.2	12.08	29.9	3.4	45.9	12.71
FeO	9.59(82)	0.30	28.8	5.74	9.17	0.30	18.4	5.14	26.25	23.70	28.8	3.61
MnO	0.08	0.02	0.2	0.04	0.08	0.02	0.17	.04	0.08	0.02	.20	.05
MgO	1.3	0.02	3.27	0.83	1.30	0.02	3.27	.84	1.34	0.30	3.04	.79
CaO	0.94	0.12	4.14	0.87	0.89	0.12	3.59	.78	1.33	0.22	4.14	1.34
Na <sub>2</sub> O	0.66	0	3.2	0.79	0.64	0.0	3.20	.75	0.74	0.0	2.50	1.09
K <sub>2</sub> O	0.83	0	3.29	1.14	0.85	0.0	3.11	.83	0.73	0.05	3.29	0.91
P <sub>2</sub> O <sub>5</sub>	0.21	0.07	0.44	0.07	0.21	0.07	0.44	.06	0.19	0.09	.39	0.07
H <sub>2</sub> O <sub>T</sub>	2.29	0.2	8.4	1.40	2.16	0.20	4.90	1.24	3.19	1.4	8.4	2.05
CO <sub>2</sub> T	2.02	0.1	17.2	3.28	1.40	0.10	8.00	1.51	6.14	.20	17.20	6.57
S	1.50	0.0	27.2	4.95	.04	0	0.43	0.07	11.19	.57	27.2	9.18
Au	593.7	1.0	10001	20934	27.2(79)	1.0	1700	190.8	4323(11)	1.0	10001	4257
Ni	19	0	69	16.6	19			17.0	17			14.6
Cr	60	5	183	36.8	61			4.2	53			7.2
Co	10	0	27	6.5	8			0.7	11			1.8
Cu	25	0	260	31.0	22			18.8	51			68.2
Zn	49	16	130	20.5	50			19.0	47			30.2
Pb	15	0	41	9.5	16			1.1	13			3.0
As	859	0	70000	7296	24			46.0	6432			5783

Note: major elements are reported in wt%, Au in ppb, and other trace elements in ppm.

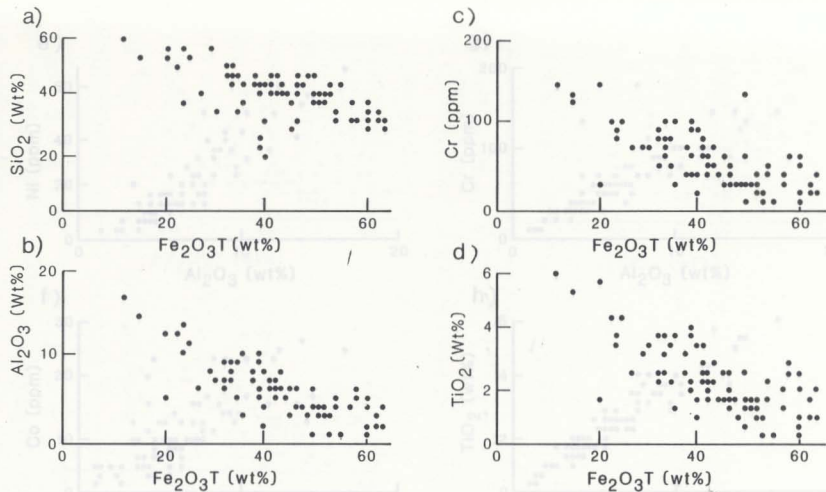
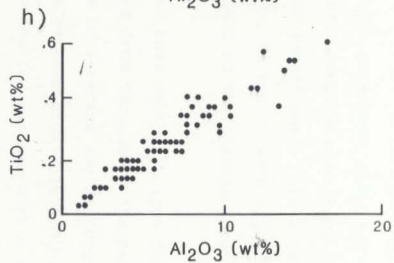
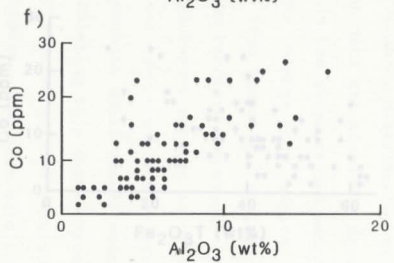
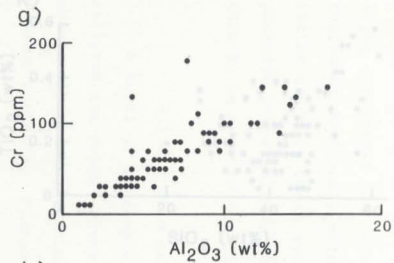
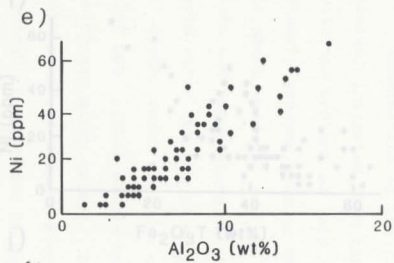
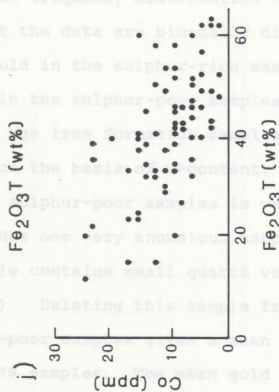
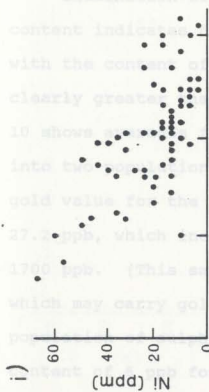
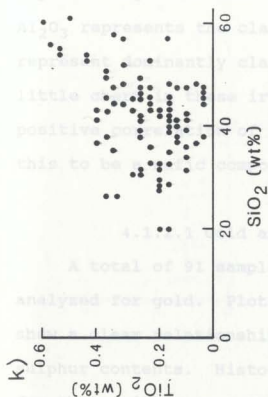


Figure 36. X-Y plots of iron formation geochemical analyses; a) SiO<sub>2</sub> vs Fe<sub>2</sub>O<sub>3</sub>T, b) Al<sub>2</sub>O<sub>3</sub> vs Fe<sub>2</sub>O<sub>3</sub>T, c) Cr vs Fe<sub>2</sub>O<sub>3</sub>T, d) TiO<sub>2</sub> vs Fe<sub>2</sub>O<sub>3</sub>T, e) Ni vs Al<sub>2</sub>O<sub>3</sub>, f) Co vs Al<sub>2</sub>O<sub>3</sub>, g) Cr vs Al<sub>2</sub>O<sub>3</sub>, h) TiO<sub>2</sub> vs Al<sub>2</sub>O<sub>3</sub>, i) Ni vs Fe<sub>2</sub>O<sub>3</sub>T, j) Co vs Fe<sub>2</sub>O<sub>3</sub>T, k) TiO<sub>2</sub> vs SiO<sub>2</sub>.





component.  $\text{Fe}_2\text{O}_3\text{T}$  probably dominantly represents the input of magnetite-hematite chemical precipitates, while  $\text{Al}_2\text{O}_3$  represents the clastic component ( $\text{SiO}_2$  may also represent dominantly clastic component as there is very little  $\text{SiO}_2$  in the iron formations). The strong positive correlation of Cr, Ni and Co with  $\text{Al}_2\text{O}_3$  suggest this to be a component of the clastic input.

4.1.1.1 and base metals in iron formation. A total of 91 samples from throughout the belt were analyzed for gold. Plots of  $\delta$  versus  $\log \delta u$  (Figure 37) show a positive relationship between high gold and high sulphur contents. Histograms for samples with  $\delta > 0.57$  and for those with  $\delta < 0.57$  are given in Figure 38a.

Examination of the frequency distribution of gold content indicates that the data are bimodally distributed, with the concentration of gold in the sulphur-rich samples clearly greater than in the sulphur-poor samples. Table 10 shows the mean values for the iron formation, divided into the sulphur-rich and sulphur-poor categories. The mean gold value for the 80 sulphur-poor samples is very low, 27.2ppb, which is only one very anomalous sample with 1760 ppb. (This sample contains small quartz veinlets which may carry gold.) Deleting this sample from the population of 79 sulphur-poor samples, the mean gold content for 79 samples is 27.2ppb. The mean gold value for the 12 sulphur-rich samples is 437ppb.

component.  $\text{Fe}_2\text{O}_3\text{T}$  probably dominantly represents the input of magnetite-hematite chemical precipitate, while  $\text{Al}_2\text{O}_3$  represents the clastic component ( $\text{SiO}_2$  may also represent dominantly clastic component as there is very little chert in these iron formations). The strong positive correlation of Cr, Ni and Co with  $\text{Al}_2\text{O}_3$  suggest this to be a mafic component of the clastic input.

#### 4.1.2.1 Gold and base metals in iron formation

A total of 91 samples from throughout the belt were analyzed for gold. Plots of S versus log Au (Figure 37) show a clear relationship between high gold and high sulphur contents. Histograms for samples with  $\text{S} > 0.5\%$  and for those with  $\text{S} \leq 0.5\%$  are given in Figure 38a.

Examination of the frequency distribution of gold content indicates that the data are bimodally distributed, with the content of gold in the sulphur-rich samples clearly greater than in the sulphur-poor samples. Table 10 shows averages for the iron formation samples, divided into two populations on the basis of S-content. The mean gold value for the 80 sulphur-poor samples is very low, 27.2 ppb, which includes one very anomalous sample with 1700 ppb. (This sample contains small quartz veinlets which may carry gold.) Deleting this sample from the population of sulphur-poor samples gives a mean gold content of 6 ppb for 79 samples. The mean gold value for the 12 sulphur-rich samples is 432ppb.

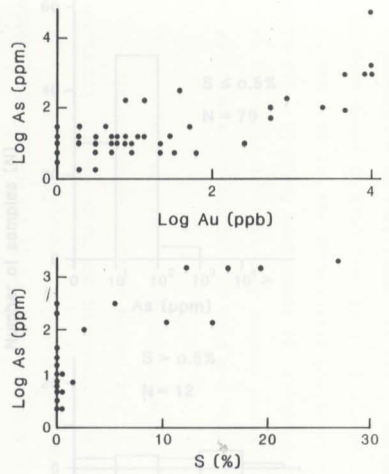
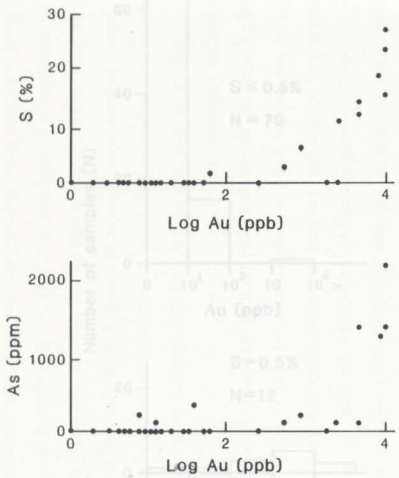


Figure 37. X-Y plots of sulphur, gold and arsenic in iron formation; a) S versus log Au, b) As versus log Au, c) log As versus log Au, and d) log As versus S.

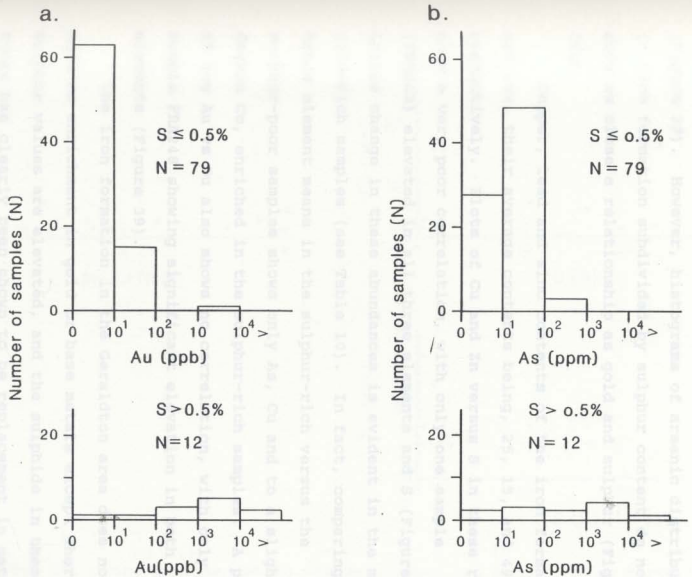


Figure 38. Histograms of gold and arsenic content of iron formation, subdivided by sulphur content; a) gold , b) arsenic.

Arsenopyrite is very common in the sulphide replacement zones in iron formation. Plots of log Au vs log As, and S vs log As, show a weak positive correlation (Figure 37). However, histograms of arsenic distribution in iron formation subdivided by sulphur content do not show as close a relationship as gold and sulphur (Figure 38b).

Copper, lead and zinc contents of the iron formation are low, their average contents being, 25, 15, and 49 ppm, respectively. Plots of Cu and Zn versus S in these rocks show a very poor correlation, with only one sample (FRA248) elevated in all three elements and S (Figure 39). Little change in these abundances is evident in the more gold-rich samples (see Table 10). In fact, comparing the trace element means in the sulphur-rich versus the sulphur-poor samples shows only As, Cu and to a slight degree Co, enriched in the sulphur-rich samples. A plot of log Au vs Cu also shows no correlation, with only sample FRA248 showing significant elevation in both elements (Figure 39).

The iron formation in the Geraldton area does not show an enrichment in gold or base metals except where sulphur values are elevated, and the sulphide in these rocks has clearly been shown to be replacement in nature (see Chapter 2, section 2.2.2.3). The background gold content of the iron formation is very low (compare with Crockett, 1974) and therefore this rock is probably not a

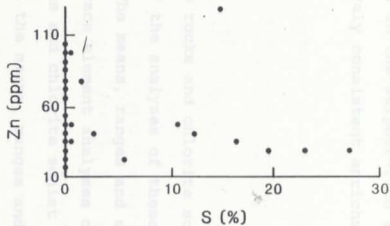
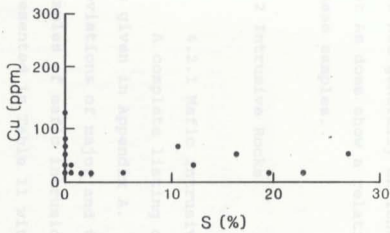
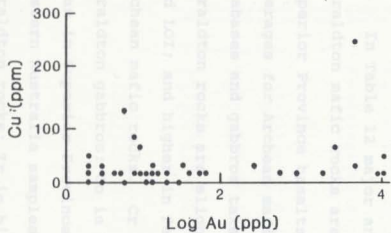


Figure 39. X-Y plots of base metals versus sulphur and gold in iron formation;  
 a) Cu versus log Au, b) Cu versus S, and c) Zn versus S.

primary source for the gold in the veins. Cu, Pb and Zn are not generally enriched in the sulphur-rich samples, but As does show a relatively consistent enrichment in these samples.

#### 4.2 Intrusive Rocks

##### 4.2.1 Mafic intrusive rocks and chlorite schists

A complete listing of the analyses of these samples is given in Appendix A. The means, ranges and standard deviations of major and trace element analyses of 40 samples of mafic intrusions and chlorite schist are presented in Table 11 with the means, ranges and standard deviations for hornblende gabbro and chlorite schist as separate groups.

In Table 12 major and trace element averages for the Geraldton mafic rocks are given with averages for Archean Superior Province basalts taken from Goodwin (1977) and averages for Archean mafic flows and Western Australia diabbases and gabbros taken from Condie (1981). The Geraldton rocks are slightly lower in  $\text{TiO}_2$ ,  $\text{Al}_2\text{O}_3$ ,  $\text{CaO}$ , and LOI; and higher in  $\text{Fe}_2\text{O}_3$ ,  $\text{MgO}$  and  $\text{K}_2\text{O}$  than the other Archean mafic rocks. Cr and Sr are higher in the Geraldton gabbros; Co is higher in the Geraldton rocks than in Superior Province basalts, but lower than the Western Australia samples; Zn, Cu, and V are lower in the Geraldton rocks; Zr is higher in the Superior Province

Table 11. Means, ranges and standard deviation of major and trace element analyses of mafic intrusions and chlorite schist, Geraklitos.

	Hornblende Gabbro N = 23				Chlorite Schist N = 16				Total Mafics N = 38			
	mean	min.	max.	S.D.	mean	min.	max.	S.D.	mean	min.	max.	S.D.
SiO <sub>2</sub>	49.32	43.3	65.6	6.52	50.72	46.6	65.3	6.10	49.99	43.5	65.4	5.16
TiO <sub>2</sub>	0.89	0.3	1.96	0.27	0.89	0.2	1.28	0.32	0.89	0.2	1.58	0.28
Al <sub>2</sub> O <sub>3</sub>	13.65	10.0	20.3	2.65	13.71	8.30	16.4	1.93	13.68	8.3	20.3	2.23
Fe <sub>2</sub> O <sub>3</sub>	3.44	3.8	9.9	2.44	5.85	2.40	10.10	3.51	3.97	0.8	10.1	2.78
FeO	7.53	3.4	11.0	(11)	2.23	7.07	5.8	9.0	1.70	0.3	3.4	1.1.0
MnO	0.19	0.07	0.46	0.074	0.17	0.09	0.28	0.05	0.13	0.07	0.46	0.06
MgO	2.48	3.22	13.5	3.19	6.90	2.76	10.84	2.31	4.18	2.74	14.6	3.17
CaO	0.08	0.06	0.31	0.08	0.08	0.04	0.31	0.08	0.08	0.04	0.31	0.08
Na <sub>2</sub> O	2.33	0.0	5.56	1.86	2.50	0.32	5.2	1.28	2.64	0.0	5.56	1.37
K <sub>2</sub> O	0.67	0.02	2.90	0.59	1.20	0.15	2.71	0.84	0.83	0.02	2.90	0.73
P <sub>2</sub> O <sub>5</sub>	0.139	0.03	0.27	0.06	0.13	0.07	0.23	0.04	0.13	0.03	0.27	0.05
LOI	3.911	1.20	9.24	1.93	7.18	6.68	10.04	1.89	11.1	5.45	1.2	10.06
Total Fe (as FeO)	12.09	5.3	18.6	2.22	11.95	5.88	14.31	1.93	12.03	5.3	18.6	2.08
TOTAL												
H <sub>2</sub> O <sup>+</sup>	4.255	2.9	5.2	(11)	0.71	3.73	3.0	6.2	0.31	0.1	4.11	2.90
CO <sub>2</sub> <sup>+</sup>	1.791	0.2	5.6	(11)	1.53	4.83	1.2	7.6	3.05	0.1	2.60	2.20
S	0.04	0.0	0.3	(11)	0.09	0.32	0.03	1.15	0.35	0.1	1.14	0.0
Au (ppb)	1.5	1.0	3.0	(12)	0.7	0.29	1	180	66	(7)	12	1.0
Ni (ppm)	136	35	420	(24)	111	85	19	210	40	16	115	14
Cr	943	10	1900	(24)	510	225	0	562	178	16	396	0
Co	95	2	110	(24)	30	47	0	59	13	16	57	19
Cu	84	36	130	(24)	21	91	28	314	65	(16)	87	28
Zn	5	0	21	(7)	5	7	0	15	4	(16)	6	0
Pb	19	4	33	(11)	10	29	14	52	17	(6)	22	4
As	21	4	73	(24)	15	35	7	85	23	(16)	26	4
Mo	21	86	133	(24)	34	8	5	485	100	22	30	181
V	21	1	42	(24)	8	23	0	72	22	71	17	28
Zr	70.5	29	140	30	73	17	149	31	71	17	144	30
Y	3	0	6	28	1	3.5	2	7	3	0	7	1
Nb	304	156	407	(16)	68	374	151	496	91	(23)	336	151
Rb	134	16	400	(14)	123	300	40	817	246	(12)	211	16.0
												817.0
												204

Note: N = number of samples except where otherwise indicated by number in parentheses.

S.D. = standard deviation

TABLE 12: Average major and trace element analyses for Geraldton mafic rocks, Archean Superior Province basalts (Goodwin, 1977) and Archean mafic flows and Western Australian gabbro and diabase (Condie, 1981)

	Geraldton		Goodwin (1977)			Condie (1981)	
	hornblende gabbro	chlorite schist	Timmins-Kirkland Lake	Wabigoon	Uchi	Archean flows	Western Australia gabbro and diabase
SiO <sub>2</sub>	49.5	50.72	49.1	49.5	49.1	51.4	50.8
TiO <sub>2</sub>	.89	.89	1.15	1.02	0.95	0.02	1.16
Al <sub>2</sub> O <sub>3</sub>	13.65	13.71	14.6	14.6	15.2	14.8	14.5
Fe <sub>2</sub> O <sub>3</sub>	3.44(11)	5.45(4)	2.69	2.70	2.69		
FeO	7.43(10)	7.07(3)	8.51	9.20	8.78		
MnO	.19	.17	0.21	0.21	0.19		
MgO	8.44	6.00	6.18	6.33	6.02	6.7	6.9
CaO	7.44	4.74	8.95	8.90	8.55	10.7	9.9
Na <sub>2</sub> O	2.53	2.80	2.62	2.26	2.22	2.7	2.7
K <sub>2</sub> O	.67	1.20	0.51	0.40	0.38	0.18	0.25
P <sub>2</sub> O <sub>5</sub>	.14	.13	0.14	0.27	0.12		
LOI	3.91	7.18	-	-	5.29		
Fe <sub>2</sub> O <sub>3,t</sub>	12.09	11.95	-	-		10.4	11.7
H <sub>2</sub> O	4.26	3.73	3.3	2.33			
CO <sub>2</sub>	1.79	1.2	1.17	2.23			
S	0.4	.03					
Ni	136	85	170(484)	160	105(58)	161	145
Cr	443	225	245(487)	257	250(57)	395	314
Co	47(11)	47	36(483)	37	41	59	57
Cu	55	45	106	90	111	98	111
Zn	84	91	81	110	139	112	107
Pb	5	7	3.9	6.0	7.9		
Rb	21	35				9	9
Sr	331	140	172	174	219	105	91
Y	21	23				22	22
Zr	71	73	84	121	153	60	54
Nb	3	4					
V	304(14)	374(12)	372(488)	337	387	320	307
Ba	134(14)	300(12)	152	136	107		
	23	15	503	171	62	123	84

(except where noted in parentheses)

basalts and lower in the Western Australian rocks than in the Geraldton samples; and Ni, Pb and Ba are the approximately the same.

REE plots of four Geraldton gabbro samples are shown in Figure 40. (A listinf of REE data is given in Appendix D.) Sample 254A is a basalt from the Sturgeon Lake area (sampled by J.M. Franklin) and was analyzed for comparison. The gabbro patterns are essentially flat with a very slight light rare earth element (LREE) enrichment, with values 10-30X chondrite, and heavy rare earth element (HREE) 6-15X chondrite. Condie (1981) presented average compositions and REE plots for Archean basaltic komatiites (BK) (Condie, 1981, p.93), and Archean tholeiites which he subdivided into two groups (TH1 and TH2) (Condie, 1981, p.98) (Figure 41). TH1 is characterized by flat REE patterns (approximately 10X chondrite) with or without small Eu anomalies and TH2 is characterized by enriched LREE and a sloping REE pattern (Figure 41). Both TH1 and TH2 differ from BK by their higher  $TiO_2$ ,  $Al_2O_3$ ,  $Na_2O$ ,  $K_2O$ , Ba, Sr, Zr, Y, Zr/Y, and Ti/V and by their lower MgO/FeO (<1), Cr, Ni, Co and Ni/Co. TH1 and TH2 have slightly higher REE abundances than BK. BK range from slight LREE enrichment to extreme LREE depletion. TH1 differs from TH2 by its higher  $TiO_2$ ,  $K_2O$ ,  $P_2O_5$ , V, Zr, Sr, Y and Zr/Y and by its lower CaO, Cr, FeO/Fe<sub>2</sub>O<sub>3</sub>, and Ti/Zr.

Based on the above criteria, the Geraldton mafic intrusive rocks best approximate Condie's TH group and not

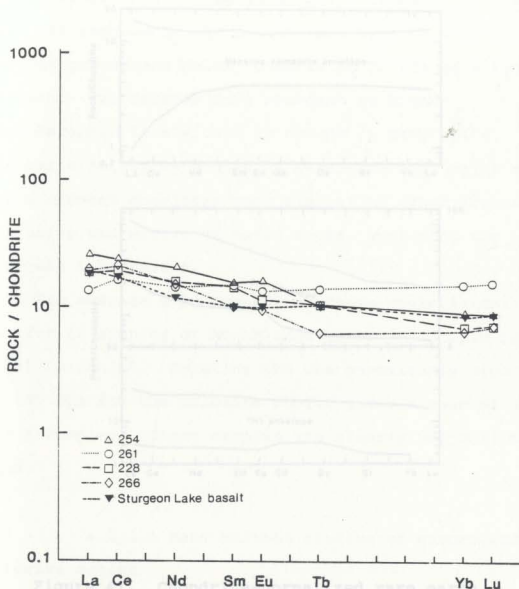


Figure 40. Chondrite-normalized rare earth element plots of mafic intrusive rocks. One sample of Sturgeon Lake basalt (sample collected by J.M. Franklin) is plotted for comparison.

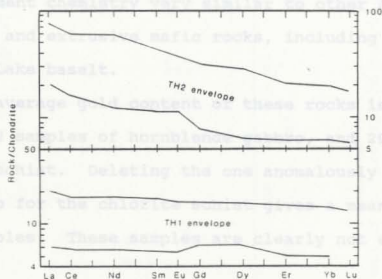
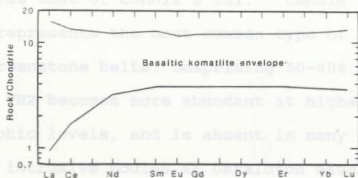


Figure 41. Chondrite-normalized rare earth element plots of a) Archean basaltic komatilitites, and b) Archean tholeiites (after Condie, (1981) pages 93 and 98).

BK. The REE pattern of the Geraldton intrusive rocks best approximates that of Condie's TH1. Condie (1981) states that TH1 represents the most common type of volcanic rock in most greenstone belts, comprising 50-80% of a typical section. TH2 becomes more abundant at higher stratigraphic levels, and is absent in many belts. Thus, the mafic intrusive bodies at Geraldton have major and trace element chemistry very similar to other Archean intrusive and extrusive mafic rocks, including the Sturgeon Lake basalt.

The average gold content of these rocks is only 1.5 ppb for 12 samples of hornblende gabbro, and 29.0 ppb for chlorite schist. Deleting the one anomalously high value of 180 ppb for the chlorite schist gives a mean of 3.8 ppb for 6 samples. These samples are clearly not enriched in gold.

#### 4.2.1.1 Mass balance studies of gabbro and chlorite schist

Table 11 illustrates that there are some obvious geochemical differences between the Geraldton hornblende gabbro and chlorite schist samples. However, the similarity in trace element composition between the gabbro and chlorite schist samples is very clear (a plot of Cr versus MgO and Zr versus  $TiO_2$  is given in Figure 42 for 5 samples of gabbro and 3 of chlorite schist from the Highway 11 Fault Rock outcrops).

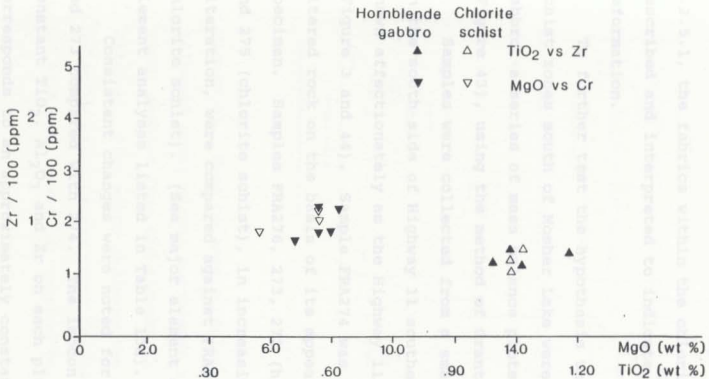


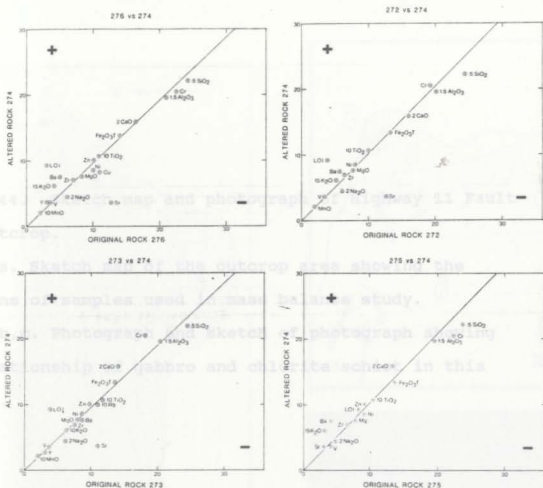
Figure 42. Zr versus  $\text{TiO}_2$  and Cr versus MgO in hornblende gabbro and chlorite schist samples from the Highway 11 Fault Rock Outcrop.

In chapter two the relationships of these rocks in outcrop were described, and it was postulated that the chlorite schists were derived from hornblende gabbro by deformation and alteration. In Chapter 3, section 3.2.5.1, the fabrics within the chlorite schist zones were described and interpreted to indicate dextral shear deformation.

To further test the hypothesis that the chlorite schist zones south of Mosher Lake were derived from the gabbro, a series of mass balance plots were produced (Figure 43), using the method of Grant (1986).

Samples were collected from a small area of outcrop on the south side of Highway 11 southeast of Mosher Lake, known affectionately as the Highway 11 Fault Rock outcrop (Figure 3 and 44). Sample FRA274 was chosen as the most altered rock on the basis of its appearance in hand specimen. Samples FRA276, 273, 272 (hornblende gabbro) and 275 (chlorite schist), in increasing order of apparent alteration, were compared against FRA274 (most altered chlorite schist). (See major element and selected trace element analyses listed in Table 13a).

Consistent changes were noted for samples 276, 272, and 273 compared with 274. The isocon is chosen for constant  $TiO_2$ ,  $Al_2O_3$  and Zr on each plot. This corresponds to an approximately constant  $Fe_2O_3T$ , MnO, MgO, CaO (except 273 vs 274), Ni and V. A slight loss in  $SiO_2$  and  $Na_2O$ , a slight gain in Ba and  $K_2O$ , a large loss of Sr



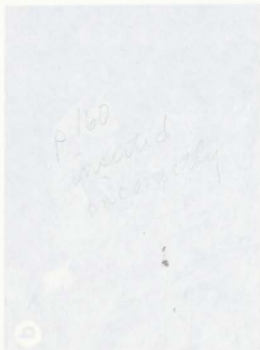
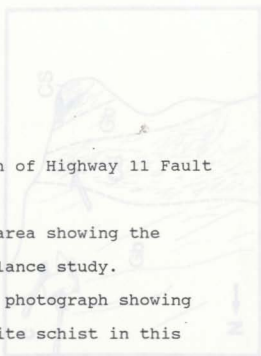
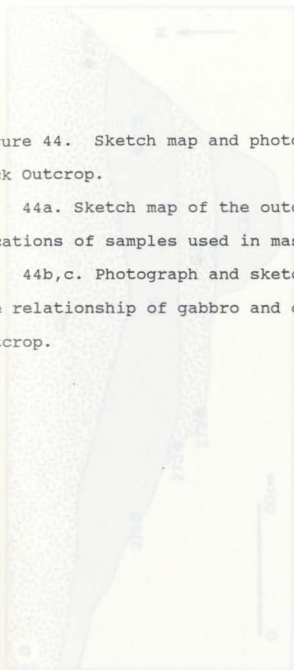
All reactions assuming constant  $\text{TiO}_2$ , Zr,  $\text{Al}_2\text{O}_3$

Figure 43. Mass balance plots of chlorite schist (altered rock) versus hornblende gabbro (unaltered rock) samples from the Highway 11 Fault Rock Outcrop. Plus signs indicate the direction of relative gains, minus signs indicate the direction of relative losses, of components.

Figure 44. Sketch map and photograph of Highway 11 Fault Rock Outcrop.

44a. Sketch map of the outcrop area showing the locations of samples used in mass balance study.

44b,c. Photograph and sketch of photograph showing the relationship of gabbro and chlorite schist in this outcrop.



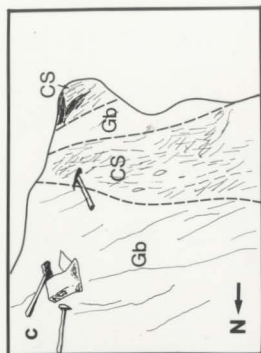
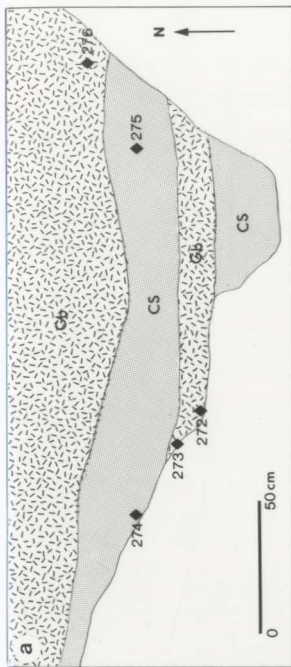


TABLE 13. a) Major element and selected trace element analyses and densities of samples illustrated in mass balance plots (Figure 43). b) Equation of the isocons based on constant  $TiO_2$  and  $Al_2O_3$ .

Sample	272	273	274	275	276
$SiO_2$	48.7	48.9	44.4	47.4	48.3
$TiO_2$	0.99	1.18	1.07	1.03	1.09
$Al_2O_3$	13.40	13.6	13.1	13.0	14.0
$Fe_2O_3$	-	-	-	-	-
FeO	-	-	-	-	-
MnO	0.19	0.20	0.21	0.21	0.20
MgO	7.59	8.03	7.70	7.70	8.30
CaO	8.02	7.06	7.95	6.59	8.24
$Na_2O$	3.03	3.12	2.24	2.37	3.04
$K_2O$	0.34	0.42	0.41	0.21	0.27
$P_2O_5$	0.09	0.10	0.09	0.09	0.10
LOI	3.94	3.91	9.25	8.10	2.98
Total Fe (as $Fe_2O_3$ )	13.29	13.60	13.38	13.60	14.00
TOTAL	99.58	100.12	99.80	100.30	100.52
Density ( $\rho$ )	2.917	2.922	2.795	2.790	2.973
Cu	86	84	82	80	110
Zn	91	98	101	101	101
Ni	80	87	86	90	100
Cr	192	181	205	224	225
Rb	9	11	10	7	10
Sr	127	110	37	30	127
Zr	64	76	70	65	71

272 = slightly sheared gabbro  
 273 = slightly sheared gabbro  
 274 = chlorite schist  
 275 = chlorite schist  
 276 = massive hornblende gabbro

b)

Equation of the isocon through points of equal geochemical concentration:

$$C^A = (M^O/M^A) C^O$$

$$\frac{M^O}{M^A} = \text{Slope of the isocon (from plots).}$$

if constant volume is assumed:

$$C^A = (\rho^O/\rho^A) C^O$$

$$\frac{V^A}{V^O} = \frac{1}{\text{slope}} \times \frac{\rho^O}{\rho^A}$$

I. 276 vs 274  $\frac{M^O}{M^A} = 0.946$   $\frac{\rho^O}{\rho^A} = \frac{2.973}{2.795}$

$$\frac{V^A}{V^O} = 1.057 \times \frac{2.973}{2.795} = 1.124$$

II. 272 vs 274  $\frac{M^O}{M^A} = 1.03$   $\frac{\rho^O}{\rho^A} = \frac{2.917}{2.795}$   $\frac{V^A}{V^O} = 1.013$

III. 273 vs 274  $\frac{M^O}{M^A} = 0.95$   $\frac{\rho^O}{\rho^A} = \frac{2.922}{2.795}$   $\frac{V^A}{V^O} = 1.100$

IV. 275 vs 274  $\frac{M^O}{M^A} = 1.047$   $\frac{\rho^O}{\rho^A} = \frac{2.790}{2.795}$   $\frac{V^A}{V^O} = 0.953$

Note: o = unaltered sample  
 A = altered sample  
 $\rho$  = specific gravity  
 V = volume of sample  
 M = mass of sample

and a large gain in volatiles (LOI) were also noted in all three comparisons of unaltered against the altered sample.

Comparing the two chlorite schist samples, 274 versus 275, almost all components fall on the constant  $TiO_2$ ,  $Al_2O_3$ , Zr isocon (which is very close to the constant mass line) including Sr and volatiles. A slight gain is recorded in CaO, Ba and  $K_2O$ .

In each case of 276, 273 and 272 versus 274,  $TiO_2$ ,  $Al_2O_3$ , MgO,  $Fe_2O_3T$ , Zr, V, and Y all lie on or very close to a line through the origin and therefore probably represent a consistent isocon. In each case the isocon closely approximates the constant mass line, whose slope is 1.00. This is good evidence for the chlorite schist in this outcrop being derived from the gabbro. The order of alteration for these samples from least altered to most altered as indicated by the mass balance studies is;  $276 < 273 \leq 272 < 275 \leq 274$ . The volume factors for these four comparisons are 1.124, 1.100, 1.013, and 0.953 respectively (Table 13b). Thus the most altered samples show a volume decrease compared to the least altered samples. Chemically the most altered samples show an increase in volatiles and loss in Sr. This probably represents a hydration of the rocks during deformation which led to the volume increase, and destruction of the feldspars with resulting loss in Sr.

In comparing the two most altered samples, 275 versus 274 (both chlorite schist), volatiles and Sr both lie on

the isocon, small gains are shown in  $K_2O$ , Ba and CaO. This may reflect the inhomogeneity that these rocks develop when they are most intensely deformed, i.e. chlorite-rich laminae versus quartz-carbonate-feldspar laminae. Sample 275 has lost volume compared to 274 indicating that samples which are most intensely deformed suffer a volume decrease.

#### 4.2.2 Felsic intrusive rocks

The compositions of the felsic intrusive rocks in the Geraldton area were studied; 1) to compare the eastern and the western porphyritic intrusions, 2) to document the changes in these rocks due to alteration, and 3) to comment on the possible association between these rocks and gold mineralization.

The results of analyses of 17 samples of felsic rocks, 12 of the western porphyry (WP) and 5 of the eastern porphyry (EP) are given in Table 14. These rocks were analyzed for major, minor and trace elements, and 5 WP and 2 EP were analyzed for REE (Figure 45). In addition, one sample of the Croll Lake Stock, a large granodioritic pluton to the east of the thesis area (Figure 2) was similarly analyzed.

Table 14. Major and trace element analyses of selected quartz-feldspar and feldspar porphyritic intrusions, Geraldton.

Sample No.	WESTERN PORPHYRIES PORPHYRY HILL					MOSHER-EAST MOSHER- WEST					BANKFIELD					EASTERN PORPHYRIES WOODS-					ROCHE LONGE LAC MAC				
	214	156	221	215	146	220	222	226	259	268	209	202	205	207	208	209	202	205	207	208					
wt % oxides																									
SiO <sub>2</sub>	62.3	63.8	64.1	66.0	64.30	66.90	64.30	63.8	65.0	65.80	64.90	68.50	63.70	65.90	65.50	64.80	65.60	63.70	65.90	65.50					
TiO <sub>2</sub>	17.35	1.33	1.2	1.31	1.32	1.27	1.33	1.34	1.30	1.40	1.38	1.31	1.39	1.35	1.35	1.34	1.36	1.39	1.39	1.35					
Fe <sub>2</sub> O <sub>3</sub>	1.0	15.2	16.36	16.40	15.50	16.20	16.40	15.80	15.10	16.30	14.80	15.10	15.10	16.20	15.50	15.10	15.30	15.00	16.20	15.50					
FeO	2.3	-	1.70	-	-	2.00	-	-	-	-	-	-	-	-	-	-	-	-	-	-					
MnO	0.4	0.3	0.4	0.3	0.3	0.3	0.2	0.3	0.3	0.3	0.4	0.3	0.5	0.6	0.5	0.5	0.5	0.6	0.5	0.7					
MgO	3.86	1.14	3.58	3.09	3.2	3.2	3.2	3.2	3.2	3.2	3.2	3.2	3.2	3.2	3.2	3.2	3.2	3.2	3.2	3.2					
CaO	3.07	4.37	3.30	2.07	3.02	1.31	2.55	3.24	3.79	1.53	2.28	2.30	3.90	3.83	4.58	3.63	4.58	3.63	4.64	4.64					
Na <sub>2</sub> O	5.2	3.19	4.40	6.14	4.77	6.60	3.96	5.00	4.68	5.09	5.69	4.96	4.90	4.58	4.41	5.00	4.58	4.41	5.00	5.43					
K <sub>2</sub> O	2.1	2.1	2.1	2.1	2.1	2.1	2.1	2.1	2.1	2.1	2.1	2.1	2.1	2.1	2.1	2.1	2.1	2.1	2.1	2.1					
P <sub>2</sub> O <sub>5</sub>	0.14	0.09	0.12	0.10	0.08	0.09	0.17	0.11	0.14	0.09	0.10	0.10	0.16	0.15	0.15	0.16	0.18	0.16	0.15	0.16					
L.O.I.	-	5.71	-	3.08	4.13	-	2.92	4.01	4.35	2.78	2.93	2.46	3.00	1.91	2.05	3.11	2.05	3.11	1.48	1.48					
Total Fe (as Fe <sub>2</sub> O <sub>3</sub> )	1.77	2.50	2.41	1.75	3.00	1.74	3.83	1.95	3.69	4.55	1.96	4.04	3.95	5.34	4.24	4.38	4.24	4.38	4.24	4.38					
H <sub>2</sub> O <sup>T</sup>	2.0	1.7	1.40	-	1.4	1.60	-	-	-	-	-	-	2.1	-	-	2.1	-	-	1.5	-					
CO <sub>2</sub> T	3.4	4.8	3.90	-	2.4	3.30	-	-	-	-	-	-	1.6	-	-	1.6	-	-	0.3	-					
S	0.25	0.51	0.00	-	1.23	0.40	-	-	-	-	-	-	0.10	-	-	0.10	-	-	0.13	-					
Au(ppb)	8	214	1	1	4	270	140	172	4	-	-	-	1	10	1	20	12	-	-	-					
Ni(ppm)	6	4	12	1	1	11	3	4	-	3	23	3	15	18	13	16	16	16	16	16					
Cr	7	63	16	27	29	26	2	24	-	12	81	8	64	45	36	51	51	51	51	51					
Co	16	-	9	-	-	7	-	-	-	-	-	-	-	-	-	-	-	-	-	-					
Cu	64	16	3	12	14	17	30	33	14	11	13	23	48	35	55	221	245	245	245	245					
Zn	20	37	55	28	5	54	10	11	31	12	14	16	20	38	31	40	37	40	37	40					
Pb	22	0	23	5	5	19	3	3	7	6	4	4	2	0	10	8	20	8	20	8					
As	64	72	13	-	-	88	-	-	-	-	-	-	-	-	-	-	-	-	-	-					
Rb	64	50	71	55	79	38	96	80	71	81	54	36	52	81	79	68	31	68	31	68					
Sr	242	530	540	561	242	384	319	421	419	260	122	517	812	493	528	932	621	932	621	932					
Y	5	1	8	6	3	7	6	5	1	6	9	4	9	13	9	9	9	9	9	9					
Zr	124	110	127	101	94	96	58	92	58	98	82	85	135	138	121	133	130	133	130	133					
Nb	4	4	4	4	3	6	3	6	3	5	3	4	6	9	7	6	9	7	6	9					
V	5	5	5	5	5	5	5	5	5	5	5	5	5	5	5	5	5	5	5	5					
Ba	890	1052	947	915	643	-	724	353	703	661	444	692	868	481	638	906	638	906	638	906					

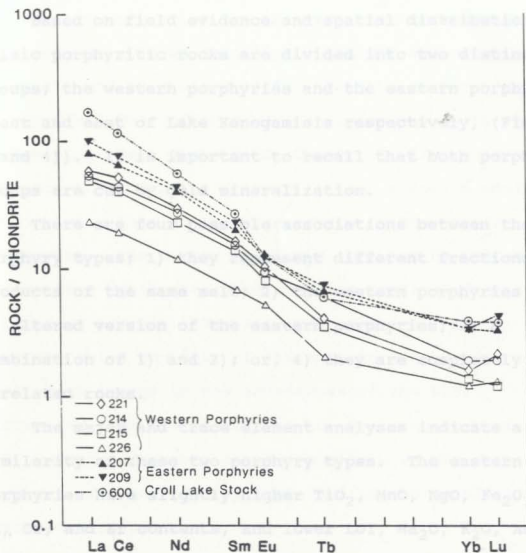


Figure 45. Chondrite-normalized rare earth element plots of felsic porphyritic intrusive rocks, including Eastern Porphyries, Western Porphyries and one sample of the Croll Lake Stock (see Figure 2).

4.2.2.1 Comparison of eastern and western felsic porphyritic rocks

Based on field evidence and spatial distribution the felsic porphyritic rocks are divided into two distinct groups; the western porphyries and the eastern porphyries, (west and east of Lake Kenogamisis respectively, (Figures 3 and 4)). It is important to recall that both porphyry groups are cut by gold mineralization.

There are four possible associations between the two porphyry types; 1) they represent different fractionation products of the same melt; 2) the western porphyries are an altered version of the eastern porphyries; 3) a combination of 1) and 2); or, 4) they are completely unrelated rocks.

The major and trace element analyses indicate a similarity of these two porphyry types. The eastern porphyries have slightly higher  $TiO_2$ ,  $MnO$ ,  $MgO$ ,  $Fe_2O_3T$ ,  $Ni$ ,  $Cr$ , and  $Zr$  contents, and lower  $LOI$ ,  $Na_2O$ ,  $K_2O$ ,  $Au$ , and  $Ba$  contents than the western porphyries. The REE patterns are essentially identical in shape for both groups, but the eastern porphyry has higher abundances.

The similarity of REE patterns suggests that the two porphyry types were generated by a similar petrogenetic process and were probably derived from a similar magmatic source. The similar spatial and timing relationships (similar structural history) of the two porphyry groups also implies that they are probably genetically related,

and therefore that the slight differences in their composition are due to fractionation and/or alteration. The western porphyries are in every location more strongly deformed and altered (based on a greater sericite, carbonate and sulphide content) than the eastern porphyries. The differences in plagioclase phenocryst composition (see probe data, Chapter 2, Figure 23) also suggests an alteration process, either a sodium addition or a calcium loss in the phenocrysts in the western porphyries. The higher  $K_2O$ ,  $Na_2O$ , LOI and Ba contents of the western porphyries also may have resulted from an alteration process. However, the relatively higher ferromagnesian contents of the eastern porphyries, the consistent change in the abundances of the REEs, decreasing from the eastern to the western porphyries, and the presence of quartz phenocrysts only in the western porphyry, are more easily explained as the result of a fractionation process.

A plot of  $Al_2O_3$  versus  $SiO_2$  (Figure 46, not corrected for volatiles) does not show a separation of the two porphyry groups, consistent with the similarity in quartz-feldspar dominant mineralogy of these rocks. On the plot of Cr versus  $Al_2O_3$  (Fig 46f), Cr is negatively correlated with  $Al_2O_3$  and the two populations overlap. In contrast, plots of  $Fe_2O_3T$ , and  $FeOT + MgO$  versus  $SiO_2$  (Figs 46a and c) show two distinct populations, the latter plot showing a distinct separation of the two groups, the EP being more

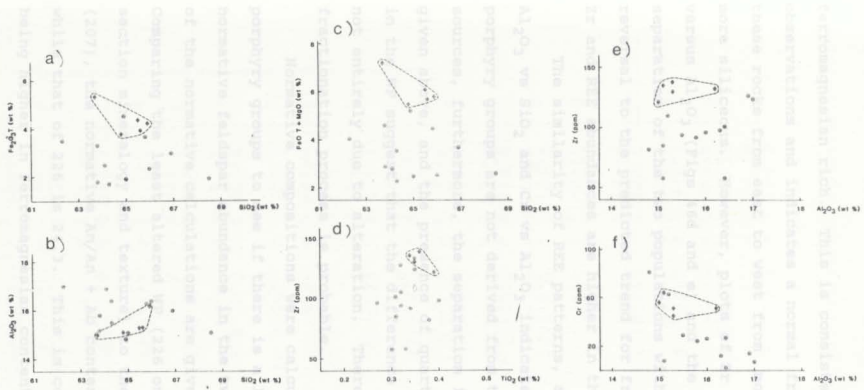


Figure 46. X-Y plots of selected element analyses for comparison of Eastern versus Western porphyries; a)  $Fe_2O_3T$  vs  $SiO_2$ , b)  $Al_2O_3$  vs  $SiO_2$ , c)  $FeOT + MgO$  vs  $SiO_2$ , d)  $Zr$  vs  $TiO_2$ , e)  $Zr$  vs  $Al_2O_3$  and f)  $Cr$  vs  $Al_2O_3$ . The Eastern Porphyries are represented by the diamond-shaped symbol and are outlined by the dashed line. The Western Porphyries are plotted with circles.

ferromagnesian rich. This is consistent with petrographic observations and indicates a normal fractionation trend in these rocks from east to west from more ferromagnesian to more siliceous. However, plots of Zr versus  $TiO_2$  and Zr versus  $Al_2O_3$  (Figs 46d and e) and the REE patterns show a separation of the two populations with an apparent reversal to the predicted trend for fractionation in that Zr and REE abundances are higher in the EP.

The similarity of REE patterns, and relationships of  $Al_2O_3$  vs  $SiO_2$  and Cr vs  $Al_2O_3$  indicates that the two porphyry groups are not derived from two different sources, furthermore, the separation in the other plots given above, and the presence of quartz phenocrysts only in the WP suggest that the difference in the two groups is not entirely due to alteration. Therefore some type of fractionation process is probable.

Normative compositions were calculated for the two porphyry groups to see if there is a large difference in normative feldspar abundance in the two groups. Results of the normative calculations are given in Table 15. Comparing the least altered WP (226 on the basis of thin section mineralogy and texture) to the least altered EP (207), the normative An/An + Ab content of 207 is 27.5 while that of 226 is 24.3. This is consistent with the EP being higher in ferromagnesian content. Total normative feldspar content is greater in the WP than the EP, but the difference is only 5-10%. This is consistent with

Table 15. Calculated normative mineralogy of Geraldton felsic porphyritic intrusive rocks.

Sample Number	011	214	156	221	215	146	220	222	226	259	264	268	209	202	205	207	208
XT <sup>o</sup>																	
Q	15.881	17.791	21.214	18.049	19.808	14.679	10.187	17.470	22.592	20.283	17.723	17.967	20.842	20.248	18.958	20.003	18.928
C	.832	0.0	.654	.657	0.000	0.00	0.0	0.0	0.0	2.253	0.0	0.0	0.0	0.0	0.0	0.879	0.0
OR	13.803	13.299	16.612	13.346	17.715	9.613	26.010	15.531	14.316	17.999	13.440	9.10	8.969	12.702	9.733	9.161	4.989
Al	46.436	46.790	39.158	54.265	43.168	60.536	52.618	44.255	42.216	46.574	49.611	60.448	42.762	39.626	38.372	42.823	46.685
AN	15.115	12.728	17.647	10.044	13.486	7.708	6.783	13.863	14.380	7.247	9.252	5.678	15.333	15.223	16.874	17.236	15.166
Total Fsp	75.374	72.817	72.417	77.655	74.369	77.857	83.411	73.649	70.912	69.82	72.303	75.236	67.064	67.651	64.979	69.22	66.84
AN/AN + AB norm ratio	23.47	20.41	29.81	14.85	22.75	10.72	10.83	22.80	24.30	13.29	14.95	8.13	25.26	26.71	29.30	27.50	23.44
DI	0.0	6.525	0.0	0.0	1.573	0.0	4.036	1.291	3.651	0.0	1.219	4.175	2.617	1.813	2.878	0.0	4.152
HE	0.0	0.0	0.0	0.0	0.0	0.0	0.0	.482	0.0	0.0	.915	0.0	.163	.511	1.533	0.0	1.631
EN	2.43	0.0	1.519	1.015	1.911	2.278	0.0	2.397	.299	2.887	2.329	.212	4.181	4.686	4.838	5.042	3.314
FS	2.097	0.0	0.0	0.0	0.0	1.679	0.0	1.026	0.0	1.858	2.005	0.0	.298	1.515	2.956	1.915	1.493
MT	1.531	0.0	1.535	2.105	0.0	1.186	.185	2.791	.743	2.611	2.809	.508	3.20	2.624	2.773	2.715	2.667
IL	.702	.289	.659	.238	.069	.198	.198	.676	.243	.472	.696	.312	1.754	.524	.703	.673	.598
HV	0.0	1.769	.730	.240	1.872	1.542	1.542	.267	1.215	0.0	0.0	1.394	0.0	1.394	.382	.352	.377
AP	.343	.222	.293	.242	.199	.841	.411	.340	.216	0.0	.235	.427	.383	.427	.382	.352	.377

## Key to Symbols:

Q = quartz  
 C = corundum  
 OR = orthoclase  
 AB = albite  
 AN = anorthite  
 Fsp = feldspar  
 DI = diopside  
 HE = hedenbergite  
 EN = enstatite  
 FS = forsterite  
 MT = magnetite  
 AP = apatite  
 PV = pyrite  
 HV = hematite

petrographic observations that the amount of phenocryst feldspar is not greatly different between the two groups.

On a triangular plot of normative quartz-K-feldspar-plagioclase, the Geraldton feldspar and quartz feldspar porphyries plot in the granodiorite-quartz monzodiorite field of the IUGS (1973) modal mineral classification plot (Figure 47). The normative quartz and plagioclase mineralogy of these rocks appears to be close to their modal composition except in K-feldspar content, which is too high in the normative calculations. The composition of the Geraldton porphyrites would probably be better described as tonalite to quartz diorite.

The REE patterns have no significant Eu anomaly in either EP or WP despite the large amount of modal feldspar in these rocks. The shape of the REE patterns are very similar for each group with a slightly smaller difference in the middle REEs between the EP and the WP than between the heavy REE and the light REE of the two groups (Figure 45). The patterns are typical of those interpreted to be the result of melts formed in the presence of residual garnet (Drury, 1979). The EP are probably the result of slightly higher temperature melting which fused slightly more of each of the residual phases (zircon, biotite and possibly hornblende) without changing the shape of the REE patterns, but only increasing REE, Zr and ferromagnesian abundances. Therefore, the EP and the WP are thought to be derived from varying degrees of partial melting of the

GEFALDTON NORMPLOT - QFP 5

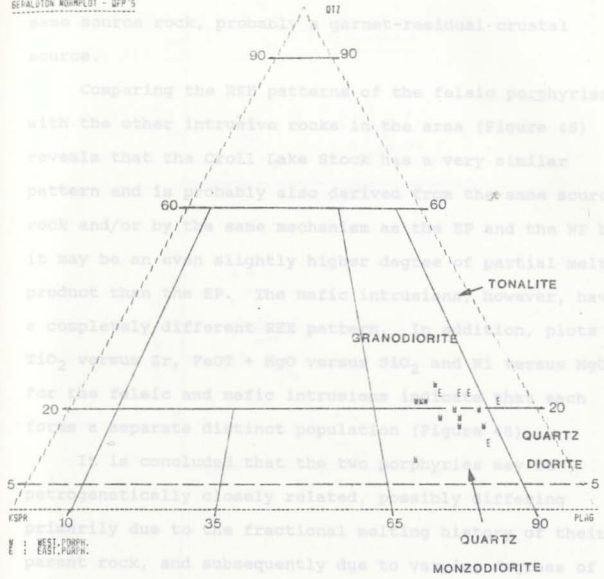


Figure 47. Plot of calculated normative quartz-plagioclase-K-feldspar on an IUGS modal mineral ternary classification plot for plutonic rocks. The normative quartz and plagioclase of the felsic intrusive rocks is close to their modal composition, but the normative K-feldspar is too high. Therefore, these rocks are probably better classified as tonalite and quartz diorite.<sup>8</sup>

The WP are all variably altered, even within single outcrops. The alteration consists of feldspar phenocrysts being altered to almost pure albite, with variable development of sericite, carbonate and quartz. The matrix is variably altered to sericite, carbonate and quartz with some chlorite. These changes imply that the alteration

same source rock, probably a garnet-residual crustal source.

Comparing the REE patterns of the felsic porphyries with the other intrusive rocks in the area (Figure 45) reveals that the Croll Lake Stock has a very similar pattern and is probably also derived from the same source rock and/or by the same mechanism as the EP and the WP but it may be an even slightly higher degree of partial melt product than the EP. The mafic intrusions, however, have a completely different REE pattern. In addition, plots of  $TiO_2$  versus Zr,  $FeOT + MgO$  versus  $SiO_2$  and Ni versus MgO for the felsic and mafic intrusions indicate that each forms a separate distinct population (Figure 48).

It is concluded that the two porphyries may be petrogenetically closely related, possibly differing primarily due to the fractional melting history of their parent rock, and subsequently due to varying degrees of alteration.

#### 4.2.2.2 Alteration of the felsic porphyritic rocks

The WP are all variably altered, even within single outcrops. The alteration consists of feldspar phenocrysts being altered to almost pure albite, with variable development of sericite, carbonate and quartz. The matrix is variably altered to sericite, carbonate and quartz with some chlorite. These changes imply that the alteration

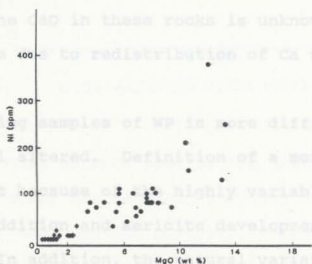
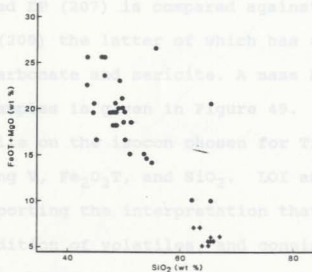
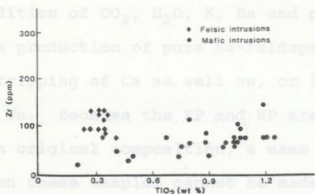


Figure 48. Plots of a) Zr versus TiO<sub>2</sub>, b) FeOT + MgO versus SiO<sub>2</sub>, and c) Ni versus MgO for comparison of felsic and mafic intrusive rocks.

involved addition of  $\text{CO}_2$ ,  $\text{H}_2\text{O}$ , K, Ba and possibly Na, although the production of pure Na-feldspar may be the result of stripping of Ca as well as, or instead of, addition of Na. Because the EP and WP are slightly different in original composition, a mass balance comparison on these samples cannot be made. Instead, the least altered EP (207) is compared against the most altered EP (209) the latter of which has a small amount of secondary carbonate and sericite. A mass balance plot of these two samples is given in Figure 49. Most of the components lie on the isocon chosen for  $\text{TiO}_2$ ,  $\text{Al}_2\text{O}_3$  and Zr, including V,  $\text{Fe}_2\text{O}_3$ , T, and  $\text{SiO}_2$ . LOI and CaO were gained, supporting the interpretation that alteration involved addition of volatiles, and consistent with the petrographic observations for these two samples. The source of the CaO in these rocks is unknown. Losses and gains may be due to redistribution of Ca with  $\text{CO}_2$  alteration.

Comparing samples of WP is more difficult because they are all altered. Definition of a most-altered sample is difficult because of the highly variable amount of carbonate addition and sericite development between outcrops. In addition, the natural variation in the composition of these rocks makes comparing samples from two different outcrop areas somewhat unreliable. For this reason, mass balance comparisons were done on pairs of samples from the same outcrop area (except for one

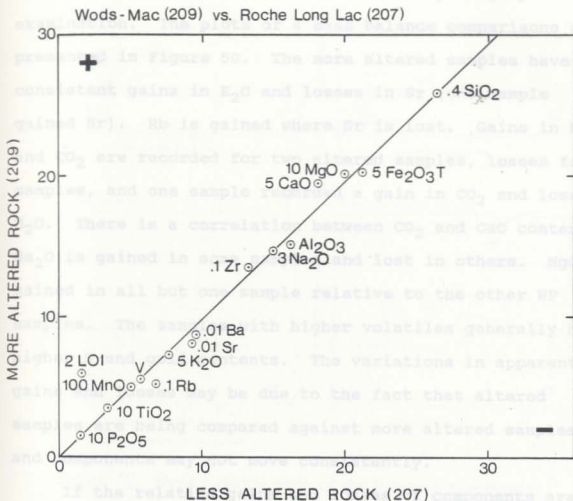


Figure 49. Mass balance plot of two Eastern porphyritic intrusive rocks; the Wods Mac porphyry (sample FRA209), the most altered Eastern porphyry, versus the Roche Long Lac porphyry (sample FRA207) the least altered Eastern porphyry.

comparison, which probably included samples from the same porphyry body), and categorizing less altered versus more altered samples was done on the basis of petrographic examination. The plots of 4 mass balance comparisons are presented in Figure 50. The more altered samples have consistent gains in  $K_2O$  and losses in Sr (one sample gained Sr). Rb is gained where Sr is lost. Gains in  $H_2O$  and  $CO_2$  are recorded for two altered samples, losses for 2 samples, and one sample recorded a gain in  $CO_2$  and loss of  $H_2O$ . There is a correlation between  $CO_2$  and CaO content.  $Na_2O$  is gained in some samples and lost in others. MgO is gained in all but one sample relative to the other WP samples. The samples with higher volatiles generally have higher S and gold contents. The variations in apparent gains and losses may be due to the fact that altered samples are being compared against more altered samples, and components may not move consistently.

If the relative gains and losses of components are compared with the normative  $An/An+Ab$  values for each of these samples (Table 15), there is a consistent correlation between the relative addition of  $Na_2O$  to the rock and its normative albite content. An increase of  $Na_2O$  corresponds to a decrease in the normative  $An/An+Ab$ . There does not seem to be the same correlation with addition of CaO and normative feldspar composition. The behaviour of CaO may be due to variable carbonate composition. The four anomalously high gold samples



(>100ppb) also have lower An/An+Ab normative feldspars (<21).

In summary, the fluids that altered the western porphyritic rocks consistently introduced K and Mg, removed Sr, and generally introduced volatiles, including S, thus hydrating, carbonatizing and pyritizing the WP relative to the EP. CaO increases with CO<sub>2</sub> and Na<sub>2</sub>O is variably lost or gained. The normative feldspar content reflects the Na<sub>2</sub>O gains and losses. Generally Rb is gained and Sr is lost in the more altered samples. Plots of K<sub>2</sub>O versus Al<sub>2</sub>O<sub>3</sub> for the two porphyry groups overlap in Al<sub>2</sub>O<sub>3</sub>, but the WP have higher K<sub>2</sub>O and Sr versus Al<sub>2</sub>O<sub>3</sub> shows the EP to be higher in Sr (Figure 51), supporting the above conclusions.

The presence of abundant sericite alteration indicates that the fluid responsible for the alteration was probably moderately acidic, since both sericite and albite are stable and K-feldspar is not. The albite and oligoclase phenocrysts show alteration to sericite, suggesting that sericitization continued after albite formation. The fluid was also CO<sub>2</sub>, K<sup>+</sup>, Mg<sup>++</sup> and S - bearing, and mobilized Na<sub>2</sub>O. The loss of Sr and gain in Rb reflect the destruction of feldspar and development of mica as observed petrographically. A very significant indicator of alteration in the WP is the presence of unzoned, almost pure albitic feldspar, with sericite and carbonate. Evidently the alteration process involved

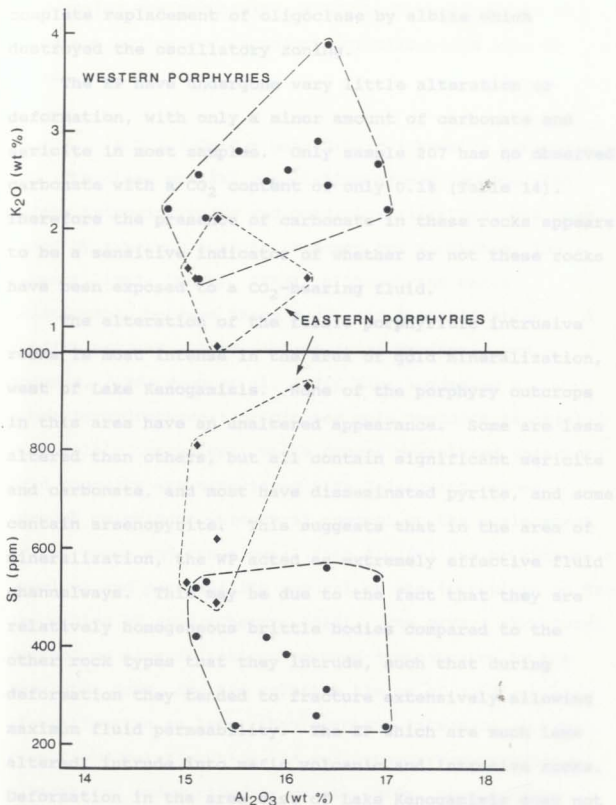


Figure 51. Plots of  $K_2O$  and Sr versus  $Al_2O_3$  for Eastern versus Western felsic porphyritic intrusive rocks. Data for the Eastern porphyries are plotted as diamonds and outlined with short dashes. Data for the Western porphyries are plotted with circles and outlined with long dashes.

complete replacement of oligoclase by albite which destroyed the oscillatory zoning.

The EP have undergone very little alteration or deformation, with only a minor amount of carbonate and sericite in most samples. Only sample 207 has no observed carbonate with a  $\text{CO}_2$  content of only 0.1% (Table 14). Therefore the presence of carbonate in these rocks appears to be a sensitive indicator of whether or not these rocks have been exposed to a  $\text{CO}_2$ -bearing fluid.

The alteration of the felsic porphyritic intrusive rocks is most intense in the area of gold mineralization, west of Lake Kenogamisis. None of the porphyry outcrops in this area have an unaltered appearance. Some are less altered than others, but all contain significant sericite and carbonate, and most have disseminated pyrite, and some contain arsenopyrite. This suggests that in the area of mineralization, the WP acted as extremely effective fluid channelways. This may be due to the fact that they are relatively homogeneous brittle bodies compared to the other rock types that they intrude, such that during deformation they tended to fracture extensively allowing maximum fluid permeability. The EP which are much less altered, intrude into mafic volcanic and intrusive rocks. Deformation in the area east of Lake Kenogamisis does not appear to have been as intense as in the west, and in addition, much of the deformation in this area may have been taken up by the less competent mafic rocks

surrounding the porphyries, allowing them to remain as competent bodies and therefore not allowing access to fluids.

4.2.2.3 Gold - porphyritic intrusion association

The close spatial association between porphyritic felsic intrusive rocks and gold mineralization, has been noted by numerous authors (Hodgson and MacGeehan, 1982; Marmont, 1983; Cherry, 1983), although the exact relationship between these rocks and mineralization remains unclear. Some authors (e.g. Macdonald and Hodgson, 1986; Wood et al, 1986) have suggested a magmatic-hydrothermal origin for gold deposits associated with felsic intrusions, while others postulated that some gold deposits are associated with felsic intrusions through coincident structural control on the emplacement of the magma and the mineralizing fluids, and/or through a chemical and permeability control by the intrusions on the deposition of gold (Cherry, 1983). The strong structural control on mineralization has been demonstrated in the Geraldton area, and the relative timing of gold mineralization as later than porphyry intrusion is obvious from field relationships, as sericite-carbonate-pyrite alteration, and auriferous quartz veins, crosscut the felsic porphyritic intrusions. However, the absolute timing of magma emplacement and gold mineralization must be known before the exact relationship of these rocks may

be determined. For this reason, isotopic studies including U/Pb zircon dating of the felsic intrusions, and Pb isotope analyses of pyrite from mineralized areas, were undertaken to try to resolve the absolute timing of magmatism and mineralization and therefore to determine the relationship between gold mineralization and the felsic intrusive rocks in the Geraldton area.

#### 4.3 Isotopic studies

##### 4.3.1 Uranium-lead zircon dating of a felsic

##### porphyritic intrusion

The Wods Mac porphyry (sample 209, see Figure 2) was chosen for U/Pb zircon dating as it is close to the main area of mineralization, but it appears to be only slightly altered, and good euhedral zircons were observed in thin section. Approximately 20 kilograms of this rock were collected and submitted to the Geochronology Laboratory of the Geological Survey of Canada. Procedures used for the concentration of zircon and preparation of zircon fractions, chemical extraction of U and Pb from zircon and isotopic analyses of U and Pb are described in van Breemen et al (1986). The uranium decay constants and isotopic composition recommended by Steiger and Jaeger (1977) were used to calculate the U/Pb ages.

The zircon concentrate from sample 209 consisted of relatively uniform purple, translucent, euhedral finely

zoned crystals. Some crystals have small overgrowths of a clearer, lighter colour on their terminations, while a few have multiple terminations. Some crystals have darker, purplish inner zones, but most are uniform. Polished sections of grain mounts were etched with HF fumes to determine if these zircons contained inherited cores. Zoning is continuous from the central area into the clear overgrowths and therefore the central darker areas represent a U-rich zone and not an inherited core. The length to width ratios generally fall into the 3:1 to 4:1 range but many of the crystals are broken, especially in the larger fractions. Clear bubble inclusions and fractures are common.

The zircons were sieved and hand-picked into three fractions. Five fractions were then analyzed, two abraded (Krogh, 1982) and three not abraded; all compositions lie below concordia. The analytical results are presented in Table 16 and the concordia diagram is given in Figure 52. Regression analysis yields upper and lower intercept ages of  $2691 \pm 3/-2$  Ma and  $328 \pm 79/-74$  Ma. The continuous growth zoning, euhedral habit and absence of inherited cores in these zircons indicate crystallization from a cooling silicate melt. Therefore the upper intercept age is interpreted as the age of intrusion of the Wods Mac feldspar porphyry.

For comparison, a U/Pb zircon age was determined for a porphyritic rhyolite from northwest of the the Onaman

TABLE 16: U/Pb zircon analytical results, G = Wods Mac Porphyry, sample 209, OL = Onaman Lake Rhyolite

Label	Size Fraction	Wt (mg)	U (ppm)	Pb (ppm)	Measured $^{206}\text{Pb}/^{238}\text{Pb}$	Isotopic Abundances			Isotopic ratios		Age (Ma) $^{207}\text{Pb}/^{235}\text{Pb}$
						$^{238}\text{Pb}$	$^{207}\text{Pb}$	$^{206}\text{Pb}$	$^{206}\text{Pb}/^{238}\text{U}$	$^{207}\text{Pb}/^{235}\text{U}$	
G-1	-105,74 A	0.019	301.5	167.0	2328	0.0107	18.526	8.961	0.50685	12.856	2689
G-2	-105,74 A	1.54	228.8	123.6	1842	0.0435	18.853	11.160	0.49041	12.390	2682
G-3	-105,74	0.68	733.6	390.1	3234	0.0220	18.557	10.843	0.48129	12.136	2679
G-4	-74+62	3.15	297.0	157.8	6331	0.0120	18.459	11.133	0.47837	12.078	2681
G-5	-62+35	3.17	245.3	129.1	5380	0.0174	18.503	12.040	0.47127	11.885	2679
OL-1	-105,74 A	0.38	105.0	64.40	1362	0.0166	19.429	18.797	0.51799	13.734	2762
OL-2	-74+62 A	0.69	179.5	110.07	1172	0.0651	19.961	22.366	0.51054	13.501	2758
OL-3	-105,74	1.21	260.4	147.6	767	0.1213	20.398	23.809	0.47360	12.366	2737
OL-4	-74+62	1.11	2239	124.7	634	0.1356	20.572	25.078	0.46247	12.073	2736

Note: A = abraded fraction

Figure 52. Concordia diagram for U/Pb zircon analysis of the Wods Mac porphyry (sample 209) and the Onaman Lake rhyolite volcanic (sample 16). The analytical results are presented in Table 16.

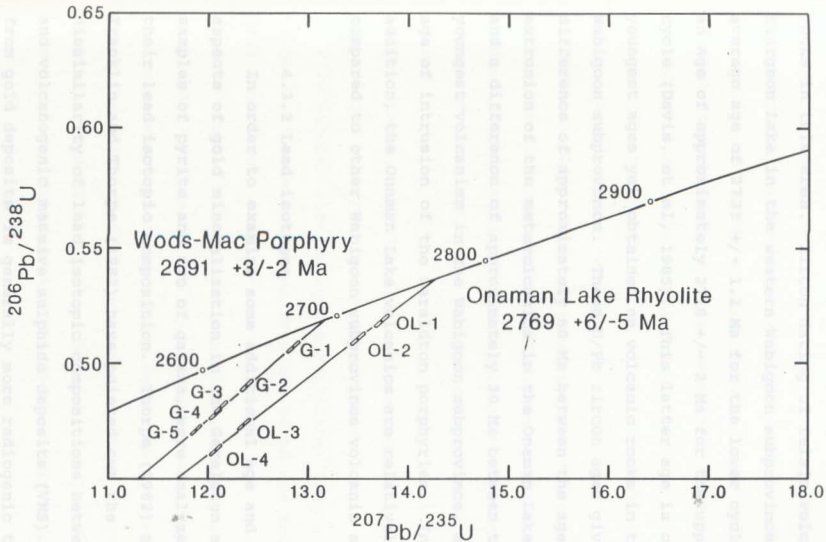


Figure 52. Concordia diagram for U/Pb zircon analyses of the Wods-Mac porphyry (sample FRA209) and the Onaman Lake rhyolitic volcanic (sample FRA602). The analytical results are presented in Table 16.

Lake area, north of the Beardmore-Geraldton belt (Figure 1a). This gave an age of  $2769 \pm 5$  for the metavolcanic rocks in this area. Zircon dating of felsic volcanism at Sturgeon Lake in the western Wabigoon subprovince gives an average age of  $2735 \pm 1.2$  Ma for the lower cycles, and an age of approximately  $2718 \pm 2$  Ma for the uppermost cycle (Davis, et al, 1985). This latter age is one of the youngest ages yet obtained on volcanic rocks in the Wabigoon subprovince. These U/Pb zircon ages give a difference of approximately 80 Ma between the age of extrusion of the metavolcanics in the Onaman Lake area, and a difference of approximately 30 Ma between the age of youngest volcanism in the Wabigoon subprovince, and the age of intrusion of the Geraldton porphyries. In addition, the Onaman Lake volcanics are relatively old compared to other Wabigoon subprovince volcanic sequences.

#### 4.3.2 Lead isotopes

In order to examine some additional age and genetic aspects of gold mineralization in the Geraldton area, 14 samples of pyrite and two of galena, were analyzed for their lead isotopic composition. Thorpe (1982) and Franklin and Thorpe (1982) have pointed out the dissimilarity of lead isotopic compositions between gold and volcanogenic massive sulphide deposits (VMS). Galena from gold deposits is generally more radiogenic than galena from VMS deposits. Franklin et al (1983) noted

that the lead isotopic composition of pyrite in most massive sulphide deposits is close to that for galena from the same deposits, but in gold deposits, pyrite samples have comparatively radiogenic compositions; in some of these deposits these latter samples yield a linear array of isotopic compositions that is amenable to interpretation by conventional two-stage techniques.

Samples were selected to examine several types of gold mineralization including:

- 1) Three samples of disseminated pyrite from gold zones within the albite porphyry bodies; one of these bodies (sample 202) is similar to the porphyry body that is the source of the zircons for the age determination discussed above;
- 2) One sample of pyrite from an intermediate intrusion mineralized with pyrite and arsenopyrite.
- 3) Five samples (including one replicate) from a zone of sulphidized iron formation from the North Ore Zone of the Hard Rock Mine;
- 4) Five samples from the Solomons Pillar's deposit, a small gold occurrence which is a fracture-controlled pyrite-arsenopyrite replacement zone totally within iron formation, similar to but much smaller than (3);
- 5) Galena from two deposits within the Geraldton district (the Bankfield Mine and the Bema Property at Watson Lake).

#### 4.3.2.1 Lead isotope methods

The samples of galena and pyrite were mechanically separated from the silicate portions of the rock by a combination of magnetic and super-panner methods. The samples were analyzed by Geospec Consultants Ltd., Edmonton, Alberta. They were prepared by dissolving a small amount in 10 ml of high purity 2N HNO<sub>3</sub>, and evaporating the solution slowly until Pb(NO<sub>3</sub>)<sub>2</sub> crystallized. The crystals were extracted from the solution, washed in 4N HCl, dried and dissolved in water. An aliquot of 1 to 2 micrograms was loaded onto a rhenium filament in a silica gel-phosphoric acid mixture and analyzed on a Micromass MM-30 mass spectrometer. The data are presented in Table 17. A discussion of the errors associated with the lead isotope analyses is included as Appendix C.

Data sets which form distinctive linear arrays were subjected to linear regression using the method of York (1969). Upon inspection of the data, linear arrays were subjected to two-stage calculations following the method of Russell and Farquhar (1960). Model ages were calculated using the Stacey-Kramers (1975) model and models developed by Thorpe (pers. comm, 1986) using a set of galena analyses from massive sulphide deposits from the Abitibi belt and the western Superior subprovince for which the ages are well constrained by U-Pb (zircon) age determinations.

**TABLE 17: Lead isotope analyses**

Sample No.	Deposit	Mineral	Pb isotope ratios			
			206/204	207/204	208/204	
83FRA	-235	Bema, Watson L.	gn	16.122	15.383	35.364
	-202	Roche Long Lac	py	17.306	15.514	36.818
	-212A	Hard Rock Mine	py	15.749	15.196	35.289
	-212B	Hard Rock Mine	py	16.250	15.238	35.921
	-212C	Hard Rock Mine	py	15.362	15.041	34.977
	-212D	Hard Rock Mine	py	16.345	15.297	36.008
	-214	Porphyry Hill	py	21.050	16.150	39.214
	-215	Mosher Hydroline	py	19.168	15.833	38.002
	-327	Ashmore	py	18.189	15.688	37.927
	-366	Solomons Pillars	py	15.026	15.051	34.731
	-369	Solomons Pillars	py	14.947	15.005	34.541
	-370	Solomons Pillars	py	14.929	14.980	34.459
	-380	Solomons Pillars	py	15.683	15.068	35.275
	-382	Solomons Pillars	py	15.608	15.283	35.315
	TQ82	-130	Bankfield Mine	gn	13.910	14.793

#### 4.3.2.2. Theory of lead isotopes

The theory of lead isotopes has been discussed by Franklin et al (1983) and is treated in detail by Russell and Farquhar (1960) and Faure (1977) and will only briefly be discussed here.

Lead in any mineral is a mixture of isotopes;  $^{204}\text{Pb}$ ,  $^{206}\text{Pb}$ ,  $^{207}\text{Pb}$  and  $^{208}\text{Pb}$ , the latter three of which are the radiogenic isotope end products of radioactive decay of  $^{238}\text{U}$ ,  $^{235}\text{U}$  and  $^{232}\text{Th}$  respectively.  $^{204}\text{Pb}$  has no known parent isotope. The abundances of the radiogenic isotopes have increased with time and therefore so have the ratios  $^{206}\text{Pb}/^{204}\text{Pb}$  (6/4),  $^{207}\text{Pb}/^{204}\text{Pb}$  (7/4), and  $^{208}\text{Pb}/^{204}\text{Pb}$  (8/4). Very old lead-bearing minerals that have remained isolated from U and Th since they were formed will have the smallest ratios.

In a single-stage model,  $^{206}\text{Pb}/^{204}\text{Pb}$ ,  $^{207}\text{Pb}/^{204}\text{Pb}$ , and  $^{208}\text{Pb}/^{204}\text{Pb}$  grow along curved paths from a starting point ( $a_0$ ,  $b_0$ ,  $c_0$ ) representing primeval lead. The growth curve that the sample follows depends on the initial starting composition, and the U/Pb and Th/Pb ratios of the host environment. If a Pb-bearing mineral (eg galena), evolved from primeval material, was separated from its parent U and Th at a given time,  $t$ , and remained a closed chemical system with no subsequent addition of radiogenic lead, this galena will have a unique 7/4 vs 6/4 set of ratios and from this the age of separation may be

calculated assuming a  $t_0$ , or age of formation of the Earth, and a primeval lead starting composition ( $a_0$ ,  $b_0$ ,  $c_0$ ).

However, a simple single-stage model in which all the lead is derived from the mantle does not account for complex crustal and mantle interactions, remelting of crustal material, or geophysical evidence of considerable inhomogeneity in the upper mantle (Franklin et al, 1983). Three models have recently been proposed which attempt to reconcile geological considerations, and yield reasonable agreement between model lead ages and independently determined wallrock ages; a) Cumming and Richards (1975), b) Stacey and Kramers (1975), which will be used in this study and c) Doe and Zartman (1979). In addition, models are being developed by Thorpe (1986, pers. comm.) for specific areas in the Superior subprovince (see above).

Galena and pyrite were the minerals chosen for lead isotopic analysis in this study. Galenas are high lead-bearing minerals which are not strongly affected by addition of radiogenic lead. Because of the amount of lead in these minerals they are most likely to have formed at the time of mineralization. Although model ages for galenas from gold deposits may be difficult to determine, the lead in the galena may be a relatively good indicator of the composition of lead in the mineralizing fluid. Model ages may be valid for these minerals, providing that a model consistent with the composition of the source

rocks for the lead can be applied. However, most lead isotope models have been generated for volcanogenic massive sulphide deposits, where the processes of ore formation and source of fluids and metals are better constrained than models for gold deposits.

Lead in pyrite is a relatively minor component and therefore the lead isotopic composition is more readily subject to modification after crystallization of the pyrite by radiogenic addition of Pb from included U and Th. The problem of source of the common lead, U and Th is much greater with pyrites because the source of these components could include both the immediate wall rocks and/or the mineralizing fluid.

Often, lead isotopic compositions form linear arrays on plots of  $^{207}\text{Pb}/^{206}\text{Pb}$  versus  $^{206}\text{Pb}/^{204}\text{Pb}$  (7/4 vs 6/4), and  $^{208}\text{Pb}/^{204}\text{Pb}$  versus  $^{206}\text{Pb}/^{204}\text{Pb}$  (8/4 vs 6/4). Colinear anomalous leads may be interpreted in several ways:

1. as a mixture of two (or more) ordinary leads, a mixing line;
2. a two-stage, or secondary isochron, lead; and,
3. multistage leads, and repetition of the two-stage process.

1. A mixture of two ordinary leads (a binary mixing line) results from mixing two homogeneous leads, one relatively non-radiogenic, the other more radiogenic. Binary mixing lines are normally very short as it would require one very radiogenic lead composition to get an

extensive binary mixing line. A long binary mixing line would only be formed in a uranium deposit, where there is a substantial amount of U to generate a large radiogenic component.

2. Two-stage and, 3. multistage leads; These result from radiogenic addition of Pb that formed in varying U/Pb environments, to a single common lead composition. The repetition of this process gives rise to multistage leads. To interpret a secondary isochron by conventional two-stage analysis requires that either  $t_1$  (time of addition of U and Th to the common lead component) or  $t_2$  be fixed based on independent age estimates or otherwise geologically reasonable criteria. In addition, two specialized limiting cases may be examined;  $t_{\max}$ , when there has been continuous addition of radiogenic lead to the present and  $t_2$  is therefore set to 0; and,  $t_{\min}$  (or  $t_{\text{instantaneous}}$ ) which indicates that U and Th were added to the mineral sometime before, and removed sometime after, this calculated time. This latter calculation is a limiting case only and has virtually no significance in the case of pyrite.

#### 4.3.2.3 Discussion of the lead isotope data

##### I. Model ages

Model lead ages were calculated using both the Stacey-Kramers model and the models of Thorpe (per comm,

1986) for all minerals analyzed. The results are presented in Table 18. As outlined above, model ages determined on galenas are much more reliable than those determined on pyrite because the former are very lead-rich minerals and therefore are not very susceptible to modification by radiogenic addition of lead.

The model ages on the Bankfield sample give a range of ages from 2474 Ma by Thorpe's Abitibi model, to 2563 Ma by the Stacey-Kramer's model. These are relatively young ages which may indicate time of emplacement of this galena (ie. time of removal of the lead from its parent U and Th). The Bema sample gives ages ranging from 1360 Ma to 1512 Ma which are interpreted to be too young to represent age of formation of the galena and are therefore anomalous. However, so little is known about the conditions under which the lead minerals in gold deposits were formed, for example the source of the fluids or the lead, that it makes the application of any model age system suspect.

The galena samples from the immediate Geraldton area have moderately to very radiogenic compositions. The sample from the Bema property has a composition close to the main cluster of pyrite samples from iron formation-hosted deposits (this sample comes from a small vein cutting chert oxide iron formation). The sample from the Bankfield Mine is much less radiogenic, and is at the top end of the main cluster of galena compositions for

TABLE 18. Model lead ages

Sample location & no.		Mineral	Model: Stacey-Kramers (1975)	Thorpe (pers. comm., 1986)	
				Abitibi	Western Superior
Bankfield	TQ82-130	gn	2563	2474	2516
Bema	FRA83-235	gn	1512	1360	1402
Roche Long Lac	FRA83-202	py	827	645	690
Mosher	FRA83-215	py	0	-331	-282
Porphyry Hill	FRA83-214	py	-555	-1319	-1263
Ashmore	FRA83-327	py	500	0	254
Hard Rock	FRA83-212A	py	1497	1442	1486
	FRA83-212B	py	1150	1113	1158
	FRA83-212C	py	1555	1576	1620
	FRA83-212D	py	1184	1104	1149
Solomon's Pillars	FRA83-366	py	1884	1841	1884
	FRA83-369	py	1876	1857	1900
	FRA83-370	py	1848	1847	1890
	FRA83-380	py	1314	1359	1403

Superior Province gold deposits (Figures 53 and 54); deposits in this cluster yield model ages in the 2700 to 2550 Ma range (Thorpe, 1982; Franklin and Thorpe, 1982). The Bankfield is a relatively big deposit compared to Bema which is a small occurrence, and therefore, more lead may have been derived from the mineralizing fluid at the Bankfield than at Bema where wallrock lead may be a more significant component.

#### Pyrites

All of the model ages on the pyrites are anomalous, particularly the pyrites in the felsic porphyritic rocks, two of which give "future" model ages (Table 18).

#### II. Secondary isochrons on pyrite samples

On plots of  $^{207}\text{Pb}/^{204}\text{Pb}$  versus  $^{206}\text{Pb}/^{204}\text{Pb}$  and  $^{208}\text{Pb}/^{204}\text{Pb}$  versus  $^{206}\text{Pb}/^{204}\text{Pb}$  the pyrite data clearly fall into two distinct populations; a) the felsic and intermediate intrusive rocks and, b) iron formation (Figures 54 and 55).

##### a) Felsic and intermediate intrusive rocks:

The isotopic compositions of these samples are clearly anomalous. They are far too radiogenic to be interpreted as representing a primary isochron or a simple single-stage lead isotopic evolution. Initial inspection of the 7/4 vs 6/4 plot shows a general colinearity of the four intrusive rocks, however, the intermediate, Ashmore, intrusion (sample 327), is slightly different. The 8/4 vs

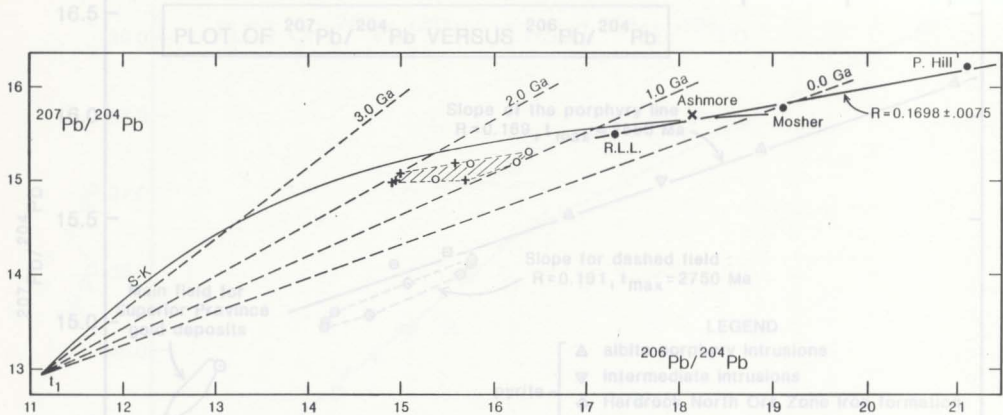


Figure 53. Geraldton lead isotope data superimposed on a Stacey-Kramers (1975) growth curve and selected isochrons. The iron formation data is plotted with crosses (Solomon's Pillars) and open circles (Hard Rock), the porphyry data is plotted with closed circles, and the one intermediate intrusive sample is plotted with an "x" (see Figures 54 and 55). galena showing the main field for Superior Province massive sulphides and gold deposits (Franklin and Thorpe, 1982).

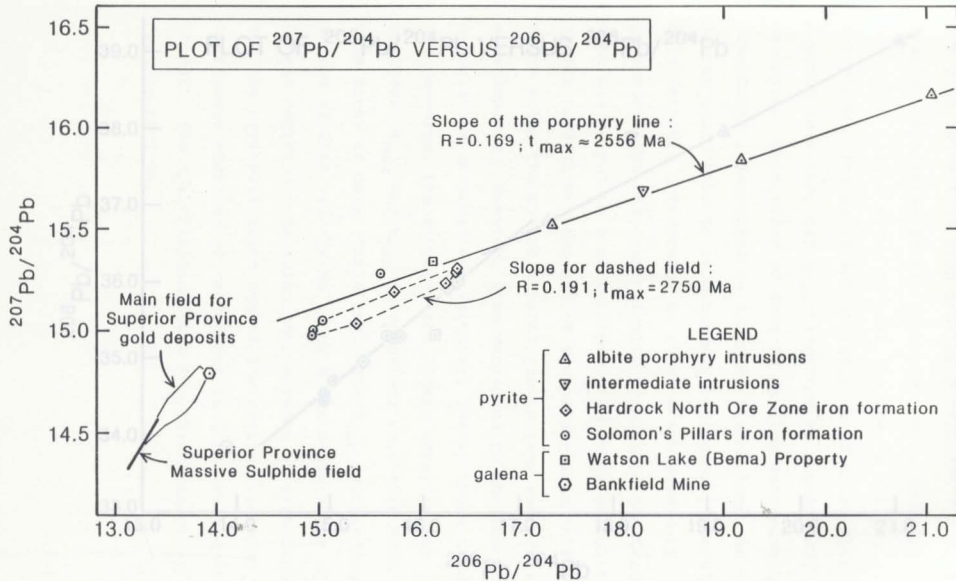


Figure 54.  $^{207}\text{Pb}/^{204}\text{Pb}$  versus  $^{206}\text{Pb}/^{204}\text{Pb}$  plot of lead isotope analyses of pyrites and galena showing the main field for Superior Province massive sulphides and gold deposits (Franklin and Thorpe, 1982).

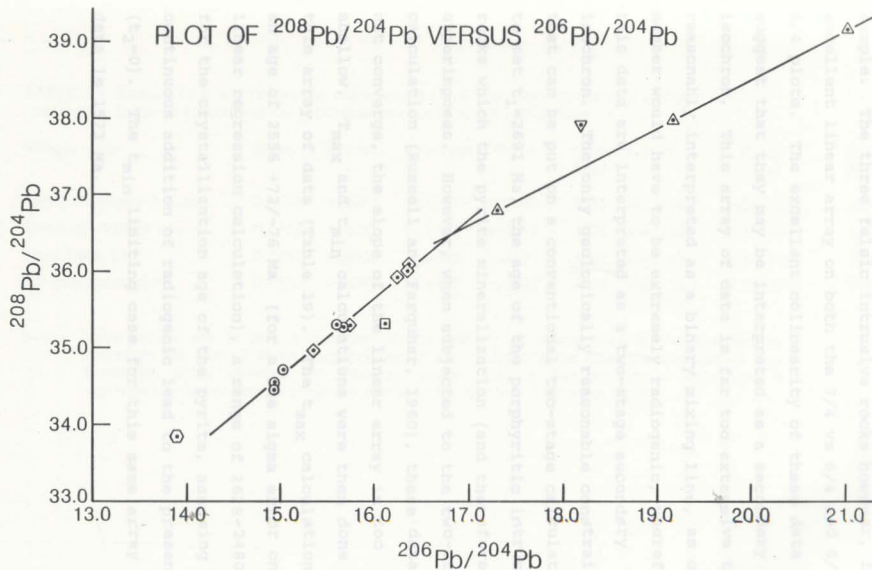


Figure 55.  $^{208}\text{Pb}/^{204}\text{Pb}$  versus  $^{206}\text{Pb}/^{204}\text{Pb}$  plot of lead isotope analyses.

6/4 plot reveals an even greater difference for this sample. The three felsic intrusive rocks however, form an excellent linear array on both the 7/4 vs 6/4 and 8/4 vs 6/4 plots. The excellent colinearity of these data suggest that they may be interpreted as a secondary isochron. This array of data is far too extensive to be reasonably interpreted as a binary mixing line, as one end member would have to be extremely radiogenic, therefore, this data are interpreted as a two-stage secondary isochron. The only geologically reasonable constraint that can be put on a conventional two-stage calculation is to set  $t_1=2691$  Ma, the age of the porphyritic intrusive rocks which the pyrite mineralization (and therefore gold) superimposes. However, when subjected to the two-stage calculation (Russell and Farquhar, 1960), these data do not converge, the slope of the linear array is too shallow.  $T_{\max}$  and  $t_{\min}$  calculations were then done on this array of data (Table 19). The  $t_{\max}$  calculation gave an age of  $2556 \pm 72/-76$  Ma (for a one sigma error on the linear regression calculation), a range of 2628-2480 Ma, for the crystallization age of the pyrite, assuming continuous addition of radiogenic lead to the present ( $t_2=0$ ). The  $t_{\min}$  limiting case for this same array of data is 1573 Ma.

**TABLE 19.** Results of linear regression calculations for a two-stage continuous addition secondary isochron (tmax) and for a t-instantaneous (tmin) limiting case

Sample suite	Slope	/ Error	Intercept	/ Error	tmax (Ma)	/ Error	Range (Ma)	tmin (Ma)
Felsic Porphyry-3 points	0.1699	±.0075	12.5751	±.0060	2556	+72/-76	2628-2480	1573
Solomon's Pillars I.F.	0.1718	±.0057	12.4575	±.0217	2576	+54/-57	2630-2519	1587
Hard Rock I.F.	0.2232	±.0060	11.6384	±.0191	3002	+44/-42	3046-2960	1931
All Iron Formation	0.1910	±.0040	12.1422	±.0102	2750	+28/-36	2778-2714	1713

Note: slope errors are in part a function of the number of points used in the calculation, therefore the line of three porphyry points has a higher error than the clusters of iron formation data, whereas the intercept error reflects the scatter of data and is significantly lower for the porphyry line than for the iron formation data.

b) Iron formation: were introduced into the pyrite from

The iron formation pyrite samples are from sulphide replacement zones in oxide iron formation from a) the North ore zone of the Hard Rock Mine and b) from the Solomon's Pillars property, a small showing northwest of Jellicoe. The iron formation data are collectively less radiogenic than that of the porphyries, and the compositions are more scattered on the  $^{207}\text{Pb}/^{204}\text{Pb}$  vs.  $^{206}\text{Pb}/^{204}\text{Pb}$  plot. The calculated present-day  $^{232}\text{Th}/^{238}\text{U}$  of the porphyries is 2.2 while that of the iron formation is 3.8 (calculated by method shown in Faure, 1977). However they still form a broad linear trend, (Figure 54) with a slope similar to that for the data for the pyrite samples from the porphyry-hosted mineralization. The data from Solomon's Pillars give a calculated  $t_{\text{max}}$  of 2576 Ma, very similar to that for the porphyry line (Table 19).

The scatter of data in the iron formation may represent a common lead component that originated by binary mixing of lead from the chemical and clastic components of these rocks. The samples from the Solomon's Pillars deposit include the least radiogenic pyrite of this study. On the  $^{208}\text{Pb}/^{204}\text{Pb}$ - $^{206}\text{Pb}/^{204}\text{Pb}$  plot (Figure 55), they define a linear trend which is broadly coincident with the data for the samples from the Hard Rock Mine. The Hard Rock deposit is substantially larger than the Solomon's Pillars occurrence, and the more radiogenic nature of the lead in the former may indicate

that more U and Th were introduced into the pyrite from the mineralizing fluid at the Hard Rock than at Solomon's Pillars. The oldest of which is significantly younger than

Although the data for both the Hard Rock and Solomon's Pillars deposits cannot be collectively subjected to rigorous two-stage analysis, the similar slope of the Solomon's Pillars data to that of the porphyries indicates that radiogenic addition was produced from the same starting time as for the porphyry samples. The samples from the two iron formation deposits share a common  $^{208}\text{Pb}/^{204}\text{Pb}$  vs  $^{206}\text{Pb}/^{204}\text{Pb}$  line which is very distinct from the line for the porphyries (Figure 55), indicating that the U/Th ratio of the iron formation pyrites was very different from the felsic porphyry pyrites. Therefore, the immediate host rocks appear to be the major controlling factor on the lead isotopic composition of the pyrite, as there is no reason to assume two entirely different mineralizing systems in the felsic porphyries and the iron formation samples from the district.

than the main field of galena from Superior Province gold deposits (Figure 54) (Franklin and Charpe, 1982).  
4.3.3 Implications of U/Pb zircon and Pb isotope results for genetic models of gold deposits

Taking the continuous addition model as being the most reasonable interpretation of the secondary isochron of the pyrite in the felsic porphyritic intrusive rocks, gives an age of crystallization of the pyrite of 2560 Ma.

Taking into account a one sigma error on the linear regression calculation gives a range of ages of 2628 to 2480 Ma, the oldest of which is significantly younger than the crystallization age of the felsic porphyritic intrusive rocks determined by U/Pb zircon dating to be 2691  $\pm$  3/-2 Ma. This indicates a significant difference in time of magmatism and time of emplacement of gold of between 63 and 211 Ma with a best estimate around 130 Ma. Therefore, the mineralization is not a product of a magmatic-hydrothermal system associated with these porphyries.

The Stacey-Kramers (1975) model age of 2563 Ma on the Bankfield galena is consistent with the calculated continuous addition secondary isochron age of the pyrites in the porphyries, as is the calculated secondary isochron age of 2576 Ma of the pyrites from the Solomon's Pillars property.

The lead isotopic compositions of the pyrites and galenas from the Geraldton area are significantly more radiogenic than the main field of galenas from Superior Province gold deposits (Figure 54) (Franklin and Thorpe, 1982), possibly indicating that they developed in a more uranium-rich environment than the latter, and therefore indicating a greater crustal component to the fluids in the Geraldton area than in other Superior Province gold camps. It is interesting to note that regionally the Geraldton area is characterized by a greater amount of

sedimentary rock than typical Superior province Archean gold camps such as Timmins and Val d'Or which are dominated by mafic volcanic rocks. The greater amount of clastic (i.e. crustally-derived) material in the Geraldton area may be giving the mineralizing fluids their more radiogenic signature. This "local" control on the composition of the mineralizing fluids provides some support for a metamorphogenic origin for the fluids. However, gold mineralization post-dates regional metamorphism in the Geraldton area so the source of the fluids is probably not related to a regional metamorphic event. Pb, Zn, Ni and Cr do not show any enrichment in

If the mineralizing fluid were derived from a mantle-related magmatic source, a more homogeneous, less radiogenic, lead isotopic composition would be expected for the fluids derived from this melt. In addition, a single line or scatter should be developed on the  $8/4$  vs  $6/4$  plot for pyrite data from both the porphyry and the iron formation if a single magmatic source is responsible for the mineralization.

#### 4.4 Summary

1. The Geraldton clastic sedimentary rocks are not geochemically distinct from average Archean clastic sedimentary rocks; there appears to be no significant geochemical difference between the group A and group B sedimentary sequences other than the presence of more

iron-rich rocks (iron formation) in the group A and not the group B; and there appears to be no primary enrichment of gold in these rocks away from zones of deformation and quartz veining, the average gold content of both greywacke and siltstone is less than 9 ppb.

2. The background gold content of oxide iron formation in the Beardmore-Geraldton belt is also very low, at 6 ppb, for samples with less than 0.5% sulphur. The mean gold value for iron formation samples with greater than 0.5% S is 432 ppb. Increases of S and As are closely associated with elevated gold values in iron formation, but the base metal Cu, Pb, Zn, Ni and Cr do not show any enrichment in the S- and Au-rich iron formation.

3. The hornblende gabbros in the Geraldton area have compositions very similar to other Archean mafic intrusive and extrusive rocks. The mean background gold content of these rocks is 1.5 ppb. Many of the chlorite schist outcrops in the Geraldton area were derived from deformation and hydration of original hornblende gabbro. Mass balance plots indicate addition of volatiles,  $K_2O$ , and Ba, and loss of Sr,  $Na_2O$  and  $SiO_2$  in the chlorite schists compared with the hornblende gabbro. The mean background gold content of chlorite schist is 4 ppb.

4. The eastern and western felsic porphyritic intrusive rocks have very similar REE patterns, the eastern porphyries have slightly higher REE abundances, as well as being slightly higher in ferromagnesian components, and

the two groups are thought to represent slightly different amounts of partial melting from the same source. However, both porphyry groups are cut by gold mineralization.

The most distinctive difference between the two porphyry groups is the degree of alteration they have undergone. The western porphyry is everywhere more altered than the eastern porphyry, with extensive development of sericite, carbonate and pyrite and quartz veinlets in the former. In addition, the phenocryst composition of the western porphyries is albite, whereas that of the eastern porphyries is oligoclase, and this is thought to be a result of stripping of Ca from the feldspars in the western porphyries by CO<sub>2</sub>-rich fluids to form carbonate.

The alteration of the porphyries is characterized by addition of CO<sub>2</sub>, H<sub>2</sub>O, S, K, Ba and possibly Na and Mg, as well as gold. The fluids must be moderately acidic as they stabilize albite + muscovite rather than K-feldspar + muscovite.

5. U/Pb zircon dating of the Wods Mac feldspar porphyry gives an age of crystallization of 2691  $\pm$  3/-2 Ma. This is significantly younger than the age of 2769  $\pm$  6/-5 Ma determined on a porphyritic rhyolite volcanic rock from the Onaman Lake area, approximately 60 km to the northwest of the Geraldton area. The age of the Geraldton felsic porphyritic intrusion is also significantly younger than the upper cycle rhyolite at Sturgeon Lake which at 2717 Ma

represents the youngest dated volcanics in the Wabigoon subprovince.

6. A continuous addition secondary isochron determined on pyrite from the Geraldton porphyritic felsic intrusions gives an age of crystallization of the pyrite, and therefore of gold emplacement, of  $2556 \pm 72/-76$  Ma. This places the timing of gold emplacement approximately 130 Ma younger than the intrusion of the felsic porphyritic magmas, thus negating the hypothesis that there is a direct magmatic-hydrothermal association between the gold and these intrusions. This calculated secondary isochron age is in agreement with a Stacey-Kramers (1975) model age calculated on a galena from the Bankfield property which gives a model date of 2563 Ma.

7. The lead isotopic compositions of pyrites and galenas from the Geraldton area are all relatively radiogenic when compared to other Superior province Pb-isotopic data. This may possibly be reflecting a greater amount of clastic material in the Geraldton area than in other Superior province gold camps, which in turn implies a "local" control on some aspects of the mineralizing fluid chemistry.

## CHAPTER 5

GOLD MINERALIZATION IN THE GERALDTON AREA: SELECTED  
EXAMPLES

## 5.0 Introduction

Two gold deposit types, exposed at the time of this study, are described in this chapter; 1) mineralization hosted in iron formation, exposed in an open stope on the North Ore Zone of the Hard Rock Mine, and 2) porphyry-associated mineralization, observed at "Porphyry Hill" on the Hard Rock and MacLeod-Cockshutt properties, and at the Bankfield property. These two deposit types exhibit several important structural, textural and geochemical aspects of the mineralization at Geraldton. Descriptions of several other deposits are summarized from the literature for comparison.

5.1 Relationship of gold mineralization to iron formation;  
North Ore Zone, Hard Rock Mine

The North Ore Zone, or No. 30 Vein System, of the Hard Rock Mine is exposed in outcrop and pit faces where the mine workings broke through to surface (Figure 56). This open stope is located 200m south of highway 11 approximately 750m east of the intersection of highways 11

Figure 56. Aerial photograph of the Open Stope exposure of the North Ore Zone on the Hard Rock property. Note the Z-shape of the workings. The pit is approximately 80 metres long. The photograph is oriented with north toward the top of the page. (Photograph courtesy of A.J. Macdonald, Ontario Geological Survey, Toronto, Ontario, 1983).



and 584 (Figure 3). The pit is in the shape of a large Z (Figure 56) 80m long by 35m wide at its greatest width. This exposure was mapped in detail (Figure 57) to document the distribution of quartz veins and to examine the controls acting on the emplacement of the veins and the massive sulphide lenses. Rock types exposed at the pit include; interbedded thin banded oxide iron formation (magnetite, hematite, minor chert and jasper) and fine-grained siltstone laminae, medium-grained greywacke, and a quartz-carbonate-sericite(-chlorite)-pyrite rock (probably a highly altered intrusive rock). Gold-bearing quartz veins and irregular replacement lenses of sulphide and quartz crosscut the above rock types (Figure 58a). All of the rocks in the immediate vicinity of the pit are strongly deformed and carbonatized. Minor folding has been extensive, with a dominant z-asymmetry to the folds. Carbonate minerals are secondary, overgrowing all primary minerals, thus carbonate alteration post-dates the peak of metamorphism in the area.

The quartz veins exposed in the outcrops surrounding the pit and in the pit walls (Figure 57) are dominantly of approximately east-west strike and are fairly continuous along strike. In addition there are irregular veins which follow contacts or occupy fractured or brecciated zones at the contacts between iron formation and altered intrusive or iron formation and greywacke, and smaller, more irregular veinlets that may show "ladder" or sigmoidal

Figure 57. Detailed map of the Open Stope exposure of the North Ore Zone, Hard Rock property.

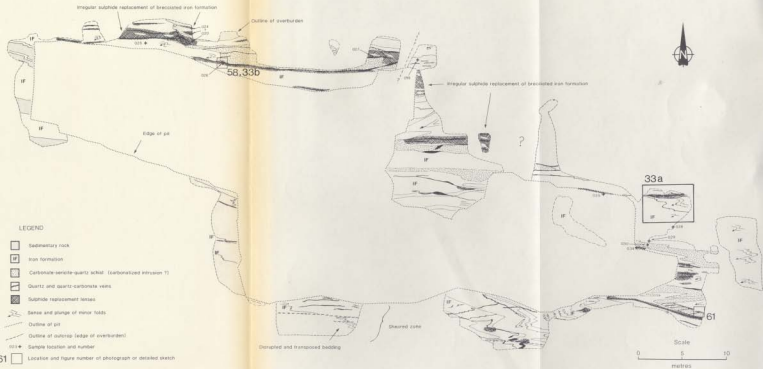
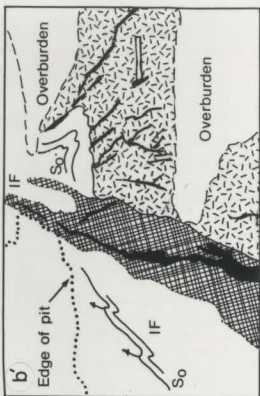
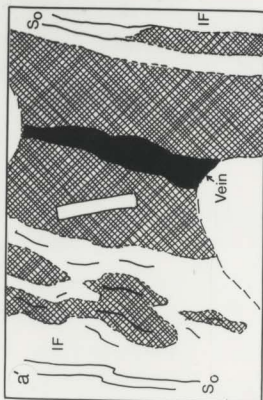


Figure 58. Photographs and sketches of sulphide replacement lenses at the Open Stope exposure. (See Figure 57 for location of photographs and legend for sketches.)

58a. Sulphide replacement lens in banded oxide iron formation at the borders of a crosscutting quartz vein. Note: the lighter-coloured material immediately adjacent to the vein is fresh sulphide, exposed by chipping away weathered material. The dark rubbly surface next to it is oxidized sulphide. The dark, smooth surface is oxide iron formation. 58a'. Sketch of 58a.

58b. Photograph of quartz veins and sulphide replacement lenses localized at the contact between banded oxide iron formation and highly carbonatized intrusive (now a quartz-carbonate-sericite-(chlorite)-pyrite schist). Note the small cleavage-parallel veinlets in the intrusive that are not found in the more competent iron formation. Veins crosscut the iron formation where it has fractured, as in the hinge area of minor folds. Sulphide replacement lenses are formed at the margins of the quartz veins where they are in contact with the iron formation. Note also the different orientation of the veins in the intrusive as opposed to the iron formation. It appears that cleavage (schistosity) controls the site of veins in the intrusive, while ductility contrasts between different rock types and along layers of different composition, and the tendency of the more competent rock to fracture, control the emplacement of veins in the iron formation. (See also Figure 61.) 58b' Sketch of 58b.



form and appear to be tension gashes off the main vein zones.

The quartz veins crosscut folds in the iron formation and greywacke, along fractures subparallel to the fold hinge lines (Figure 58b), and are often continuous into veins that follow bedding in the sedimentary rocks, or contacts with the altered intrusive. The quartz veins also cut earlier carbonate veins. The main quartz veins exposed at the open stope are variable in width, from less than a centimetre to 20 centimetres wide. Horwood and Pye (1955) report that the veins attain widths of up to two feet (70 cm) in underground exposures.

The veins are often bordered by irregular gold-bearing sulphide lenses which replace the sedimentary rocks outward from the vein walls where the veins crosscut iron formation or ferruginous greywacke (Figure 58a). The individual lenses generally strike approximately east-west, dip steeply, and are variable in size. The lenses are reported to attain lengths up to 100 metres and widths up to 10 metres (Horwood and Pye, 1955).

Collectively these lenses formed a strong ore-zone which was hosted along the north limb and in the trough of a large synformal fold in the greywacke and iron formation that plunges 30 degrees W (Figure 57 and 59, and 60). The ore zone persisted along strike and down dip (85 degrees S) to the eastern and lower limits of the fold in the iron formation (Horwood and Pye, 1955). The ore zone

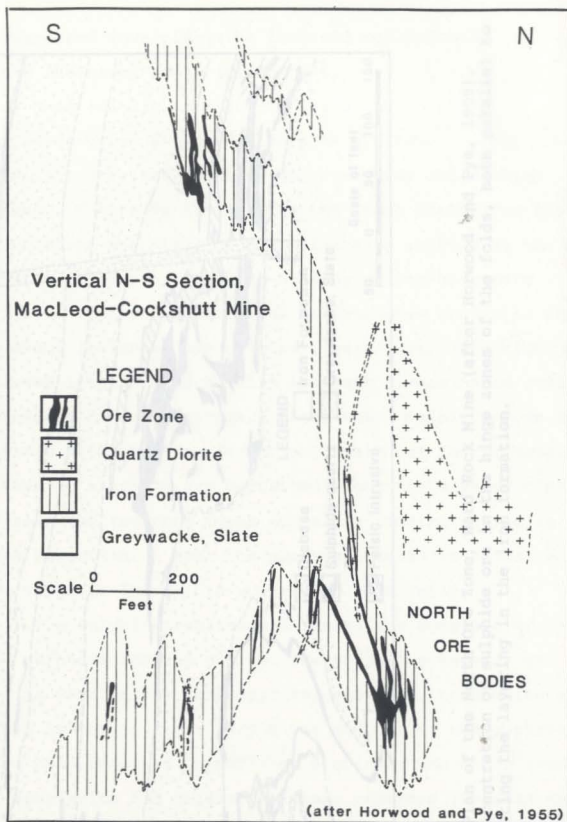


Figure 59. Vertical north-south cross-section of the North Ore Zone, MacLeod-Cockshutt Mine (after Horwood and Pye, 1955). Note the distribution of the sulphide lenses; a) in the hinge zones of folds roughly parallel with the axial planes of the folds, and b) along the contacts between the intrusive rocks and the iron formation.

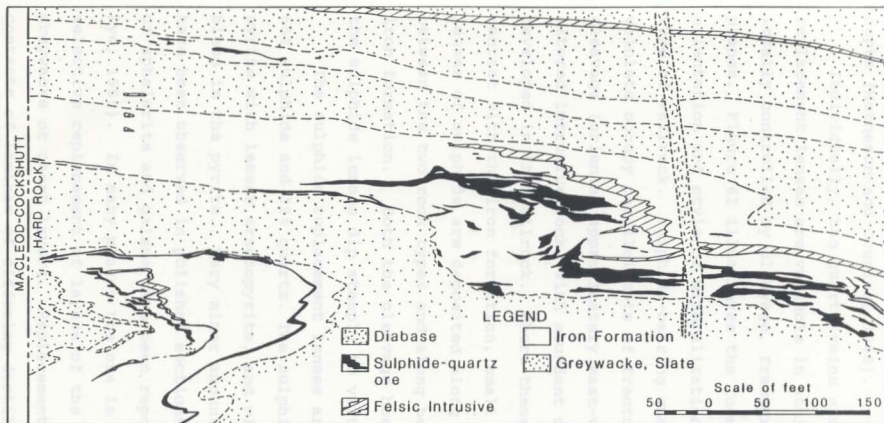


Figure 60. Plan of the North Ore Zone, Hard Rock Mine (after Horwood and Pye, 1955). Note the concentration of sulphide ore in the hinge zones of the folds, both parallel to and crosscutting the layering in the iron formation.

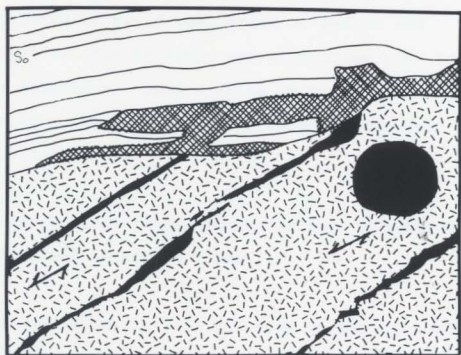
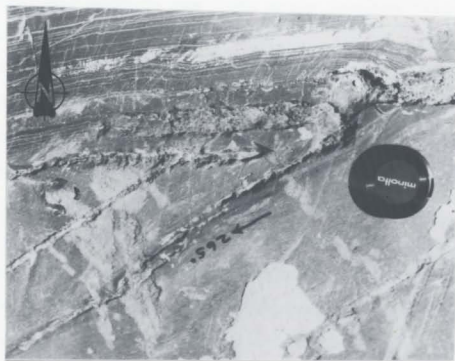
disappeared down plunge as the fold straightened out at depth (Matheson and Douglas, 1948).

Individually, the quartz veins and sulphide replacement lenses are variable in attitude as they are locally controlled by cleavage, fractures and bedding planes. Figure 61 illustrates the local control on the orientation and style of mineralization exerted by the type of wallrock. Sulphide-bearing quartz-carbonate veinlets occupy parallel sets of fractures hosted in the cleavage (oriented approximately east-west) in a highly altered intrusive rock, with abundant disseminated pyrite developed in the wallrock. Where these veinlets come into contact with the iron formation, small but fairly massive lenses of sulphide are deposited along the sheared contact between the two rock types and along bedding planes in the iron formation. Both the cleavage hosted veinlets and the sulphide lenses dip steeply to vertically.

The sulphide replacement lenses are composed of up to 65% sulphide and 35% quartz. The sulphides consist of pyrite with lesser arsenopyrite, and minor pyrrhotite as blebs in the pyrite. Very minor amounts of chalcopyrite have been observed in polished sections, and minor amounts of sphalerite and galena have been reported (Horwood and Pye, 1955). In many places the ore is banded due to the selective replacement of layers of the iron oxide between greywacke or chert layers. Replacement begins along contacts of laminae of differing ductility, in this case

Figure 61. Photograph illustrating the control exerted by rock type on the form and emplacement of quartz veins and sulphide replacement lenses, Open Stope exposure, Hard Rock property.





between iron oxide and siltstone laminae, and progressively engulfs the iron oxide laminae (Figures 13 and 14, Chapter 2).

The pyrite varies from coarse to fine grained (less than 2mm grain size). In many samples, arsenopyrite appears to be earlier than the pyrite. It displays good rhombohedral and lath-shaped forms which are often fractured and surrounded by pyrite grains. The arsenopyrite also ranges in grain size from laths 5 mm long to very fine grained crystals less than 1 mm long.

Gold is intimately associated with the pyrite and arsenopyrite in the replacement lenses (Figure 62). Gold grains are found; 1) associated with, and at the edges of, inclusions in inclusion-rich pyrite, (Figure 62a), 2) at the contacts of grain boundaries of pyrite and arsenopyrite (Figure 62b), and 3) filling tiny fractures in the sulphides. Hand samples of sulphide replacement lenses from the open stope exposure consistently assayed over 10,000 ppb Au.

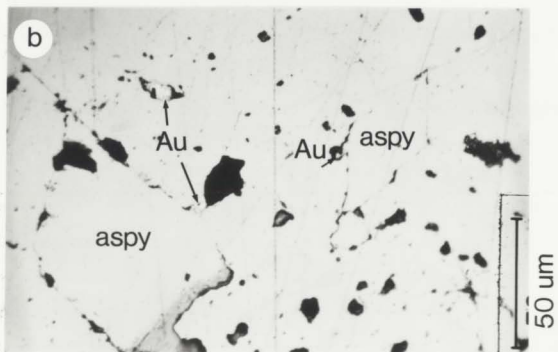
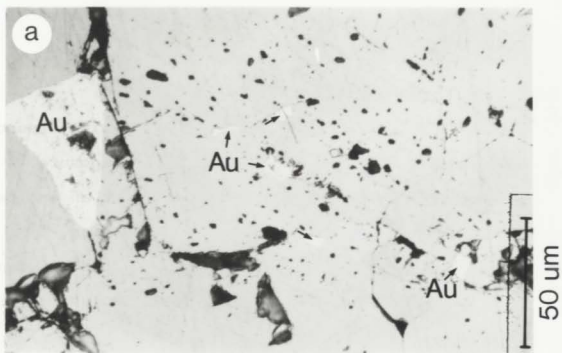
## 5.2 Porphyry-associated mineralization; MacLeod-Cockshutt, Hard Rock and Bankfield Mines

At the Porphyry Hill outcrops on the Hard Rock and MacLeod-Cockshutt properties, fractured and altered massive quartz-feldspar porphyry (QFP) hosts numerous parallel quartz veinlets associated with disseminated

Figure 62. Photomicrographs of gold in pyrite-arsenopyrite sulphide replacement lenses, Open Stope exposure.

62a. Gold grains scattered throughout an inclusion-rich pyrite grain, and along grain boundaries.

62b. Gold grains along grain boundaries between pyrite and arsenopyrite, and along margins of inclusions within the pyrite.



pyrite and arsenopyrite. The porphyry is strongly sheared, and alteration consists of sericitization and carbonatization as described in Chapters 2 and 4. The quartz and quartz-carbonate veinlets occupy cleavage-parallel fractures which strike approximately east-west and dip vertically. Individual veinlets are seldom greater than 2 cm wide and most are less than 1 cm. Outcrops of QFP immediately to the north of the mill building on the Bankfield property exhibit this style of mineralization (Figure 32a and b, Chapter 3; and Figure 16, map of Bankfield property, Chapter 2).

In addition to these quartz stringer zones hosted entirely in porphyry, mineralization is hosted in fractured and deformed sedimentary rocks at the contacts with the porphyry bodies. To the west of the main Porphyry Hill outcrops, tongues of the porphyry intrude into greywacke and lean, slaty iron formation beds. Near the contacts, small replacement lenses of sulphide are developed in the sedimentary rocks. Similarly, on the Bankfield property, a favourable site for veins is at the sheared contacts between the QFP sills and greywacke (Figure 16, Chapter 2). Sulphides are hosted within veins and where the strike of the contact changes slightly, the veins may show an increase in width and amount of sulphide.

At both the Hard Rock and MacLeod-Cockshutt mines important orebodies were associated with the quartz

feldspar porphyry intrusive rocks. Horwood and Pye (1955) described several of the porphyry-associated orebodies to which they had underground access during their study. They identified two types of mineralization, similar to those observed in outcrop, associated with porphyries at these mines:

1) quartz veins and mineralized zones in greywacke and lean iron formation along the contacts of, and in, the porphyry. Examples of this type include;

a) the No. 1 vein system at the Hard Rock mine: a 75 cm wide zone, striking N85E and dipping steeply S, of narrow parallel quartz stringers in fractured albite porphyry and, to the east, at the contact between porphyry and sedimentary rocks;

b) the South Ore Zone on the MacLeod-Cockshutt property (Figure 63): a zone of shearing and fracturing striking N83°W dipping 75°S, along the main contact between sedimentary rocks and porphyry intrusive, characterized by numerous small lenses of almost massive sulphide in the sedimentary rocks, and disseminated gold-bearing sulphides in the porphyry;

c) the No.210 vein and No.517 drift zone, MacLeod-Cockshutt Mine: gold-bearing quartz veins hosted within porphyry.

2) large, low grade bodies composed of auriferous quartz stringers in sheared and fractured greywacke and porphyry along the contacts of porphyry tongues. The stringers consistently strike approximately east-west and dip steeply to vertically. Where the strike of the contacts change, the stringers often coalesce to form large "replacement" lenses. Examples of this second type include;

a) the A and D zones of the Hard Rock Mine: quartz stringer zones in sedimentary rocks at the contacts with the porphyry;

b) the F-zone of the MacLeod-Cockshutt Mine (Figure 64): innumerable quartz veins and stringers localized in a wide zone of shearing and fracturing along the north contact of the main porphyry intrusive body. The stringers strike N80W and dip steeply S, are generally less than 10cm wide but persistent along strike, and collectively formed a very large, important orebody. The ore body plunged to the west following the contact of the porphyry.

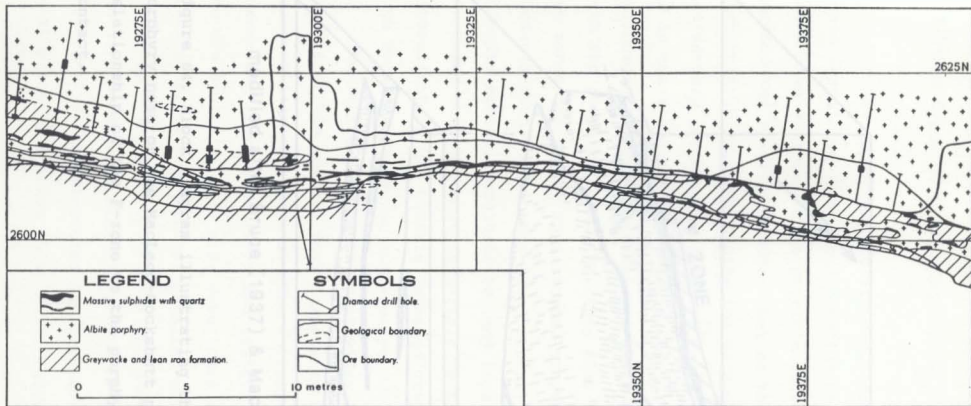
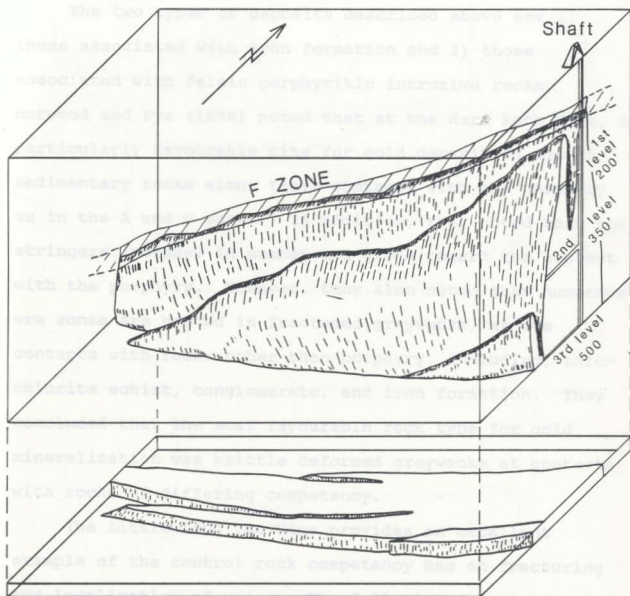


Figure 63. Plan of the South Ore Zone, 349-foot level, of the MacLeod-Cockshutt Mine, illustrating the nature of the sulphide lenses in relation to the porphyry-sediment contact (after Horwood and Pye, 1955).

## 4.3 Other types of mineralization



modified after Bruce (1937) & Macdonald (1984)

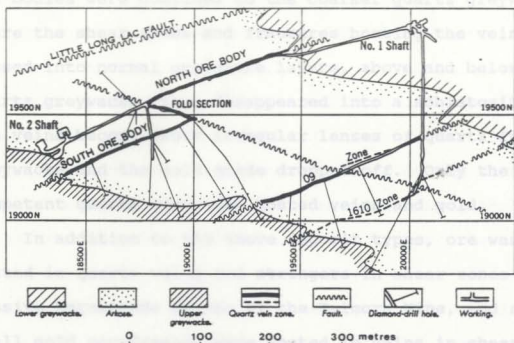
Figure 64. Block diagram illustrating the shape of the porphyry nose on the MacLeod-Cockshutt property and the relationship of the F-zone to the porphyry-sediment contact.

### 5.3 Other types of mineralization

The two types of deposits described above are 1) those associated with iron formation and 2) those associated with felsic porphyritic intrusive rocks. Horwood and Pye (1955) noted that at the Hard Rock Mine, a particularly favourable site for gold deposition was in sedimentary rocks along their contacts with the porphyry, as in the A and D zones. In addition, they noted that the stringers increase in number and grade toward the contact with the porphyry. However, they also noted that numerous ore zones are hosted in fractured greywacke, at its contacts with rocks other than porphyry, including, talc-chlorite schist, conglomerate, and iron formation. They concluded that the most favourable rock type for gold mineralization was brittle deformed greywacke at contacts with rocks of differing competency.

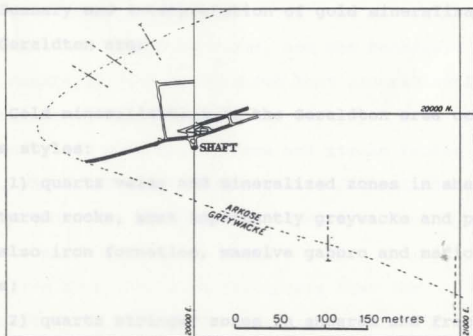
The Little Long Lac Mine provides an excellent example of the control rock competency has on fracturing and localization of veins. The following description is summarized from Bruce (1935 and 1937a), and Pye (1952). The ore bodies at this mine were lodes made up of narrow, continuous, closely-spaced, parallel quartz veins occupying shear planes striking approximately east-west and dipping steeply south in fractured quartz greywacke (Figure 65). The fractures approximately paralleled the axial plane of a large fold in the sedimentary rocks. The

a.



(after Pye, 1952)

b.



(after Bruce, 1937a)

Figure 65. Geological plans of the Little Long Lac Mine.

65a. Plan of the second level of the Little Long Lac Mine (after Bruce, 1937a).

65b. Plan of the 16th (2,214-foot) level of the Little Long Lac Mine (after Pye, 1952).

ore bodies were confined to the coarser quartz greywacke. Where the shear zones and fractures hosting the veins passed into normal greywacke layers, above and below the quartz greywacke, they disappeared into a schistosity. The veins become short irregular lenses of quartz in the greywacke and the gold grade dropped off. Only the more competent quartz greywacke hosted veins and gold.

In addition to the above deposit types, ore was hosted in quartz veins and stringers in shear zones in massive hornblende gabbro at the Talmora Mine, and several small gold occurrences were hosted in veins in sheared and carbonatized volcanic rocks (Pye, 1952).

#### 5.4 Summary and interpretation of gold mineralization in the Geraldton area

Gold mineralization in the Geraldton area occurs in three styles:

- 1) quartz veins and mineralized zones in sheared and fractured rocks, most importantly greywacke and porphyry, but also iron formation, massive gabbro and mafic volcanic rocks;
- 2) quartz stringer zones in sheared and fractured greywacke and porphyry; and,
- 3) sulphide replacement lenses in oxide iron formation.

As is the iron formation is obvious from Figures 29 and 30, which illustrate the axial planar

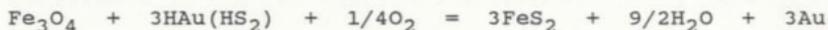
The most important control on the site of individual orebodies was the development of a zone of fracturing or shearing that allowed the mineralizing fluids access to the rocks. These zones may be developed in competent rocks where they have been folded and fractured, often parallel to the axial plane of folds, as at the Little Long Lac mine or the North Ore Zone of the Hard Rock Mine. Zones of shearing and brecciation are commonly developed at the contacts between rocks of differing ductilities, as between greywacke and porphyry, and greywacke and iron formation. These zones represented some of the largest and most important ore bodies in the Geraldton area, including the F-zone and South Ore Zone of the MacLeod-Cockshutt Mine, and the North Ore Zone of the MacLeod-Cockshutt and Hard Rock Mines, and the Bankfield Mine.

Generally, the zones which host mineralization strike approximately east-west and dip steeply. This orientation is consistent with shear zones and strike faults in the area, which reflect the compressive dextral shear deformation that acted on the rocks in a roughly NW-SE direction.

Iron formation is a favourable host for mineralization because it acts as a relatively competent rock during deformation and therefore is susceptible to fracturing. The strong structural control on mineralization in the iron formation is obvious from Figures 59 and 60, which illustrate the axial planar

orientation of many of the ore lenses in the North Ore Zone of the Hard Rock Mine. The iron formation appears to exert an additional control on mineralization in that it acts as a chemical trap for the sulphur-arsenic-gold-bearing solutions. The replacement character of the sulphide lenses where quartz veins crosscut bands containing iron oxide minerals has been clearly shown in Chapter 2 and above.

Phillips et al (1984) suggest that the iron formation acts as the source of iron for the formation of pyrite during the interaction of these rocks with the mineralizing fluid. Gold shows a strong spatial association with pyrite in the mineralization and therefore they suggest that the interaction of iron-rich host rocks and sulphide-bearing solutions is an effective mechanism for precipitating gold. They present the equation;



which represents the oxidation of sulphur ( $\text{S}^{2-}$ ) to form pyrite ( $\text{S}^-$ ) as the mechanism by which aurous complexes are reduced to native gold.

The close spatial association between ore zones and intrusive quartz feldspar porphyry bodies appears to be largely due to structural control. The porphyries

represent a rock type of different ductility to the sedimentary rocks that they intrude, and provide zones of weakness at their contacts where shearing and brecciation are localized. The porphyry bodies in the vicinity of mineralization are all moderately to strongly altered. As discussed in chapter 4, none of the western porphyries have any remnant oligoclase phenocrysts, and all have abundant sericite and carbonate, indicating that the alteration, although variable in degree, has affected this entire suite of rocks. This suggests that these porphyries were very susceptible to alteration, probably by the mineralizing fluids. One explanation of this is that the quartz feldspar porphyry, being a more competent rock, tends to fracture more completely during deformation than the surrounding rocks, and therefore is more permeable to fluid penetration.

No primary sulphide or carbonate facies of iron formation were observed anywhere in the Geraldton belt. All sulphide and carbonate in iron formation was clearly a later overprint on primary oxide minerals. Gold has a very distinctive association with sulphide, suggesting it is also introduced very late. That the sedimentary rocks in the area could be a primarily-enriched source of gold

## CHAPTER 6

## SUMMARY AND DISCUSSION

## 6.1 Summary of observations

## 6.1.1 Sedimentary environment

The Geraldton area is characterized by turbiditic sedimentary rocks with associated oxide iron formation and polymict pebble conglomerate. The group A sedimentary rocks consist of graded greywacke-siltstone (mudstone) turbidites with minor coarse greywacke, polymict matrix-supported conglomerate and iron formation. To the south the group B sequence consists entirely of graded greywacke-siltstone and mudstone with no conglomerate or iron formation. The lack of iron formation in the group B assemblage indicates that there was either no source of iron to form a chemical precipitate in this area, or the clastic sedimentation rates were higher and/or more consistent so that no distinctive iron-sediments were produced.

No primary sulphide or carbonate facies of iron formation were observed anywhere in the Geraldton belt. All sulphide and carbonate in iron formation was clearly a later overprint on primary oxide minerals. Gold has a very distinctive association with sulphide, suggesting it is also introduced very late. That the sedimentary rocks in the area could be a primarily-enriched source of gold

is not likely as the background gold content of both clastic and chemical sedimentary rocks is less than 10 ppb throughout the Geraldton area.

Two of the most distinctive rock types in the Geraldton area are the extensive linear conglomerate horizons and the iron formation. There is a close spatial association of both these rocks with the major deformation zone, and specifically the Bankfield-Tombill Fault zone, in the Geraldton area. In addition, it has been observed by many of the earlier workers that similar conglomerate beds are commonly associated with faults and shear zones throughout the belt (Bruce, 1937a, b). These conglomerate horizons may have been generated due to uplift along a fault-scarp, and may be indicative of the deformation zone being a very long-lived feature. The added spatial coincidence of an anomalous accumulation of iron formation in the area also suggests the presence of some early syn-sedimentary structure(s) that focussed the exhalative activity necessary to form these chemical sediments. These syn-depositional structures may have been listric or basin-margin faults.

While the group A and the group B clastic sedimentary rocks are not distinctive geochemically, there is no iron formation or conglomerate within the group B sequence. These rocks therefore must have been in a different sedimentary/tectonic environment than the group A when they were deposited.

The relationship of the sedimentary rocks to the mafic volcanic rocks in the Geraldton area is unknown as the contacts between the two are generally occupied by faults. The mafic volcanics are submarine in nature, and do not appear to host interbedded clastic sediment.

patterns suggest that these rocks are derived from a

#### 6.1.2 Intrusive rocks of crustal material.

The sedimentary and volcanic rocks in the Geraldton area were intruded by mafic magma, and then by felsic porphyritic bodies, the latter of which are largely confined to the group A sedimentary panel immediately south of Geraldton. Both intrusive rock types show an anomalous abundance in the Geraldton area.

The mafic intrusive rocks are dominantly gabbro and hornblende gabbro. Their composition is similar to some typical Archean intrusive and extrusive mafic volcanic rocks. They do not show a background enrichment in gold. The outcrop pattern of these intrusive rocks suggests that they may be structurally controlled. They are emplaced into both the group A sedimentary rocks and the volcanic rocks to the north, but not into the group B sedimentary rocks.

The felsic intrusive rocks in the Geraldton area have an even more restricted spatial distribution than the mafic intrusive rocks in that they intrude only the group A rocks and the mafic volcanic rocks immediately adjacent to the group A sequence. They crosscut the gabbros and

they appear to post-date at least some deformation of these mafic intrusions. Chemically they are quite distinct from the mafic intrusions in the area and therefore they appear to have both a distinct source and time of emplacement from the mafic intrusions. Their REE patterns suggest that these rocks are derived from a garnet-residual partial melt of crustal material. There is a strong spatial association of the felsic intrusive rocks and the Bankfield-Tombill Fault zone. The porphyries are distributed as long linear features, parallel and close to the fault zone. The fault may have acted as a conduit for these magmas.

### 6.1.3 Structural settings

The Geraldton area is characterized by a major zone of intense deformation, roughly centered on the Bankfield-Tombill Fault zone. Within the area, this zone is spatially coincident with a package of rocks that has an anomalous accumulation of chemical sediment, conglomerate, and intrusive rocks, all of which are distributed roughly parallel to the fault zone. The gold deposits also have a strong spatial association with the areas of most intense deformation.

The change in structural facing direction between the group A and group B sedimentary rock packages may be indicative of an early, large scale deformation. This deformation may have been a large fold or fault that

juxtaposed the two opposing facing packages. The structural discontinuity between the two packages also roughly coincides with the Bankfield-Tombill Fault zone.

At some time these rocks were subjected to an isoclinal folding event that generated upright folds with steep fold axes, possibly associated with the development of a pervasive regional cleavage, which probably postdated the intrusion of the mafic rocks, as they appear to be folded about the same axes. Subsequent to the isoclinal folding, a dextral shearing deformation flattened pre-existing folds, produced a dominant z-shaped asymmetry in minor folds, developed sheared and dilatant zones in massive gabbro and along contacts of rocks of differing ductility, and opened fractures in competent rocks.

The intense dextral shearing developed mylonitized chlorite schist zones in massive hornblende gabbro. Mass balance calculations on these chlorite schists indicate that a) the chlorite schists are derived from the gabbro and b) these rocks have undergone a volume increase (due to hydration) followed by a decrease during deformation. Chemically, the chlorite schists show an increase in volatiles and a loss in Sr, relative to the massive gabbro. This represents a hydration of the gabbro during deformation and the destruction of feldspar resulting in the loss of Sr. The volume decrease is associated with laminated zones in the chlorite schists that are the result of recrystallization into mineralogically

distinctive zones, chlorite alternating with quartz-feldspar layers.

6.1.4 Structural controls on and relative timing of quartz vein emplacement

Quartz veins are hosted in zones of dilatancy localized a) in cleavage, b) in fracture zones parallel to, and commonly occupying, the fold axes of asymmetric folds, and c) in highly deformed areas localized at the contact of rocks of differing ductility. Iron formation was an especially competent lithology within the sedimentary sequence and pervasive fractures within it effectively allowed access of the mineralizing fluids.

The structures which host quartz veins crosscut all Archean rock types in the area including the felsic porphyritic intrusive rocks, and crosscut the later Z-shaped asymmetric minor folds associated with the later dextral shearing event which affected these rocks. Therefore these veins are relatively late features in the structural development of the belt. The lack of high background contents of gold in any of the rock types in the Geraldton area (relative to the common content of gold in all rock types on a world-wide basis), particularly the chemical sediments, and the relatively younger time of emplacement of the quartz veins is strong evidence against a syngenetic or exhalative origin for these deposits. In addition, the lack of base metal enrichment associated

with the gold mineralization at Geraldton is a feature that has been used by Kerrich (1983) as evidence that these deposits are not formed by a process similar to volcanogenic massive sulphides, as has been suggested by Hutchinson and Burlington (1984), and Valliant and Bradbrook (1986) for some Archean lode gold deposits.

6.1.5 The absolute timing of emplacement of gold mineralization

The close spatial association between gold mineralization and felsic intrusions in Superior Province gold camps has been well-documented (Marmont, 1983; Hodgson and MacGeehan, 1982). In most areas, however, the relative timing of the intrusion and mineralization events is not known precisely, although mineralization consistently overprints felsic intrusions. A U/Pb zircon date on a felsic porphyritic intrusion in the Geraldton area gave an age of intrusion of  $2691 \pm 3/-2$  Ma.

To determine the absolute age of mineralization, a continuous addition Pb isochron age was determined on pyrite from the mineralized felsic porphyries. The time of formation of pyrite, and by inference, the time of gold mineralization is calculated to be 2560 Ma. This age is not model dependent as it is calculated as a two-stage isochron with  $t_2 = \text{zero}$ . Even taking a one sigma error into account on the slope of the linear regression calculation, the range of ages obtained is 2628 to 2480

Ma, the oldest of which is significantly younger than the crystallization age of the porphyry. This indicates a difference of 63 to 211 Ma, and probably on the order of 130 Ma, in the time of magmatism and the time of gold emplacement. This long time interval suggests that the gold mineralization is probably not derived from a magmatic hydrothermal system directly associated with the felsic porphyries.

It is interesting to note that the time interval between magmatism and mineralization determined for the Geraldton gold deposits is consistent with recent high resolution step-heating  $^{40}\text{Ar}/^{39}\text{Ar}$  studies done in the Val d'Or and Timmins Archean gold camps. At the Sigma Mine in Val d'Or Hanes et al (1986) obtained a  $^{40}\text{Ar}/^{39}\text{Ar}$  age of 2578 +/- 4 Ma on coarse muscovite from gold-bearing veins. They also determined the timing of regional metamorphism with a metamorphic hornblende, which gave an age of 2687 +/- 18 Ma, thus bracketing gold mineralization to within 110 Ma. Similarly, Masliwec et al (1985) dated fuchsite alteration and the Dome and Hollinger Mines in the Timmins camp by the same  $^{40}\text{Ar}/^{39}\text{Ar}$  step-heating method. They obtained ages of alteration of 2560 +/- 8 to 2633 +/- 6 Ma. A preliminary U/Pb zircon age of 2685 +/- 3 Ma has been reported for the Millerton porphyry in the Hollinger Mine (Masliwec et al, 1985). This also gives a difference in age of magmatism and mineralization on the order of 52 to 125 Ma.

These  $^{40}\text{Ar}/^{39}\text{Ar}$  ages are cooling ages on alteration minerals and therefore may only be used as a minimum estimate of the time of mineralization, but their similarity to the calculated lead isotope age from Geraldton suggests that similar processes have operated in many Archean gold camps whereby mineralization is significantly ( $> 50 \text{ Ma}$ !) younger than the porphyry emplacement, thus negating a magmatic-hydrothermal association with these intrusive rocks (but not ruling out the possibility of a magmatic association with some other, unexposed, magma at depth).

#### 6.1.6 Alteration

Associated with the gold mineralization is an extensive development of carbonate, sericite, and pyrite alteration, with a variable amount of chlorite and arsenopyrite, in all rock types except the diabase dykes (which cross-cut mineralization). Mass balance studies have shown that addition of  $\text{CO}_2$ , S, As, K, Ba and  $\text{H}_2\text{O}$ , and loss of Sr are characteristic of the alteration in the Geraldton area. Mineralogically, massive pyrite-arsenopyrite-iron carbonate alteration is observed in the iron formation, whereas, sericite-carbonate-pyrite(-arsenopyrite) alteration is developed in the felsic porphyritic rocks, and chlorite-sericite-pyrite-(arsenopyrite)-carbonate alteration in clastic sedimentary rocks. In all cases, the degree and type of alteration

appears to be wall-rock controlled, with the host rock contributing cations (ie Fe in the iron formation to make the abundant pyrite and arsenopyrite) and the mineralizing fluid contributing anions.

The thoroughness of alteration of the western porphyries as compared to the eastern porphyries may be a result of the amount of deformation, and therefore fracturing, that affected the two different rocks. The eastern porphyries are not as deformed, foliated or fractured as the western porphyries, and therefore fluids would not have as ready access to these rocks as they would to the fractured western porphyries.

#### 6.1.7 Source of the mineralization fluids

The lead isotopic compositions of pyrites and galenas from the Geraldton area are significantly more radiogenic than the main field of galenas from Superior Province gold deposits (Franklin and Thorpe, 1982), possibly indicating a greater crustal component to the fluids in the Geraldton area than in other Superior Province gold camps. It is interesting that regionally the Geraldton area is characterized by a greater amount of sedimentary material than typical Archean gold camps such as Timmins or Val d'Or, which are dominated by mafic volcanic rocks. This greater amount of clastic material may be giving the fluids in the Geraldton area a more radiogenic signature. This "local" influence on the chemical composition of the

fluids might be invoked to support a metamorphic origin for these fluids, but gold mineralization post-dates regional metamorphism in the Geraldton area and therefore mineralization is probably not related to this metamorphic event. The long time interval between felsic porphyritic magmatism and gold emplacement discussed above precludes a direct magmatic-hydrothermal association between the two, but it does not rule out the possibility of some magmatic source at depth.

## 6.2 Discussion

The principal problems facing geologists in attempting to understand the formation of Archean lode gold deposits are; timing of emplacement of the mineralization; the source of the fluids; and, the cause and mechanism of focussing of the fluids. A comprehensive model of Archean gold deposits has been proposed by the Ontario Geological Survey (Colvine et al, 1984). Many of their general observations apply to the Geraldton area, including the strong structural control on the deposits, the characteristic alteration associated with this style of mineralization, and the close spatial association of gold with felsic porphyritic intrusive rocks. However, the ultimate source of the gold, and the absolute timing of its emplacement is still unclear.

In the Geraldton area, as in many other Archean gold camps, mineralization is associated with major deformation zones and structural "breaks"; the Cadillac-Malartic Break in Val d'Or, the Porcupine-Destor Fault in Timmins, and the Larder Lake Break in Kirkland Lake. The Bankfield-Tombill Fault zone in Geraldton is part of a similar major structure. This fault zone is within a major deformed zone of dextral shear, and may represent a late brittle deformation within the zone. The deformation zone itself coincides with a reversal in structural facing between two packages of sedimentary rocks, shows evidence of being a long-lived zone of structural weakness and possible tectonic activity, and is parallel to and roughly part of spatially coincident with the subprovince boundary between the Wabigoon subprovince to the north and the Quetico subprovince to the south. This zone may represent a collisional tectonic margin, and more specifically a "docking" area between the two major tectonic zones, (Wabigoon and Quetico), similar to that envisioned for accreted suspect terranes in the Appalachian (Williams and Hatcher, 1983) and the Cordillera (Coney et al, 1980).

Williams (1986) interprets the Beardmore-Geraldton belt to be part of an accretionary prism consisting of trench and fore-arc sedimentary material which has been interspersed with layers of mafic volcanics and gabbros, cut by midly discordant gabbros and major and minor intrusions of leucogranite. He states that layer-parallel

shearing, thrusting and strain inhomogeneity have been well-documented as the dominant mechanisms of deformation in modern accretionary prisms, and that these features are present in the Beardmore-Geraldton belt. He interprets the predominance of a dextral shear component as evidence for oblique subduction. Williams concludes that the "Beardmore-Geraldton belt is an accretionary prism which developed on the southern margin of the Onaman Plutonic Complex" to the north, "which represent(s) a volcanic arc typical of the Wabigoon Subprovince".

The long-lived tectonic activity of this zone is suggested by the presence of conglomerate and iron formation along the entire length of the northern part of the Beardmore-Geraldton belt. This distribution suggests that the deposition of these rocks was controlled by some sort of basin-margin faults or listric-type faults. Thus what was originally a marginal basinal zone, may have eventually become the site of subduction and subsequently, dextral shearing.

The presence of discontinuous linear bodies of felsic porphyry localized within this zone may be a result of compressional shear melting at the base of the crust during subduction and/or dextral shear deformation similar to that suggested by Strong (1980) for granitoid plutonism in the Appalachians. He postulated that the magmatism following subduction and the closure of Iapetus was "related to crustal melting caused by thickening due to

continued plate compression, and to both shearing and extensional processes resulting from relative plate motion, which produced a 'megashear' environment". Alternatively, the magmas may be produced by decompressional melting of the lower crust with or without addition of volatiles. These sources are consistent with the garnet-residual REE patterns of the porphyries which suggest a lower-crustal source area. It is interesting to note that the REE patterns of the Geraldton felsic porphyritic intrusions are very similar in both shape and abundance to the Timmins porphyries (Maloney, 1982) and these latter porphyries also show a distinct spatial coincidence with the Porcupine-Destor Fault.

The timing of gold emplacement in the Geraldton area has been shown to be coincident with relatively late structural features, and in absolute terms, mineralization post-dated porphyry emplacement by 130 Ma, thus negating a magmatic-hydrothermal association between these magmas and the gold mineralization. In both the Timmins and Val d'Or gold camps preliminary age dating work suggests that there is a similar large time gap between magmatism and mineralization. Thus gold was emplaced after the period of magmatism that probably coincided with the subduction event. The accretionary process may have been largely complete, and the gold-bearing fluids introduced during later, transcurrent faulting of a "new" craton.

From the above observations it appears that the spatial association of felsic porphyritic intrusions and gold mineralization in Archean lode gold deposits may be a somewhat fortuitous structural superposition, with the porphyries being the result of a major shear zone acting as a producer of these magmas and a conduit for their emplacement, and subsequently the same zone acting as a source?, and most surely as a conduit for the gold-bearing fluids, and providing sites of dilatancy and permeability for deposition of gold. The porphyritic intrusions are therefore a significant indicator of the tectonic environment required to ultimately produce lode gold deposits, although they probably do not have a primary control on mineralization. in relatively young

The major alteration features in the Geraldton area include the introduction of  $\text{CO}_2$  and Au and the loss of Sr. The latter is probably a result of the complete destruction of feldspars within these major shear zones. However, the source of the fluids, the  $\text{CO}_2$  and the gold in Archean lode gold deposits continues to be one of the major unresolved problems in determining the mode of origin of these deposits.

4. The gold deposits are hosted in a major, long-lived deformation zone, roughly coincident with the boundary between the Wabigoon subprovince to the north and the Quetico subprovince to the south.

## CHAPTER 7

## CONCLUSIONS

1. There is no primary enrichment of gold in any of the rocks in the Geraldton area. The background gold content of all rock types is less than 10 ppb.
2. There is no primary sulphide or carbonate facies iron formation in the Geraldton belt. All sulphide and carbonate minerals in iron formation are secondary alteration features associated with gold mineralization.
3. Gold-bearing veins occur in relatively young structures that crosscut all Archean rock types in the area, and overprint several earlier phases of deformation.
4. The major control on emplacement of veins is cleavage-parallel fractures and dilations, and zones of intense deformation localized at the contacts of rocks of differing ductility.
4. The gold deposits are hosted in a major, long-lived deformation zone, roughly coincident with the boundary between the Wabigoon subprovince to the north and the Quetico subprovince to the south.

5. The U/Pb zircon age of felsic porphyry intrusions is 2691  $\pm$  3/-2 Ma.

6. The age of gold mineralization is 2556  $\pm$  72/-76 Ma as determined by a secondary, continuous addition, lead isochron on pyrite from mineralized felsic porphyries.

7. The alteration associated with gold mineralization in the Geraldton area is characterized by addition of CO<sub>2</sub>, S, As, K, Ba and H<sub>2</sub>O, and loss of Sr.

- Barratt, T.J. and Fiala, P.V., 1973, Sediment redeposition in Archean gneisses, Ontario, Canada. *Journal of Metamorphic Geology*, 1, p. 1-11.
- Berthé, D., Gauthier, P. and Jopson, F., 1979, Orthogneiss, gneissite and non-orogenic deformation of granites: the example of the South American Shear Zone. *Journal of Structural Geology*, 1, p. 31-41.
- Blackburn, C.H., Boyd, F.D., Brooks, F.V., Davis, D.V., Edwards, C.H., Foyen, K.H., Fyfe, W.F. and Wood, J., 1985, Evolution of Archean volcanic-sedimentary sequences of the Western Yukon Subprovince and its margin: a review. In Ayres, L.D., Thurston, P.C., Cord, J.B. and Veizer, V., eds. *Evolution of Archean Supracrustal Sequences*. GAC Special Paper 28, 1985.
- Burrows, H.J., 1976, "Structural Facies" (Shackleton's Hole) and the Palaeozoic rocks of the Salguife Complex near Val de Roble, SE Spain. In *Proceedings from Koninklijke Nederlandse Akademie van Wetenschappen, Amsterdam, Series B vol 79*, p. 330-336.
- Bruce, H.L., 1932, Little Long Lac gold area, Ontario Department of Mines Annual Report vol 44, pt 3.
- Bruce, H.L., 1937a, The Eastern part of the Sturgeon River area; Ontario Department of Mines Annual Report vol 45, pt 2, p. 1-59.
- Bruce, H.L., 1937b, New developments in the Little Long Lac area; Ontario Department of Mines Annual Report vol 45, pt 2, p. 119-140.
- Buck, S., and Williams, H.S., 1964, A traverse across a gold-bearing deformation zone, Geraldton. [also] *Geoscience Research Seminar and Open House '84*. 622.

## REFERENCES

- Abbey, S., 1968, Analysis of rocks and minerals by atomic absorption spectroscopy; Part 2; Determination of total iron, magnesium, calcium sodium and potassium. Geological Survey of Canada Paper 68-20.
- Ayres, L.D., 1978, Metamorphism in the Superior Province of northwestern Ontario and its relationship to crustal development, in Fraser, J.A. and Heywood, W.W, eds. Metamorphism in the Canadian Shield, Geol. Surv. Can., Paper 78-10, p.25-36, 1978.
- Barrett, T.J. and Fralick, P.W., 1985, Sediment redeposition in Archean iron formation: examples from the Beardmore-Geraldton greenstone belt, Ontario, Journal of Sedimentary Petrology, v.55, no.2, p.205-212.
- Benedict, P.C. and Titcomb, J.A., 1948, Northern Empire Mine, in Structural Geology of Canadian Ore Deposits - a Symposium. CIMM Special Volume.
- Berthe D., Choukroune, P. and Jegouzo, P., 1979, Orthogneiss, mylonite and non-coaxial deformation of granites: the example of the South American Shear Zone. Journal of Structural Geology, v.1, p.31-42.
- Blackburn, C.E., Bond, W.D., Breaks, F.W., Davis, D.W., Edwards, G.R., Poulsen K.H., Trowell, N.F. and Wood, J., 1985, Evolution of Archean volcanic-sedimentary sequences of the Western Wabigoon Subprovince and its margins: a review. in Ayres, L.D., Thurston, P.C., Card, K.D. and Weber, W., eds. Evolution of Archean Supracrustal Sequences. GAC Special Paper 28, 1985.
- Borradaille, G.J., 1976, "Structural facing" (Shackleton's Rule) and the Paleozoic rocks of the Malaguide Complex near Velez Rubio, SE Spain, in Proceedings Koninklijke Nederlandse Akademie van Wetenschappen, Amsterdam, Series B vol 79, p.330-336.
- Bruce, E.L., 1935, Little Long Lac gold area, Ontario Department of Mines Annual Report vol 44, pt 3.
- Bruce, E.L., 1937a, The Eastern part of the Sturgeon River area; Ontario Department of Mines Annual Report vol 45, pt 2, p.1-59.
- Bruce, E.L., 1937b, New developments in the Little Long Lac area; Ontario Department of Mines Annual Report vol 45, pt 2, p.118-140.
- Buck, S., and Williams, H.R., 1984, A traverse across a gold bearing deformation zone, Geraldton. [abs] Geoscience Research Seminar and Open House '84. OGS.

- Card, K.D., 1983, Regional geological synthesis, central Superior Province: reconnaissance investigations in the Nakina area, Ontario; in Current Research, Part A, Geological Survey of Canada, Paper 83-1A, p.25-27.
- Cherry, M.E., 1983, The association of gold and felsic intrusions - examples from the Abitibi belt, in Colvine, A.C. ed. The Geology of Gold in Ontario, Ontario Geological Survey Miscellaneous Paper 110, p.48-55.
- Colvine, A.C., Andrews, A.J., Cherry, M.E., Durocher, M.E., Fyon, A.J., Lavigne Jr., M.J., Macdonald, A.J. Marmont, Soussan, Poulsen, K.H., Springer, J.S., and Troop, D.G., 1984; An integrated model for the origin of Archean Lode Gold Deposits, Ontario Geological Survey Open File Report 5524, 98p.
- Condie, K.C., 1981, Archean Greenstone Belts, Elsevier, Amsterdam.
- Coney, P.J., Jones, D.L., and Monger, J.W.H., 1980, Cordilleran suspect terranes, Nature, v.288, p.329-333.
- Cummins, W.A. and Shackleton, R.M., 1955, The Ben Lui recumbent syncline (S.W. Highlands). Geological Magazine v.92, p.353-363.
- Davis, D.W., Krough, T.E., Hinzer, J., and Nakamura, E., 1985; Zircon dating of polycyclic volcanism at Sturgeon Lake and implications for base metal mineralization, Economic Geology, v.80, p.1942-1952.
- Doe, B.R., and Zartman, R.E., 1979, Plumbotectonics I, the Phanerozoic; in Geochemistry of Hydrothermal ore deposits, 2nd edition, H.L.Barnes, ed.; John Wiley and Sons, New York.
- Drury, S.A., 1979, Rare-earth and other trace element data bearing on the origin of Archean granitic rocks from Yellowknife, Northwest Territories, Canadian Journal of Earth Sciences, v. 16, p. 809-815.
- Faure, G. 1977, Principles of Isotope Geology. Smith-Wiley Intermediate Geology Series.
- Franklin, J.M., Roscoe, S.M., Loveridge, W.D., and Sangster, D.F., 1983, Lead isotope studies in Superior and Southern Provinces. Geological Survey of Canada Bulletin 351.
- Franklin, J.M., and Thorpe, R.I., 1982, Comparative metallogeny of the Superior, Slave and Churchill provinces; in H.S. Robinson Memorial Volume, Precambrian Sulphide Deposits, R.W. Hutchinson, C.D. Spence, and J.M. Franklin, editors. Geological Association of Canada Special Paper 25, p.3-90.

- Goodwin, A.M., 1977, Archean volcanism in Superior Province, Canadian Shield, in Baragar, W.R.A., Coleman, L.C., and Hall, J.M., eds., Volcanic Regimes in Canada, Geological Association of Canada Special Paper 16, p.205-241.
- Grant, J.A., 1986, The Isocon Diagram - a simple solution to Gresens' equation for metasomatic alteration, *Economic Geology*, v. 81, p.1976-1982.
- Gross, G.A., 1965 Geology of iron deposits of Canada - Volume 1, General geology and evaluation of iron deposits, Geological Survey of Canada, Economic Geology Report No.22, 181p.
- Hanes, J. A., Archibald, D.A., and Hodgson, C.J., 1986, Timing of Archean Au-mineralization in Sigma Mine by  $^{40}\text{Ar}/^{39}\text{Ar}$  Dating, (unpublished abstract for GAC-MAC meeting, Saskatoon, 1986).
- Hanmer, S., 1986, Asymmetrical pull-aparts and foliation fish as kinematic indicators. *Journal of Structural Geology*, vol.8, p.113-122.
- Hodgson, C.J. and MacGeehan, P.J., 1982, Geological characteristics of gold deposits in the Superior Province of the Canadian Shield, in Hodder, R.W. and Petruk, W. editors, *Geology of Canadian Gold Deposits*, CIM Special Volume 24.
- Horwood, H.C., 1948, General structural relationships of ore deposits in the Little Long Lac - Sturgeon River area in *Structural Geology of Canadian Ore Deposits - a Symposium*, Canadian Institute of Mining and Metallurgy.
- Horwood, H.C. and Pye, E.C., 1955, *Geology of Ashmore Township*, Ontario Department of Mines Annual Report, vol 60, part 5, 105 pp.
- Hutchinson, R.W., 1976, Lode gold deposits: the case for volcanogenic derivation. in *Proceedings Volume Pacific Northwest Mining and Metals Conference* Portland, Oregon, 1975. Oregon Dept Geology and Mineral Ind., p.64-105.
- Hutchinson, R.I. and Burlington, J.L., 1984, Some broad characteristics of greenstone belt lode gold deposits, in Foster, R.P., ed., *Gold '82: The geology, geochemistry and genesis of gold deposits*: Geological Society of Zimbabwe, Special Paper No. 1, p.339-371.
- IUGS (International Union of Geological Sciences) 1973, Plutonic rocks - classification and nomenclature recommended by the IUGS Subcommission on the Systematics of Igneous Rocks, *Geotimes*, October, p.26-30.

- Kehlenbeck, M.M, 1986, Folds and folding in the Beardmore-Geraldton fold belt, Canadian Journal of Earth Sciences, vol. 23, p.158-171.
- Kehlenbeck, M.M, 1983, Structural studies in the Beardmore-Geraldton area, Ontario Geological Survey Miscellaneous Paper 116, p.210-203.
- Kerrich, R., 1983, Geochemistry of gold in the Abitibi greenstone belt, Canadian Institute of Mining and Metallurgy Special Paper 27, 75p.
- Krogh, T.E., 1982, Improved accuracy of U-Pb zircon ages by the creation of more concordant systems using an air abrasion technique, Geochimica et Cosmochimica Acta, v.46, p.637-649.
- Lavigne, M.J., 1983, Gold deposits of the Geraldton area, Ontario Geological Survey Miscellaneous Paper 116, p.198-200.
- Macdonald, A.J., 1983, The iron formation - gold association: evidence from Geraldton area, in Colvine, A.C. ed., The Geology of Gold in Ontario, Ontario Geological Survey Miscellaneous Paper 110, p.75-83.
- Macdonald, A.J., 1984, Gold mineralization in Ontario; I; the role of banded iron formation, in CIM Special Volume 34, Chibougamau Stratigraphy and Mineralization, p.412-430.
- Macdonald, A.J. and Hodgson, C.J., 1986, The case for the magmatic-hydrothermal origin of Archean lode gold deposits, in Gold '86 Poster Paper Abstracts volume, p.98-99.
- MacDonald, R.D., 1943, Geology of the Hutchinson Lake area, Ontario Department of Mines Annual Report vol 50, part 3, 21p.
- Mackasey, W.O. 1975, Geology of Dorothea, Sandra, and Irwin Townships, District of Thunder Bay; Ontario Geological Survey, Geological Report 122, 83p.
- Mackasey, W.O., Blackburn, C.E., and Trowell, N.F., 1974, A regional approach to the Wabigoon-Quetico belts and its bearing on exploration in northwestern Ontario; Ontario Division of Mines, Miscellaneous Paper 58, 29p.
- Maloney, J.A., 1982, A comparison of the geology and geochemistry of alkali rich rocks of the Timiskaming Group, with felsic porphyritic igneous rocks found in the Dome Mine, Timmins, Ontario., unpub BSc thesis, University of Waterloo, 78p.
- Marmont, S., 1983, The role of felsic intrusions in gold mineralization, in Colvine, A.C. ed., The Geology of Gold in Ontario, Ontario Geological Survey Miscellaneous Paper 110, 38-47.

- Maslivec, A., York, D., Kuybida, P., and Hall, C.M., 1985, The dating of Ontario's gold deposits: Grant 233; *in* V.G. Milne, ed., Geoscience Research Grant Program, Summary of Research 1984-1985: Ontario Geological Survey Miscellaneous Paper 127, p.223-228.
- Mason, J.K., and McConnell, C.D., 1982, Gold mineralization in the Beardmore-Grealdton area, *in* Colvine, A.C. ed., The Geology of Gold in Ontario, Ontario Geological Survey Miscellaneous Paper 110, p.84-97.
- Mason, J., White, G., and McConnell, C., 1985, Field guide to the Beardmore-Geraldton metasedimentary-metavolcanic belt; Ontario Geological Survey Open File Report 5538, 73p.
- Matheson, A.F., 1948a, Jellicoe Mine, *in* Structural Geology of Canadian Ore Deposits, CIMM Special Volume, p.399-401.
- Matheson, A.F., 1948b, Bankfield and Tombill Mines, *in* Structural Geology of Canadian Ore Deposits, CIMM Special Volume, p.401-406.
- Matheson, A.F., and Douglas, J.H., 1948, Hard Rock Mine, *in* Structural Geology of Canadian Ore Deposits, CIMM Special Volume, p.406-413.
- Maxwell, J.A., 1968, Rock and mineral analysis. Interscience, New York, p.393-396.
- McGlynn, J.C., 1970, Geology of the Canadian Shield-Superior Province; *in* R.J. Douglas, ed., Geology and Economic Minerals of Canada, Economic Geology Report No.1, p.54-71.
- McKay, G.A., Cormie, A.M., and Coulson, C.J., 1948, Leitch Mine, *in* Structural Geology of Canadian Ore Deposits, CIMM Special Volume.
- Ojakangas, R.W., 1985, Review of Archean clastic sedimentation, Canadian Shield: major felsic volcanic contributors to turbiditic and alluvial fan facies associations, *in* Ayres, L.D., Thurston, P.C. Card, K.D., and Weber, W., eds., Evolution of Archean Supracrustal Sequences, Geological Association of Canada Special Paper 28.
- Pettijohn, F.J., 1975, Sedimentary Rocks: New York, Harper and Row, Third edition, 628p.
- Phillips, G.N., Groves, D.I., and Martyn, J.E., 1984, An epigenetic origin for Archean banded iron-formation-hosted gold deposits, Economic Geology v.79, no.1, p.162-171.

- Pirie, J. and Mackasey, W.O., 1978. Preliminary examination of regional metamorphism in parts of Quetico Metasedimentary Belt,, Superior Province, Ontario; in *Metamorphism in the Canadian Shield*, Geol. Surv. Can., Paper 78-10, p.37-48, 1978.
- Platt, J.P., 1984, Secondary cleavages in ductile shear zones. *Journal of Structural Geology*, v. 6, p.439-442.
- Ponce de Leon, M.I. and Choukroune, P., 1980, Shear zones in the Iberian Arc. *Journal of Structural Geology*, v. 2, p.63-68.
- Poulsen, K.H., Borradaile, G.J., and Kehlenbeck, M.M., 1980, An inverted Archean succession at Rainy Lake, *Canadian Journal of Earth Sciences*, vol.17, p.1358-1369.
- Pye, E.G., 1952, Geology of Errington Township, Little Long Lac area, Ontario Department of Mines Annual Report, vol 60, part 6, 140p.
- Pye, E.G., Harris, F.R., Fenwick, K.G., and Baillie, J., Tashota-Geraldton Sheet, Thunder Bay and Cochrane Districts, 1965; Ontario Department of Mines Geological Compilation Series Map 2102, scale 1 inch to 4 miles or 1:253,440.
- Ramsay, J.G., 1967, *Folding and Fracturing of Rocks*, McGraw-Hill Book Company, 568p.
- Reid, J.A., 1945, The Hardrock Porphyry of the Little Long Lac. *Economic Geology*, v. 40, p.509-516.
- Russell, R.D. and Farqhar, R.M., 1960, *Lead Isotopes in Geology*. Interscience Publishers Inc., New York, 243 pages.
- Shegelski, R.J., 1978, Stratigraphy and geochemistry of Archean iron formations in the Sturgeon Lake-Savant Lake greenstone terrain, Northwestern Ontario. PhD thesis, unpublished, University of Toronto, 251p.
- Sinclair, A.J., 1976, Applications of probability graphs in mineral exploration, Special Volume No. 4, The Association of Exploration Geochemists.
- Stacey, J.S., and Kramers, J.D., 1975, Approximation of terrestrial two-stage lead isotope evolution by two-stage model, *Earth and Planetary Science Letters*, volume 6, p.16-25.
- Steiger and Jager, 1977, Subcommittee on geochronology: convention on the use of decay constants in geo- and cosmochronology, *Earth and Planetary Science Letters*, v.36, p.359-362.

- Stockwell, C.H., 1964, Age determinations and geological studies part II: Fourth report on structural provinces, orogenies and time classification of rocks of the Canadian Precambrian Shield, Geological Survey of Canada Paper 64-17, p.1-29.
- Strong, D.F., 1980, Granitoid rocks and associated mineral deposits of Eastern Canada and Western Europe, in D.W. Strangway ed., The Continental Crust and its Mineral Deposits, Geological Association of Canada Special Paper 20, p.741-769.
- Taylor, S.R. and Gorton, M.P., 1977, Geochemical application of spark source mass spectrography - III. Element sensitivity, precision and accuracy, *Geochimica et Cosmochimica Acta*, v.41, p.1375-1380.
- Thorpe, R.I., 1982, Lead isotope evidence regarding Archean and Proterozoic metallogeny in Canada, *Revisita Brasileira de Geologicas*, volume 12, p.510-521.
- Valliant, R.I., and Bradbrook, C.J., 1986, Relationship between stratigraphy, faults and gold deposits, Page-Williams Mine, Hemlo, Ontario, Canada, in A.J. Macdonald ed., *Gold '86 Proceedings Volume*, Toronto, 1986, p.355-361.
- van Breemen, O., Davidson, A., Loveridge, W.D., and Sullivan, R.W., 1986, U-Pb zircon geochronology of Grenville tectonites, granulites and igneous precursors, Parry Sound, Ontario, in Moore, J.M., Davidson, A. and Baer, A.J., eds., *The Grenville Province*, Geological Association of Canada Special Paper 31, p.191-207.
- Walker, R.G., 1979, Turbidites and associated coarse clastic deposits, in Walker, R.G., ed., *Facies Models*, Geoscience Canada Reprint Series 1. Fourth Printing, 1981, p.91-104.
- Weijermars, R., and Rondeel, H.E., 1984, Shear band foliations as an indicator of sense of shear: Field observations in central Spain. *Geology*, v.12, p.603-606.
- Williams, H., and Hatcher, R.D. Jr., 1983, Appalachian suspect terranes. *Geological Society of America Memoir* 158, p.33-53.
- Williams, H.R., 1986, Grant 242 Structural studies in the Beardmore-Geraldton Belt, Northern Ontario, in Milne, V.G. ed. *Geoscience Research Grant Program Summary of Research, 1985-1986*, Ontario Geological Survey Miscellaneous Paper 130, p.138-146.
- Wood, P.C, Burrows, D.R., Thomas, A.V and Spooner, E.T.C., 1986, The Hollinger-McIntyre Au-quartz vein system, Timmins, Ontario, Canada; geologic characteristics, fluid properties and light stable isotope geochemistry, in A.J. Macdonald ed., *Gold '86 Proceedings Volume*, Toronto, 1986, p.56-80.

York, D., 1969, Least squares fitting of a straight line with correlated errors, Earth and Planetary Science Letters v. 5, p.320-324.

#### Appendix A-1. Sedimentary rocks

The geochemical analyses of Geraldton clastic sedimentary rocks are listed in Tables A-1 and A-2. All major element analyses were done at the Geological Survey of Canada (GSC) except samples 486, 488, 489 and 500 which were done at Memorial University (MUN). All trace element analyses were done at the GSC except for the same four samples listed above which were done at MUN. All Ba and V analyses were done at MUN. (See Appendix B for analytical methods. All SIFRA samples of all rock types were analysed for gold at Xray Assay Laboratories (XRAL), and all SIFRA were analysed for gold at Chemex Laboratories, Ltd.)

Table A-1. Major element geochemistry of sedimentary rocks

Table A-2. Trace element geochemistry of sedimentary rocks

## APPENDIX A - LISTING OF GEOCHEMICAL ANALYSES

## Appendix A-I. Sedimentary rocks

The geochemical analyses of Geraldton clastic sedimentary rocks are listed in Tables A-1 and A-2. All major element analyses were done at the Geological Survey of Canada (GSC) except samples 486, 488, 499 and 500 which were done at Memorial University (MUN). All trace element analyses were done at the GSC except for the same four samples listed above which were done at MUN. ALL Ba and V analyses were done at MUN. (See Appendix B for analytical methods. All 82FRA samples of all rock types were analysed for gold at Xray Assay Laboratories (XRAL), and all 83FRA were analysed for gold at Chemex Laboratories, Ltd.).

Table A-1. Major element geochemistry of sedimentary rocks

Table A-2. Trace element geochemistry of sedimentary rocks

Table A-1.

MAJOR ELEMENT GEOCHEMISTRY OF SEDIMENTARY ROCKS, GERALDTON

SAMPLE NO.:	S102	T102	AL2O3	FeO	Fe2O3	MnO	MgO	CaO	Na2O	K2O	P2O5	LOI	FE2O3+K2O	CO2	S	C	TOT
82FRAB81	58.6	0.66	14.0	5.300	1.40	0.88	4.84	1.25	1.90	4.41	0.17	0-	0-	3.78	1.18	0.83	100.9
82FRAB82	62.7	0.44	4.200	2.30	0.86	2.97	1.81	3.90	1.93	0.33	0.17	0-	0-	2.60	1.90	0.20	100.4
82FRAB85	47.1	1.16	15.1	8.700	3.00	1.17	3.95	4.33	2.00	1.23	0.21	0-	13.9	3.90	6.60	0.09	100.4
82FRAB12	64.6	0.68	15.6	4.500	1.60	0.87	2.63	1.03	3.30	2.81	0.11	0-	6.68	2.69	1.60	0.10	100.5
82FRAB37	54.7	0.79	19.3	6.700	1.40	0.99	4.17	6.64	5.20	3.48	0.16	0-	0-	3.30	0.90	0.00	100.8
82FRAB38	55.1	0.66	19.3	6.300	1.40	0.99	4.12	3.41	0.99	3.09	0.19	0-	0-	2.00	1.90	0.00	100.5
82FRAB59	64.9	0.60	15.8	4.500	1.50	0.86	2.63	1.23	2.80	2.38	0.13	0-	8.40	4.00	1.50	0.07	100.2
82FRAB67	53.1	0.76	15.2	5.900	2.48	0.85	3.45	0.74	2.60	3.18	0.14	0-	0-	3.70	0.30	0.15	100.3
82FRAB68	58.0	0.62	16.2	4.900	1.40	0.85	3.05	0.74	2.60	3.18	0.14	0-	0-	3.70	0.30	0.15	100.3
82FRAB71	68.9	0.69	17.2	5.600	1.80	0.91	3.52	0.83	3.20	2.52	0.13	0-	12.9	4.40	2.60	0.00	100.5
82FRAB76	55.6	0.62	15.9	8.900	3.00	0.89	3.45	1.98	1.10	2.54	0.13	0-	0-	4.40	2.60	0.00	100.5
82FRAB88	62.6	0.90	13.3	6.300	1.40	0.86	3.42	1.53	3.00	1.37	0.11	0-	8.40	3.50	2.30	0.40	100.3
82FRAB159	65.7	0.61	14.4	5.100	1.10	0.85	2.43	0.91	3.10	1.79	0.12	0-	6.80	2.60	1.70	0.16	100.9
82FRAB173	47.4	0.44	11.5	12.60	5.50	0.86	2.68	1.87	2.70	2.76	0.18	0-	0-	1.30	12.1	0.29	100.5
82FRAB179	56.2	0.61	14.5	5.400	1.50	0.38	3.14	4.54	1.00	3.05	0.13	0-	7.50	2.40	8.50	0.00	100.4
82FRAB246	65.9	0.51	13.5	5.100	0.80	0.87	1.96	2.33	2.40	2.09	0.11	0-	5.40	2.50	3.50	0.27	100.2
82FRAB249	57.1	0.68	17.7	5.600	1.50	0.89	2.49	2.60	1.70	3.15	0.18	0-	6.50	3.20	5.40	0.12	100.5
82FRAB251	58.0	0.75	16.8	7.900	1.80	0.89	2.66	1.92	0.00	2.70	0.13	0-	10.3	4.10	4.40	0.08	100.3
82FRAB257	60.9	0.13	15.3	0-	0-	0-	0-	0-	0-	3.58	0.14	3.74	4.68	0-	0-	0-	86.92
82FRAB328	56.7	0.75	18.7	6.200	1.90	0.87	3.70	2.79	2.70	2.76	0.18	0-	8.80	4.60	1.00	0.04	100.3
82FRAB333	58.2	0.74	18.3	5.800	2.00	0.87	2.40	0.75	1.70	3.21	0.13	0-	8.10	4.60	5.50	0.05	100.0
82FRAB335	61.9	0.60	15.9	4.200	1.60	0.87	2.48	1.44	2.30	2.32	0.13	0-	6.10	3.50	2.00	0.07	99.10
82FRAB336	61.9	0.60	15.9	4.200	1.60	0.87	2.48	1.44	2.30	2.32	0.13	0-	6.10	3.50	2.00	0.07	99.10
82FRAB338	61.9	0.60	15.9	4.200	1.60	0.87	2.48	1.44	2.30	2.32	0.13	0-	6.10	3.50	2.00	0.07	99.10
82FRAB344	54.5	0.89	16.1	5.200	1.00	0.88	6.42	1.44	4.60	0.21	0.15	0-	9.40	4.30	1.60	0.00	100.9
82FRAB351	58.9	0.64	14.8	6.800	1.60	0.83	3.35	0.26	0.00	3.31	0.11	0-	14.3	4.20	0.68	0.00	100.3
82FRAB353	73.9	0.14	4.90	3.000	9.80	0.33	0.97	0.90	0.40	0.66	0.09	0-	14.0	2.70	1.68	0.00	100.2
82FRAB357	67.3	0.59	16.4	4.100	0.70	0.86	1.53	0.50	2.50	2.93	0.14	0-	5.20	3.40	0.68	0.01	100.9
82FRAB358	66.5	0.56	14.9	4.200	0.90	0.87	2.07	0.95	3.80	1.56	0.09	0-	5.90	3.30	1.10	0.05	100.2
82FRAB359	58.7	0.72	17.8	3.600	5.80	0.18	3.54	1.22	3.30	2.26	0.16	0-	9.00	4.60	1.20	0.07	100.9
82FRAB361	67.1	0.59	15.9	3.200	1.50	0.83	2.14	0.33	2.80	2.57	0.14	0-	5.10	3.60	0.70	0.03	100.6
82FRAB361	67.6	0.49	14.8	3.000	0.80	0.85	1.63	1.71	2.30	2.56	0.09	0-	4.10	2.50	2.40	0.01	99.30
82FRAB384	55.4	0.67	16.3	3.300	6.20	0.89	1.25	2.07	0.00	3.87	0.17	0-	9.80	4.20	3.40	0.37	99.70
82FRAB386	59.3	0.36	11.1	4.900	2.4	0.7	1.56	0.33	8.00	1.98	0.22	0-	27.8	3.00	0.40	0.01	100.9
82FRAB386	63.6	0.56	15.1	4.400	1.20	0.87	2.19	2.11	5.50	0.65	0.16	0-	6.10	3.00	2.00	0.21	100.9
82FRAB397	66.7	0.58	14.5	3.800	1.60	0.87	1.88	1.13	3.30	2.46	0.13	0-	4.90	3.20	1.70	0.08	99.40
82FRAB398	66.7	0.59	15.2	2.900	1.20	0.87	1.93	0.16	3.00	3.90	0.18	0-	3.90	3.10	0.80	0.11	100.2
82FRAB399	66.7	0.59	15.2	2.900	1.20	0.87	1.93	0.16	3.00	3.90	0.18	0-	3.90	3.10	0.80	0.11	100.2
82FRAB400	66.7	0.59	15.2	2.900	1.20	0.87	1.93	0.16	3.00	3.90	0.18	0-	3.90	3.10	0.80	0.11	100.2
82FRAB401	66.7	0.59	15.2	2.900	1.20	0.87	1.93	0.16	3.00	3.90	0.18	0-	3.90	3.10	0.80	0.11	100.2
82FRAB402	66.7	0.59	15.2	2.900	1.20	0.87	1.93	0.16	3.00	3.90	0.18	0-	3.90	3.10	0.80	0.11	100.2
82FRAB429	59.4	0.64	15.4	6.700	4.40	1.00	3.00	0.70	1.00	3.32	0.23	0-	11.9	4.40	1.20	0.04	100.2
82FRAB431	68.4	0.61	15.9	6.200	2.60	0.87	1.93	2.48	3.90	5.48	0.22	0-	5.40	4.20	3.70	0.04	99.48
82FRAB432	64.6	0.50	14.0	3.600	1.00	0.87	2.36	2.45	2.60	2.85	0.13	0-	5.00	3.00	3.60	0.19	100.3
82FRAB441	67.4	0.53	11.6	3.900	0.70	1.00	2.20	3.31	2.40	1.43	0.18	0-	5.10	3.30	2.70	0.08	99.80
82FRAB442	66.0	0.58	15.1	3.800	1.40	0.87	2.09	1.70	3.70	1.82	0.15	0-	5.70	3.60	1.80	0.12	100.3
82FRAB443	62.9	0.62	16.4	4.400	1.00	0.86	3.39	1.13	3.00	2.31	0.20	0-	5.90	4.10	1.30	0.00	100.9
82FRAB444	58.5	0.63	14.9	5.200	0.90	0.11	4.41	3.18	2.10	2.69	0.17	0-	6.70	4.10	2.50	0.06	100.4
82FRAB474	68.4	0.65	14.5	6.900	5.00	0.85	4.24	2.16	4.00	2.42	0.12	0-	6.00	2.90	0.88	0.07	100.2
82FRAB486	64.0	0.36	15.0	0-	0-	0-	0-	0-	0-	2.73	0.15	3.20	5.09	0-	0-	0-	98.05
82FRAB488	76.7	0.30	11.8	0-	0-	0-	0-	0-	0-	3.11	0.08	2.11	2.16	0-	0-	0-	99.90
82FRAB499	70.4	0.16	13.2	0-	0-	0-	0-	0-	0-	3.11	0.08	2.11	2.16	0-	0-	0-	99.25
82FRAB500	69.3	0.16	14.6	0-	0-	0-	0-	0-	0-	1.78	0.09	4.00	4.40	0-	0-	0-	99.19

Table A-2.  
TRACE ELEMENT GEOCHEMISTRY OF SEDIMENTARY ROCKS, BERKALDON

SAMPLE NO.	Cu	Pb	Zn	Ni	Co	Cr	Au	As	Ba	V	Br	U	Th	Rb	Sr	Zr	Y	Nb	
82FR0091	36	28	84	93	28	185	1	54	1142	154	2	0	30	133	356	145	17	5	
82FR0092	42	22	76	55	225	1	35	482	92	4	0	12	10	35	232	159	14	7	
82FR0095	39	10	90	44	46	261	22	7	454	393	6	12	10	35	232	159	24	2	
82FR0017	54	20	100	52	35	150	2	51	514	165	0	23	12	64	152	151	18	5	
82FR0032	12	12	125	95	32	203	2	20	1160	153	0	0	0	101	173	146	12	1	
82FR0038	17	31	100	76	27	166	2	15	1060	147	11	5	16	93	336	165	17	5	
82FR0058	10	16	81	54	33	155	1	20	544	140	1	0	10	82	151	130	12	5	
82FR0067	45	15	87	55	22	212	10	267	672	289	0	0	8	113	75	136	15	3	
82FR0068	9	6	77	58	26	173	10	6	606	164	0	0	7	182	73	139	8	1	
82FR0071	53	15	100	64	17	191	1	25	915	168	0	0	11	130	62	125	19	4	
82FR0076	8	6	83	78	20	181	16	0	804	175	0	0	5	86	73	101	13	4	
82FR0088	86	10	44	55	25	171	6	45	0	-0-	0	0	0	35	91	131	18	1	
82FR0159	47	17	84	51	23	141	8	46	0	-0-	0	4	7	58	110	145	16	5	
82FR0173	81	11	59	45	24	119	6	1	948	141	0	0	6	70	104	72	14	3	
82FR0179	65	11	74	65	33	175	17	199	766	143	0	0	4	90	152	131	19	2	
82FR0246	41	4	77	46	21	130	21	60	0	-0-	14	5	13	77	290	190	11	5	
82FR0249	58	0	64	75	23	160	8	75	0	-0-	0	3	14	120	210	160	15	6	
82FR0251	81	0	91	95	32	130	6	52	0	-0-	5	6	11	97	170	130	13	5	
82FR0257	15	0	31	30	0	80	0	0	609	117	0	0	3	0	81	310	89	8	
82FR0320	55	11	110	79	31	160	1	60	0	-0-	35	3	3	9	160	8	7	1	
82FR0328	53	4	79	63	29	200	2	65	0	-0-	3	7	12	100	77	130	19	7	
82FR0333	53	4	79	63	29	200	2	65	0	-0-	2	2	15	73	190	150	13	6	
82FR0334	45	9	69	59	27	140	1	22	0	-0-	4	4	7	17	330	62	6	7	
82FR0335	44	9	69	74	37	200	1	22	0	-0-	0	4	2	7	17	330	62	6	7
82FR0344	13	0	69	74	37	200	1	22	0	-0-	0	4	2	7	17	330	62	6	7
82FR0344	13	0	69	74	37	200	1	22	0	-0-	0	4	2	7	17	330	62	6	7
82FR0351	99	4	85	75	29	150	4	13	0	-0-	0	5	7	140	43	95	15	5	
82FR0353	26	0	46	17	7	42	1	6	0	-0-	3	1	4	27	39	24	10	0	
82FR0357	48	0	47	64	9	150	1	12	0	-0-	0	3	5	11	99	93	160	11	6
82FR0358	33	0	59	43	16	130	1	28	0	-0-	3	6	12	55	170	150	12	5	
82FR0359	50	0	81	78	29	170	1	42	0	-0-	0	3	4	11	78	120	140	18	5
82FR0360	18	0	65	31	17	150	3	16	0	-0-	0	4	5	69	130	260	6	5	
82FR0361	15	0	58	38	20	86	1	48	0	-0-	2	3	7	79	140	100	6	4	
82FR0384	52	1	75	77	30	170	57	130	0	-0-	11	7	16	110	200	140	17	8	
82FR0386	26	6	57	34	16	90	1	11	0	-0-	1	5	8	84	45	71	10	5	
82FR0396	62	11	71	46	20	130	1	27	0	-0-	6	18	16	570	190	10	6	6	
82FR0397	50	1	77	43	19	140	52	22	0	-0-	11	7	19	87	200	300	9	5	
82FR0398	26	19	120	16	7	120	3	700	0	-0-	1	4	19	94	250	140	7	5	
82FR0400	71	3	96	55	24	140	2	140	0	-0-	2	5	10	56	140	150	12	6	
82FR0400	71	3	96	55	24	140	2	140	0	-0-	2	5	10	56	140	150	12	6	
82FR0421	46	6	93	100	20	130	0	35	0	-0-	2	3	12	120	110	120	16	5	
82FR0422	12	11	55	100	21	340	0	34	0	-0-	8	7	20	90	270	190	13	6	
82FR0441	44	2	54	24	150	0	1	5	0	-0-	2	5	14	75	370	150	6	4	
82FR0442	55	12	70	48	14	130	0	13	0	-0-	8	4	9	53	220	130	11	4	
82FR0443	34	4	51	69	21	210	0	24	0	-0-	14	9	14	69	320	140	10	5	
82FR0443	34	4	51	69	21	210	0	24	0	-0-	9	7	10	82	390	150	9	5	
82FR0444	44	5	84	90	25	320	0	15	0	-0-	0	4	12	59	340	140	12	6	
82FR0474	38	5	66	49	17	150	1	62	0	-0-	0	4	11	87	120	180	10	6	
82FR0486	38	16	22	53	0	189	0	0	887	131	0	0	7	96	288	123	14	5	
82FR0488	29	7	25	23	0	68	0	0	868	67	0	0	13	109	153	109	10	7	
82FR0499	34	7	41	31	0	123	0	0	727	72	0	0	1	91	208	131	12	6	
82FR0500	35	14	65	34	0	109	0	0	556	105	0	2	15	59	240	121	15	8	

## Appendix A-II. Iron formation

The geochemical analyses of Geraldton iron formation samples are listed in Tables A-3 and A-4. All major and trace element analyses were done at the GSC, except for Ba and V, and sample 465 which were analysed at MUN.

Table A-3. Major element geochemistry of iron formation

Table A-4. Trace element geochemistry of iron formation

Table A-3.

Major element geochemistry of iron formation, Geraldton

Sample No.	SiO <sub>2</sub>	TiO <sub>2</sub>	Al <sub>2</sub> O <sub>3</sub>	FeO	MnO	MgO	CaO	Na <sub>2</sub> O	K <sub>2</sub> O	P <sub>2</sub> O <sub>5</sub>	Total
465	51.2	0.1	15.8	28.5	0.5	12.5	0.2	0.1	0.1	0.1	108.6
466	51.5	0.1	16.0	28.8	0.5	12.6	0.2	0.1	0.1	0.1	109.0
467	51.8	0.1	16.2	29.1	0.5	12.7	0.2	0.1	0.1	0.1	109.4
468	52.1	0.1	16.4	29.4	0.5	12.8	0.2	0.1	0.1	0.1	109.8
469	52.4	0.1	16.6	29.7	0.5	12.9	0.2	0.1	0.1	0.1	110.2
470	52.7	0.1	16.8	30.0	0.5	13.0	0.2	0.1	0.1	0.1	110.6
471	53.0	0.1	17.0	30.3	0.5	13.1	0.2	0.1	0.1	0.1	111.0
472	53.3	0.1	17.2	30.6	0.5	13.2	0.2	0.1	0.1	0.1	111.4
473	53.6	0.1	17.4	30.9	0.5	13.3	0.2	0.1	0.1	0.1	111.8
474	53.9	0.1	17.6	31.2	0.5	13.4	0.2	0.1	0.1	0.1	112.2
475	54.2	0.1	17.8	31.5	0.5	13.5	0.2	0.1	0.1	0.1	112.6
476	54.5	0.1	18.0	31.8	0.5	13.6	0.2	0.1	0.1	0.1	113.0
477	54.8	0.1	18.2	32.1	0.5	13.7	0.2	0.1	0.1	0.1	113.4
478	55.1	0.1	18.4	32.4	0.5	13.8	0.2	0.1	0.1	0.1	113.8
479	55.4	0.1	18.6	32.7	0.5	13.9	0.2	0.1	0.1	0.1	114.2
480	55.7	0.1	18.8	33.0	0.5	14.0	0.2	0.1	0.1	0.1	114.6
481	56.0	0.1	19.0	33.3	0.5	14.1	0.2	0.1	0.1	0.1	115.0
482	56.3	0.1	19.2	33.6	0.5	14.2	0.2	0.1	0.1	0.1	115.4
483	56.6	0.1	19.4	33.9	0.5	14.3	0.2	0.1	0.1	0.1	115.8
484	56.9	0.1	19.6	34.2	0.5	14.4	0.2	0.1	0.1	0.1	116.2
485	57.2	0.1	19.8	34.5	0.5	14.5	0.2	0.1	0.1	0.1	116.6
486	57.5	0.1	20.0	34.8	0.5	14.6	0.2	0.1	0.1	0.1	117.0
487	57.8	0.1	20.2	35.1	0.5	14.7	0.2	0.1	0.1	0.1	117.4
488	58.1	0.1	20.4	35.4	0.5	14.8	0.2	0.1	0.1	0.1	117.8
489	58.4	0.1	20.6	35.7	0.5	14.9	0.2	0.1	0.1	0.1	118.2
490	58.7	0.1	20.8	36.0	0.5	15.0	0.2	0.1	0.1	0.1	118.6
491	59.0	0.1	21.0	36.3	0.5	15.1	0.2	0.1	0.1	0.1	119.0
492	59.3	0.1	21.2	36.6	0.5	15.2	0.2	0.1	0.1	0.1	119.4
493	59.6	0.1	21.4	36.9	0.5	15.3	0.2	0.1	0.1	0.1	119.8
494	59.9	0.1	21.6	37.2	0.5	15.4	0.2	0.1	0.1	0.1	120.2
495	60.2	0.1	21.8	37.5	0.5	15.5	0.2	0.1	0.1	0.1	120.6
496	60.5	0.1	22.0	37.8	0.5	15.6	0.2	0.1	0.1	0.1	121.0
497	60.8	0.1	22.2	38.1	0.5	15.7	0.2	0.1	0.1	0.1	121.4
498	61.1	0.1	22.4	38.4	0.5	15.8	0.2	0.1	0.1	0.1	121.8
499	61.4	0.1	22.6	38.7	0.5	15.9	0.2	0.1	0.1	0.1	122.2
500	61.7	0.1	22.8	39.0	0.5	16.0	0.2	0.1	0.1	0.1	122.6
501	62.0	0.1	23.0	39.3	0.5	16.1	0.2	0.1	0.1	0.1	123.0
502	62.3	0.1	23.2	39.6	0.5	16.2	0.2	0.1	0.1	0.1	123.4
503	62.6	0.1	23.4	39.9	0.5	16.3	0.2	0.1	0.1	0.1	123.8
504	62.9	0.1	23.6	40.2	0.5	16.4	0.2	0.1	0.1	0.1	124.2
505	63.2	0.1	23.8	40.5	0.5	16.5	0.2	0.1	0.1	0.1	124.6
506	63.5	0.1	24.0	40.8	0.5	16.6	0.2	0.1	0.1	0.1	125.0
507	63.8	0.1	24.2	41.1	0.5	16.7	0.2	0.1	0.1	0.1	125.4
508	64.1	0.1	24.4	41.4	0.5	16.8	0.2	0.1	0.1	0.1	125.8
509	64.4	0.1	24.6	41.7	0.5	16.9	0.2	0.1	0.1	0.1	126.2
510	64.7	0.1	24.8	42.0	0.5	17.0	0.2	0.1	0.1	0.1	126.6
511	65.0	0.1	25.0	42.3	0.5	17.1	0.2	0.1	0.1	0.1	127.0
512	65.3	0.1	25.2	42.6	0.5	17.2	0.2	0.1	0.1	0.1	127.4
513	65.6	0.1	25.4	42.9	0.5	17.3	0.2	0.1	0.1	0.1	127.8
514	65.9	0.1	25.6	43.2	0.5	17.4	0.2	0.1	0.1	0.1	128.2
515	66.2	0.1	25.8	43.5	0.5	17.5	0.2	0.1	0.1	0.1	128.6
516	66.5	0.1	26.0	43.8	0.5	17.6	0.2	0.1	0.1	0.1	129.0
517	66.8	0.1	26.2	44.1	0.5	17.7	0.2	0.1	0.1	0.1	129.4
518	67.1	0.1	26.4	44.4	0.5	17.8	0.2	0.1	0.1	0.1	129.8
519	67.4	0.1	26.6	44.7	0.5	17.9	0.2	0.1	0.1	0.1	130.2
520	67.7	0.1	26.8	45.0	0.5	18.0	0.2	0.1	0.1	0.1	130.6
521	68.0	0.1	27.0	45.3	0.5	18.1	0.2	0.1	0.1	0.1	131.0
522	68.3	0.1	27.2	45.6	0.5	18.2	0.2	0.1	0.1	0.1	131.4
523	68.6	0.1	27.4	45.9	0.5	18.3	0.2	0.1	0.1	0.1	131.8
524	68.9	0.1	27.6	46.2	0.5	18.4	0.2	0.1	0.1	0.1	132.2
525	69.2	0.1	27.8	46.5	0.5	18.5	0.2	0.1	0.1	0.1	132.6
526	69.5	0.1	28.0	46.8	0.5	18.6	0.2	0.1	0.1	0.1	133.0
527	69.8	0.1	28.2	47.1	0.5	18.7	0.2	0.1	0.1	0.1	133.4
528	70.1	0.1	28.4	47.4	0.5	18.8	0.2	0.1	0.1	0.1	133.8
529	70.4	0.1	28.6	47.7	0.5	18.9	0.2	0.1	0.1	0.1	134.2
530	70.7	0.1	28.8	48.0	0.5	19.0	0.2	0.1	0.1	0.1	134.6
531	71.0	0.1	29.0	48.3	0.5	19.1	0.2	0.1	0.1	0.1	135.0
532	71.3	0.1	29.2	48.6	0.5	19.2	0.2	0.1	0.1	0.1	135.4
533	71.6	0.1	29.4	48.9	0.5	19.3	0.2	0.1	0.1	0.1	135.8
534	71.9	0.1	29.6	49.2	0.5	19.4	0.2	0.1	0.1	0.1	136.2
535	72.2	0.1	29.8	49.5	0.5	19.5	0.2	0.1	0.1	0.1	136.6
536	72.5	0.1	30.0	49.8	0.5	19.6	0.2	0.1	0.1	0.1	137.0
537	72.8	0.1	30.2	50.1	0.5	19.7	0.2	0.1	0.1	0.1	137.4
538	73.1	0.1	30.4	50.4	0.5	19.8	0.2	0.1	0.1	0.1	137.8
539	73.4	0.1	30.6	50.7	0.5	19.9	0.2	0.1	0.1	0.1	138.2
540	73.7	0.1	30.8	51.0	0.5	20.0	0.2	0.1	0.1	0.1	138.6
541	74.0	0.1	31.0	51.3	0.5	20.1	0.2	0.1	0.1	0.1	139.0
542	74.3	0.1	31.2	51.6	0.5	20.2	0.2	0.1	0.1	0.1	139.4
543	74.6	0.1	31.4	51.9	0.5	20.3	0.2	0.1	0.1	0.1	139.8
544	74.9	0.1	31.6	52.2	0.5	20.4	0.2	0.1	0.1	0.1	140.2
545	75.2	0.1	31.8	52.5	0.5	20.5	0.2	0.1	0.1	0.1	140.6
546	75.5	0.1	32.0	52.8	0.5	20.6	0.2	0.1	0.1	0.1	141.0
547	75.8	0.1	32.2	53.1	0.5	20.7	0.2	0.1	0.1	0.1	141.4
548	76.1	0.1	32.4	53.4	0.5	20.8	0.2	0.1	0.1	0.1	141.8
549	76.4	0.1	32.6	53.7	0.5	20.9	0.2	0.1	0.1	0.1	142.2
550	76.7	0.1	32.8	54.0	0.5	21.0	0.2	0.1	0.1	0.1	142.6
551	77.0	0.1	33.0	54.3	0.5	21.1	0.2	0.1	0.1	0.1	143.0
552	77.3	0.1	33.2	54.6	0.5	21.2	0.2	0.1	0.1	0.1	143.4
553	77.6	0.1	33.4	54.9	0.5	21.3	0.2	0.1	0.1	0.1	143.8
554	77.9	0.1	33.6	55.2	0.5	21.4	0.2	0.1	0.1	0.1	144.2
555	78.2	0.1	33.8	55.5	0.5	21.5	0.2	0.1	0.1	0.1	144.6
556	78.5	0.1	34.0	55.8	0.5	21.6	0.2	0.1	0.1	0.1	145.0
557	78.8	0.1	34.2	56.1	0.5	21.7	0.2	0.1	0.1	0.1	145.4
558	79.1	0.1	34.4	56.4	0.5	21.8	0.2	0.1	0.1	0.1	145.8
559	79.4	0.1	34.6	56.7	0.5	21.9	0.2	0.1	0.1	0.1	146.2
560	79.7	0.1	34.8	57.0	0.5	22.0	0.2	0.1	0.1	0.1	146.6
561	80.0	0.1	35.0	57.3	0.5	22.1	0.2	0.1	0.1	0.1	147.0
562	80.3	0.1	35.2	57.6	0.5	22.2	0.2	0.1	0.1	0.1	147.4
563	80.6	0.1	35.4	57.9	0.5	22.3	0.2	0.1	0.1	0.1	147.8
564	80.9	0.1	35.6	58.2	0.5	22.4	0.2	0.1	0.1	0.1	148.2
565	81.2	0.1	35.8	58.5	0.5	22.5	0.2	0.1	0.1	0.1	148.6
566	81.5	0.1	36.0	58.8	0.5	22.6	0.2	0.1	0.1	0.1	149.0
567	81.8	0.1	36.2	59.1	0.5	22.7	0.2	0.1	0.1	0.1	149.4
568	82.1	0.1	36.4	59.4	0.5	22.8	0.2	0.1	0.1	0.1	149.8
569	82.4	0.1	36.6	59.7	0.5	22.9	0.2	0.1	0.1	0.1	150.2
570	82.7	0.1	36.8	60.0	0.5	23.0	0.2	0.1	0.1	0.1	150.6
571	83.0	0.1	37.0	60.3	0.5	23.1	0.2	0.1	0.1	0.1	151.0
572	83.3	0.1	37.2	60.6	0.5	23.2	0.2	0.1	0.1	0.1	151.4
573	83.6	0.1	37.4	60.9	0.5	23.3	0.2	0.1	0.1	0.1	151.8
574	83.9	0.1	37.6	61.2	0.5	23.4	0.2	0.1	0.1	0.1	152.2
575	84.2	0.1	37.8	61.5	0.5	23.5	0.2	0.1</			

Table A-3.

MAJOR ELEMENT GEOCHEMISTRY OF IRON FORMATION, GERALDTON

SAMPLE NO.	SiO2	TiO2	Al2O3	FeO	Fe2O3	MnO	MgO	CaO	Mn2O	K2O	P2O5	LOI	Fe2O3T	H2O	CO2	S	C	TOT
3-FRAN03	60.6	0.50	13.5	5.00	10.0	0.05	1.66	0.43	1.66	2.83	0.19	0-	0-	2.40	1.10	0.01	0-	100.4
3-FRAN10	44.3	0.17	4.50	12.8	25.8	0.06	1.85	3.59	0.00	0.23	0.22	0-	33.8	1.80	5.50	0.12	0-	100.9
3-FRAN25	47.4	0.03	1.00	6.38	30.8	0.04	0.39	0.59	0.00	0.44	0.12	0-	0-	0.20	2.20	0.00	0-	98.70
3-FRAN28	39.9	0.17	5.90	6.58	38.6	0.03	1.14	0.59	0.18	2.98	0.19	0-	0-	0.20	6.80	0.00	0-	99.00
3-FRAN29	57.9	0.18	4.40	0.38	59.2	0.07	1.78	0.93	0.00	0.07	0.19	0-	59.5	2.50	3.00	0.05	0-	100.6
3-FRAN31	52.3	0.19	3.70	0-	45.9	0.05	1.16	0.22	0.00	0.11	0.19	0-	45.9	6.40	1.10	0.24	0-	105.7
3-FRAN74	43.0	0.29	6.60	13.1	26.5	0.10	1.54	2.66	0.40	0.82	0.27	0-	41.1	1.80	2.30	0.69	0-	98.90
3-FRAN75	38.0	0.25	6.20	14.9	28.6	0.17	2.28	2.77	0.00	0.57	0.26	0-	45.2	2.30	2.70	0.27	0-	99.30
3-FRAN150	52.6	0.22	6.60	4.08	27.0	0.04	1.78	0.33	0.20	2.39	0.14	0-	32.3	1.60	1.70	0.00	0-	99.40
3-FRAN164	42.2	0.15	4.50	6.20	42.0	0.09	0.63	0.53	0.00	1.35	0.20	0-	48.9	1.20	0.80	0.15	0-	100.1
3-FRAN166	36.5	0.41	8.60	14.9	29.5	0.13	2.27	0.85	0.30	0.04	0.19	0-	0-	1.60	1.80	0.00	0-	100.0
3-FRAN167	28.7	0.20	4.40	16.7	41.5	0.10	1.13	1.10	3.20	0.04	0.14	0-	0-	1.00	2.30	0.87	0-	98.60
3-FRAN168	36.2	0.21	5.50	15.7	36.2	0.17	0.69	0.47	1.80	0.09	0.27	0-	0-	1.00	1.10	0.00	0-	99.60
3-FRAN175	46.6	0.26	7.20	9.08	26.9	0.06	1.25	1.64	0.00	1.90	0.21	0-	37.8	1.60	3.00	0.82	0-	100.6
3-FRAN180	48.9	0.25	7.20	11.0	26.0	0.11	2.29	2.44	1.40	0.96	0.26	0-	32.2	1.30	4.30	0.00	0-	100.5
3-FRAN182	43.6	0.42	7.70	11.7	21.9	0.15	3.27	2.19	0.60	0.62	0.23	0-	0-	2.60	3.40	0.00	0-	98.50
3-FRAN347	37.5	0.32	3.70	13.2	41.6	0.06	1.11	0.31	0.80	0.80	0.21	0-	56.3	1.10	0.30	0.00	0-	100.3
3-FRAN350	34.6	0.34	1.80	2.7	38.3	0.03	3.04	0.84	0.80	0.75	0.29	0-	20.7	4.50	1.20	0.47	0-	98.30
3-FRAN352	26.8	0.30	1.80	2.8	34.0	0.06	3.28	1.14	2.38	0.47	0.15	0-	34.0	1.50	17.2	0.27	0-	98.90
3-FRAN353	36.3	0.19	4.00	0-	30.8	0.12	1.72	0.73	0.18	1.03	0.19	0-	45.8	1.60	1.20	0.25	0-	98.40
3-FRAN323	40.4	0.14	3.50	15.2	33.5	0.15	1.57	1.63	0.00	1.91	0.23	0-	50.4	1.80	1.50	0.28	0-	100.0
3-FRAN324	57.1	0.36	10.5	9.68	13.1	0.05	2.33	0.65	0.10	1.91	0.29	0-	33.7	3.60	0.50	0.06	0-	100.3
3-FRAN330	55.0	0.33	7.90	10.4	16.9	0.05	2.76	0.42	0.10	1.11	0.23	0-	26.5	3.30	0.50	0.19	0-	100.2
3-FRAN331	48.0	0.17	4.60	12.8	27.3	0.07	1.42	1.39	0.40	0.69	0.23	0-	41.5	1.60	1.90	0.06	0-	100.6
3-FRAN337	39.2	0.17	4.00	14.9	33.5	0.08	1.73	1.31	0.70	0.80	0.27	0-	50.0	1.10	1.70	0.00	0-	96.60
3-FRAN338	32.6	0.15	2.60	18.3	42.1	0.05	0.59	0.37	0.00	0.06	0.22	0-	62.4	0.50	0.40	0.83	0-	98.60
3-FRAN339	33.8	0.16	1.90	18.4	41.8	0.04	0.82	0.30	0.00	0.23	0.15	0-	62.2	0.90	0.30	0.00	0-	99.70
3-FRAN340	36.8	0.06	1.80	13.7	45.2	0.07	0.89	0.49	0.00	0.03	0.15	0-	60.4	0.50	0.60	0.00	0-	99.50
3-FRAN341	38.2	0.04	1.00	4.00	55.8	0.02	0.82	0.22	0.10	0.04	0.12	0-	60.2	0.20	0.20	0.00	0-	100.0
3-FRAN342	42.8	0.20	5.80	13.6	27.1	0.10	1.85	1.19	1.40	0.03	0.25	0-	42.2	2.30	1.60	0.43	0-	98.70
3-FRAN343	42.7	0.29	7.90	13.6	26.0	0.09	1.95	0.32	0.60	1.34	0.10	0-	43.1	3.10	0.40	0.00	0-	100.4
3-FRAN344	46.8	0.14	3.60	12.1	32.5	0.04	0.81	0.66	0.00	1.14	0.22	0-	46.0	0.80	0.80	0.00	0-	99.00
3-FRAN347	46.1	0.04	0.90	9.70	42.4	0.03	0.15	0.34	0.00	0.01	0.10	0-	52.1	0.40	0.50	0.00	0-	99.30
3-FRAN348	32.3	0.09	1.30	16.8	43.2	0.06	0.59	1.06	0.20	1.00	0.27	0-	51.9	0.50	1.20	0.01	0-	98.60
3-FRAN349	32.5	0.21	5.60	10.3	35.1	0.07	1.62	1.75	0.00	0.16	0.27	0-	49.2	0.70	0.80	0.00	0-	100.5
3-FRAN351	32.5	0.19	4.20	14.6	41.4	0.07	1.02	0.75	0.00	0.11	0.27	0-	49.2	0.30	0.40	0.00	0-	100.4
3-FRAN352	32.5	0.19	4.20	14.6	41.4	0.07	0.73	1.36	1.50	0.02	0.24	0-	49.2	0.30	0.40	0.00	0-	99.60
3-FRAN355	44.3	0.34	7.30	17.2	26.1	0.16	1.78	0.99	0.70	0.90	0.18	0-	40.4	2.80	1.50	0.06	0-	100.2
3-FRAN356	32.2	0.24	*2.20	17.2	39.0	0.10	1.06	0.56	0.00	0.53	0.21	0-	53.1	1.90	1.00	0.17	0-	100.2
3-FRAN357	38.3	0.13	3.60	0-	35.3	0.05	0.81	0.24	0.00	0.63	0.13	0-	35.3	2.40	1.60	0.19	0-	102.4
3-FRAN366	20.7	0.16	4.60	0-	39.1	0.02	0.72	0.66	0.00	0.57	0.20	0-	39.1	2.30	0.30	0.23	0-	98.40
3-FRAN369	36.1	0.21	5.30	0-	34.7	0.20	1.67	1.86	2.20	0.05	0.20	0-	24.8	2.10	0.8	0.48	0-	97.70
3-FRAN373	44.1	0.34	8.70	5.50	33.6	0.04	0.61	0.43	1.10	1.02	0.26	0-	39.8	3.40	0.60	0.01	0-	100.6
3-FRAN374	44.4	0.23	6.00	3.90	34.7	0.08	1.32	2.60	0.30	1.12	0.44	0-	39.0	1.90	3.50	0.01	0-	100.7
3-FRAN378	44.8	0.24	6.90	8.70	23.5	0.13	1.14	0.75	3.20	0.13	0.21	0-	33.2	3.60	6.60	0.02	0-	100.0
3-FRAN380	56.3	0.15	4.90	0-	19.8	0.06	0.82	2.46	2.20	0.10	0.09	0-	19.8	1.60	5.90	5.70	0-	100.1
3-FRAN381	23.0	0.16	3.60	1.90	49.7	0.06	0.78	0.40	0.00	0.44	0.38	0-	51.8	1.90	0.50	0.83	0-	99.30
3-FRAN382	31.6	0.09	2.60	0-	39.7	0.03	0.30	0.26	0.00	0.34	0.18	0-	39.7	3.50	0.30	0.22	0-	106.1
3-FRAN383	41.3	0.26	6.60	0-	27.2	0.02	0.53	0.24	0.00	1.49	0.19	0-	27.2	4.30	0.20	0.64	0-	98.80
3-FRAN385	44.9	0.15	4.00	2.60	42.6	0.07	0.53	0.39	0.30	0.53	0.24	0-	45.5	1.40	1.30	0.60	0-	99.00
3-FRAN387	44.6	0.03	1.30	1.10	50.7	0.03	0.05	0.74	0.00	0.12	0.22	0-	51.3	0.60	0.60	0.08	0-	100.3
3-FRAN393	42.1	0.10	1.70	4.90	40.6	0.07	1.09	0.75	0.70	0.15	0.25	0-	41.8	1.20	0.20	0.40	0-	99.10
3-FRAN390	38.6	0.11	2.60	3.80	47.6	0.15	0.12	0.12	0.00	1.03	0.10	0-	51.8	2.10	0.60	0.05	0-	99.30

## MAJOR ELEMENT GEOCHEMISTRY OF IRON FORMATION, GERALDTON (CONT.)

SAMPLE NO.	5102	1102	AL2O3	FE0	FE2O3	PMO	M60	CAO	MA2O	K2O	P2O5	LOI	FE2O3T H2O	CO2	S	C	TOT
33FRM331	46.7	0.31	9.90	3.00	29.6	0.13	0.72	0.40	1.90	1.65	0.29	-0-	32.9	3.40	0.40	0.85	100.5
33FRM332	45.1	0.22	6.80	2.60	39.8	0.06	0.61	0.35	1.50	0.80	0.25	-0-	42.7	2.70	0.60	0.81	100.1
33FRM334	45.2	0.25	7.40	1.90	38.1	0.16	0.40	0.24	0.40	0.91	0.19	-0-	58.2	3.10	0.30	0.81	99.60
33FRM335	41.3	0.09	2.70	1.60	58.7	0.05	0.11	0.20	0.00	0.77	0.18	-0-	40.4	1.80	0.30	0.80	99.80
33FRM401	47.0	0.34	9.20	11.9	21.1	0.06	2.23	0.86	1.70	0.84	0.17	-0-	34.3	2.50	1.60	0.86	100.0
33FRM402	45.1	0.17	5.20	13.7	29.0	0.08	1.13	0.86	1.90	0.23	0.36	-0-	44.2	1.00	3.20	0.14	100.2
33FRM405	45.1	0.04	1.00	11.1	42.3	0.03	0.87	0.19	0.00	0.00	0.10	-0-	54.6	0.40	0.10	0.88	100.4
33FRM406	39.0	0.26	6.9	8.9	18.3	0.09	0.93	0.95	0.70	0.00	0.14	-0-	37.0	1.00	0.10	0.85	100.4
33FRM407	42.5	0.18	6.20	12.9	24.7	0.08	2.72	0.83	0.70	0.76	0.19	-0-	36.9	3.70	1.00	0.85	100.4
33FRM408	42.5	0.24	6.50	12.9	31.3	0.06	1.02	0.83	1.10	1.19	0.10	-0-	45.7	1.20	0.00	0.85	99.60
33FRM409	36.1	0.10	2.10	14.2	44.3	0.07	0.40	0.95	0.50	0.00	0.15	-0-	60.0	0.50	1.20	0.00	100.6
33FRM410	29.7	0.19	4.50	13.5	47.8	0.04	1.40	0.32	0.00	0.39	0.19	-0-	62.8	1.80	0.70	0.00	100.4
33FRM411	31.2	0.27	5.00	18.2	37.7	0.09	2.06	0.53	1.00	0.07	0.22	-0-	57.9	2.30	0.60	0.00	100.7
33FRM412	47.0	0.11	2.70	12.0	34.8	0.03	0.51	0.23	0.30	0.25	0.12	-0-	48.1	0.80	0.40	0.00	99.20
33FRM413	31.1	0.25	5.60	17.2	40.6	0.10	0.93	0.35	0.70	0.52	0.16	-0-	59.8	1.80	0.60	0.81	100.0
33FRM415	33.4	0.08	2.20	8.90	53.4	0.06	0.05	0.44	0.70	0.00	0.22	-0-	63.1	0.30	0.10	0.00	99.70
33FRM465	-0-	-0-	-0-	-0-	-0-	-0-	-0-	-0-	-0-	-0-	-0-	-0-	-0-	-0-	-0-	-0-	-0-
33FRM466	44.1	0.31	6.60	3.50	33.6	0.10	0.67	0.92	1.70	1.32	0.28	-0-	37.5	2.90	1.80	0.00	99.60
33FRM467	38.5	0.38	13.5	-0-	23.6	0.08	1.46	0.74	1.90	3.29	0.16	-0-	23.6	4.30	5.40	1.34	99.90
33FRM468	37.4	0.13	3.90	6.60	51.1	0.06	0.02	0.37	4.30	0.04	0.31	-0-	51.8	2.80	0.70	0.83	98.00
33FRM469	42.6	0.10	2.00	6.10	45.0	0.04	0.63	0.40	0.00	0.33	0.20	-0-	51.7	1.60	0.50	0.00	100.2
33FRM470	44.1	0.23	5.90	1.40	41.0	0.10	0.30	0.25	1.20	0.70	0.24	-0-	43.2	3.20	3.80	0.82	100.30
33FRM471	54.3	0.54	14.4	18.6	2.80	0.11	7.4	7.06	1.90	1.81	0.19	-0-	14.7	4.60	3.80	0.15	99.30
33FRM472	43.1	0.04	4.30	6.00	42.5	0.06	0.90	0.33	0.50	0.60	0.17	-0-	43.2	2.80	0.40	0.83	99.20
33FRM475	53.1	0.45	11.7	3.00	20.6	0.05	1.40	0.81	0.80	3.11	0.22	-0-	24.8	3.30	1.00	0.85	100.5
33FRM476	43.0	0.23	7.30	0.70	41.4	0.13	0.49	0.40	1.40	1.05	0.26	-0-	42.2	3.20	0.50	0.00	100.2
33FRM477	59.1	0.60	16.6	6.40	4.50	0.09	2.39	0.42	2.10	2.93	0.19	-0-	11.6	4.60	0.20	0.86	100.4
33FRM478	50.9	0.31	8.40	5.20	27.5	0.10	1.40	0.51	0.50	1.57	0.18	-0-	33.3	2.90	0.30	0.84	99.60
33FRM479	46.9	0.23	7.10	7.50	32.0	0.04	1.49	0.50	0.20	1.18	0.22	-0-	48.4	2.80	0.20	0.84	100.5
33FRM480	43.1	0.17	4.70	5.30	41.0	0.07	1.23	0.27	0.00	0.45	0.15	-0-	46.3	2.50	0.40	0.82	99.40
33FRM481	49.7	0.37	9.40	5.40	26.3	0.03	2.16	0.31	0.30	1.75	0.20	-0-	37.3	4.10	0.10	0.83	100.2
33FRM502	45.0	0.38	10.4	6.90	27.4	0.03	2.33	0.44	0.00	1.90	0.32	-0-	35.1	4.70	0.10	0.85	100.1
33FRM503	35.4	0.16	4.0	2.90	50.6	0.05	0.91	0.20	0.00	0.82	0.20	-0-	53.3	3.00	0.80	0.05	99.20
33FRM504	52.3	0.45	12.3	9.30	13.0	0.07	3.11	1.20	0.00	2.49	0.37	-0-	25.2	4.90	1.20	0.84	100.4
33FRM505	50.7	0.37	8.30	5.00	26.7	0.04	2.36	0.27	0.00	1.38	0.10	-0-	33.2	3.90	0.20	0.80	100.4
33FRM506	46.0	0.25	5.60	4.10	37.4	0.05	1.54	0.20	0.00	0.70	0.21	-0-	45.0	3.30	0.20	0.80	99.60
33FRM507	55.1	0.57	12.4	6.10	13.7	0.10	2.73	0.63	1.50	2.63	0.20	-0-	20.4	4.30	0.30	0.83	99.60

Table A-4.

TRACE ELEMENT GEOCHEMISTRY OF IRON FORMATION, GERALDTON

SAMPLE NO.	Cu	Pb	Zn	Ni	Co	Cr	Au	As	Ba	V	Br	U	Th	Rb	Sr	Zr	Y	Nb	
82FRAN03	36	21	78	53	27	146	1	6	952	-0-	93	3	0	9	122	153	130	18	3
82FRAN10	12	27	61	17	20	44	2	45	-0-	-0-	0	13	0	12	138	95	10	4	0
82FRAN26	20	25	39	0	5	14	1700	0	165	16	0	28	0	0	18	6	0	1	0
82FRAN46	11	24	37	10	5	33	1	8	817	67	0	0	0	0	65	46	25	5	0
82FRAN49	18	34	52	29	15	42	2	37	1434	36	14	0	0	150	93	98	15	10	0
82FRAN72	39	46	40	0	9	47	4403	1455	-0-	-0-	0	0	0	0	1	9	35	1	0
82FRAN74	21	24	57	13	14	70	3	2	351	75	7	0	0	0	39	72	70	70	5
82FRAN75	38	25	97	15	14	64	2	246	81	0	0	0	0	0	24	83	54	12	1
82FRAN150	19	17	47	15	6	56	14	0	618	52	4	0	0	0	77	65	61	11	4
82FRAN164	24	25	58	12	11	36	31	7	527	66	0	0	0	0	46	19	33	2	0
82FRAN166	7	36	95	37	23	118	2	22	117	105	0	0	0	0	2	184	79	10	2
82FRAN167	14	28	104	19	15	76	11	22	101	123	4	0	0	0	6	67	32	9	1
82FRAN168	6	28	49	18	13	75	0	0	106	116	4	0	0	0	2	67	30	8	0
82FRAN175	15	35	45	15	16	41	34	327	1365	70	0	66	0	0	72	66	51	14	0
82FRAN180	35	31	57	24	12	83	12	176	452	79	4	3	7	44	103	53	13	7	4
82FRAN247	11	21	37	0	4	31	8	8	-0-	-0-	5	4	0	0	28	88	96	20	8
82FRAN248	260	4	130	40	24	92	4800	120	-0-	-0-	5	4	18	36	15	22	15	5	0
82FRAN249	38	17	30	20	18	15	22	12	-0-	-0-	0	5	13	20	50	22	5	4	0
82FRAN250	18	17	36	18	13	32	4	11	11	11	11	11	21	11	180	95	5	2	0
82FRAN251	70	17	46	9	24	40	2350	130	-0-	-0-	0	7	13	40	54	34	2	3	0
82FRAN273	17	26	48	23	13	28	5	25	-0-	-0-	5	16	13	15	37	14	6	3	0
82FRAN274	31	10	58	32	18	66	3	7	-0-	-0-	3	7	10	79	68	73	9	5	0
82FRAN330	41	8	84	14	11	70	1	10	-0-	-0-	4	7	14	47	16	61	5	2	0
82FRAN331	11	10	61	1	3	40	18	6	-0-	-0-	2	9	11	28	40	26	4	1	0
82FRAN337	6	11	40	0	7	36	12	20	-0-	-0-	6	16	24	6	55	14	1	0	0
82FRAN338	3	15	42	0	2	23	1	0	-0-	-0-	0	26	4	15	29	12	1	0	0
82FRAN339	3	15	48	0	2	16	3	8	-0-	-0-	5	27	33	21	12	8	1	0	0
82FRAN340	6	22	41	0	0	11	1	15	-0-	-0-	6	37	12	28	10	0	1	0	0
82FRAN341	4	28	16	0	0	5	25	18	-0-	-0-	8	26	36	18	17	2	0	2	0
82FRAN342	19	11	51	18	9	53	5	6	-0-	-0-	1	11	16	7	65	25	7	0	0
82FRAN343	14	11	50	18	9	71	1	19	-0-	-0-	12	15	19	42	21	37	4	0	0
82FRAN344	12	16	32	7	4	33	1	19	-0-	-0-	10	12	24	15	32	16	4	0	0
82FRAN345	11	19	14	2	3	17	5	15	-0-	-0-	5	13	21	19	46	6	0	0	0
82FRAN347	11	19	14	2	3	30	20	2	-0-	-0-	5	13	21	19	46	6	0	0	0
82FRAN348	34	16	50	25	10	54	2	0	-0-	-0-	7	16	33	44	40	29	6	3	0
82FRAN508	7	12	22	3	3	13	6	70	-0-	-0-	11	17	17	12	24	4	2	0	0
82FRAN552	20	20	43	12	5	41	1	24	-0-	-0-	12	24	41	10	63	19	4	2	0
82FRAN555	27	11	60	32	15	82	1	19	-0-	-0-	9	12	20	38	52	38	8	0	0
82FRAN556	20	27	52	17	13	64	13	20	-0-	-0-	0	18	27	30	55	23	0	2	0
82FRAN566	16	5	27	14	7	26	9250	1300	-0-	-0-	0	1	18	22	18	1	0	0	0
82FRAN569	23	14	31	10	6	41	10001	70000	-0-	-0-	93	2	2	15	62	28	7	0	0
82FRAN370	15	8	39	18	9	51	500	94	-0-	-0-	6	9	20	4	97	28	4	0	0
82FRAN373	28	7	55	35	16	93	1	30	-0-	-0-	8	10	19	44	47	61	9	2	0
82FRAN374	52	11	30	13	10	66	1	13	-0-	-0-	5	10	17	42	120	49	11	0	0
82FRAN376	76	0	52	30	9	60	8	220	-0-	-0-	31	4	7	4	130	32	2	1	0
82FRAN380	16	12	26	12	9	32	895	260	-0-	-0-	2	22	36	27	42	21	5	0	0
82FRAN381	16	12	26	12	9	46	8	24	-0-	-0-	2	1	9	53	15	19	6	5	0
82FRAN382	5	17	39	0	5	21	10001	2300	-0-	-0-	30	7	12	26	57	27	4	1	0
82FRAN383	47	18	33	21	7	43	9400	1907	-0-	-0-	10	12	30	17	30	4	1	0	0
82FRAN385	18	15	32	7	7	43	4	24	-0-	-0-	3	18	31	17	30	4	1	0	0
82FRAN387	9	13	17	0	4	6	1	5	-0-	-0-	0	8	16	15	56	28	1	0	0
82FRAN389	31	4	48	10	8	43	1	5	-0-	-0-	0	4	19	27	50	15	13	0	0
82FRAN390	14	16	47	4	7	22	1	3	-0-	-0-	4	4	19	27	50	15	13	0	0

TRACE ELEMENT GEOCHEMISTRY OF IRON FORMATION, GERALDTON (CONT.)

SAMPLE NO.	Cu	Pb	Zn	Ni	Co	Cr	Au	As	Ba	V	Br	U	Th	Rb	Sr	Zr	Y	Nb
33FR431	18	16	48	28	12	82	2	14	0-	0-	9	9	17	70	63	51	9	7
33FR433	14	17	40	14	6	57	5	18	0-	0-	1	12	24	41	45	36	4	2
33FR434	29	11	41	24	9	67	1	20	0-	0-	5	14	18	74	33	58	6	2
33FR435	13	9	29	0	5	21	1	8	0-	0-	1	19	24	30	15	12	0	0
33FR440	20	2	69	42	14	84	1	7	0-	0-	7	7	11	35	51	51	9	3
33FR442	14	3	29	13	7	39	9	7	0-	0-	2	8	12	13	75	22	4	1
33FR445	5	15	17	0	0	9	13	17	0-	0-	2	15	28	12	8	5	0	2
33FR446	6	13	44	19	4	59	3	6	0-	0-	3	14	19	9	70	27	5	1
33FR447	31	40	97	44	14	100	1	27	0-	0-	2	13	43	13	54	63	0	3
33FR448	24	29	41	17	7	55	1	15	0-	0-	4	12	16	43	17	32	4	3
33FR449	17	22	28	0	0	24	1	3	0-	0-	18	36	59	27	16	2	0	2
33FR450	11	7	26	12	3	24	12	3	0-	0-	6	20	36	14	47	33	11	1
33FR451	5	16	70	26	10	67	1	3	0-	0-	6	20	36	14	47	33	11	1
33FR452	15	13	27	8	2	78	48	41	0-	0-	3	27	28	19	17	17	1	2
33FR453	14	25	52	19	6	58	4	43	0-	0-	12	27	40	29	51	33	6	1
33FR454	4	19	23	0	0	0	22	10	23	0-	1	24	44	16	31	9	2	0
33FR455	0	7	79	19	0-	79	0-	2.75	161	0-	0	5	43	158	57	18	0	3
33FR456	25	10	59	31	11	78	2	21	0-	0-	0	7	18	59	99	54	7	3
33FR457	20	8	82	46	15	92	57	7	0-	0-	1	3	11	140	110	86	7	5
33FR458	14	19	43	7	7	35	13	0	0-	0-	7	22	25	13	56	21	2	3
33FR459	12	12	38	3	0	25	1	8	0-	0-	6	23	29	24	26	15	2	3
33FR470	14	11	41	12	3	51	13	0	0-	0-	3	12	20	35	40	36	2	2
33FR471	25	0	81	57	13	130	1	16	0-	0-	0	8	17	74	100	110	11	5
33FR472	13	20	39	8	4	140	1	16	0-	0-	3	10	25	30	70	110	14	5
33FR473	15	14	48	18	15	88	1	14	0-	0-	3	9	29	42	53	33	4	
33FR474	17	14	48	18	15	88	1	15	0-	0-	3	9	29	42	53	33	4	
33FR475	57	0	75	69	26	150	9	13	0-	0-	3	8	12	130	69	129	16	6
33FR476	57	0	75	69	26	150	9	13	0-	0-	3	8	12	130	69	129	16	6
33FR478	20	7	40	27	11	69	1	12	0-	0-	0	5	13	60	37	56	0	3
33FR479	17	15	49	21	9	58	1	12	0-	0-	4	11	19	47	32	41	6	2
33FR480	15	11	35	10	6	36	1	18	0-	0-	0	16	23	25	42	24	2	2
33FR481	32	5	51	26	14	57	1	15	0-	0-	0	7	8	73	31	60	10	4
33FR482	45	8	69	51	24	110	2	15	0-	0-	6	7	14	81	37	55	11	2
33FR483	16	13	43	13	11	37	1	29	0-	0-	7	24	36	36	17	19	6	4
33FR484	44	2	64	52	23	110	1	9	0-	0-	2	3	8	100	71	85	14	2
33FR485	25	0	45	41	17	100	1	15	0-	0-	9	10	14	56	25	43	8	4
33FR486	25	10	40	16	8	65	1	14	0-	0-	2	14	18	34	27	27	7	22
33FR487	65	0	64	62	25	150	1	12	0-	0-	1	5	6	89	37	69	10	5

## Appendix A-III. Mafic intrusive rocks

The geochemical analyses of Geraldton mafic intrusive rocks are listed in Tables A-5 and A-6. All major element analyses of 82FRA samples were done at the GSC. All major element analyses of 83FRA samples, except sample numbers 328, 329, 419, 423, 425, 439, and 451, were done at MUN. The samples listed above were analysed at the GSC. All trace element analyses of 82FRA samples were done at the GSC, except Ba and V which were done at MUN. All 83FRA samples were analysed for trace elements at MUN except for the samples listed above which were analysed at the GSC.

Table A-5. Major element geochemistry of mafic intrusive rocks

Table A-6. Trace element geochemistry of mafic intrusive rocks



Table A-6.

TRACE ELEMENT GEOCHEMISTRY OF MAFIC INTRUSIVE ROCKS, SERIALATION

SAMPLE NO.	Cu	Pb	Zn	Ni	Co	Cr	Au	As	Ba	V	Br	U	Th	Rb	Sr	Zr	Y	Nb	
82FRA036	55	6	49	58	34	156	2	31	400	186	0	2	0	23	84	111	17	3	
82FRA061	95	13	63	14	31	60	180	52	0	-0-	10	8	0	0	12	62	144	35	4
82FRA083	2	0	98	110	40	58	3	35	0	0	0	0	0	31	190	91	26	0	
82FRA106	129	18	85	131	63	176	2	33	0	0	0	0	0	4	762	74	6	0	
82FRA157	31	8	99	30	43	236	1	14	0	0	0	1	1	21	224	90	18	3	
82FRA165	13	15	123	77	51	329	5	18	0	0	0	4	1	2	31	211	90	22	3
82FRA183	103	21	103	79	50	362	1	23	0	-0-	0	13	12	15	1159	186	21	0	
83FRA203	83	4	61	51	0	30	0	117	322	0	0	0	0	37	210	59	26	4	
83FRA228	36	2	94	254	0	795	1	194	365	0	0	0	0	25	382	38	15	1	
83FRA254	14	2	91	157	0	562	0	204	230	0	0	0	0	19	711	33	18	1	
83FRA258	56	8	48	54	0	645	0	207	243	0	0	0	0	15	180	103	0	0	
83FRA268	4	0	28	65	0	155	0	429	418	0	0	3	12	37	136	71	25	3	
83FRA261	21	0	57	46	0	112	0	138	407	0	0	0	0	17	125	73	31	4	
83FRA262	3	6	59	83	0	162	0	181	427	0	0	2	15	146	56	19	4		
83FRA263	0	7	69	101	0	179	0	267	496	0	5	8	49	57	78	35	4		
83FRA266	2	0	65	386	0	878	0	130	290	0	0	0	0	11	23	96	49	13	
83FRA267	36	5	80	66	0	176	0	723	391	0	0	0	0	66	482	17	8		
83FRA271	86	0	98	111	0	32	0	87	340	0	2	0	0	13	114	41	1		
83FRA273	84	0	98	87	0	181	0	87	376	0	0	0	0	13	118	76	31	4	
83FRA274	82	6	101	66	0	205	2	76	376	0	0	0	0	10	37	78	27	5	
83FRA275	60	0	101	90	0	224	4	40	404	0	4	3	7	30	65	28	2		
83FRA276	110	10	101	100	0	225	3	50	358	0	1	10	10	127	71	30	3		
83FRA325	58	5	94	114	0	125	0	18	235	0	4	3	4	419	88	17	5		
83FRA326	31	0	74	105	0	221	0	66	213	0	0	5	6	153	79	11	3		
83FRA328	94	7	95	78	0	171	7	62	213	0	6	3	5	16	89	140	25	6	
83FRA429	82	3	92	105	0	239	1	16	0	0	0	1	1	21	208	108	10	5	
83FRA482	56	0	54	35	0	18	0	376	0	0	11	5	9	28	368	42	12	2	
83FRA484	0	0	46	88	0	150	0	179	0	0	0	2	7	73	478	79	15	4	
83FRA485	0	7	45	100	0	142	0	271	423	0	6	1	5	7	71	75	32	3	
83FRA487	44	12	314	77	0	278	0	817	322	0	0	4	5	6	113	78	29	4	
83FRA328	52	0	86	110	49	84	1	6	0	0	0	0	3	4	127	66	29	3	
83FRA329	73	0	130	424	69	100	1	0	0	0	3	2	8	8	96	120	42	5	
83FRA423	55	9	118	388	67	1080	0	22	0	0	0	10	16	16	300	85	21	4	
83FRA425	33	2	36	62	19	220	0	18	0	0	0	0	0	19	124	62	35	3	
83FRA439	58	0	100	46	47	43	0	4	0	0	0	1	0	38	172	51	20	2	
83FRA451	27	1	82	190	47	750	0	19	0	151	0	5	13	85	289	128	16	7	

## Appendix A-IV. Felsic intrusive rocks

The geochemical analyses of Geraldton felsic intrusive rocks are listed in Tables A-7 and A-8. All major and trace element analyses of 82FRA samples were done at the GSC except Ba and V which were analysed at MUN. All major and trace element analyses of 83FRA samples were done at MUN.

Table A-7. Major element geochemistry of felsic intrusive rocks

Table A-8. Trace element geochemistry of felsic intrusive rocks

Table A-7.

## MAJOR ELEMENT GEOCHEMISTRY OF FELSIC INTRUSIVE ROCKS, GERALDTON

SAMPLE NO.:	SiO <sub>2</sub>	TiO <sub>2</sub>	Al <sub>2</sub> O <sub>3</sub>	FeO	Fe <sub>2</sub> O <sub>3</sub>	MnO	MgO	CaO	Na <sub>2</sub> O	K <sub>2</sub> O	P <sub>2</sub> O <sub>5</sub>	LOI	FeCO <sub>3</sub>	H <sub>2</sub> O	CO <sub>2</sub>	S	C	TOT
83FRA011	62.3	0.35	17.0	2.308	1.08	0.04	0.86	3.07	5.20	2.21	0.14	0-	3.50	2.00	3.40	0.25	0-	100.3
83FRA106	66.3	0.37	16.0	2.388	0.88	0.03	0.89	3.10	4.00	1.56	0.09	0-	3.00	1.60	3.30	0.40	0-	100.3
83FRA152	65.1	0.37	15.9	0.708	-0.70	0.05	0.89	3.54	4.60	2.67	0.12	0-	2.50	1.40	3.90	0.00	0-	100.5
83FRA202	65.6	0.36	15.3	0.708	-0.70	0.05	0.89	3.83	4.50	2.10	0.18	1.91	3.95	0-	0-	0-	0-	100.3
83FRA205	63.7	0.39	15.0	0-	0-	0.05	2.41	4.58	4.41	1.60	0.16	2.05	5.34	0-	0-	0-	0-	99.66
83FRA207	65.9	0.35	16.2	0-	0-	0.05	2.00	3.63	5.00	1.53	0.15	0.81	4.24	0-	0-	0-	0-	99.67
83FRA208	65.5	0.35	15.3	0-	0-	0.07	2.07	4.64	5.43	0.83	0.16	1.48	4.38	0-	0-	0-	0-	100.2
83FRA209	64.8	0.34	15.1	0-	0-	0.05	2.10	3.90	4.90	1.47	0.16	3.00	4.04	0-	0-	0-	0-	100.4
83FRA214	63.8	0.33	15.2	0-	0-	0.03	1.14	4.37	5.19	2.11	0.09	5.71	1.77	0-	0-	0-	0-	99.57
83FRA215	64.3	0.32	15.5	0-	0-	0.03	0.92	3.07	4.77	2.80	0.08	4.13	1.75	0-	0-	0-	0-	97.42
83FRA220	64.3	0.33	16.4	0-	0-	0.02	0.72	2.55	5.96	3.89	0.17	2.92	1.74	0-	0-	0-	0-	96.77
83FRA221	66.0	0.31	16.4	0-	0-	0.03	0.39	2.07	6.10	2.16	0.10	3.08	2.41	0-	0-	0-	0-	98.90
83FRA222	63.8	0.34	15.8	0-	0-	0.03	1.15	3.24	5.00	2.51	0.11	4.01	3.83	0-	0-	0-	0-	99.62
83FRA226	65.0	0.30	15.1	0-	0-	0.03	0.75	3.79	4.68	2.27	0.14	4.35	1.95	0-	0-	0-	0-	98.29
83FRA256	67.3	0.01	13.2	0-	0-	0.04	1.43	1.09	0.57	10.1	0.00	2.15	2.65	0-	0-	0-	0-	98.40
83FRA259	65.8	0.40	16.3	0-	0-	0.03	1.12	1.53	5.04	2.94	0.09	2.74	3.69	0-	0-	0-	0-	99.57
83FRA264	64.9	0.39	14.8	0-	0-	0.04	1.11	2.28	5.60	2.17	0.00	2.93	4.55	0-	0-	0-	0-	98.73
83FRA266	68.5	0.31	15.1	0-	0-	0.03	0.84	2.30	6.96	2.90	0.10	2.48	3.96	0-	0-	0-	0-	99.71
83FRA403	66.7	0.13	16.6	0-	0-	0.03	0.58	1.70	5.10	2.64	0.10	2.89	2.49	0-	0-	0-	0-	98.38
83FRA414	57.4	0.23	14.8	0-	0-	0.05	4.15	4.76	4.76	2.06	0.09	0.36	3.61	0-	0-	0-	0-	99.68
83FRA431	64.9	0.40	17.4	0-	0-	0.03	2.55	2.69	7.10	1.33	0.10	0.74	2.16	0-	0-	0-	0-	100.6
83FRA483	74.8	0.13	13.0	0-	0-	0.01	0.28	1.09	7.10	0.85	0.02	0.72	1.01	0-	0-	0-	0-	99.93
83FRA600	67.9	0.25	15.5	0-	0-	0.05	1.84	3.41	3.76	3.92	0.12	0.65	2.69	0-	0-	0-	0-	100.1

Table A-8.

## TRACE ELEMENT GEOCHEMISTRY OF FELSIC INTRUSIVE ROCKS, GERRALDTON

SAMPLE NO.	Cu	Pb	Zn	Ni	Co	Cr	Au	As	Ba	V	Br	U	Th	Rb	Sr	Zr	Y	Nb		
03FRM011	64	22	36	6	15	7	6	64	1018	-0	53	0	22	10	64	242	124	5	4	
03FRM146	17	19	54	11	7	26	14	270	84	-0	947	6	14	15	38	308	96	7	6	
03FRM156	3	23	55	12	9	14	1	15	-0	-0	-0	12	15	71	540	127	8	4	4	
03FRM282	35	0	30	18	-0	45	18	-0	481	56	-0	4	0	4	81	493	138	13	9	
03FRM285	55	10	31	13	-0	56	1	-0	638	64	-0	6	6	79	528	121	9	7	7	
03FRM297	221	0	40	16	-0	51	20	-0	906	57	-0	4	0	4	68	332	133	9	6	
03FRM298	245	0	20	15	-0	51	12	-0	373	57	-0	4	10	31	621	130	9	9	9	
03FRM299	16	-0	2	37	4	-0	63	214	-0	1052	56	-0	0	5	52	812	135	1	6	
03FRM214	16	-0	2	37	4	-0	63	214	-0	1052	56	-0	-0	-0	3	79	242	194	3	4
03FRM215	14	5	5	1	-0	29	4	-0	643	53	-0	0	0	6	96	319	59	6	3	
03FRM220	38	3	10	3	-0	2	140	-0	724	93	-0	0	0	6	96	319	59	6	3	
03FRM221	33	3	20	1	-0	27	1	-0	919	53	-0	1	5	55	561	101	6	4	4	
03FRM222	33	3	11	4	-0	24	172	-0	565	70	-0	3	3	80	421	92	5	6	6	
03FRM226	14	0	3	11	-0	-0	4	-0	705	55	-0	0	2	71	419	58	1	1	1	
03FRM227	14	0	3	11	-0	-0	4	-0	705	55	-0	0	4	221	395	100	5	6	6	
03FRM259	11	6	12	3	-0	12	0	-0	163	49	-0	4	0	6	54	129	82	9	3	
03FRM254	13	4	14	23	-0	81	-0	-0	464	113	-0	1	6	54	129	82	9	3	3	
03FRM268	23	4	16	3	-0	8	-0	-0	652	59	-0	0	0	1	36	517	85	4	4	
03FRM483	13	12	25	6	-0	7	1	-0	972	56	-0	0	5	78	443	107	6	4	4	
03FRM414	11	5	30	20	-0	355	1	-0	758	92	-0	0	4	76	260	58	5	2	2	
03FRM415	11	5	30	20	-0	355	1	-0	758	92	-0	0	4	76	260	58	5	2	2	
03FRM403	21	3	4	1	-0	4	-0	-0	222	58	-0	0	0	24	380	74	6	1	1	
03FRM600	9	29	33	19	-0	62	1	-0	1071	32	-0	9	20	133	673	123	11	10	10	

## APPENDIX B - ANALYTICAL METHODS

B-I. Major and trace element analytical procedures at the Geological Survey of Canada Laboratories.

Tables B-1 and B-2 list the analytical accuracy of major element analyses and trace element analyses, respectively, as determined by the Analytical Chemistry Section, Geological Survey of Canada, Ottawa, Ontario.

Whole rock components (Table B-1) were determined by X-Ray Fluorescence Wavelength Dispersive Analyses (XRF), except FeO, H<sub>2</sub>O, CO<sub>2</sub>, and S which were analysed by rapid chemical methods. All whole rock components are reported in weight per cent (wt %). Fe<sub>2</sub>O<sub>3</sub> = Fe<sub>2</sub>O<sub>3</sub> (XRF) - 1.11134 FeO (volumetric). Volatiles represent all constituents lost on ignition other than CO<sub>2</sub>, H<sub>2</sub>O, and S.

Trace elements are reported in parts per million (ppm). As, Nb, Rb, Sr, Th, U, Y and Zr were analysed by Energy Dispersive XRF. Co, Cr, Cu, Ni, Pb, and Zn, were determined by Atomic Absorption (AA) Spectrometry.

Blank spaces represent values below detection limits.

Table B-1. Accuracy of whole rock analyses as reported by the Geological Survey of Canada.

ELEMENT	CALIBRATION		ESTIMATE OF ERROR		DETERMINATION LIMIT
	RANGE (%)	ESTIMATE	ABSOLUTE	RELATIVE %	
SiO <sub>2</sub>	0 - 100	10	0.40	1	0.40
TiO <sub>2</sub>	0 - 3	30	0.02	10	0.02
Al <sub>2</sub> O <sub>3</sub>	0 - 60	10	0.40	10	0.40
Fe <sub>2</sub> O <sub>3</sub>	0 - 90	30	0.10	10	0.10
FeO	0 - 30	10	0.20	10	0.20
MnO	0 - 1	10	0.01	10	0.01
MgO	0 - 50	30	0.10	10	0.10
CaO	0 - 35	30	0.10	10	0.10
Na <sub>2</sub> O	0 - 10	10	0.50	10	1.50
K <sub>2</sub> O	0 - 15	10	0.05	10	0.05
H <sub>2</sub> O	0 - 5	10	0.10	10	0.10
CO <sub>2</sub>	0 - 20	10	0.05	10	0.05
P <sub>2</sub> O <sub>5</sub>	0 - 1	7	0.02	10	0.02
S	0 - 3	10	0.04	10	0.04

Table B-2. Accuracy of trace element analyses as reported by the Geological Survey of Canada.

ELEMENT	ESTIMATE OF ERROR	
	ABSOLUTE (ppm)?	RELATIVE (% OF CONC.)
As	30	10
Nb	10	10
Pb	30	10
Rb	10	10
Sr	10	10
Th	30	10
U	30	10
Y	10	10
Zr	10	10
Co	10	10
Cr	10	10
Cu	7	10
Ni	15	10
Zn	7	10

B-II. Analytical procedures at Memorial University of Newfoundland (MUN). ... calibrated against standards, and every slide ... to this monitor.

Major element contents were determined at MUN (G. Andrews, analyst) using a Perkin-Elmer 306 atomic absorption spectrophotometer. The techniques used are adapted from Langmyr and Paus (1968) and Abbey (1968). Phosphorus contents were determined by colorimetric techniques of Maxwell (1968).

From replicate analyses, analytical errors are estimated at; less than 2% for  $\text{SiO}_2$  and  $\text{Al}_2\text{O}_3$ , less than 5% for  $\text{MgO}$ ,  $\text{CaO}$ , and  $\text{Fe}_2\text{O}_3\text{T}$ , less than 10% for  $\text{MnO}$ ,  $\text{Na}_2\text{O}$ ,  $\text{K}_2\text{O}$ , and  $\text{LOI}$ , and greater than 10% for  $\text{TiO}_2$  and  $\text{P}_2\text{O}_5$ . The large errors in  $\text{TiO}_2$  and  $\text{P}_2\text{O}_5$  analyses are considered due to the low abundances of these elements in the rocks analysed (less than 0.5% and less than 0.3% respectively).

For trace element analyses, pressed sample pellets were prepared. The sample pellets consisted of 10 grams (+/- 0.05 g) of rock powder mixed with 1.50 grams (+/- 0.05 g) of bakelite resin. The mixture was pressed into 40mm diameter pellets at 25 tons pressure and then baked at 200°C to set the binding compound.

The trace element sample pellets were analysed with a Phillips 1450 X-ray fluorescence spectrometer. To reduce

instrument drift between sample runs, a monitor saturated with trace elements was calibrated against standards, and every element ratioed to this monitor.

Based on replicate analyses, the precision of the XRF data is estimated to be within 10% for Rb, Sr, Y, Ba and Zr, within 15% for Ni, Cr, Cu and Zn, and higher for U, Th, Nb and Pb.

Standard Bureau of Standards NBS981 standards and use of  $^{87}\text{Rb}$ ,  $^{86}\text{Sr}$ , and  $^{89}\text{Y}$  for the ratios  $^{87}\text{Rb}/^{86}\text{Sr}$ ,  $^{89}\text{Y}/^{86}\text{Sr}$ ,  $^{208}\text{Pb}/^{206}\text{Pb}$ , and  $^{207}\text{Pb}/^{206}\text{Pb}$ . Analyses for duplicate pairs (were not strictly duplicates) submitted by J. J. Sharpe of the Geological Survey of Canada to the laboratory, and repeat analyses completed to check on within-run reproducibility indicate maximum uncertainty of  $\pm 0.002$ ,  $0.002$ ,  $0.001$ , and  $0.001$  respectively.

## APPENDIX C - LEAD ISOTOPE ERRORS

The data were obtained from Geospec Consultants Limited of Edmonton Alberta, and performed on a Micromass MM-30 mass spectrometer. The uncertainties in reproducibility, quoted at the two-sigma level of error, quoted by Geospec Consultants were derived by repeated analysis of National Bureau of Standards NBS981 standard, and are 0.042, 0.052, 0.058, and 0.028% for the ratios  $^{206}\text{Pb}/^{204}\text{Pb}$ ,  $^{207}\text{Pb}/^{204}\text{Pb}$ ,  $^{208}\text{Pb}/^{204}\text{Pb}$ , and  $^{207}\text{Pb}/^{206}\text{Pb}$ . Analyses for specimen pairs (some not strictly duplicates) submitted by R.I.Thorpe of the Geological Survey of Canada to the Geospec laboratory, and repeat analyses completed to check on within-run reproducibility indicate maximum uncertainty of 0.058, 0.060, 0.061, and 0.044% respectively.

Table D-1. Rare earth element analyses of mafic and felsic intrusive rocks.

Analyses were done by Nuclear Activation Services, Hamilton, Ontario by induced neutron activation

ELEMENT	DET. LIM.***	MAFIC INTRUSIONS				STURGEON LAKE BASALT (3 REPEATS OF 1 SAMPLE)			
		SAMP. NO.	254	261	228	266			
Ba	20.00	260	220	290	160	240	260	240	
La	0.10	0.2	4.2	5.0	5.9	6.2	6.5	6.2	
Nb	0.20	0.9	1.9	1	1.3	1.2	1.5	1.2	
Ta	0.50	-0.5	-0.5	-0.5	-0.5	-0.5	-0.5	-0.5	
Mn	1.00	12	-9	-10	19	6	110	10	
Au**	5.00	-5	-5	7	6	-5	-5	-5	
Ce	1.00	19	19	15	17	13	14	14	
Nd	3.00	12	8	9	9	7	7	7	
Sm	0.10	2.97	2.05	2.74	1.93	1.86	1.91	1.92	
Eu	0.05	1.15	0.95	0.81	0.68	0.65	0.64	0.71	
Tb	0.10	0.5	0.7	0.5	0.3	0.3	0.4	0.5	
Yb	0.05	1.04	3.08	1.42	1.23	1.7	1.76	1.74	
Lu	0.01	0.20	0.49	0.23	0.22	0.27	0.28	0.28	
Sr	100.00	1000	100	400	100	100	200	200	
Rb	5.00	18	22	37	35	15	22	15	

ELEMENT	DET. LIM.***	WESTERN PORPHYRIES			EASTERN PORPHYRIES			CLS****	
		SAMP. NO.	221	214	215	226	207		207(rep.)
Ba	20.00	070	1000	590	420	880	090	960	1300
La	0.10	10.7	16.9	15.5	7.4	25.0	27.3	31.9	53.0
Nb	0.20	3.2	3.2	3.2	2.2	4	3.7	3.9	4.1
Ta	0.50	0.5	0.6	0.5	0.5	0.8	0.8	1	1.9
Mn	1.00	98	110	62	96	110	110	110	220
Au**	5.00	-5	270	9	5	10	21	5	-5
Ce	1.00	43	37	32	16	53	59	61	97
Nd	3.00	18	17	14	7	25	25	26	34
Sm	0.10	3.22	3.03	2.67	1.33	3.99	4.21	4.52	5.28
Eu	0.05	0.77	0.69	0.6	0.38	0.94	1.05	0.86	0.96
Tb	0.10	0.2	0.3	0.2	0.1	0.3	0.4	0.3	0.3
Yb	0.05	0.33	0.4	0.29	0.25	0.73	0.75	0.73	0.82
Lu	0.01	0.07	0.06	0.04	0.04	0.11	0.11	0.14	0.13
Sr	100.00	600	500	300	500	1000	1000	900	600
Rb	5.00	78	65	200	100	85	92	74	190

## Notes

-0.5 denotes less than 0.5

\*\*These samples were crushed in a tungsten carbide shatter box so there may be some W contamination

\*\*\*All analyses are reported in ppm except for Au which is in ppb

\*\*\*\*DET. LIM. = detection limit

\*\*\*\*\*CLS = Crell Lake Stock

110881

Table D-2. Chondrite normalization values used for REE plots.  
Values are from Taylor and Gorton (1977).

ELEMENT	NORMALIZATION FACTOR
La	0.315
Ce	0.813
Pr	0.116
Nd	0.597
Sm	0.192
Eu	0.0722
Gd	0.259
Tb	0.049
Dy	0.325
Ho	0.0730
Er	0.213
Tm	0.0300
Yb	0.208
Lu	0.0323





